1-1-2012

Ruthenium polypyridyl complexes that utilize azo-dyes to enhance absorption of visible photons

Akram Hazeen
Eastern Illinois University

THESIS MAINTENANCE AND REPRODUCTION CERTIFICATE

TO: Graduate Degree Candidates (who have written formal theses)

SUBJECT: Permission to Reproduce Theses

An important part of Booth Library at Eastern Illinois University's ongoing mission is to preserve and provide access to works of scholarship. In order to further this goal, Booth Library makes all theses produced at Eastern Illinois University available for personal study, research, and other not-for-profit educational purposes. Under 17 U.S.C. § 108, the library may reproduce and distribute a copy without infringing on copyright; however, professional courtesy dictates that permission be requested from the author before doing so.

By signing this form:

- You confirm your authorship of the thesis.
- You retain the copyright and intellectual property rights associated with the original research, creative activity, and intellectual or artistic content of the thesis.
- You certify your compliance with federal copyright law (Title 17 of the U.S. Code) and your right to authorize reproduction and distribution of all copyrighted material included in your thesis.
- You grant Booth Library the non-exclusive, perpetual right to make copies of your thesis, freely and publicly available without restriction, by means of any current or successive technology, including but not limited to photocopying, microfilm, digitization, or Internet.
- You acknowledge that by depositing your thesis with Booth Library, your work is available for viewing by the public and may be borrowed through the library's circulation and interlibrary departmenst or accessed electronically.
- You waive the confidentiality provisions of the Family Educational Rights and Privacy Act (FERPA) (20 U.S.C. § 1232g; 34 CFR Part 99) with respect to the contents of the thesis, including your name and status as a student at Eastern Illinois Univerity.

Petition to Delay:

I respectfully petition that Booth Library delay maintenance and reproduction of my thesis until the date specified and for the reasons below. I understand that my degree will not be conferred until the thesis is available for maintenance and reproduction.

Date:

Reasons:

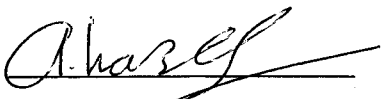

Author's Signature

7/3/2012

Date

This form must be submitted in duplicate.

Ruthenium Polypyridyl Complexes that Utilize Azo-dyes to Enhance Absorption of Visible Photons

(TITLE)

BY

Akram Hazeen

THESIS

SUBMITTED IN PARTIAL FULLMENT OF THE REQUIREMENTS
FOR THE DEGREE OF

Master of Science in Chemistry

IN THE GRADUATE SCHOOL, EASTERN ILLINOIS UNIVERSITY
CHARLESTON, ILLINOIS

2012
YEAR

I HEREBY RECOMMEND THAT THIS THESIS BE ACCEPTED AS FULFILLING
THIS PART OF THE GRADUATE DEGREE CITED ABOVE

Mark E McGuire	7/2/12		6/26/12
THESIS COMMITTEE CHAIR	DATE	DEPARTMENT/SCHOOL CHAIR OR CHAIR'S DESIGNEE	DATE
	6/26/12		
THESIS COMMITTEE MEMBER	DATE	THESIS COMMITTEE MEMBER	DATE
	6/26/12		
THESIS COMMITTEE MEMBER	DATE	THESIS COMMITTEE MEMBER	DATE

Ruthenium Polypyridyl Complexes That Utilize Azo-dyes to Enhance Absorption of Visible Photons

Starting graduate school is a journey that has to end someday. In my journey at EIU I wish to thank Mrs. Maria Dust and Mrs. Mini Gupta from the stockroom for their effort to find the chemicals I need. I would like to extend my thanks to the faculty members for their help, cooperation and kindness during my stay at EIU. I am deeply thankful for my advisor Dr. Mark McGuire, he was there whenever I need his help. This journey couldn't be done without Dr. McGuire's guidance.

Abstract

Research in the field of dye sensitized solar cells has been growing rapidly. The challenge in this field is to prepare molecules that absorb in the visible region. An azo dye ligand based on 1,0-phenanthroline, "phen-azo-phenol", was prepared and found to absorb at 380 nm in MeOH. UV-Vis spectra of this ligand were recorded in different solvents and in the presence of added acid or base and it appeared that the spectra were shifted to longer wavelength (around 500 nm) in the presence of base and/or basic solvents. This was attributed to deprotonation of the phenol portion of the ligand.

Three Ru (II) polypyridyl complexes based on phen-azo-phenol were prepared and purified by size exclusion chromatography: $[(dcbpy)_2Ru^{II}(phen\text{-}azo\text{-}phenol)]^{2+}$, $[(mcbpy)_2Ru^{II}(phen\text{-}azo\text{-}phenol)]^{2+}$, and $[(dmbpy)_2Ru^{II}(phen\text{-}azo\text{-}phenol)]^{2+}$, where dcbpy = 4,4'-dicarboxy-2,2'-bipyridine, mcbpy = 4-methyl-4'-carboxy-2,2'-bipyridine, and dmbpy = 4,4'-dimethyl-2,2'-bipyridine. The complexes were characterized by UV-Vis and ^{1}H-NMR. Cyclic voltammetry scans were obtained for the three complexes in DMF and/or CH_3CN using 0.1 M TBAH as the electrolyte.

Table of Contents

Introduction 1

References: 14

Experimental section: 17

Methods 17

Syntheses 18

I.1 Synthesis of 5-nitro-1,10-phenanthroline (5-NO_2-phen): 18

Materials: 18

Procedure: 18

I.2 Preparation of 5-amino-1,10-phenanthroline (5-NH_2-phen): 19

I.3- Preparation of phen-azo-phenol: 19

I.4 Preparation of ruthenium complexes 22

I.4.1 Synthesis of cis-dichloro-bis(4'-carboxy-4-methyl-2,2'-bipyridine)Ru(II) 22

[cis-$Ru^{II}(mcbpy)_2Cl_2$] 22

I.4.2 Synthesis of bis(4'-carboxy-4-methyl-2,2'-bipyridine)(phen-azo-phenol) ruthenium(II)hexafluorophosphate ([$(mcbpy)_2Ru^{II}$(phen-azo-phenol)]$(PF_6)_2$) 23

I.4.3 Synthesis of bis(4,4'-dimethyl-2,2'-bipyridine)(phen-azo-phenol)ruthenium(II) hexafluorophosphate [$(dmbpy)_2Ru^{II}$(phen-azo-phenol)]$(PF_6)_2$ 25

I.4.4 Synthesis of 4,4'-dicarboxy-2,2'-bipyridine (dcbpy) 28

I.4.5 Synthesis of 4,4'-dimethoxycarbonyl-2,2'-bipyridine (dmcbpy) 29

I.4.6 Synthesis of cis-dichloro-bis(4,4'-dimethoxycarbonyl-2,2'-bipyridine)ruthenium(II) [cis-$Ru^{II}(dmcbbpy)_2Cl_2$] 30

I.4.7 Synthesis of bis[(4,4'-dimethoxycarbonyl-2,2'-bipyridine)(phen-azo-phenol)ruthenium(II)]hexafluorophosphate[$(dmcbpy)_2Ru^{II}$(phen-azo-phenol)]$(PF_6)_2$ 31

I.5 Synthetic attempts at phen-indigo dye 33

I.5.1 Synthesis of 5-Br-phenanthroline (5-Br-phen) 33

I.5.2 Synthetic attempt at 2-((1,10-phenanthrolin-5-yl)amino)acetic acid (N-acetyl-1,10-phen) 34
I.5.3 Synthetic attempt at the preparation of indolin-3-ol (indoxyl) 35
I.5.4 Synthesis of 2-phenylamino-3-phenylimino-3H-indole 36
II.5.5 Synthesis of indoline-2,3-dione (isatin) 37
II.5.6 Reduction of indoline-2,3-dione (isatin) to indolin-3-ol (indoxyl) 38
I.5.7 Synthetic attempt at N,N'-(5H-pyrrolo[2,3-f][1,10]phenanthroline-6,7-diylidene)bis(1,10-phenanthrolin-5-amine) (phen-isatin) 39
I.5.8- Another alternative attempt for the synthesis of indoline-2,3-dione (isatin) 40

Results and discussions 44

I. Syntheses 44
I.1 Synthesis of phen-azo-phenol 44
I.2 Synthesis of ruthenium polypyridyl complexes 44
I.3 Synthetic attempts at phen-indigo: 47
I.3.1 Synthetic attempt at 2-((1,10-phenanthrolin-5-yl)amino)acetic acid (N-acetyl-1,10-phen) 47
I.3.2 Synthetic attempt at the preparation of indolin-3-ol (indoxyl) 47
I.3.3 Synthetic attempt at N,N'-(5H-pyrrolo[2,3-f][1,10]phenanthroline-6,7-diylidene)bis(1,10-phenanthrolin-5-amine) (phen-isatin): 48

II. ^{1}H-NMR spectra 49
II.1 5-NO_2-phen 49
II.2 5-NH_2-phen 50
II.3 Phen-azo-phenol 51
II.4 4,4'-Dimethyl-2,2'-bipyridine (dmbpy) 52
II.5 4,4-Dicarboxy-2,2'-bipyridine (dcbpy) 53
II.6 4,4'-Dimethoxycarbonyl-2,2'-bipyridine (dmcbpy) 53
II.7 4'-Carboxy-4-methyl-2,2'-bipyridine (mcbbpy) 54
II.8 $[(dmbpy)_2Ru^{II}(phen\text{-}azo\text{-}phenol)]^{2+}$ 55
II.9 $[(dcbpy)_2Ru^{II}(phen\text{-}azo\text{-}phenol)](PF_6)_2$ 56
II.10 ^{1}H-NMR for $[(mcbpy)_2Ru^{II}(phen\text{-}azo\text{-}phenol)](PF_6)_2$ 57

II.11 ^{1}H-NMR for the reduction of isatin: 58

III. IR data 60

IV. X-ray crystallography of phen-azo-phenol 60

V. UV-Vis spectra 61

V.1 UV-Vis of phen-azo-phenol 61

V.2 UV-Vis spectra of ruthenium polypyridyl complexes 63

VI. Cyclic voltammetry for Ruthenium(II) polypyridyl complexes 66

VI.1 Cyclic voltammetry (CV) for phen-azo-phenol: 66

VI.2- Cyclic voltammetry of ruthenium(II) polypyridyl complexes 67

VII. Future work 72

References: 73

List of Figures

Figure 1a: ^{1}H-NMR spectrum of 5-NO_2-phen in d_6-DMSO..... 75
Figure 1b: ^{1}H-NMR spectrum for 5-NO_2-phen in d_6-DMSO..... 75
Figure 2a:^{1}H-NMR spectrum of 5-NH_2 -phen in d_6-DMSO..... 76
Figure 2b: 1H-NMR spectrum of 5-NH2 -phen in d6-DMSO expanded..... 76
Figure 3a: ^{1}H-NMR of phen-azo-phenol crude product in d_6-DMSO..... 77
Figure 3b: ^{1}H-NMR spectrum of phen-azo-phenol crude product in d_6-DMSO expanded. 77
Figure 3c:^{1}H-NMR spectrum for phen-azo-phenol in d_6-DMSO..... 78
Figure 3d:^{1}H-NMR spectrum for phen-azo-phenol in d_6-DMSO..... 78
Figure 3e: UV-Vis spectra of phen-azo-phenol 79
Figure 3f: UV-Vis spectra of phen-azo-phenol 80
Figure 3g: UV-Vis spectra of phen-azo-phenol in acetone and in acetone with added acid or base..... 80
Figure 3h: UV-Vis spectra of phen-azo-phenol in DMSO and in DMSO with added acid or base..... 81
Figure 3i: UV-Vis spectra of phen-azo-phenol in MeOH and in MeOH with added acid and base..... 81
Figure 3j: Crystal structure of phen-azo-phenol 82
Figure 3k: Crystal packing of phen-azo-phenol 83
Figure 4a: ^{1}H-NMR of 4-carboxy-4'-methyl-2,2'-bipyridine in d_6-DMSO..... 84
Figure 4b: ^{1}H-NMR of 4-carboxy-4'-methyl-2,2'-bipyridine in d_6-DMSO expanded. .. 85
Figure 4c: ^{1}H-NMM of 4-carboxy-4'-methyl-2,2'-bipyridine in d_6-DMSO expanded showing the methyl protons..... 85
Figure 4d: UV-Vis spectrum in MeOH for the reaction of $RuCl_3.3H_2O$ with 4-carboxy-4'-methyl-2,2'-bipyridine initially after mixing..... 86
Figure 4e: UV-Vis spectrum in MeOH for the reaction of $RuCl_3.3H_2O$ with 4-carboxy-4'-methyl-2,2'-bipyridine after 1 h of the reaction..... 86
Figure 4f: UV-Vis spectrum in MeOH for the reaction of $RuCl_3.3H_2O$ with 4-carboxy-4'-methyl-2,2'-bipyridine after 3 h of the reaction..... 87
Figure 4g: UV-Vis of $Ru^{II}(mcbpy)_2Cl_2$ in MeOH..... 88

Figure 5a: UV-Vis for the reaction of $Ru^{II}(mcbpy)_2Cl_2$ with phen-azo-phenol after 30 min of reaction using MeOH as a solvent. 89
Figure 5b: UV-Vis for the reaction of $Ru^{II}(mcbpy)_2Cl_2$ with phen-azo-phenol after 1 h of reaction using MeOH as a solvent..... 89
Figure 5c: UV-Vis for the reaction of $Ru^{II}(mcbpy)_2Cl_2$ with phen-azo-phenol after 1.5 h of reaction using MeOH as a solvent. 90
Figure 5d: UV-Vis for the reaction of $Ru^{II}(mcbpy)_2Cl_2$ with phen-azo-phenol after 3.5 h of reaction using MeOH as a solvent. 90
Figure 5e: UV-Vis spectrum of $[(mcbpy)_2Ru^{II}(phen\text{-}azo\text{-}phenol)](PF_6)_2$ crude product in MeOH. 91
Figure 5f: The UV-Vis spectrum of the yellow band from purification of $[(mcbpy)_2Ru^{II}(phen\text{-}azo\text{-}phenol)](PF_6)_2$ in CH_3OH:CH_3COOH (90:10)..... 91
Figure 5g: UV-Vis spectrum of the orange band from the purification of 92
$[(mcbpy)_2Ru^{II}(phen\text{-}azo\text{-}phenol)](PF_6)_2$ in MeOH:CH_3COOH (90:10)..... 92
Figure 5h: UV-Vis spectra from size exclusion chromatography. 93
Figure 5i: UV-Vis of $[(mcbpy)_2Ru^{II}(phen\text{-}azo\text{-}phenol)](PF_6)_2$ (3^{rd} fraction in MeOH. .. 94
Figure 5j: UV-Vis of $[(mcbpy)_2Ru^{II}(phen\text{-}azo\text{-}phenol)](PF_6)_2$ (4^{th} fraction in MeOH. .. 95
Figure 5k: ^{1}H-NMR for the last three fractions (3^{rd}, 4^{th}, and 5^{th}) of $[(mcbpy)_2Ru^{II}(phen\text{-}azo\text{-}phenol)](PF_6)_2$ in d_6-DMSO. 96
Figure 5l: ^{1}H-NMR for the last three fractions (3^{rd}, 4^{th}, and 5^{th}) of $[(mcbpy)_2Ru^{II}(phen\text{-}azo\text{-}phenol)](PF_6)_2$ in d_6DMSO expanded. 97
Figure 5m: ^{1}H-NMR for $[(mcbpy)_2Ru^{II}(phen\text{-}azo\text{-}phenol)](PF_6)_2$ 3^{rd} fraction in d_6-DMSO. 98
Figure 5n: ^{1}H-NMR for $[(mcbpy)_2Ru^{II}(phen\text{-}azo\text{-}phenol)](PF_6)_2$ 4^{th} fraction in DMSO. 99
Figure 5o: ^{1}H-NMR for $[(mcbpy)_2Ru^{II}(phen\text{-}azo\text{-}phenol)](PF_6)_2$ in d_6-DMSO for the 4^{th} fraction showing the rest of the spectrum. 99
Figure 5p: ^{1}H-NMR for $[(mcbpy)_2Ru^{II}(phen\text{-}azo\text{-}phenol)](PF_6)_2$ 5^{th} fraction in d_6-DMSO. 100
Figure 5q: ^{1}H-NMR for $[(mcbpy)_2Ru^{II}(phen\text{-}azo\text{-}phenol)](PF_6)_2$ 5^{th} fraction expanded in d_6-DMSO 100

Figure 6a: UV-Vis spectrum for the reaction of $Ru^{II}(dmbpy)_2Cl_2$ with phen-azo-phenol using 95% EtOH as a solvent after 1 h of reflux. 101
Figure 6b: UV-Vis spectrum for the reaction of $Ru^{II}(dmbpy)_2Cl_2$ with phen-azo-phenol using 95% EtOH as a solvent after 3 h of reflux. 102
Figure 6c: UV-Vis spectrum for the reaction of $Ru^{II}(dmbpy)_2Cl_2$ with phen-azo-phenol using 95% EtOH as a solvent after 5 h of reflux. 102
Figure 6d: UV-Vis spectrum for the reaction of $Ru^{II}(dmbpy)_2Cl_2$ with phen-azo-phenol using 95% EtOH as a solvent after 21 h of reflux 103
Figure 6f: UV-Vis spectrum of $[(dmbpy)_2Ru^{II}(phen\text{-}azo\text{-}phenol)](PF_6)_2$ in CH_3CN. ... 103
Figure 6g: UV-Vis spectrum of $[(dmbpy)_2Ru^{II}(phen\text{-}azo\text{-}phenol)](PF_6)_2$ for the red fraction from alumina column. 104
Figure 6h: UV-Vis spectra for the two fractions from size exclusion chromatography using 80:20 $MeOH/H_2O$ as a solvent. 104
Figure 6i: UV-Vis spectrum of $[(dmbpy)_2Ru^{II}(phen\text{-}azo\text{-}phenol)](PF_6)_2$ in MeOH..... 105
Figure 6j: ^{1}H-NMR for $[(dmbpy)_2Ru^{II}(phen\text{-}azo\text{-}phenol)](PF_6)_2$ in d_6-DMSO..... 106
Figure 6k: ^{1}H-NMR for $[(dmbpy)_2Ru^{II}(phen\text{-}azo\text{-}phenol)](PF_6)_2$ in d_6-DMSO expanded. 107
Figure 6l: ^{1}H-NMR for $[(dmbpy)_2Ru^{II}(phen\text{-}azo\text{-}phenol)](PF_6)_2$ in d_6-DMSO expanded. 107
Figure 6m: ^{1}H-NMR for $[(dmbpy)_2Ru^{II}(phen\text{-}azo\text{-}phenol)](PF_6)_2$ in d_6-DMSO expanded showing the methyl protons. 108
Figure 6n: ^{1}H-NMR of an authentic sample of 4,4'-dimethyl-2,2'-bipyridine in $CDCl_3$. 109
Figure 6o: IR spectrum for 4,4'-dicarboxy-2,2'-bipyridine 110
Figure 6p: ^{1}H-NMR (MEM2A413) for 4,4'-dicarboxy-2,2'-bipyridine in D_2O/NaOD. 111
Figure 7a: IR spectrum of 4,4'-dimethoxycarbonyl-2,2'-bipyridine (expanded). 112
Figure 7b: ^{1}H-NMR of 4,4'-dimethoxycarbonyl-2,2'-bipyridine in $CDCl_3$. 113
Figure 7c: ^{1}H-NMR of 4,4'-dimethoxycarbonyl-2,2'-bipyridine in $CDCl_3$ expanded.. 114
Figure 7d: ^{1}H-NMR of 4,4'-dimethoxycarbonyl-2,2'-bipyridine in $CDCl_3$ expanded in the aromatic region. 114

Figure 8a: UV-Vis spectrum for the reaction of $RuCl_3.3H_2O$ with (4,4'-dimethoxy-2,2'-bipyridine) in abs. EtOH initially after mixing. 115
Figure 8b: UV-Vis spectrum for the reaction of $RuCl_3.3H_2O$ with (4,4'-dimethoxy-2,2'-bipyridine) in abs. EtOH after 2 h. 115
Figure 8c: IR spectrum of $Ru^{II}(dmcbpy)_2Cl_2$ 116
Figure 9a: UV-Vis spectra for the reaction monitoring of $Ru^{II}(dmcbpy)_2Cl_2$ with phen-azo-phenol using MeOH as a solvent. 117
Figure 9b: UV-Vis spectra for the reaction monitoring of $Ru^{II}(dmcbpy)_2Cl_2$ with phen-azo-phenol in MeOH expanded. The arrows indicate the shift in wavelength as the reaction proceeds. 118
Figure 9c: IR spectrum of $[(dmcbpy)_2Ru^{II}(phen\text{-}azo\text{-}phenol)](PF_6)_2$ 119
Figure 9d: UV-Vis spectra for the two bands collected from size exclusion chromatography in 1:1 MeOH:H_2O. 120
Figure 9e: UV-Vis spectrum of $[(dcbpy)_2Ru^{II}(phen\text{-}azo\text{-}phenol)](PF_6)_2$ in MeOH. 121
Figure 9f: ^{1}H-NMR of $[(dcbpy)_2Ru^{II}(phen\text{-}azo\text{-}phenol)](PF_6)_2$ in d_6-DMSO. 122
Figure 9g: ^{1}H-NMR of $[(dcbpy)_2Ru^{II}(phen\text{-}azo\text{-}phenol)](PF_6)_2$ in d_6-DMSO expanded. 123
Figure 9h: UV-Vis spectra of $[(mcbpy)_2Ru^{II}(phen\text{-}azo\text{-}phenol)](PF_6)_2$ 124
Figure 9i: UV-Vis spectra of $[(dmbpy)_2Ru^{II}(phen\text{-}azo\text{-}phenol)](PF_6)_2$ 125
Figure 9j: UV-Vis spectra of $[(dcbpy)_2Ru^{II}(phen\text{-}azo\text{-}phenol)](PF_6)_2$ 126
Figure 9k: UV-Vis spectrum of $[Ru^{II}(bpy)_3]Cl_2$ in abs. MeOH. 127
Figure 10a: ^{1}H-NMR for 5-Br-phen in $CDCl_3$. 128
Figure 10b: ^{1}H-NMR for 5-Br-phen in $CDCl_3$ expanded. 128
Figure 10c: IR of 4'-carboxy-4-methyl-2,2'-bipyridine 129
Figure 10d: IR of 4'-carboxy-4-methyl-2,2'-bipyridine at high resolution. 130
Figure 11a: ^{1}H-NMR for the synthetic attempt of 2-((1,10-phenanthrolin-5-yl)amino)acetic acid in d_6-DMSO. 131
Figure 12a: ^{1}H-NMR for the synthetic attempt of indoxyl in $CDCl_3$. 132
Figure 12b: ^{1}H-NMR for the synthetic attempt of indoxyl in $CDCl_3$ (expanded). 132
Figure 12c: ^{1}H-NMR for an authentic sample of triphenylphosphine oxide in $CDCl_3$. 133

Figure 12d: ^{1}H-NMR for an authentic sample of triphenylphosphine oxide in $CDCl_3$ expanded..... 133
Figure 12e: ^{1}H-NMR for the indoxyl attempt upper graph and an authentic sample of triphenylphosphine oxide lower graph in $CDCl_3$. 134
Figure 13a: ^{1}H NMR spectrum of 2-phenylamino-3-phenylimino-3H-indole in $CDCl_3$. 135
Figure 13b: ^{1}H-NMR spectrum for 2-phenylamino-3-phenylimino-3H-indole in $CDCl_3$ (expanded). 136
Figure 14a:^{1}H- NMR spectrum of isatin in acetone-d_6..... 137
Figure 14b:^{1}H-NMR spectrum for isatin in acetone-d_6 (expanded). 137
Figure 14a: ^{1}H-NMR spectrum for the product of isatine reduction in d_6-DMSO..... 138
Figure 14b:^{1}H-NMR spectrum for the product of isatin reduction in d_6-DMSO showing pyridine peaks in the spectrum as the major impurity..... 138
Figure 14c: ^{1}H-NMR spectra for the product of isatin reduction upper spectrum (green color) and an authentic sample of indigo dye lower spectrum (blue color) in d_6-DMSO..... 139
Figure 14d: ^{1}H-NMR spectrum for the product of isatin reduction in d_6-DMSO showing the integration values of indigo dye peaks. 140
Figure 14e: ^{1}H-NMR spectrum for an authentic sample of indigo dye in d_6-DMSO.... 141
Figure 14f: ^{1}H-NMR spectrum for an authentic sample of indigo dye in d_6-DMSO expanded..... 141
Figure 14g: UV-Vis spectra of an authentic sample of indigo dye and the product of isatin reduction in DMSO..... 142
Figure 16a: ^{1}H- NMR spectrum for the synthetic attempt at phen-isatin in d_6-DMSO. 143
Figure 16b: ^{1}H- NMR spectrum for the synthetic attempt at phen-isatin in d_6-DMSO. The spectrum matched the starting material 5-NH_2-phen (Figure 2b). 144
Figure 17a: ^{1}H-NMR for the synthetic attempt of isatin in d_6-DMSO. 145
Figure 17b: ^{1}H-NMR for the synthetic attempt of isatin in d_6-DMSO (expanded)..... 145
Figure 17c: ^{1}H-NMR for the synthetic attempt of isatin in d_6-DMSO (expanded). 146
Figure 18: CV plots of: (1) Background , (2) phen-azo-phenol. They were recorded in DMF (0.1 M TBAH, sample concentrated 5×10^{-3} M). 147

Figure 19: CV of phen-azo-phenol lower graph using glassy carbon electrode and upper graph using a platinum electrode. Both CVs were recorded in DMF (0.1 M TBAH, sample concentrated 5×10^{-3} M). 148

Figure 20: CV plots of phen-azo-phenol upper graph vs the background lower graph. Both CVs were recorded in CH_3CN (0.1 M TBAH, sample concentrated 1×10^{-3} M). 149

Figure 21: CV of $[(bpy)_2Ru^{II}(phen)]^{2+}$ upper graph and the scan background recorded in DMF (0.1 M TBAH, sample concentrated 1×10^{-3} M). 150

Figure 22: CV of $[(bpy)2Ru^{II}(phen\text{-}azo\text{-}phenol)]^{2+}$ upper graph and the background scan recorded in CH_3CN (0.1 M TBAH, sample concentrated 1×10^{-3} M)..... 151

Figure 23: CV of $[(bpy)2Ru^{II}(phen\text{-}azo\text{-}phenol)]^{2+}$ showing the reductive part. It was recorded in CH_3CN (0.1 M TBAH, sample concentrated 1×10^{-3} M)..... 152

Figure 24: CV of $[(dcbpy)_2Ru^{II}(phen\text{-}azo\text{-}phenol)]^{2+}$ upper graph and the background scan recorded in DMF (0.1 M TBAH, sample concentrated 1×10^{-3} M, WE:GC, Aux; Pt, Ref: Ag wire, scan rate: 100 mV s^{-1})..... 153

Figure 25: CV for $[(mcbpy)_2Ru^{II}(phen\text{-}azo\text{-}phenol)]^{2+}$ upper graph and the background lower graph recorded in DMF (0.1 M TBAH, sample concentrated 1×10^{-3} M). 154

Figure 26: CV for $[(mcbpy)_2Ru^{II}(phen\text{-}azo\text{-}phenol)]^{2+}$ recorded in DMF (0.1 M TBAH, sample concentrated 1×10^{-3} M). 155

Figure 27: CV of $[(dmbpy)_2Ru^{II}(phen\text{-}azo\text{-}phenol)]^{2+}$ using Pt working electrode lower graph and using GC electrode upper graph recorded in CH_3CN (0.1 M TBAH, sample concentrated 1×10^{-3} M). 156

Figure 28: CV of $[(dmbpy)_2Ru^{II}(phen\text{-}azo\text{-}phenol)]^{2+}$ recorded in CH_3CN (0.1 M TBAH, sample concentrated 1×10^{-3} M). 157

Appendix 1: 158

List of Tables

Table 1: ^{1}H-NMR chemical shift for 5-NO_2-phen.....49

Table 2: ^{1}H-NMR chemical shift for 5-NH_2-phen.....50

Table 3: ^{1}H-NMR chemical shift for phen-azo-phenol.....51

Table 4: ^{1}H-NMR chemical shifts for 4,4'-dimethyl-2,2'-bipyridine.....53

Table 5: ^{1}H-NMR chemical shift for 4,4'-dicarboxy-2,2'-bipyridine 53

Table 6: ^{1}H-NMR chemical shift for 4,4'-dimethoxycarbonyl-2,2'-bipyridine.....54

Table 7: ^{1}H-NMR chemical shift for 4'-carboxy-4-methyl-2,2'-bipyridine.....55

Table 8: ^{1}H-NMR chemical shift for indigo dye 59

Table 9: Redox potential for phen-azo-phenol.....67

Table 10: Electrochemical data for $[(dcbpy)_2Ru^{II}(phen\text{-}azo\text{-}phenol)]^{2+}$, $[(mcbpy)_2Ru^{II}(phen\text{-}azo\text{-}phenol)]^{2+}$ and $[(bpy)_2Ru^{II}(phen)]^{2+}$ in DMF.....69

Table 11: Electrochemical data for $[(dmbpy)_2Ru^{II}(phen\text{-}azo\text{-}phol)]^{2+}$ and $[(bpy)_2Ru^{II}(phen)]^2$ 71

Introduction

World energy consumption will grow by 53% from 2008 to 2035 according to the US Energy Information Administration[1] (Figure I-1). Liquid fuels, coal, and natural gas will remain as the main energy supplies for our planet. Liquid fuels, mainly petroleum, are expected to grow from 85.7 million barrels per day in 2008 to 112.2 million barrels per day in 2035. Oil prices have increased from $82 per barrel in 2010 to more than $112 per barrel in 2011.[1] These energy sources are non-renewable and produce large emissions of CO_2. They are not sustainable or clean and someday they will run out, so a search for other energy sources is required. One of the alternatives is the use of sunlight to generate energy. This source of energy is clean and sustainable. The amount of energy received from sunlight is 4.3×10^{20} J/h.[2] The harvesting of solar radiation requires the design of molecules that absorb sunlight.[2]

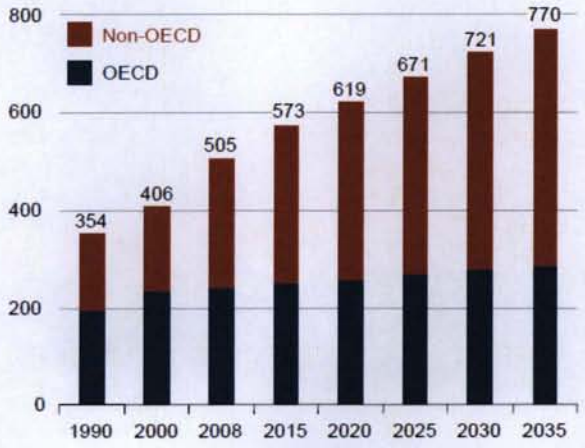

Figure I-1: World energy consumption from 1990-2035, numbers in quadrillion British Thermal Units (Btu). OECD: The Organization for Economic Cooperation and Development.[1]

Polypyridyl ruthenium(II) complexes have been investigated for possible use as light harvesting molecules.[3] They tend to exhibit high stability and synthetic flexibility. High temperatures are normally required to remove ligands or exchange them, and many are

stable even in concentrated H_2SO_4. Under suitable conditions ligands can be removed and substituted with others with retention of configuration. The substituents on polypyridyl ruthenium behave almost the same as if they were free; this helps in predicting their chemistry.[3]

The photophysical properties of polypyridyl complexes have been studied for the last 30 years.[4] Polypyridyl complexes of Ru(II) are d^6 with "local" octahedral geometry. The polypyridine ligands have σ-donor orbitals that are localized on the N-atoms and π-acceptor orbitals localized on the aromatic rings. A generalized molecular orbital (MO) diagram of a typical octahedral polypyridyl complex is shown in Figure I-2. The MO diagram shows the possible electronic transitions for polypyridyl complexes upon absorption of light. The electronic transition from a π_M to a π_L^* orbital is denoted as a metal-to-ligand charge transfer (MLCT) transition. Metal-centered (MC) or d-d transitions occur when an electron is promoted from a metal π-type orbital (π_M) to a σ-type (σ_M^*) orbital (many times labeled $t_{2g} \longrightarrow e_g$ transitions in octahedral symmetry). Ligand-centered (LC) or ligand-ligand transitions occur when an electron is excited from π_L to π_L^* orbitals on the ligands themselves.[4]

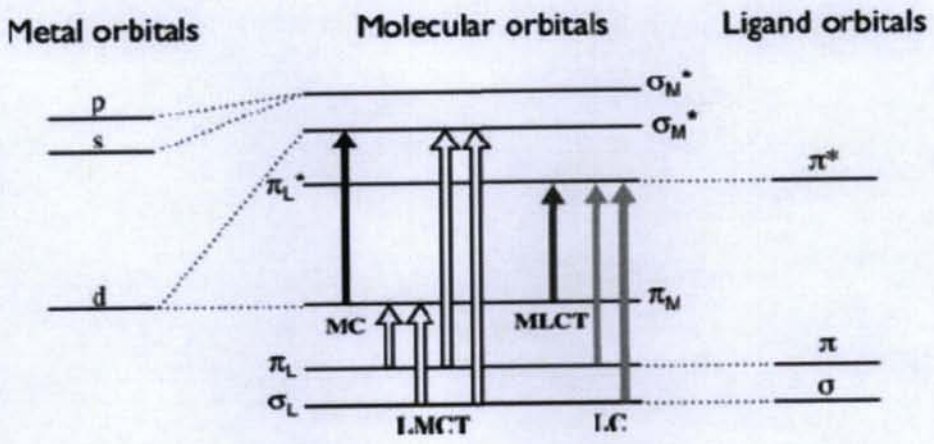

Figure I-2: Molecular orbital diagram for a typical octahedral polypyridyl complex labeled with the possible electronic transitions.[2]

In 1950, Michael Kasha proposed that the excited states of molecules undergo transitions to the first (or lowest) excited state regardless of the energy of the light absorbed (Kasha's rule).[5b] These transitions between upper excited states and the lowest excited state occur in less than one picosecond. This indicates that at room temperature electronic excitation of all molecules will be ultimately populate their lowest excited state (Figure I-3).[5a]

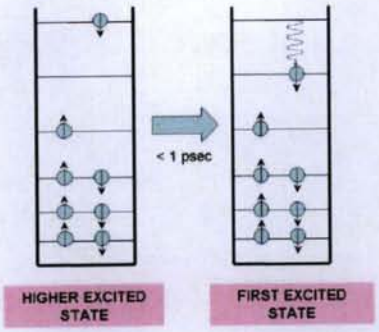

Figure I-3: Transitions between upper excited states back to the lowest excited state.[5a]

The photophysical properties of polypyridyl ruthenium(II) complexes depend on the population of the lowest excited state. There are actually three possible lowest excited states in polypyridyl ruthenium(II) complexes: MC, LC and MLCT. The MC excited state lifetime is short and does not produce luminescence emission. It can lead to ligand dissociation reactions or deactivation by radiationless relaxation to the ground state. MLCT and LC excited states do not undergo fast radiationless deactivation to the ground state compared to the MC excited state. Therefore, MLCT excited states have longer lifetimes and can give luminescence emission at room temperature (Figure I-4). [4]

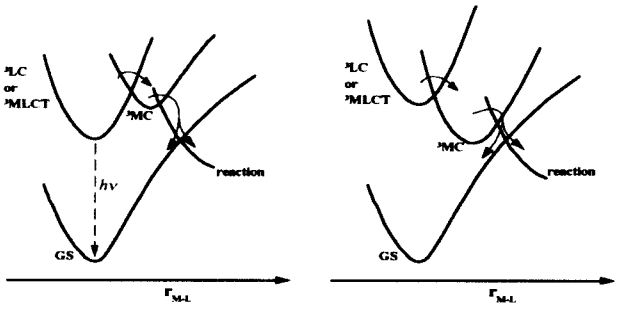

Figure I-4: Triplet excited states of LC, MC and MLCT and their relaxation to the ground state (GS).[4]

In polypyridyl ruthenium(II) complexes the MLCT state dominates and it is typically the lowest energy excited state. The electronic transitions giving rise to the MLCT state produce absorption maxima in the visible region. The transition involves promotion of an electron from a HOMO with metal character (π_M) to a LUMO with ligand π^* character (π_L^*). The compound $[Ru(bpy)_3]^{2+}$ (bpy = 2,2`-bipyridine) has been used as a model for studying electronic transitions of polypyridyl ruthenium(II) complexes. The UV-Vis spectrum of this compound is shown in Figure I-5 with the assigned electronic transitions.[4]

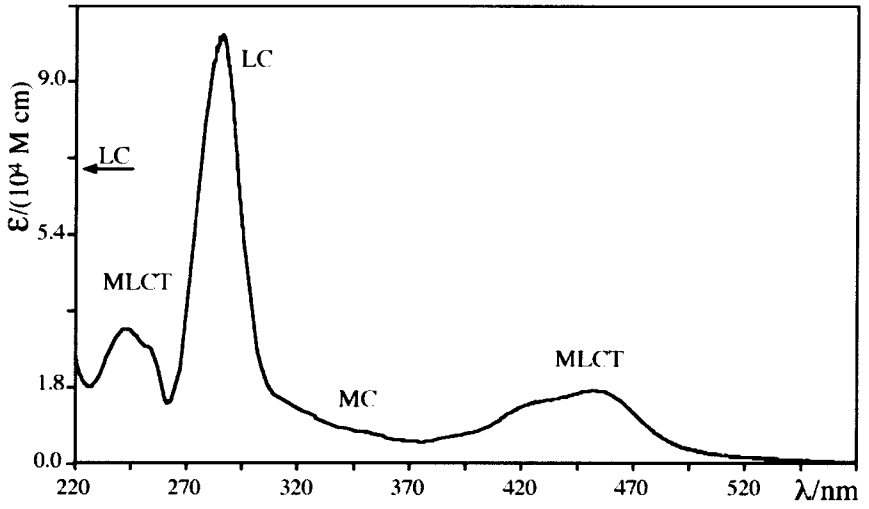

Figure I-5: UV-Vis spectrum of $[Ru(bpy)_3]^{2+}$ in ethanol.[4]

In the last 30 years ruthenium(II) polypyridyl complexes have been studied for their ability to harness the energy of visible light. The solar spectrum shows that a significant portion of solar radiation is received in the visible region of the spectrum (Figure I-6). The literature contains numerous examples of polypyridyl ruthenium(II) compounds that were synthesized and investigated for their enhanced ability to absorb light in the visible region (Figure I-7). Some of the polypyridyl used ligands were 4,4`-bis(carboxyethyl)-2,2`-bipyridine [$(EtCO_2)_2bpy$], 4,4`-dimethyl-2,2`-bipyridine (Me_2bpy), 4,4`,5,5`-tetramethyl-2,2`-bipyridine ($Me_4bpy$), 2,3-bis(2-pyridyl)-pyrazine (dpp), 6,7-dimethyl-2,3-bis(2-pyridyl)quinoxaline ($Me_2dpq$), 2,3-bis(2-pyridyl)-quinoxaline (dpq), 2,3-bis(2-pyridyl)-1,4-diazaanthracene (dpa), 2-(2`-pyridyl)pyrimidine (pypm), 2,2`-bipyrazine (bpz), 2,2`-bipyrimidine, and 2,2`-bipyridine (bpy).[6,7]

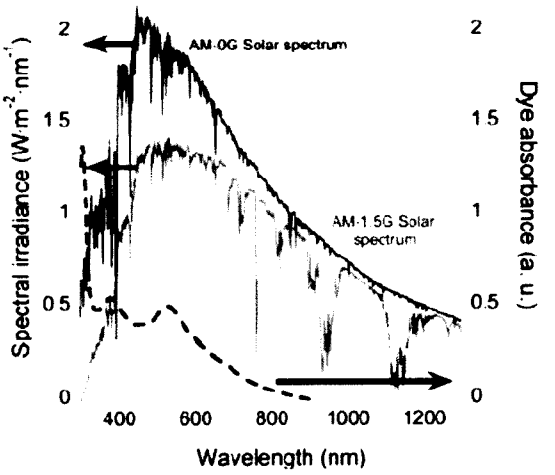

Figure I-6: Solar spectrum (AM-0G solid line, AM-1.5G grey line) and the absorption spectrum of cis-dithiocyanato-bis(4,4`-dicarboxy-2,2`-bipyridine)ruthenium(II) (dashed line).[2]

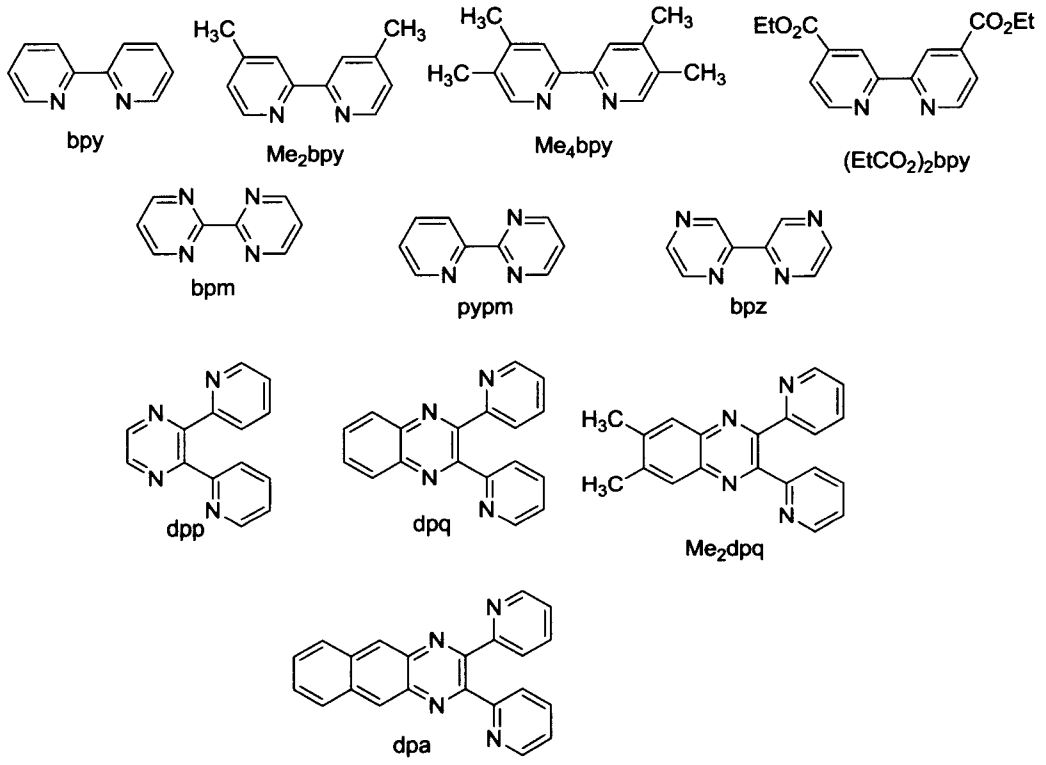

Figure I-7: Polypyridyl ligands.[6,7]

In 1992, Grätzel published a paper about the design of a dye-sensitized cell for the conversion of light to energy.[8] The cell was different from other semiconductor devices in that it separated the charge carrier transport and the light absorption molecules (Figure I-8). In this cell, current is generated when an electron is injected into the conduction band of a semiconductor (TiO_2) upon the absorption of a photon by the dye molecule. The cell was constructed by deposition of a thin film of TiO_2 on a conducting glass sheet (Indium Tin Oxide, ITO) followed by a deposition of a monolayer of a ruthenium(II) polypyridyl complex. Excitation of the dye (the Ru(II) complex) causes electrons to be injected into the conduction band of the TiO_2 and these electrons flowed to the counter electrode (Pt) through an external circuit. Electrons that arrived at the counter electrode were used to reduce I_3^- to I^- and the I^- was used to reduce Ru(III) back to Ru(II). This prototype cell showed stability at high temperature.[8,9]

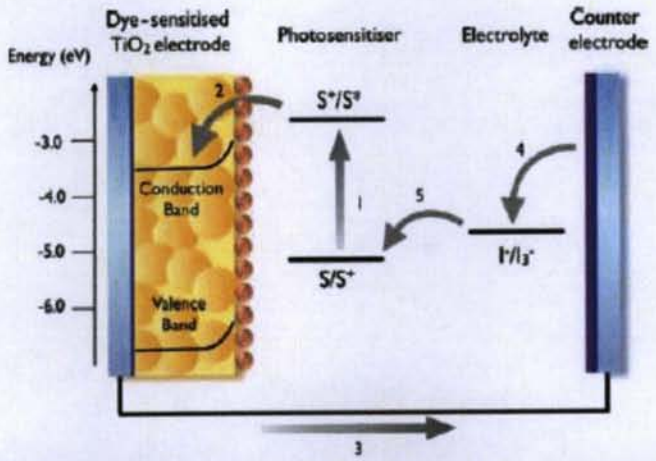

Figure I-8: Schematic representation of the Grätzel dye-sensitized solar cell. S = sensitizer (dye), S^* = excited sensitizer, S^+ = oxidized sensitizer, I^-/I_3^- = redox system.[2]

Scheme 1: Processes in the dye-sensitized cell.[2]

Photoexcitation: $S + h\nu \longrightarrow S^*$ (S^* = excited state Ru(II) polypyridyl complex)

Electron injection: $S^* + TiO_2 \longrightarrow S^+ + \bar{e}\text{-}TiO_2$ (S^+ = Ru(III) polypyridyl complex)

Electrolyte regeneration: $I_3^- + 2\bar{e} \longrightarrow 3I^-$

Reduced dye regeneration: $2S^+ + 3I^- \longrightarrow 2S + I_3^-$ (S = ground state Ru(II) polypyridyl complex)

Grätzel was able to synthesize a dye molecule that harvests/absorbs light in a greater portion of the visible spectrum than the $Ru^{II}(bpy)_3^{2+}$ prototype. The compound $(4,4`\text{-}(COOH)_2\text{-}2,2`\text{-bipyridine})_2Ru^{II}(NCS)_2$, or N_3 dye, was attached to TiO_2 and used in the Grätzel cell. The use of carboxylic acid groups were required since they were the anchoring groups that bind with TiO_2. In addition, electron withdrawing groups lower the π^*_L which caused a red shift of the light absorption (MLCT band) of the molecule.[9] Thiocyanate is an electron donor ligand that destabilizes the HOMO energy of Ru^{II} π_M resulting in a decrease of the energy gap between HOMO and LUMO. This decrease in energy gap also causes a shift of the absorption spectra to longer wavelengths.[2]

In general, polypyridyl ruthenium(II) complexes can be "tuned" to maximize their absorbance in the visible region. Three methods are: 1) Introduction of electron withdrawing groups on the polypyridyl ligands that lower the energy of the π^* LUMO orbital of the ligand; 2) Raising the energy level of the HOMO of the complex by using π-donor ligands; and 3) Introduction of a polypyridyl ligand that itself absorbs visible light (acting as "antenna").[2]

The photophysical and electrochemical properties of three ruthenium(II) complexes were investigated in this thesis. The ligand phen-azo-phenol (**1**) is an example of an "antenna" ligand that itself absorbs visible light. This absorption can be "tuned" because of the pH and solvent dependent phenol moiety on this azo dye derivative. In addition, the electron withdrawing and donating substituents on the bipyridine ligands can "tune"

the MLCT absorption. The goal was to synthesize and characterize a set of Ru(II) complexes showing enhanced absorption in the visible spectrum (compared to the prototype $Ru^{II}(bpy)_3^{2+}$ complex). Two of these complexes can theoretically be attached to TiO_2-coated ITO electrodes.

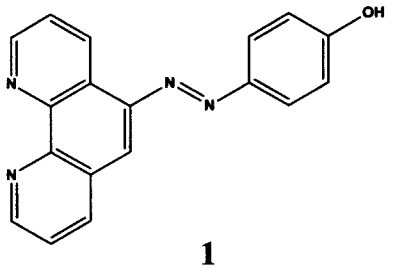

1

The three complexes were: bis(4,4`-dicarboxy-2,2`-bipyridine)Ru^{II}(phen-azo-phenol), $[(dcbpy)_2Ru^{II}(phen\text{-}azo\text{-}phenol)]^{2+}$; bis(4-methyl-4`-carboxy-2,2`-bipyridine)Ru^{II}(phen-azo-phenol), $[(mcbpy)_2Ru^{II}(phen\text{-}azo\text{-}phenol)]^{2+}$; and bis(4,4`-dimethyl-2,2`-bipyridine)Ru^{II}(phen-azo-phenol), $[(dmbpy)_2Ru^{II}(phen\text{-}azo\text{-}phenol)]^{2+}$ (Figure I-9).

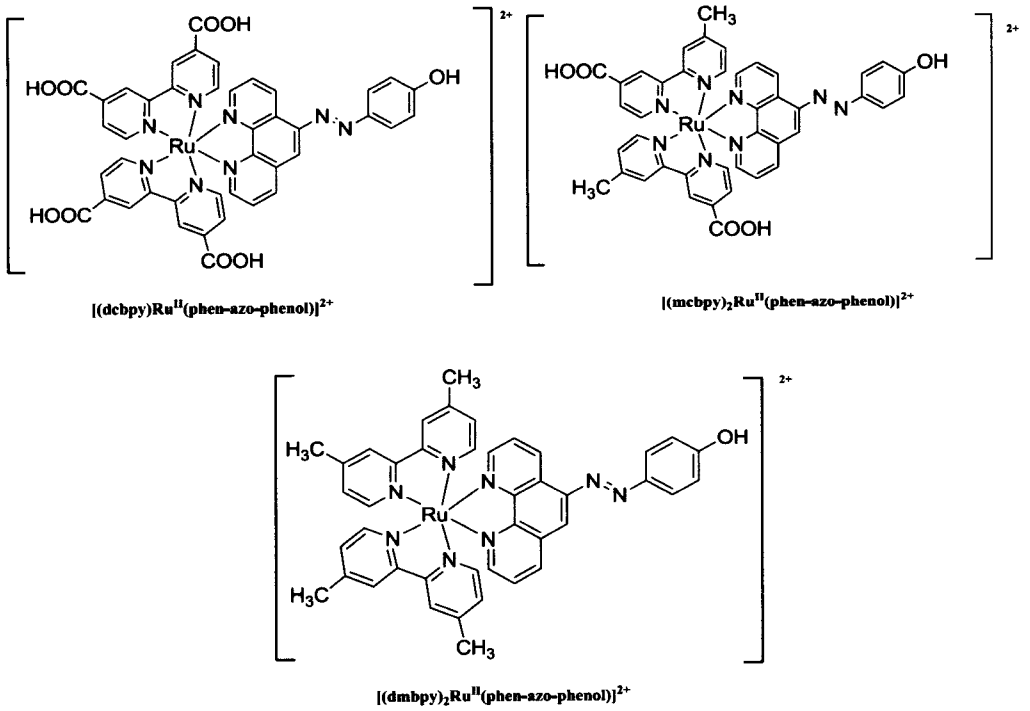

Figure I-9: Ruthenium(II) complexes.

It was reported previously by the McGuire research group[10] that the presence of carboxylic acid groups in conjunction with the presence of phen-azo-phenol may have an exaggerated effect on the absorption spectra of polypyridyl ruthenium(II) complexes at different pHs and in various solvents. To study this effect, the three Ru(II)-phen-azo-phenol complexes prepared have four (-COOH) groups, two (-COOH) groups and no (-COOH) groups, respectively.

Another approach to increasing the visible light absorption of Ru(II) complexes presented in this thesis was to synthesize another polypyridyl ligand that itself absorbs in the visible region. This ligand would be an indigo dye derivative of 1,10-phenanthroline. Indigo dye absorbs red light and appears blue. It has been used to dye textiles, (blue jeans).[11] The proposed ligand (phen-indigo, **2)** is expected to absorb light in the visible region (mostly red light) due to the fact that it is a combination of an indigo chromophore and two1,10-phenanthroline rings (Figure I-10). The ultimate goal is to use this ligand to produce the polypyridyl ruthenium(II) complex **(3)**.

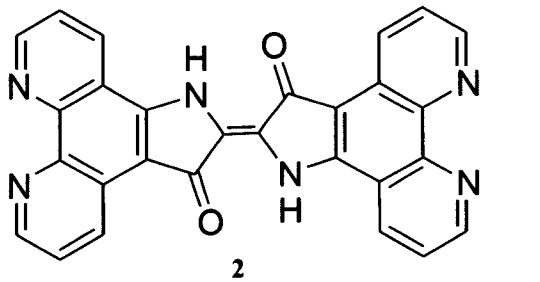

2

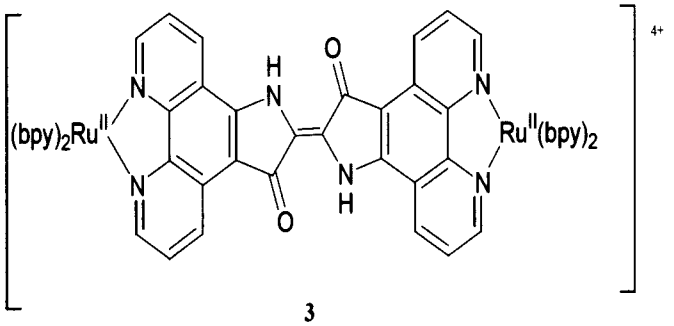

3

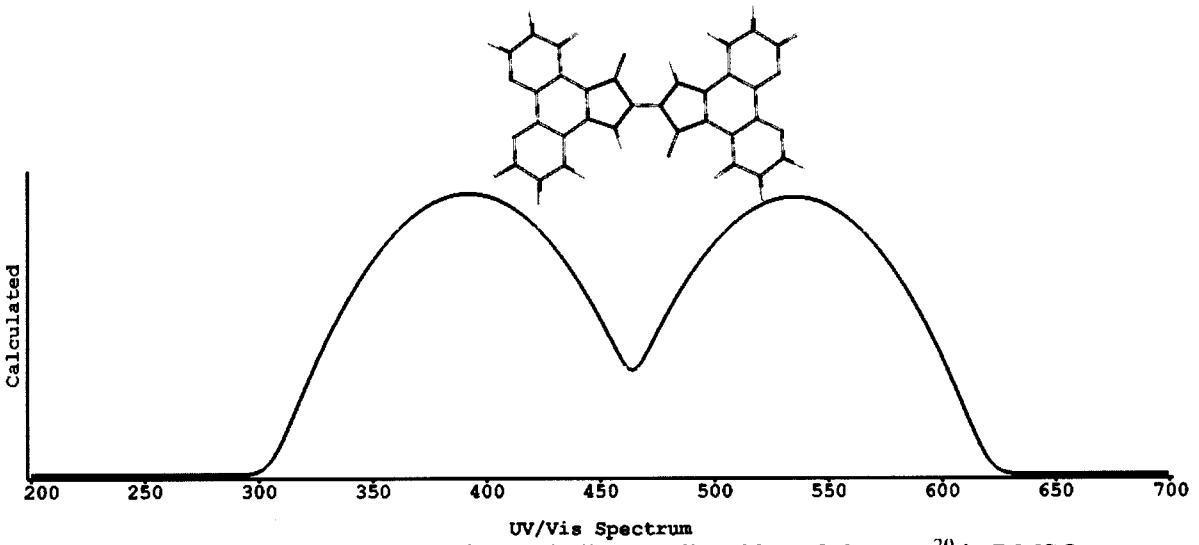

Figure I-10: UV-Visible spectrum of phen-indigo predicted by PC Spartan[20] in DMSO.

The redox properties of polypyridyl ruthenium(II) complexes depend on the ligands attached to the metal. Reduction of these complexes involves the addition of one electron to a LUMO orbital (π^*_L) of a ligand or to a metal centered orbital (σ^*_M) of the metal. If the ligands are easily reduced then the reduction process takes place on the ligands. However, if the ligands are hard to reduce/electron rich, then the metal could be reduced and electrons would be placed in the (σ^*_M).[2,12]

When the ligand is reduced; the electron is localized on a single ligand.

$[Ru^{II}(LL)_3]^{2+} + \bar{e} \xrightarrow{\text{Red}} [Ru^{II}(LL)_2(LL^-)]^{2+}$, LL = bidentate ligand.

The model complex $[Ru^{II}(bpy)_3]^{2+}$ shows six reduction waves (using cyclic voltammetry, CV) in DMF at -54 °C in the potential range -1.33 and -2.85 V (vs SCE). The reduction waves were assigned to the first and second reductions of each of the three bpy ligands .[12]

Oxidation of ruthenium(II) polypyridyl complexes takes place on the metal center orbital π_M (t_{2g}), producing a Ru(III) metal center.[6] In addition, ligands can be oxidized if

they have oxidizable groups. For example, phen-azo-phenol has a phenol ring that can be oxidized.

$$[Ru^{II}(L)_3]^{2+} \xrightarrow{Ox} [Ru^{III}(L)_3]^{3+} + \bar{e}$$

The oxidation of Ru^{II} to Ru^{III} is observed around +1.25 V (vs SCE)[11] in CH_3CN. Electron donating ligands can shift the oxidation to as low as +0.3 V (vs SCE)[11] since these ligands will stabilize Ru^{III} by donating electrons to the π_M orbital. On the other hand, electron withdrawing ligands (CN^-, SCN^-) and π-acceptor ligands increase the oxidation potential to as high as +1.9 V (vs SCE).[11] This shift in potential is due to the fact that the acceptor orbitals possess the correct symmetry to interact with the t_{2g} orbitals of the metal. The mixing of these orbitals with t_{2g} which results in lowering the energy of the t_{2g} energy levels.[13]

Bis-polypyridyl ruthenium(II) complexes (containing two bpy ligands and 2 Cl^- ligands) were synthesized from $RuCl_3.3H_2O$ by refluxing in dimethylformamide (DMF) and using the appropriate bipyridine ligands. The synthesis of these complexes was carried out under reduced light and N_2 to prevent isomerization to a complex with trans polypyridyl ligands. The attachment of phen-azo-phenol to the bis(polypyridyl) ruthenium(II) was achieved by refluxing in a mixture of water and methanol. The progress of these reactions was monitored using UV-Vis spectroscopy. Purification was carried out using alumina and size exclusion chromatography and the final products were characterized by ^{1}H-NMR.

The photophysical and electrochemical properties of the three Ru(II) complexes were studied using UV-Vis spectroscopy and cyclic voltammetry (CV), respectively. The effect of the changes in pH and solvent polarity on the UV-Vis absorption of the Ru(II)

complexes was measured and recorded. The reduction potential was measured in 0.1 M tetrabutylammonium hexafluorophosphate (TBAH) in DMF and acetonitrile (CH_3CN) using ferrocene (Fc^+/Fc) as an internal standard.

Several attempts were made to synthesize phen-indigo ligand. The first attempt was to attach glycine to 5-NH_2-phen followed by cyclization to form indoxyl.[14,15] The second attempt was to use oxalyl chloride and DMF to form phen-isatine which then would be reduced by $LiAlH_4$ to indoxyl.[16,17] The third was to use zeolite to do a one step synthesis of isatin from 5-NH_2-phen and oxalyl chloride.[18] The fourth method was to use chloral hydrate and 5-NH_2-phen to prepare an intermediate compound that goes to indoxyl upon the addition of sulfuric acid.[19] These attempts will be discussed further in the Results and Discussion section of this thesis.

References:

1. International Energy Outlook 2011. http://205.254.135.7/forecasts/ieo/pdf-/0484%282011%29.pdf (accessed 4/25/2012).
2. Palomares, E.; Reynal, A. Ruthenium Polypyridyl Sensitisers in Dye Solar Cells Based on Mesoporous TiO_2. *Eur. J. Inorg. Chem.* **2011**, 4509-4526.
3. Kelly, J.M.; Vos, J.G. Ruthenium Polypyridyl Chemistry; from Basic Research to Applications and Back Again. *Dalton Trans.* **2006**, 4869-4883.
4. Balzani, V.; Bergamini, G.; Campagna, S.; Nastasi, F.; Puntoriero, F. Photochemistry and Photophysics of Coordination Compounds: Ruthenium. *Top Curr. Chem.* **2007**, 117-214.
5. a) Topic 7: The Behavior of Photo-Excited Molecules:Biological Actions and Biotechnological Applications. http://www.centenary.edu/attachments-/biophysics/bphy304/07a.pdf (accessed 5/4/2012).
   b) Kasha, M. Characterization of Electronic Transitions in Complex Molecules. Disc. Faraday Soc. **1950**, *9*, 14-19.
6. Blanton, C.B.; Boldaji, M.; Bundy, S.; Jackman, D.C.; Meyer, T.J.; Rillema, D.P.; Shaver, R.J.; Worl, L.A. MLCT-dd Energy Gap in Pyridyl-Pyrimidine and Bis(pyridine) Complexes of Ruthenium(II). *Inorg. Chem.* **1992**, *31*, 1600-1606.
7. Anderson, P.A.; Keene, F.R.; Meyer, T.J.; Strouse, G.F.; Treadway, J.A. Black MLCT Absorbers. *Inorg. Chem.* **1994**, *33*, 3863-3864.
8. Grätzel, M.; O'Regan, B. A Low-Cost, High-efficiency Solar Cell Based on Dye-Sensitized Colloidal TiO_2 films. *Nature*, **1991**, *353*, 737-740.

9. Grätzel, M. Dye-sensitized Solar Cells. *J. of Photochem. And Photobiol. C: Photochem. Rev.* **2003**, *4*, 145-153.

10. Malinowski, L.; McGuire, M.E. Incorporation of a Ru(II) Complex Containing a Phenanthroline-Based Azo Dye into a Grätzel-Type Solar Cell. ACS National Meeting, New Orleans, LA, March 2003.

11. Schatz, F.P. Indigo and Tyrian Purple-In Nature and in the Lab. *J. Chem. Ed.* **2001**, *78*, 1442-1443.

12. Balzani, V.; Juris, A.; Venturi, M. Luminescent and Redox-Active Polynuclear Transition Metal Complexes. *Chem. Rev.* **1996**, *96*, 759-833.

13. Fielder, S.S.; Lever, A.B.P.; Osborne, M.C.; Pietro, W.J. First-Principles Interpretation of Ligand Electrochemical ($E_L(L)$) Parameters. Factorization of the σ and π Donor and π Acceptor Capabilities of Ligands. *J. Am. Chem. Soc.* **1995**, *117*, 6990-6993.

14. Kalluraya, B.; Lingappa, B.; Puranic, V.G.; Rai, N.S.; Shenoy, S. Convenient Access to 1,3,4-Trisubstituted Pyrazoles Carrying 5-Nitrothiophene Moiety via 1,3-Dipolar Cycloaddition of Sydnones with Aacetylenic Ketones and Their Antimicrobial Evaluation. *Eur. J. of Med. Chem.* **2008**, *43*, 1715-1720.

15. Hendrickson, J.B.; Hussoin, Md.S. Reactions of Carboxylic Acids with "Phosphonium Anhydrides". *J. Org. Chem.* **1989**, *54*, 1144-1149.

16. Hennig, A.; Hubber, S.M.; Pühlhofer, F.G.; Weiss, R. From DMF to Isatine: A Novel and General One-Pot Synthesis of Isatine and Its N-Unsubstituted Derivatives via Nucleophilic Substitution Reactions on 1,2-Bis(dimethylamino)-1,2-dichloroethene. *J. Heterocycl. Chem.*, **2009,** *46*, 421-427.

17. Khoshtariya, T.E.; Kurkovskaya, L.N.; Mirziashvili, N.T.; Sikharulidze, M.I.; Tsintsadze, T.G. Novel Route For Obtaining Isomeric Benzo[*b*]Thiophenoindoles. *Chem. of Heterocycl. Compd.* **2002**, *38,* 472-476.

18. Mahamadali Shaikh, T.; Raj, I.V.P.; Sudalai, A. H-β Zeolite: an Efficient, Reusable Catalyst for One-Pot Synthesis of Isatins from Anilines. *Acta Chim. Slov.* **2010,** *57,* 466–469.

19. Blackburn, A.G.; Denny, W.A.; Rewcastle, G.W.; Sutherland, H.S.; Weir, C.A. An Improved Synthesis of Isonitrosoacetanilides. *Tetrahedron Lett.* **2005**, *46*, 8719–872.

20. PC Spartan 10 ^{TM}, v: 1.1.0, **2011**.

Experimental section

Methods

^{1}H-NMR spectra were recorded on a Bruker Avance FT-NMR spectrometer (400 MHz). X-ray data was collected on a Bruker APEXII CCD diffractometer. UV-Vis spectra were recorded using a Shimadzu UV-3100 UV-Vis-NIR recording spectrometer or an Ocean Optics UV-enabled UV-Vis spectrometer (SN: USP2E1423). IR data was obtained using a Thermoscientific Avatar 360 FT-IR.

Cyclic voltammetry (CV) was carried out using a Princeton Applied Research (PAR) Model 263A Potentiostat/Galvanostat. The instrument was controlled and data collected by a PC using PowerSuite CV™ software. Data were saved in .txt format and later plotted using Origin 8™. The CVs were typically obtained in a single cup using ~ 2 mL of solvent/electrolyte. The solvents used were DMF (Sigma-Aldrich, 99.9%, Lot # 01540AB, dried over 3Å Molecular Sieves ™) or CH_3CN (EIU Chemistry Stockroom, dried over 3Å Molecular Sieves ™). The electrolyte was tetrabutylammoinum hexafluorophosphate (TBAH, Aldrich, 98%, Lot # 281026) that had been previously recrystallized and dried in a vacuum oven. The electrolyte concentration was 0.10 M for all runs; the concentration of analyte was often targeted at ~1×10^{-3} M, but in some cases the exact concentration was not determined. Ferrocene was used as an internal standard. Solutions were purged with N_2 for 30 min before starting measurements. The measurements were obtained using three electrodes: the working electrode was either glassy carbon (GC, disk diameter 3 mm) or platinum (Pt, disk diameter 1.6 mm), the auxiliary electrode was a Pt wire and the reference electrode was a silver (Ag) wire or (NaCl) saturated calomel electrode (SSCE). The working electrodes were polished with

alumina, rinsed with water, and gently sonicated before use. In all experiments the potential scan rate was 100 mVs^{-1}.

Syntheses

I.1 Synthesis of 5-nitro-1,10-phenanthroline (5-NO_2-phen):

Materials:

1,10-Phenanthroline (1,10-phen, Aldrich, 99+%, Lot# 07601JZ), H_2SO_4 (Fisher, A.C.S. reagent-min 95%, Lot# 903025), d_6-DMSO (Cambridge Isotope Laboratories, D 99.9%, Lot # DLM-10). HNO_3 (16 *M*) and $NaHCO_3$ were obtained from the EIU Chemistry Stockroom.

Procedure:

This ligand was prepared as described in the literature.[1] 1,10-Phen (2.0063 g, 11.133 mmol) was transferred to a 3-neck flask. Concentrated H_2SO_4 (25 mL) was added and the mixture was stirred; all the phenanthroline dissolved. The solution was heated to 160°C. Concentrated HNO_3 (13 mL) was then added dropwise using a separatory funnel while the mixture was maintained at 160°C. The temperature of the solution dropped by approximately 2°C after each addition of HNO_3. Brown fumes also formed during and after the addition of HNO_3. The mixture was then heated for 3 h at 115°C, cooled to room temperature, and poured into a beaker containing cold water (300 mL) immersed in an ice bath, resulting in a yellow solution. The pH was adjusted to 4-5 with solid $NaHCO_3$. The precipitate that formed was collected using a course porosity glass frit funnel (60 mL). The solid was washed with cold water and dried under vacuum for 2 h. A light yellow solid resulted (111511-A-AH, 1.6940 g, 67.56 % yield based on 1,10-phen).

The filtrate was extracted with CH_2Cl_2 (3 ×100 mL) and the combined extracts were dried over anhydrous Na_2SO_4. The CH_2Cl_2 was then removed under vacuum. A yellow

solid formed (111511-B-AH, 0.3803 g, 15.17 % yield based on 1,10-phen).[1]H-NMR for sample 111511-A-AH (MEM2A373, Figures 1a-b) (400 MHz, d_6-DMSO) δ (ppm) = 7.95 (m, 2H), 8.78 (dd,J= 1.7, 8.2 Hz, 1H), 8.89 (dd, J= 1.59, 8.59 Hz, 1H), 9.05 (s, 1H), 9.24 (dd, J= 1.60, 4.26 Hz, 1H), 9.28 (dd, J= 1.80, 4.34 Hz, 1H).

I.2 Preparation of 5-amino-1,10-phenanthroline (5-NH_2-phen):

Materials:

5-NO_2-phen (111511-A-AH), hydrazine monohydrate (N_2H_4. H_2O, Sigma-Aldrich, 64-65% reagent grade, Lot # 207942), 10% Pd/C (Aldrich, Lot # 06829LF). d_6-DMSO (Cambridge Isotope Laboratories, D 99.9%, Lot # DLM-10). Abs. EtOH was obtained from the EIU Chemistry Stockroom.

Procedure:

This ligand was prepared according to a literature method.[2] 5-NO_2-phen (1.0174 g, 4.5178 mmol) was transferred to a 3-neck flask (100 mL), abs. EtOH (250 mL) and 10% Pd/C (0.6005 g) were added under N_2, and the mixture was stirred. N_2H_4. H_2O (2.00 mL, 0.0412 mol), previously diluted in abs. EtOH (30 mL), was added dropwise at room temperature. The resulting mixture was refluxed for 3 h under N_2, cooled to room temperature, and gravity filtered using Whatman #2 filter paper (24.0 cm). The filtrate had a greenish color, and it was left in the hood to let the solvent evaporate, resulting in a brownish solid (111611-A-AH). Yield: 0.7206 g (81.6% based on 5-NO_2-phen). [1]H-NMR (MEM2A374, Figures 2a-b) (400 MHz, d_6-DMSO) δ (ppm) = 9.05 (dd, J= 1.6, 4.2 Hz, 1H), 8.68 (d, 1H), 8.67 (dd, J= 1.6, 4.3 Hz, 1H), 8.04 (dd, J= 1.6, 8.2 Hz, 1H), 7.74 (m, 1H), 7.51 (m, 1H), 6.86 (s, 1H), 6.15 (s, 2H).

I.3- Preparation of phen-azo-phenol:

Materials:

Phenol (Aldrich, 99+%, A.C.S. Reagent, Lot # 08811PQ), $NaNO_2$ (Fisher, A.C.S. certified, Lot # 734954), NaOH pellets (Fischer, Lot # AD-10313-11), d_6-DMSO (Aldrich, 99.9 atom % D,0.03 % TMS, Lot # 296147), 5-NH_2-phen (050211-A-AH), Al_2O_3 (Fisher, 80-200 mesh, Lot # 000496), 6 M HCl, abs. EtOH, MeOH, DMSO, acetone, 2 M HCl, dioxane, CH_3CN, $CHCl_3$, pyridine, DMF, THF, concentrated HCl and CH_2Cl_2 were obtained from the EIU Chemistry Stockroom.

Procedure:

This ligand was prepared by modifying a method described in a previous thesis.[3] 5-NH_2-phen (0.1962 g, 1.006 mmol) was dissolved in 6 M HCl (4 mL) resulting in a red color; no precipitate was observed. The solution was immersed in an ice bath and stirred for 2 min. $NaNO_2$ (0.0713 g, 1.03 mmol) was dissolved in water (2 mL) and immersed in an ice bath. Then, the $NaNO_2$ solution was added all at once to the 5-NH_2-phen solution and the resulting mixture was stirred for 3 min. Foam formed at the surface, the color remained red, and no precipitate formed. Phenol (0.0950 g, 1.01 mmol) was dissolved in 10% (w/w) aqueous NaOH (10 mL) and this solution was stirred for 2 min in an ice bath. It was then added to the red 5-NH_2-phen solution all at once resulting in a precipitate. The pH of the mixture was measured using pH paper and it was found to be greater than 10. After this the mixture was stirred for 4 h in an ice bath (0-10 °C). After removing the mixture from the ice bath the pH was adjusted to 6 with 2 M HCl. The color of the mixture darkened as the pH decreased to 6. After this mixture was left stirring at room temperature for 30-45 min, it was filtered on a fine porosity glass frit funnel (15 mL). The resulting solid was washed with cold water and then dried under vacuum for 3 h. A

brown solid was collected (053011-A-AH, 0.2018 g, 66.82 % yield based on 5-NH_2-phen).^{1}H NMR (MEM2A243, Figures 3a-b) (400 MHz, d_6-DMSO).

The crude phen-azo-phenol was purified on a 20 × 1 cm column of alumina. The alumina was loaded as a slurry using CH_2Cl_2: abs. EtOH (50:50). Phen-azo-phenol (50.1 mg) was dissolved in EtOH:MeOH:CH_2Cl_2 (25:25:50) and filtered using a fine porosity glass frit funnel (15 mL). The filtrate was loaded onto the column. Two bands appeared from top to bottom: orange and pink. The pink band was eluted with EtOH:MeOH:CH_2Cl_2 (25:25:50) and the orange band with MeOH. The orange band was kept in the hood to let the solvent evaporate. The solid remaining was dried under vacuum for 5 h. The dried solid was orange (053111-A-AH, 32 mg, 64% yield based on 5-NH_2-phen). ^{1}H-NMR (MEM2A246, Figures 3c-d) (400 MHz, d_6-DMSO) δ (ppm) = 9.33 (dd, J = 1.77, 8.31 Hz, 1H), 9.14 (m, 1H), 8.96 (broad, 1H), 8.52 (d, 1H), 7.93 (s, 1H), 7.84 (m, 1H), 7.77 (broad, 2H), 7.69 (m, 1H), 6.30 (broad, 2H). UV-Vis spectra of this ligand were recorded in different solvents and in the presence of added acid and base by dissolving 3.2 mg of the ligand in MeOH (10 mL) resulting in a 1 mM solution. Then, 200 μL of this solution was diluted to 3 mL using different solvents; this resulted in five UV-Vis spectra with phen-azo-phenol at the same concentration in five different solvents: dioxane, CH_3CN, $CHCl_3$, MeOH, and pyridine, acetone, DMF, and DMSO (Figures 3e-f). The effects of added acid (1 drop 2 M HCl) or added base (1 drop 10% NaOH) in acetone, DMSO, and MeOH were recorded in Figures 3g-i.

Single crystals were grown from THF-concentrated HCl (1 mL-1 drop) by slow evaporation (Figures 3j-k). Crystal data: unit cell-triclinic; V =802.73(7) Å^3. Unit cell

parameters: a=7.6732(4), b=7.7894(4) and c= 14.1225(7) Å, α=78.535(3)°, β=80.379(3)° and γ= 78.212(3)° (See Appendix 1 for refinement and solution information.)

I.4 Preparation of ruthenium complexes

I.4.1 Synthesis of cis-dichloro-bis(4'-carboxy-4-methyl-2,2'-bipyridine)Ru(II) [cis-$Ru^{II}(mcbpy)_2Cl_2$]

Materials:

$RuCl_3 \cdot 3H_2O$ (Alfa, $RuCl_3$ 43.04 %, 3.8% H_2O, Lot # 100980), 4'-carboxy-4-methyl-2,2'-bipyridine (mcbpy, 070306A-SC, ^{1}H-NMR (MEM404, d_6-DMSO, Figures 4a-c)), DMF (LabGuard, Lot# 4929KLDL), d_6-DMSO (Cambridge Isotope Laboratories, D 99.9%, Lot # DLM-10-100). Abs. EtOH was obtained from the EIU Chemistry Stockroom.

Procedure:

This complex was prepared as described in the literature.[4] The synthesis was carried out under N_2 and reduced light. $RuCl_3 \cdot 3H2O$ (0.2113 g, 0.8656 mmol-based on 43.04% Ru and 3.8% H_2O) was transferred to a 100-mL 3-neck flask. DMF (50 mL) was added and the mixture was stirred for 15 min. 4-Carboxy-4'-methyl-2,2'-bipyridine (mcbpy, 0.4258 g, 1.988 mmol) was added and stirring was resumed resulting in a black mixture. The solution was refluxed and the progress of the reaction was monitored by UV-Vis using abs. EtOH as the solvent. The UV-Vis spectrum shortly after heating began showed four maxima at 300, 385, 500 and 560 nm (Figure 4d). After 1h of refluxing the peak maxima were 300, 390 and 560 nm with intensities of 3.3, 1.05 and 1.0 respectively (Figure 4e). The refluxing continued for additional 2 h and a new peak maximum appeared at 450 nm (Figure 4f). After a total of 3h, the heat was removed and the mixture was stirred for an additional 1 h. It was then filtered using a medium porosity

glass frit funnel (30 mL). The solid was collected on the filter, and the filtrate (which had a pink color) was rotavapped to dryness. The solid obtained from the filtrate was stirred in 2 M HCl (50 mL) and the solid from the filter was stirred in 20 mL of 2 M HCl, both for 4 h under reduced light. Then, solid from both solutions was collected on a fine porosity glass frit funnel (15 mL). It was dried under vacuum for 2 h resulting in a black solid (120511-B-AH, 92.6 mg, 17.8 % yield based on Ru starting material). UV-Vis spectrum in CH_3OH (Figure 4g).

I.4.2 Synthesis of bis(4'-carboxy-4-methyl-2,2'-bipyridine)(phen-azo-phenol) ruthenium(II)hexafluorophosphate ($[(mcbpy)_2Ru^{II}(phen\text{-}azo\text{-}phenol)](PF_6)_2$)

Materials:

Phen-azo-phenol (113011-B-AH), cis-$[Ru^{II}(mcbpy)_2Cl_2]$ (120511-B-AH), triflic acid (Aldrich, 98%, Lot: 15709AB), alumina (Fisher, 80-200 mesh, Lot# 000496), HPF_6 (Aldrich, 60 wt. % solution in water, Lot# 200956), Sephadex LH-20 (Sigma, 25-100 μ, Lot# 19F-0572). Glacial acetic acid, MeOH, KOH and diethyl ether were obtained from the EIU Chemistry Stockroom.

Procedure:

The preparation was carried out under N_2 and reduced light. Cis-$[Ru^{II}(mcbpy)_2Cl_2]$ (80.5 mg, 0.134 mmol) and KOH (14.8 mg, 0.264 mmol) were transferred to a 50-mL 3-neck flask. MeOH (28 mL) and H_2O (12 mL) were added to the flask and the mixture was stirred until the entire solid dissolved (a pink solution formed). Phen-azo-phenol (48.3 mg, 0.161 mmol) was added and the mixture was stirred and refluxed. The progress of the reaction was monitored by UV-Vis using MeOH as the solvent. The peak intensity maximum at 450 nm increased and the peak intensity at 540 nm decreased which confirmed the formation of the complex. After 3.5 h the reaction was judged complete

and the refluxing was stopped (Figures 5a-d). The solvent was removed using the rotavap and the solid was taken up in 0.1 M triflic acid (10 mL) containing NH_4PF_6 (86.8 mg, 0.532 mmol). This mixture was stirred for 5 min and the solid was collected using a fine porosity glass frit funnel (15 mL). The filtrate had a light red color. The solid was washed with cold water (3 mL), followed by diethyl ether, and then dried under vacuum for 2 h. Brown solid (121311-A-AH, 98.3 mg, 65.5% yield based on $Ru^{II}(mcbpy)_2Cl_2$). The UV-Vis spectrum of the crude product was recorded in MeOH (Figure 5e).

The complex was purified using alumina column chromatography. The crude product (121311-A-AH, 49.5 mg) was mixed in 3 mL of CH_3OH:CH_3COOH (90:10 by volume) and this mixture was filtered using a fine porosity glass frit funnel (15 mL). The filtrate was loaded into the 1.0 × 15 cm alumina column and CH_3OH:CH_3COOH (90:10 by volume) was used as the eluting solvent. Three bands formed from top to bottom: brown, orange and yellow. The first band was yellow and thought to be excess ligand (Figure 5f). The second (orange) band was collected and thought to contain the desired complex based on the UV-Vis spectrum (Figure 5g). The other band (brown) didn't elute and stayed on the top of the column. The solvent from the orange fraction was removed under vacuum resulting in an orange solid (032812-B-AH, 213.9 mg, yield 432 % based on 49.5 mg).

The complex was purified further by size exclusion chromatography. Sephadex gel LH-20 (50 g) was used to prepare the column (1.9 × 35 cm) using 1:1 MeOH/H_2O as eluent. $[(mcbpy)_2Ru(II)(phen\text{-}azo\text{-}phenol)](PF_6)_2$ (176.6 mg) was dissolved in 1:1 MeOH/H_2O (2 mL); it appeared to dissolve and gave an orange solution. It was filtered using a fine porosity glass frit funnel (15 mL); a white solid was collected on the filter

(thought to be alumina particles). The filtrate then was loaded into the column and eluted with the 1:1 MeOH/H_2O. Five bands formed: three red bands and two brown bands. The two brownish bands were eluted first and collected. The second three red bands were collected separately. UV-Vis spectra for the five bands were recorded using the 1:1 MeOH/H_2O as solvent (Figure 5h). The five fractions were left in the hood to let the solvent evaporate. The largest amount of material was found in the third fraction. UV-Vis spectra of the third and fourth fractions in (MeOH) are shown in Figures 5i-j. ^{1}H-NMR spectra in d_6-DMSO were obtained for the third, fourth and fifth fractions (Figures 5k-q). [(MEM2A409, Figure 5m for the 3rd fraction), (MEM2A411, Figures 5n-o for the 4th fraction), (MEM2A410, Figures 5p-q for the 5th fraction)]. Figures 5k-l show spectra directly comparing the three fractions. ^{1}H-NMR for the 4th fraction which was the most soluble and gave the clearest peaks (400 MHz, d_6-DMSO, Figures n-o) δ (ppm) = 10.79 (s broad, 0.83H), 9.45 (d, 0.93H), 9.06 (m, 2.07H), 8.98 (m, 2.64H), 8.48 (s, 0.95H), 8.21 (m, 1.24H), 8.12 (d, 1.09H), 8.08 (d, 2.10H), 7.98 (m, 2.08H), 7.88 (m, 2.07H), 7.72-7.63 (m, 4.28H), 7.45 (m, 1.88H), 7.19 (t, 1.14H), 7.11 (broad, 0.48H), 7.05 (d, 2H).

I.4.3 Synthesis of bis(4,4'-dimethyl-2,2'-bipyridine)(phen-azo-phenol)ruthenium(II) hexafluorophosphate [(dmbpy)$_2$Ru^{II}(phen-azo-phenol)](PF$_6$)$_2$

Materials:

Cis-Ru^{II}(dmbpy)$_2$Cl$_2$ (RAP-032189), phen-azo-phenol (112911-B-AH), ammonium hexafluorophosphate, NH_4PF_6 (Aldrich, Lot#: 216593), 4,4'-dimethyl-2,2'-bipyridine (Aldrich, 99%, Lot #: 245739), alumina (Fisher, 80-200 mesh, Lot# 000496), Sephadex LH-20 (Sigma, 25-100μ, Lot# 19F-0572). Abs. EtOH, 95% EtOH, diethyl ether and acetone were obtained from the EIU Chemistry Stockroom.

Procedure:

The synthesis was carried out under N_2 and reduced light. Cis-$Ru^{II}(dmbpy)_2Cl_2$ (100.3 mg, 0.1856 mmol) and phen-azo-phenol (61.7 mg, 0.205 mmol) were transferred to a 3-necked flask (100 mL). EtOH (95%, 50 mL) was added and the mixture was brought to reflux. The progress of the reaction was monitored by UV-Vis using 95% EtOH as solvent (Figure 6a). The appearance of a peak maximum at 455 nm confirmed that the target complex was formed. Water (10 mL) was added after 3 h and then MeOH (10 mL) was added after 5 h while still refluxing the solution (Figures 6b-c). The solution was kept refluxing overnight. After a total reflux time of 21 h the UV-Vis spectrum was recorded; no further progress in the reaction was observed (Figure 6d). Refluxing was stopped and solvent was removed under vacuum. Triflic acid (0.1 M, 10 mL) was added to the solid and the mixture was heated to dissolve the solid. While this mixture was hot, NH_4PF_6 (122.5 mg, 0.7521 mmol) was added and the mixture stirred. The mixture was cooled in an ice bath and the solid was collected using a fine porosity glass frit funnel (15 mL). The brown solid was washed with cold water and diethyl ether.

The solid was purified further by dissolution in acetone (20 mL), and, using a Pasteur pipette, it was dripped into a beaker containing diethyl ether (100 mL). Solid formed upon the addition to ether; it was collected on a fine porosity glass frit funnel (15 mL). The filtrate had a light red color and the solid was dark brown. The solid was dried under vacuum (010312-A-AH, 96.3 mg, yield 48.9 % based on $Ru^{II}(dmbpy)_2Cl_2$). This dark brown solid (96.3 mg) was purified further in an attempt to remove excess salt (NH_4PF_6). It was dissolved in acetone (12 mL) followed by the addition of water (10 mL). While stirring, the acetone was evaporated by bubbling N_2 into the solution. Solid

started to form as the acetone evaporated and it was collected using a fine porosity glass frit funnel (15 mL). After drying under vacuum; a brown solid formed (010512-A-AH, 64.2 mg, overall yield 32.6% based on $Ru^{II}(dmbpy)_2Cl_2$). UV-Vis spectrum (Figure 6f) using CH_3CN as solvent, λ_{max}: 460 nm and 376 nm.

Purification of the brown solid was attempted using alumina chromatography. An alumina column (1.5 × 10 cm) was poured as a slurry using CH_3COOH:MeOH (10:90) as eluent. $[(dmbpy)_2Ru^{II}(phen\text{-}azo\text{-}phenol)](PF_6)_2$ (30.6 mg) was dissolved in the eluent (4 mL) and the mixture was filtered using a fine porosity glass frit funnel (2 mL). The filtrate was loaded on the column and eluted with CH_3COOH:MeOH (10:90) . Two bands formed: red and brown. The brown band was eluted first and the red band second. The red band was collected and it was the desired compound based on the UV-Vis spectrum (Figure 6g). The red fraction was rotavapped and an orange solid formed (264.8 mg, 022212-A-AH-thought to contain alumina particles).

The complex was purified further using size exclusion chromatography. A Sephadex LH-20 column (1.9 × 35 cm) was prepared using MeOH:H_2O (80:20) as eluent. $[(dmbpy)_2Ru^{II}(phen\text{-}azo\text{-}phenol)](PF_6)_2$ (022212-A-AH) was dissolved in eluent (2 mL) and filtered on a fine porosity glass frit funnel (15 mL); a white solid was collected (might be alumina). The filtrate was loaded into the column and eluted with 80:20 MeOH/H_2O. Two bands formed: red and brown. The UV-Vis spectra of the two bands were recorded (Figure 6h). The red was eluted second and collected. The red fraction, was left in the hood to let the solvent evaporate resulted in a dark solid that was dried under vacuum (050712-B-AH, 6.0 mg). The resulting solid appeared to be the desired product based on UV-Vis spectrum (Figure 6i). ^{1}H-NMR (Figures 6j-m) (400

MHz, d_6-DMSO) δ (ppm) = 9.39 (d, 1.30H), 8.74 (d, 3.26H), 8.69 (d, 3H), 8.63 (d, 2.28H), 8.51 (s broad, 1.34H), 8.09 (s broad, 1.26H), 7.84 (m, 4.36H), 7.76 (d, 4H), 7.67 (m, 5.10H), 7.42 (m, 7.74H), 7.20 (m, 3.53H), 6.21 (d, 2H), 2.50 (d, 10.31H), 2.46 (s broad, 13.81H), total integration ≅ 63 H; theoretical = 30H.

I.4.4 Synthesis of 4,4'-dicarboxy-2,2'-bipyridine (dcbpy)

Materials:

4,4'-Dimethyl-2,2'-dipyridyl (Aldrich, 99%, Lot # 245739, MEM2A414, Figure 6n, MEM2A414, Figure 6n), $K_2Cr_2O_2$ (Fisher, A.C.S., Lot # 922563). H_2SO_4 (Fisher, reagent A.C.S., min 95%, Lot # 903025), D_2O (Aldrich, 99.9 atom %D, Lot # 15-188-2), NaOD (Aldrich, 30 wt. % solution in D_2O 99+ atom %D, Lot # 16-448-8).

Procedure:

This ligand was prepared according to a literature method.[6] 4,4'-Dimethyl-2,2'-bipyridine (2.7041 g, 14.677 mmol) was dissolved in concentrated H_2SO_4 (70 mL). After dissolving was complete, the solution was immersed in an ice bath. Then, $K_2Cr_2O_7$ (17.6046 g, 59.841 mmol) was added in portions at 0°C. The color of the solution turned to green, and then, after the complete addition of $K_2Cr_2O_7$, dark green. The solution was heated to 50 °C for 1 h. It was then poured into ice water (150 mL) and the resulting mixture was filtered using a coarse porosity glass frit funnel (60 mL). The solid obtained was washed with cold water until the filtrate was colorless. The pale-green yellow solid obtained was dried under vacuum for 1 h. This solid then was refluxed in HNO_3 (70 mL, 50% (v/v aq.)) overnight. The next day the color of the solution was greenish and the entire solid was dissolved. It was cooled to room temperature and then white solid started to precipitate. The mixture was poured into ice water (150 mL) and stirred. The mixture was filtered on a coarse porosity glass frit funnel (150 mL) and the collected solid

washed with water and acetone; the filtrate had a greenish color. The white solid was dried under vacuum for 2 h (032312-A-AH, 2.8130 g, 78.5 % yield based on 4,4'-dimethyl-2,2'-bipyridine). IR (KBr): $\bar{\upsilon}$ (C=O): 1720 cm^{-1} (Figure 6o). ^{1}H-NMR (MEM2A413, Figure 6p) (400 MHz, D_2O/NaOD) δ (ppm) = 7.63 (dd, J= 1.50, 5.01 Hz, 2H) 8.15 (s, 1H), 8.54 (d, J=5.05 Hz, 2H).

I.4.5 Synthesis of 4,4'-dimethoxycarbonyl-2,2'-bipyridine (dmcbpy)

Materials:

4,4'-Dicarboxy-2,2'-bipyridine (032312-A-AH), H_2SO_4 (Fisher, A.C.S. reagent, min 95%, Lot# 903025), $CDCl_3$ (Acros, 0.03% TMS, 99.8+ atom % D, Lot# A020378201). CH_2Cl_2, Na_2SO_4, MeOH, NaOH and ethyl acetate were obtained from the EIU Chemistry Stockroom.

Procedure:

This ligand was prepared according to the literature.[7] 4,4'-Dicarboxy-2,2'-bipyridine (1.0080 g, 4.1303 mmol) was transferred to a round bottom flask (100 mL). MeOH (40 mL) was added and the mixture was stirred. Concentrated H_2SO_4 (4 mL) was added dropwise while stirring the mixture (white suspension formed). This mixture was refluxed overnight resulting in a pink clear solution which was cooled to room temperature and poured into ice water (150 mL).

A precipitate was formed and the pH was adjusted to 8 with 25% (w/v) NaOH. The mixture was extracted with CH_2Cl_2 (3 × 50 mL) and the extracts were dried over Na_2SO_4. The organic solvent was rotovapped and the solid was dried under vacuum for 3 h resulting in a white solid (032412-A-AH, 0.9245 g, 82.3 % based on 4,4'-dicarboxy-2,2'-bipyridine). R_f(alumina in 3:97 ethyl acetate: CH_2Cl_2) = 0.7, mp: 198-200 °C. IR (KBr) $\bar{\upsilon}$(C=O): 1732 cm^{-1} (Figure 7a). ^{1}H-NMR (MEM2A381, Figures 7b-d) (400 MHz,

$CDCl_3$) δ (ppm vs TMS): 8.97 (m, 2H), 8.87 (dd, J= 0.785, 4.98 Hz, 2H), 7.91 (dd, J= 1.62, 4.95 Hz, 2H), 4.00 (s, 6H).

I.4.6 Synthesis of cis-dichloro-bis(4,4'-dimethoxycarbonyl-2,2'-bipyridine)ruthenium(II) [cis-$Ru^{II}(dmcbbpy)_2Cl_2$]

Materials:

4,4'-Dimethoxycarbonyl-2,2'-bipyridine (032412-A-AH), $RuCl_3 \cdot 3H_2O$ (Aldrich, 35-40% Ru, Lot # 206229), DMF (Sigma-Aldrich, 99%, Lot # 01540AB, dried over 4 Å Molecular Sieves ^{TM}). Abs. EtOH was obtained from the EIU Chemistry Stockroom.

Procedure:

This synthesis was done under N_2 and reduced light. The synthesis was carried out based on a literature method.[4] $RuCl_3 \cdot 3H_2O$ (65.7 mg, 0.247 mmol based on 38% Ru) was transferred to a flask (50 mL) and DMF (20 mL) was added. The mixture was stirred for 5 min and then, dmcbpy (134.5 mg, 0.494 mmol) was added and stirred. The mixture was brought to reflux and the progress of the reaction was monitored by UV-Vis using abs. EtOH as the solvent. Initially after mixing, the UV-Vis spectrum showed a maximum at 397 nm (Figure 8a). After 2 h there were three peaks at 316 nm, 416 nm and 566 nm with relative intensities 3.77, 1.03 and 1.00, respectively (Figure 8b). After that, the heating was removed and, while hot, the mixture was filtered using a medium porosity glass frit funnel (30 mL); no solid was collected on the filter. The solvent from the filtrate was removed under vacuum and the resulting black solid was dried under vacuum for 2 h (040312-A-AH, 184.3 mg, yield 104 % based on Ru). IR (KBr) $\bar{\upsilon}$ (C=O) =1726 (s) cm^{-1} (Figure 8c).

I.4.7 Synthesis of bis[(4,4'-dimethoxycarbonyl-2,2'-bipyridine)(phen-azo-phenol)ruthenium(II)]hexafluorophosphate[$(dmcbpy)_2Ru^{II}$(phen-azo-phenol)]$(PF_6)_2$

Materials:

[cis-$Ru^{II}(dmcbpy)_2Cl_2$] (040312-A-AH), Phen-azo-phenol (032612-B-AH), NH_4PF_6 (Aldrich, Lo t# 216593), D_2O (Aldrich, 99.9 atom % D, Lot # 11829CX), d_6-DMSO (Cambridge Isotope Laboratories, 99.9 atom % D, Lot # DLM-10-100), Sephadex LH-20 (Sigma 25-100 μ, Lot # 19F-0572), HPF_6 (Aldrich, 60 wt. % solution in water, Lot # 200956). NaOH, MeOH and 6 M HCl were obtained from the EIU Chemistry Stockroom.

Procedure:

This experiment was carried out under N_2 and reduced light. $Ru^{II}(dmcbpy)_2Cl_2$ (100.2 mg, 0.1398 mmol) and phen-azo-phenol (51.4 mg, 0.1712 mmol) were transferred to a 3-neck flask (50 mL). 1:1 MeOH:H_2O (25 mL) was added and the mixture was heated to reflux. The progress of the reaction was monitored by UV-Vis using MeOH as the solvent. After 5 h the reaction was judged complete and the heating was removed (Figures 9a-b). It was cooled down to room temperature and NH_4PF_6 (68.2 mg, 0.418 mmol) was added and the mixture stirred for 5 min. MeOH was removed under vacuum and the residue containing H_2O kept in the refrigerator overnight. After filtering using a fine porosity glass frit funnel (15 mL), little solid was collected and the filtrate was dark. To the filtrate an additional 22.8 mg of NH_4PF_6 was added and the mixture was kept in the refrigerator; no additional precipitate formed. MeOH (around 30 mL) was added followed by diethyl ether (around 70 mL); precipitate formed immediately after the addition of diethyl ether. The solid was collected on a fine porosity glass frit funnel (15mL); the filtrate was yellow and solid was red-brownish. The solid was dried under

vacuum for 2 h resulting in a brown solid (042712-A-AH, 68.4 mg, 44.8% yield based on $Ru^{II}(dcbpy)_2Cl_2$). IR (Figure 9c) (KBr) ν(C=O): 1605.6 (s) cm^{-1}.

The crude complex was dissolved in water (20 mL) and filtered using a fine porosity glass frit funnel (15 mL); little solid was collected. The pH of the filtrate was adjusted to 1-2 using 6 M HCl; precipitate started to form as the pH decreased. The mixture was passed through a fine porosity glass frit funnel (15 mL); the filtrate had a clear red color. The solid collected on the filter was dried under vacuum resulting in a dark black solid (042812-A-AH, 46.1 mg).

The complex was purified further using size exclusion chromatography. Sephadex LH-20 gel (50 g) was used to prepare the column (1.9 × 35 cm) using 1:1 MeOH:H_2O as the solvent. $[(Dmcbpy)_2Ru^{II}(phen\text{-}azo\text{-}phenol)](PF_6)_2$ (45.0 mg) was dissolved in 1:1 MeOH:H_2O (2 mL) and 2 drops of 10% w/w NaOH; it dissolved completely. It was loaded into the column and eluted with 1:1 MeOH:H_2O. Two bands formed: brown and red. The brown was eluted first and the second red band later. UV-Vis spectra for the two bands (brown and red) were recorded in MeOH:H_2O (Figure 9d). Another small band with yellow color was eluted slowly from the top of the column. To the red band HPF_6 was added (few drops) to decrease the pH to around 1. Solid started to form when the pH decreased to 1. The acidified red band was left in the hood to let the MeOH evaporate and then it was filtered on a fine porosity glass frit funnel (15 mL). A dark red solid was collected which was dried under vacuum (050112-B-AH, 26.8 mg). The UV-Vis of this solid was recorded using MeOH as a solvent (Figure 9e). ^{1}H-NMR (MEM2A400, Figures 9f-g) (d_6-DMSO, 400 MHz) δ (ppm) = 10.8 (broad, 1.09H), 9.47 (d, 1.43H), 9.13 (broad, 5H), 8.98 (d, 0.75H), 8.51 (s broad, 1.27H), 8.30 (broad, 1.96H), 8.23 (broad, 1.64H),

8.13 (s, 1.04H), 8.08 (d, 3.21H), 7.96 (broad, 2.37H), 7.86 (broad, 2.10H), 7.69 (broad, 3.45H), 7.598(broad, 1.02H), 7.05 (d, 2H), total integration ≅ 28H; theoretical = 24H, excluding –COOH groups.

I.5 Synthetic attempts at phen-indigo dye

I.5.1 Synthesis of 5-Br-phenanthroline (5-Br-phen)

Materials:

1,10-Phen (Aldrich, 99+%, Lot # 07601JZ), Br_2 (Aldrich, ACS reagent 99+%, Lot # 14426BS), fuming H_2SO_4 (Aldrich, free SO_3 content ~20%, Lot # 22979TR), $CDCl_3$ (Acros, 0.03% v/v TMS, 99.8+ atom % D, Lot # A020378201). Concentrated NH_4OH, $CHCl_3$, charcoal and Na_2SO_4 were obtained from the EIU Chemistry Stockroom.

Procedure:

The ligand was synthesized based on a literature method.[5] 1,10-Phen (1.8095 g, 10.0 mmol) and fuming H_2SO_4 (12 mL) were transferred to a reaction tube at 0 °C. Br_2 (0.30 ml, 5.80 mmol) was added and the tube was closed and sealed. It was heated in an oil bath at 135 °C for 23 h. After that, it was cooled to room temperature and poured into cold water (100 mL) and stirred. The mixture was neutralized with NH_4OH; a precipitate started to form as NH_4OH was added. The mixture then was extracted with CH_3Cl (2× 100 mL); the extracts had a pink color. Charcoal was added to the extracts and stirred followed by drying over Na_2SO_4. The mixture was filtered and the solvent was removed under vacuum. A pale yellow solid formed after drying under vacuum (070811-A-AH, 2.89 g, 111.0 % based on 1,10-phen). ^{1}H-NMR (MEM2A282, Figures 10a-b) (400 MHz, $CDCl_3$) δ (ppm) = 9.20 (m, 2H), 8.65 (dd, J=1.6, 8.40 Hz, 1H), 8.16 (dd, J= 1.6, 8.4, 1H), 8.12 (s, 1H), 7.74 (m, J=4.4, 4.4 Hz 1H), 7.64 (m, J=4.0, 4.0 Hz, 1H).

I.5.2 Synthetic attempt at 2-((1,10-phenanthrolin-5-yl)amino)acetic acid (N-acetyl-1,10-phen)

Materials:

5-Br-phen (070811-A-AH), glycine (Acros, 98%, Lot # B0129654C), triethanolamine (Acros, 97%, Lot # B0511480), CuI (Fisher, Lot# 701186), K_3PO_4 (J.T. Baker, Lot # 53932220), $CDCl_3$ (Acros, 0.03% v/v TMS, 99.8+ atom % D, Lot # A020378201). $CHCl_3$, 6 M HCl, Na_2SO_4, ethyl acetate, 95% EtOH and CH_2Cl_2 were obtained from the EIU Chemistry Stockroom.

Procedure:

The synthesis was based on a literature method.[8] 5-Br-phen (0.2993 g, 1.155 mmol), glycine (0.1556 g, 2.073 mmol), triethanolamine (6 mL), K_3PO_4 (0.8026 g) and water (20 mL) were transferred to a 3-neck flask (100 mL). The mixture was stirred and heated and a yellow color formed. 5-Br-phen didn't appear to dissolve. When the temperature was 55 °C, the mixture turned red and 95% ethanol was added dropwise until the entire solid dissolved. The mixture was heated to 70 °C and then CuI (41.0 mg, 2.0 mmol) was added, and an immediate dark color formed. The mixture was then heated to 90 °C for 72 h under N_2. After that, the pH was adjusted to 6 with 6 M HCl; a green solution formed which was extracted with $CHCl_3$ (2 ×50 mL). The aqueous layer was green while the organic was red. The organic layer was dried over Na_2SO_4 and the solvent was removed under vacuum. A dark red solid formed (071911-A-AH, 0.271 g).^{1}H-NMR (MEM2A287, Figure 11a) in d_6-DMSO: broad unresolved signals.

I.5.3 Synthetic attempt at the preparation of indolin-3-ol (indoxyl)

Materials:

Triphenylphosphine oxide (Aldrich, 98%, Lot # 03907TN), trifluoromethanesulfonic (triflic0 anhydride (Aldrich, Lo t# 00607AR), triethylamine (TEA, Acros, 99% pure, Lot # A0286926), $CDCl_3$ (Acros, 0.03% v/v TMS, 99.8+ atom % D, Lot # A020378201), N-Phenylglycine (Fluka, > 97%, Lot # 78560). CH_2ClCH_2Cl (distilled over P_2O_5 and stored over 4Å Molecular Sieves ^{TM}), $NaHCO_3$ (5% solution), hexane, Na_2SO_4, brine and ethyl acetate were obtained from the EIU Chemistry Stockroom.

Procedure:

This synthesis was done under N_2 and was based on a literature method.[9] Triphenylphosphine oxide (0.5582 g, 2.006 mmol) was dissolved in CH_2ClCH_2Cl (3 mL) and the solution was bubbled with N_2. Triflic anhydride (0.157 mL, 0.933 mmol) was dissolved in CH_2ClCH_2Cl (3 mL) and then it was added dropwise into the triphenylphosphine oxide solution. After stirring for 15 min, no precipitate formed and the solution turned light yellow. N-Phenylglycine (0.1525 g, 1.009 mmol) was dissolved in CH_2ClCH_2Cl (3 mL); it didn't dissolve completely and gave a yellowish color. This mixture was transferred all at once to the previous solution (triphenylphosphine oxide and triflic anhydride). An immediate brown solution formed. TEA (0.142 mL, 1.02 mmol) was added, the solution was stirred for 5 min, and then it was washed with 5% $NaHCO_3$ (3 × 10 mL), water (2×10 mL) and brine (10 mL). The organic phase was dried over Na_2SO_4 and the solvent was removed under vacuum. The resulting solid was dried under vacuum for 2 h forming a light brown solid (080211-B-AH, 0.3897 g, 290.2 % yield based on N-phenylglycine-thought to contain a mixture of triphenylphosphine oxide and

N-phenylglycine). ^{1}H-NMR (MEM2A302, Figures 12a-b) (400 MHz, $CDCl_3$) δ (ppm) = 7.67 (m, 6H), 7.55 (m, 3H), 7.47 (m, 6H).

I.5.4 Synthesis of 2-phenylamino-3-phenylimino-3H-indole

Materials:

DMF (Sigma-Aldrich, 99.9% dried over 4Å molecular sieves, Lot # 01540AB), aniline (Acros, ACS reagent, Lot # B0506038), oxalyl chloride (Acros, 98%, Lot # A0238070), $CDCl_3$ (Acros, 0.03% v/v TMS, 99.8+ atom % D, Lot # A020378201). THF (distilled from Na/benzophenone ketyl and stored over 3Å Molecular Sieves ™), triethylamine (TEA, dried over CaH_2 and distilled from P_2O_5 and stored over 3Å Molecular Sieves ™), glacial acetic acid, concentrated HCl, CH_2Cl_2, and abs. EtOH were obtained from the EIU Chemistry Stockroom.

Procedure:

This compound was synthesized as described in the literature.[10] THF (25 mL) was transferred to a 50-mL flask and the flask was sealed with a rubber septum. It was cooled in an ice bath and the mixture was bubbled with N_2. Under positive N_2 pressure, DMF (0.92 mL, 12 mmol) was added using a syringe. Oxalyl chloride (1.03 mL, 12 mmol) was then added dropwise via a syringe under N_2. A white foaming suspension formed and this was stirred under N_2 for 2 h at room temperature. The flask was placed in an ice bath and TEA (1.7 mL, 12 mmol), was added dropwise while stirring using a cannula by applying positive N_2 pressure. A precipitate formed and the mixture was orange. After stirring for 1 h in an ice bath and 2 h at room temperature, the precipitate was filtered off under N_2 using a Kontes™ glass frit funnel. The filtrate was orange and the precipitate had an orange color. The solid was air sensitive; it appeared to react with air to give white fumes. Aniline (2.3 mL, 25 mmol) was added to the filtrate under N_2 and the solution was

stirred under N_2 for 16 h at room temperature. The color changed from orange to red. After that, air was bubbled through the solution for ~6 h. This caused the color of the solution to change to dark red. The solvent was removed under vacuum and the residue was dissolved in CH_2Cl_2 (150 mL). The solution was washed with water (2 × 50 mL), the organic layer was removed under vacuum, and the residue was recrystallized from boiling abs. EtOH. After cooling in an ice bath, the solid was collected on a medium porosity glass frit funnel (15 mL). Drying under vacuum for 2 h resulted in a red solid (081211-A-AH, 0.2035 g, yield 5.70 % based on oxalyl chloride). ^{1}H-NMR (MEM2A311, Figures 13a-b) (400 MHz, $CDCl_3$) δ (ppm) = 7.93 (broad, 1H), 7.87 (m, 2 H), 7.42 (m, 4H), 7.27 (m, 2H), 7.21 (m, 1H), 7.06 (m, 3H), 6.66 (m, 2H).

II.5.5 Synthesis of indoline-2,3-dione (isatin)

Materials:

2-Phenylamino-3-phenylimino-3H-indole (081211-A-AH), acetone-d_6 (Cambridge Isotope Laboratories, 99.9 atom %D, 0.03% v/v TMS, Lot # BJ-1168). Glacial acetic acid and concentrated HCl were obtained from the EIU Chemistry Stockroom.

Procedure:

A literature method was used to prepare this compound.[10] 2-Phenylamino-3-phenylimino-3H-indole (0.2024 g, 0.6807 mmol) was transferred to a 25-mL flask. Glacial acetic acid (9 mL), concentrated HCl (1 mL) and water (1 mL) were added and the mixture was refluxed for 20 min. After cooling to room temperature the solvent was removed under vacuum. The resulting solid was triturated with water (15 mL) and the suspension was filtered using a medium glass frit funnel (15 mL). After drying under vacuum for 2 h a greenish solid formed (081311-A-AH, 48.4 mg yield 48.3 % based on

2-phenylamino-3-phenylimino-3H-indole). ^{1}H-NMR (MEM2A312, Figures 14a-b) (400 MHz, acetone-d_6) δ (ppm vs TMS) =7.63 (t, 1H), 7.55 (d, 1H), 7.13 (t, 1H), 7.02 (d, 1H).

II.5.6 Reduction of indoline-2,3-dione (isatin) to indolin-3-ol (indoxyl)

Materials:

$LiAlH_4$ (Aldrich, 95+%, Lot # 05903TT), pyridine (Fisher, certified ACS, Lot # 011205), isatin (081311-A-AH), d_6-DMSO (Cambridge Isotope Laboratories, 99.9 atom % D, Lot # 9H-430). Diethyl ether, ethyl acetate and hexane were obtained from the EIU Chemistry Stockroom.

Procedure:

The reduction was based on a literature method.[12] Pyridine (25 mL) was transferred to a 50-mL flask and the flask was cooled in an ice bath. $LiAlH_4$ (55.5 mg, 1.46 mmol) was added while the flask sat in the ice bath. A light grey mixture formed ($LiAlH_4$ has a grey color). The mixture was stirred for 5 min, and then isatin (48 mg, 0.326 mmol) was added in portions. A green colored mixture formed which changed to dark red after stirring for 10 min. Stirring was continued for 8 h at room temperature, but no further color change was observed. Water (20 mL) was added which caused foaming to appear at the surface while stirring continued for an additional 5 min. The mixture was extracted with diethyl ether (2 × 50 mL); the aqueous layer had a green color and the organic layer was blue. The organic phase was dried over Na_2SO_4 and the solvent was removed under vacuum. Drying the residue for 1 h under vacuum resulted in a bluish solid (081711-A-AH). TLC (4:6 ethyl acetate: hexane) showed 3 spots, indicative of a mixture of products. ^{1}H-NMR (MEM2A312, Figures 14a-b) (400 MHz, d_6-DMSO) δ (ppm) = 7.63 (d, 1H), 7.53 (m, 1H), 7.33 (d, 2H), 6.97 (t, 2H). ^{1}H-NMR of an authentic sample of indigo (MEM2A305, Figures 15e-f) (400 MHz, d_6-DMSO) δ (ppm) = 10.50

(broad, 2H), 7.61 (d, 2H), 7.51 (t, 2H), 7.33 (d, 2H), 6.95 (t, 2H). A UV-Vis spectrum was recorded in DMSO for the crude product (081711-A-AH) and for an authentic sample of indigo dye (Figure 15g).

I.5.7 Synthetic attempt at N,N'-(5H-pyrrolo[2,3-f][1,10]phenanthroline-6,7-diylidene)bis(1,10-phenanthrolin-5-amine) (phen-isatin)

Materials:

DMF (Sigma-Aldrich, 99.9% dried over 4Å Molecular Sieves ™, Lot # 01540AB), 5-NH_2-phen (082111-A-AH), oxalyl chloride (Acros, 98%, Lot # A0238070), d_6-DMSO (Cambridge Isotope Laboratories, 99.9 atom % D, Lot # DLM-10). THF (distilled from Na/benzophenone ketyl and stored over 3Å Molecular Sieves ™), triethylamine (TEA dried over CaH_2 and distilled from P_2O_5 and stored over 3Å Molecular Sieves), glacial acetic acid, concentrated HCl, CH_2Cl_2 and abs. EtOH were obtained from the EIU Chemistry Stockroom.

Procedure:

The preparation of this compound was based on a literature method[10] that was used for the preparation of isatin from aniline. THF (25 mL) was transferred to a 50-mL round bottom flask and sealed with a rubber septum. The flask was cooled in an ice bath and the solvent was bubbled with N_2. DMF (95 μL, 1.2 mmol) and then oxalyl chloride (0.103 mL, 1.2 mmol) were added under N_2 using a syringe. A white foamy suspension formed and the mixture was stirred for 2 h at room temperature and under N_2. The flask was then placed in an ice bath and triethylamine (0.17 mL, 1.2 mmol) was added dropwise under N_2 while stirring. A light orange suspension formed; this was stirred for 1 h in an ice bath and then 2 h at room temperature. The precipitate was filtered off under N_2 using a Kontes ™ glass frit funnel (15 mL). Both the filtrate and the precipitate were

orange. The filtrate was transferred to a 50-mL round bottom flask containing 5-NH_2-phen (0.4281 g, 2.193 mmol). This mixture was stirred for 48 h at room temperature and under N_2. The color changed to brown. After 48 h, air was bubbled through the mixture for 3 h and it was stirred overnight at room temperature. The solvent was removed under vacuum, and the residue was mixed with CH_2Cl_2 (300 mL), resulting in a suspension. This suspension was washed with water (2 × 50 mL); the washings had a red color and the organic layer had an orange color. The organic layer was dried over anhydrous Na_2SO_4 and the solvent was removed under vacuum resulting in a dark orange solid (082511-A-AH, 105.4 mg, 14.6% yield based on oxalyl chloride). ^{1}H-NMR (MEM2A316, Figures 16a-b) (400 MHz, d_6-DMSO) δ (ppm) = 9.05 (dd, J=1.6, 4.0 Hz 1H), 8.67 (m, 2H), 8.04 (dd, J=1.8, 8.2 hz 1H), 7.73 (m, 1H), 7.50 (m, 1H), 6.86 (s, 1H), 6.16 (s-broad, 2H).

I.5.8- Another alternative attempt for the synthesis of indoline-2,3-dione (isatin)

Materials:

Oxalyl chloride (Acros, 98%, Lot # A0238070), d_6-DMSO (Cambridge Isotope laboratories, 99.9 atom % D, Lot # DLM-10). Zeolite (from CHM 4915 $[Na_{86}(AlO_2)_{86}(SiO_2)_{106}]$. $264H_2O$) was heated for 4 h at 400 °C. Aniline, CH_2Cl_2 and 1,2-dichloroethane(CH_2ClCH_2Cl) were obtained from the EIU Chemistry Stockroom.

Procedure:

This synthesis was carried out under N_2 based on a literature method.[11] CH_2ClCH_2Cl (20 mL) and CH_2Cl_2 (10 mL) were transferred to a 3-necked flask (50 mL) and aniline (0.182 mL, 2.00 mmol) was added and the solution was stirred. Zeolite (52.3 mg) was added and then oxalyl chloride (0.181 mL, 2.00 mmol) was added dropwise via

a syringe [a]. A white suspension formed when oxalyl chloride was added. The mixture was heated to reflux for 42 h (color changed to yellow after refluxing) and then it was cooled to room temperature. The mixture was filtered through a medium porosity glass frit funnel (15 mL) to remove zeolite and the solvent from the filtrate was removed under vacuum. The resulting yellowish solid was dried under vacuum (090711-A-AH, 43.6 mg, 14.8 % yield based on aniline). ^{1}H-NMR (MEM2A319, Figures 17a-c) (400 MHz, d_6-DMSO) δ (ppm)= 10.84 (s, 2H), 10.71 (s, 0.68H), 7.86 (d, 5H), 7.74 (m, 9H), 7.52 (t, 8.5H), 7.35 (m, 14H), 7.15 (m, 5H).

[a] In a previous synthesis; oxalyl chloride was added all at once; both methods gave the same result.

References:

1. Ding, H.; Gao, P.; Guo, H.; Ji, S.; Li, X.; Wu, W.; Zhao, C.; Zhao, J. A Highly Selective OFF-ON Red-Emitting Phosphorescent Thiol Probe with Large Stokes Shift and Long Luminescent Lifetime. *Org. Lett.* **2010**, *12*, 2876-2879.
2. Gunnlaugsson, T.; Harte, A.J.; Leonard, J.P.; Sénéchal, K. pH Responsive Eu(III)–Phenanthroline Supramolecular Conjugate: A Novel "*Off–On–Off*" Luminescent Signaling in the Physiological pH Range. *J. Am. Chem. Soc.* **2003**, *125*, 12062-12063.
3. Mao, M. Azo Dyes Based on 1,10-phenanthroline. MS. Thesis, Eastern Illinois University, July 1997.
4. Grätzel, M.; Nazeeruddin, M.K.; Paul, D. *Inorg. Synth.* **2002**, *33*, 185-189.
5. Connick, W.B.; Eisenberg, R.; Geiger, D.K.; Hissler, M.; Lachicotte, R.J.;Lipa, D.; McGarrah, J.E. Platinum DiimineBis(acetylide) Complexes: Synthesis, Characterization, and Luminescence Properties. *Inorg. Chem.* 2000, *39*, 447-457.
6. Görl, H.; Henry, W.; Popp, J.; Rau, S.; Schäfer, B.; Schmitt, M.; Schwalbe, M.; Tschiervel, S.; Vaughan, G.; Vos, J.G. Synthesis and Characterization of Poly(bipyridine)ruthenium Complexes as Building Blocks for Heterosupramolecular Arrays. *Eur. J. Inorg. Chem.* **2008**, 3310-3319.
7. Mclaughlin, L.W.; Wiederholt, K. A 2,2′-Bipyridine Ligand For Incorporation into Oligodeoxynucleotides: Synthesis, Stability and Fluorescence Properties of Ruthenium—DNA Complexes. *Nucleic Acids Res.* **1999**, *27*, 2487-2493.
8. Lu, Z.; Twieg, R.J. Copper-Catalyzed Aryl Amination in Aqueous Media with 2-Dimethylaminoethanol Ligand. *Tetrahedron Lett.* **2005**, *46*, 2997-3001.

9. Hendrickson, J.B.; Hussoin, Md.S. Reactions of Carboxylic Acids with "Phosphonium Anhydrides". *J. Org. Chem.* **1989**, *54*, 1144-1149.

10. Hennig, A.; Huber, S.M.; Pühlhofer, F.G.; Weiss, R. A Novel and General One-Pot Synthesis of Isatine and Its N-Unsubstituted Derivatives via Nucleophilic Substitution Reactions on 1,2-Bis(dimethylamino)-1,2-dichloroethene. *J. Heterocycl. Chem.* **2009**, *46*, 421-427.

11. MahamadaliShaikh, T.; Raj, I.V.P.; Sudalai, A. H-β Zeolite: an Efficient, Reusable Catalyst for One-Pot Synthesis of Isatins from Anilines. *Acta Chim. Slov.* **2010,** *57,* 466–469.

12. Khoshtanya, T.E.; Kurkovskaya, L.N.; Mirziashrili, N.T.; Sikharnlidze, M.I.; Tsintsadze, T.G. Novel Route For Obtaining Isomeric Benzo[b]Thiophenoindolines. *Chem. Heterocycl. Comp.* **2002**, *38*, 472-476.

Results and discussions

I. Syntheses

I.1 Synthesis of phen-azo-phenol

This ligand was synthesized in three steps. The first step was the preparation of 5-nitro-1,10-phenanthroline (5-NO_2-phen) from 1,10-phenanthroline (phen) by nitration using concentrated HNO_3 and concentrated H_2SO_4. The procedure involved generation of a nitronium ion (NO_2^+) which undergoes electrophilic substitution in the phen ring.[1] The synthesis produced two products: 5-NO_2-phen and 1,10-phenanthroline-5,6-dione (phendione). The desired product (5-NO_2-phen) was precipitated when the pH of the reaction mixture was adjusted to 4 with solid $NaHCO_3$. The phendione was obtained by extraction of the aqueous solution with CH_2Cl_2.

The next step in the synthesis was to prepare 5-amino-1,10-phenanthroline (5-NH_2-phen) from 5-NO_2-phen. The 5-NH_2-phen was synthesized by the reduction of the nitro group using $N_2H_4.H_2O$. The phen-azo-phenol was then prepared from 5-NH_2-phen according to a method used in a previous thesis.[2] The method involved the preparation of the diazonium ion from 5-NH_2-phen and coupling this ion with phenol. One modification from previous preparations was that after the diazonium salt phenol solutions were combined, the mixture was left stirring at 0-10 °C for 4 h which resulted in an improved yield. Another modification involved avoiding the use of acetic acid during the purification of the ligand on an alumina column.

I.2 Synthesis of ruthenium polypyridyl complexes

The three complexes were prepared from the starting material ruthenium(III) trichloride hydrate ($RuCl_3 \cdot 3H_2O$). Cis-bis(polypyridyl)dichloro complexes were formed by refluxing $RuCl_3$ with the selected ligands in DMF. The coordination of phen-azo-

phenol to the bis-complexes was achieved by refluxing them in a mixture of MeOH and H_2O. This solvent was chosen to make sure both the bis-complex and the ligand (phen-azo-phenol) were soluble and to assist in the labilization of the Cl^- ligands. The synthesis of bis(4,4'-dimethoxycarbonyl-2,2'-bipyridine)Ru^{II}(phen-azo-phenol) hexafluoro-phosphate, $[(dmcbpy)_2R^{II}(phen\text{-}azo\text{-}phenol)](PF_6)_2$, deserves special attention. The reason this was attempted was that complexes of dmcbpy had been found in the literature to be easier to purify than those based on 4,4'-dicarboxy-2,2-bipyridine (dcbpy)[3]. The idea was to synthesize and purify $[(dmcbpy)_2Ru^{II}(phen\text{-}azo\text{-}phenol)]^{2+}$ and then simply hydrolyze the esters to acid groups to produce $[(dcbpy)_2Ru^{II}(phen\text{-}azo\text{-}phenol)]^{2+}$. The IR of $[Ru^{II}(dmcbpy)_2Cl_2]$ (Figure 8c) showed a C=O stretch (1726 cm^{-1}) that matched well with a literature value [3] (1725 cm^{-1}) for the same complex. However, when the cis-$[Ru^{II}(dmcbpy)_2Cl_2]$ was refluxed with a mixture of $MeOH/H_2O$ to attach the phen-azo-phenol, the methoxy groups were hydrolyzed forming carboxyl groups as shown by IR (Figures 8c and 9c) and ^{1}H-NMR (Figures 9f-g). The C=O stretch in the IR-spectrum of what was thought to be $[(dmcbpy)_2Ru^{II}(phen\text{-}azo\text{-}phenol)](PF_6)_2$ (1606 cm^{-1}, Figure 9c) matched that of the complex $[Ru^{II}(dcbpy)_3]^{2+}$ found in the literature (1607 cm^{-1}).[3] In addition, It was found that the $\bar{\upsilon}$(C=O) for cis-$Ru^{II}(dcbpy)_2Cl_2 \cdot 2H_2O$ is (1711 cm^{-1})[4] which is not observed in the complex $[(dmcbpy)_2Ru^{II}(phen\text{-}azo\text{-}phenol)](PF_6)_2$. Therefore, this means that the ester form of the carboxylic acid didn't survive the synthetic conditions of the phen-azo-phenol addition. Evidence of this is supported by the the ^{1}H-NMR spectrum of what was thought to be the dmcbpy complex (Figures 9f-g). The methoxy H-atoms didn't show in the ^{1}H-NMR for $[(dmcbpy)_2Ru^{II}$(phen-azo-

phenol)]$(PF_6)_2$ compared with what observed in the ^{1}H-NMR of 4,4'-dimethoxy-2,2'-bipyridine (Figure 7c).

In general, the ruthenium complexes were found to be difficult to purify. Recrystallization attempts were made and column chromatography using alumina was attempted. Later in the project, it was found that size exclusion chromatography had the best results based on UV-Vis and ^{1}H-NMR evidence. The purification of the complex $[(mcbpy)_2Ru^{II}(phen\text{-}azo\text{-}phenol)]^{2+}$ was different than the other two complexes in that it gave five bands in the size exclusion chromatography (Figure 5h). The fourth and fifth fractions had identical UV-Vis spectra. The ^{1}H-NMR spectra for the third and fourth factions were close but that for the fifth one was different as shown in Figures 5j-k. This complex was expected to have at least three different isomers as shown below.

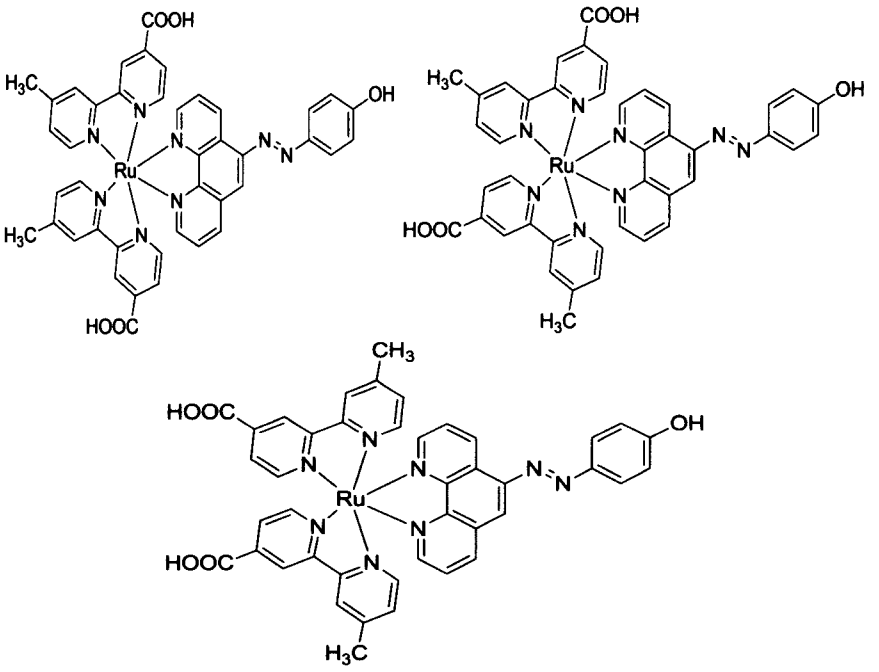

I.3 Synthetic attempts at phen-indigo:

I.3.1 Synthetic attempt at 2-((1,10-phenanthrolin-5-yl)amino)acetic acid (N-acetyl-1,10-phen)

The synthesis of this compound was attempted using a published method.[5] The first step in the synthesis was to prepare 5-bromo-1,10-phenanthroline (5-Br-phen) and then react this ligand with glycine to prepare the desired product.

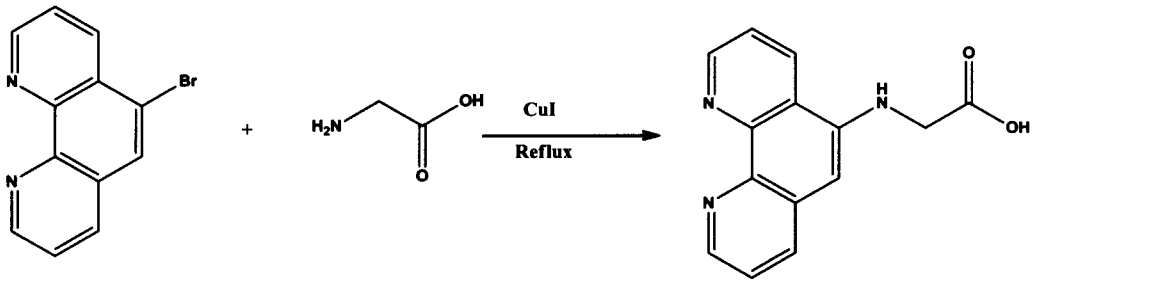

5-Br-phen glycine 2-(1,10-phenanthrolin-5-yl)amino)acetic acid (N-acetyl -1,10-phen)

The ^{1}H-NMR for the product is shown in Figure 12a; the peaks in the aromatic region were broad and difficult to assign. It was thought that the use of CuI in the synthetic procedure might coordinate with the phenanthroline ligand and, being oxidized to Cu^{II}, leads to a paramagnetic metal that would affect the ^{1}H-NMR spectrum. No further attempt to purify the compound was made.

I.3.2 Synthetic attempt at the preparation of indolin-3-ol (indoxyl)

The synthesis was done under N_2. The method involved the formation of phosphonium anhydride reagents[6] by mixing triphenylphosphine oxide ($R_3P=O$, R=phenyl) with triflic anhydride (Tf_2O, Tf = $CF_3SO_3^-$). This reagent should then react with the carboxyl group forming a bond between the phosphorus and the oxygen in the carboxylic group (P=O) bond which later undergoes C-acylation[6] as shown below.

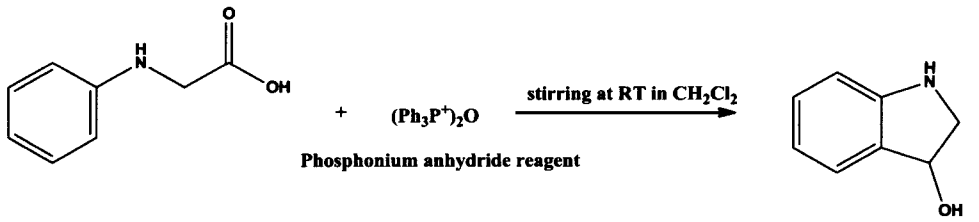

2-(phenylamino)acetic acid (N-phenylglycine)

Indoxyl

The reaction between N-phenylglycine and the phosphonium anhydride reagent didn't succeed and the product was unreacted $R_3P=O$ (Figures 13a-e). The ^{1}H-NMR of an authentic sample of $R_3P=O$ is shown in Figures 13c-e. It appeared that the formation of phosphonium anhydride reagent was not successful because Tf_2O needed to be doubly distilled before use and the quantities of this reagent of this reagent were limited.

I.3.3 Synthetic attempt at N,N'-(5H-pyrrolo[2,3-f][1,10]phenanthroline-6,7-diylidene)bis(1,10-phenanthrolin-5-amine) (phen-isatin):

This synthesis was attempted to mimic the synthesis of indoline-2,3-dione (isatin) based on a literature method.[7] Inspection of the ^{1}H-NMR spectrum of the intermediate (**I**) showed that 5-NH_2-phen didn't react and the ^{1}H-NMR spectrum was just the starting material 5-NH_2-phen (Figures 2b and 17a-b). It was thought that the intermediate **I** was not prepared due to steric issues.

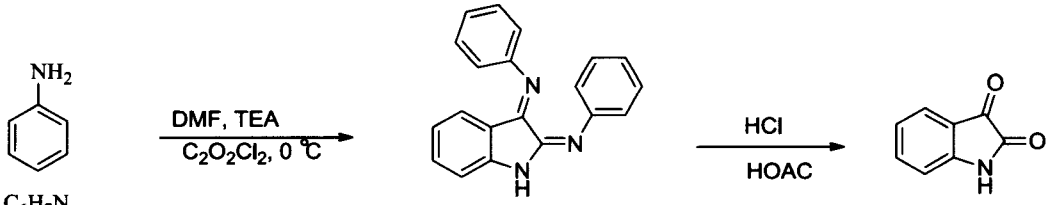

C_6H_7N

Aniline

$C_{20}H_{15}N_3$

2-Phenylamino-3-phenylimino-3H-indole

$C_8H_5NO_2$

Isatine

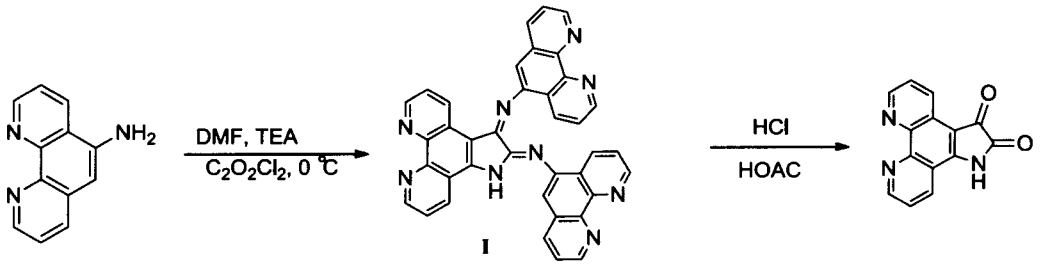

5-NH_2-phen **N,N'-(5H-pyrrolo[2,3-f][1,10]phenanthroline-6,7-diylidene)bis(1,10-phenanthrolin-5-amine)** **Phenisatine**

II. ^{1}H-NMR spectra

II.1 5-NO_2-phen

The ^{1}H-NMR spectrum of 5-NO_2-phen (in d_6-DMSO) is shown in Figures 1a-b and the values (calibrated against the DMSO solvent at 2.50 ppm) and peak assignments are summarized in Table 1. H-2 and H-9 are each assigned as a doublet of doublets and are expected to be furthest downfield due to the N-atoms in the rings. H-3 and H-8 are close to being equivalent, but the multiplet appears to be two overlapping doublet of doublets. H-4 would be expected to be slightly more deshielded than H-7 due to the $-NO_2$ group. H-6 appears as a singlet. The integration is consistent with the expected structure shown.

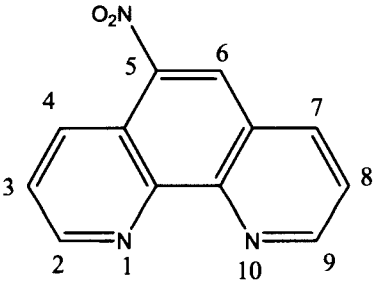

Table 1: ^{1}H-NMR chemical shift for 5-NO_2-phen.

Chemical shift δ (ppm)	9.28 (dd)	9.24 (dd)	9.05 (s)	8.89 (dd)	8.78 (dd)	7.98-7.92 (m)
J values (Hz)	1.80, 4.34	1.60, 4.26	-	1.59, 8.59	1.70, 8.20	-
# H	1	1	1	1	1	2
Position	H-2	H-9	H-6	H-4	H-7	H-3,H-8

dd: doublet of doublet.

s: singlet.

m: multiplet

II.2 5-NH_2-phen

The ^{1}H-NMR spectrum of 5-NH_2-phen (in d_6-DMSO) is shown in Figures 2a-b and the chemical shift values and peak assignments are summarized in Table 2. The appearance of a peak at 6.14 ppm with integration of 2H is consistent with the reduction of the $-NO_2$ to $-NH_2$. In addition, the effects of the electron-donating group $-NH_2$ group are evident as all the resonances are shifted upfield compared to those of 5-NO_2-phen. For example, the singlet for H-6 is shifted upfield by ~2.2 ppm. The multiplets were assigned as arising for H-3 and H-8 are better separated in 5-NH_2-phen and are shifted upfield by ~ 0.2 to 0.4 ppm. The H7/H-9 and H-4/H-7 are shifted upfield with the resonances for the H-atoms that are the fewest bonds away from the $-NH_2$ group having the larger upfield shifts. This results in greater separation between the H-2 and H-9 signals and the H-4 and H-7 signals in 5-NH_2-phen than in 5-NO_2-phen.

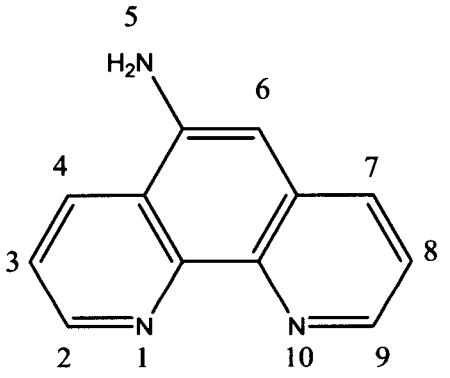

Table 2: ^{1}H-NMR chemical shift for 5-NH_2-phen.

Chemical shift δ (ppm)	9.05 (dd)	8.68 (d)	8.67 (dd)	8.04 (dd)	7.73 (m)	7.51 (m)	6.86 (s)	6.14 (s broad)
J Values (Hz)	1.60, 4.20	6.0	1.60, 4.30	1.60, 8.20	-	-	-	-
# H	1	2	1	1	1	1	1	2
Position	H-9	H-2	H-7	H-4	H-8	H-3	H-6	H-5

II.3 Phen-azo-phenol

This ligand appeared more soluble in DMSO than in $CHCl_3$, so the ^{1}H-NMR spectrum was recorded in DMSO (Table 3, Figures 3c-d). The spectrum showed the same pattern as 1,10-phenanthroline substituted at position 5 (5-NH_2-phen and 5-NO_2-phen) with two extra signals from the attached phenol ring. The phenol O-H signal didn't appear, likely due to rapid exchange with H_2O or due to deprotonation. As judged by the chemical shift of the singlet peak for H-6, the diazo group (with attached phenol) is less electron-withdrawing than $-NO_2$ and less electron-donating than $-NH_2$. The signals due to H-4 and H-6 and the signals from the phenol ring are significantly broadened. This could be due to deprotonation of –OH or due to an interchange between an "E" configuration (phenol and phenanthroline ring in "trans" position) and "Z" configuration (phenol and phenanthroline ring in "cis" position).

Table 3: ^{1}H-NMR chemical shift for phen-azo-phenol.

Chemical shift for phenanthroline ring δ (ppm)	9.33 (dd)	9.14 (m)	8.96 (broad)	8.52 (d)	7.93 (s)	7.84 (m)	7.77 (broad)
# H	1	1	1	1	1	1	1
Position	H-2	H-9	H-4	H-7	H-6	H-3	H-8
Chemical shift for phenol ring δ (ppm)	7.69 (m)	6.30 (s broad)					
# H	2	2	Phenol –O-H could not be identified. It was expected to be downfield ~ 10.50 ppm				
Position	H-11, H14	H-12, H-13					

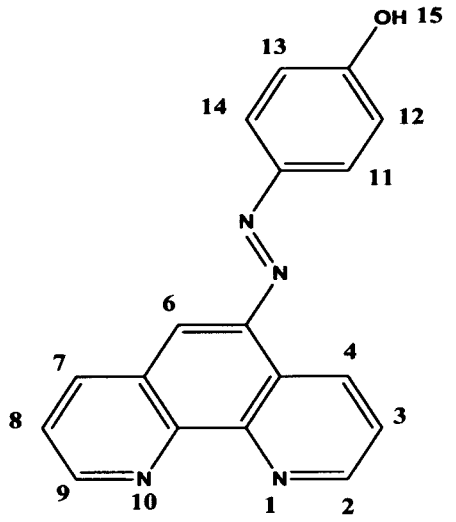

Phen-azo-phenol

II.4 4,4'-Dimethyl-2,2'-bipyridine (dmbpy)

The ^{1}H-NMR of dmbpy was recorded in $CDCl_3$ (Figure 6n) and the data is summarized in Table. The methyl protons appeared as a singlet peak as expected. The H-6, H-6' signals appeared as a doublet centered at 8.53 ppm. The H-5, H-5' signals appear as a broad and a multiplet. The H-3, H-3' would be expected to appear as a singlet peak; however a close look at the peak shows that it appears as a doublet of quartet. This might be due coupling of (H-3, H-3') with (H-5, H-5') that gives a doublet at the same time coupling of these protons with the methyl protons gives a quartet so it a doublet of quartet.

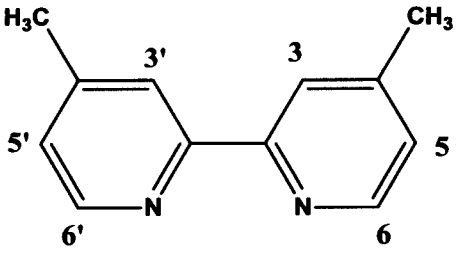

4,4'-Dimethyl-2,2'-bipyridine

Table 4: ^{1}H-NMR chemical shifts for 4,4'-dimethyl-2,2'-bipyridine.

Chemical shift δ (ppm)	8.53 (d)	8.22 (m broad)	7.13 (m)	2.44 (s)
# H	2	2	2	6
Position	H-6, H-6'	H-5, H-5'	H-3, H-3'	$-CH_3$

II.5 4,4-Dicarboxy-2,2'-bipyridine (dcbpy)

The ^{1}H-NMR for dcbpy was recorded in D_2O/NaOD. The complex didn't dissolve in water unless base was added. The addition of base caused deprotonation of the carboxyl groups which increased the solubility of the compound. The ^{1}H-NMR for dcbpy is shown in Figure 6p and the data is summarized in Table 5. There were three peaks in the spectrum with a total integration of 6H. H-3 and H-3' appear as a singlet (8.15 ppm). The carboxylic acid protons didn't appear due to deprotonation of these groups when the base sodium deuteroxide (NaOD) was added.

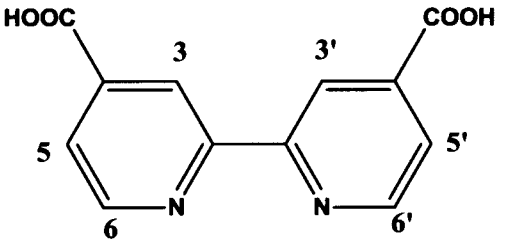

4,4'-Dicarboxy-2,2'-bipyridine

Table 5: ^{1}H-NMR chemical shift for 4, 4'-dicarboxy-2, 2'-bipyridine.

Chemical shift δ (ppm)	8.54 (d)	8.15 (s)	7.64 (d)
# H	2	2	2
Position	H-6, H-6'	H-3, H-3'	H-5, H-5'

II.6 4,4'-Dimethoxycarbonyl-2,2'-bipyridine (dmcbpy)

The ^{1}H-NMR spectrum of dmcbpy (in $CDCl_3$ is shown in Figures 7b-d and the data summarized in Table 6. The methyl protons were equivalent and integrated to 6H. The

protons at 3, 3' positions were shifted downfield due to the presence of the carbonyl groups as compared to the dmbpy (Figure 6n). The protons at positions 5, 5' (7.91 ppm) and positions 6,6' (8.87 ppm) are related by the same coupling constant (J ≅ 5 Hz).

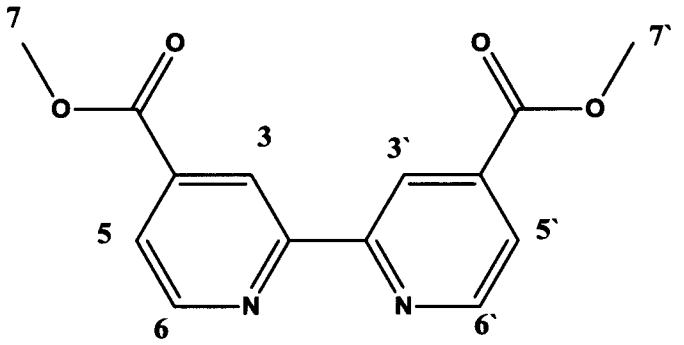

4,4'-Dimethoxycarbonyl-2,2'-bipyridine

Table 6: ^{1}H-NMR chemical shift for 4, 4'-dimethoxycarbonyl-2, 2'-bipyridine.

Chemical shift δ (ppm)	8.97 (m)	8.87 (dd)	7.91 (dd)	4.00 s
# H	2	2	2	6
Position	H-3, H-3'	H-6, H-6'	H-5, H-5'	-O-CH_3

II.7 4'-Carboxy-4-methyl-2,2'-bipyridine (mcbbpy)

The ^{1}H-NMR spectrum of mcbpy was recorded in d_6-DMSO and is shown in Figures 4a-c. The data is summarized in Table 7. The methyl protons appeared as a singlet peak at 2.42 ppm as expected for aliphatic protons. The peaks due to H-3', H-5' and H-6' were shifted downfield due to the presence of the electron-withdrawing group (-COOH). While, the peaks due to H-3, H-5 and H-6 appeared upfield due to the presence of the electron donating group (-CH_3).

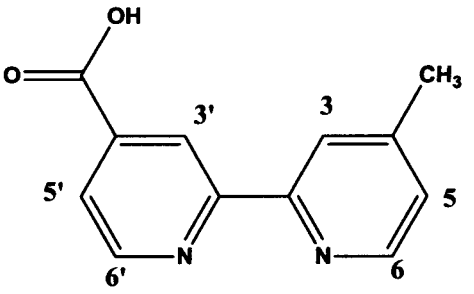

4'-Carboxy-4-methyl-2,2-bipyridine

Table 7: ^{1}H-NMR chemical shift for 4'-carboxy-4-methyl-2,2'-bipyridine.

Chemical shift δ (ppm)	8.83 (m)	8.81 (m)	8.56 (d)	8.26 (s broad)	7.84 (dd)	7.32 (d)	2.42 (s)
# H	1	1	1	1	1	1	3
Position	H-3'	H-5'	H-6'	H-6	H-5	H-3	$-CH_3$

II.8 $[(dmbpy)_2Ru^{II}(phen\text{-}azo\text{-}phenol)]^{2+}$

The ^{1}H-NMR was recorded in d_6-DMSO (Figures 6j-m). The identity of this complex is not clear and it is under investigation. The distinguishable peaks were assigned to the phen-azo-phenol ligand. The H-12, H-13 appears as a doublet centered at 6.21 ppm. The doublet centered at 7.76 ppm could be assigned as the H-14, H-11 positions. The H-6 position on the phenanthroline portion of phen-azo-phenol could be associated with the singlet at 8.51 ppm. The methyl protons from dmbpy appeared upfield as expected but there are two peaks (~2.54 ppm and 2.45 ppm) and each integrates differently: one integrates to 10.31H and the other to 13.81H. Interestingly, the spectrum appears to integrate to approximately twice the expected number of H-atoms when reasonable guesses are made on integration of key peaks (such as phen-azo-phenol peaks). Moreover, the large water peak (determined to be due to the added complex) appears to make integration over the whole spectrum challenging due to phasing problems.

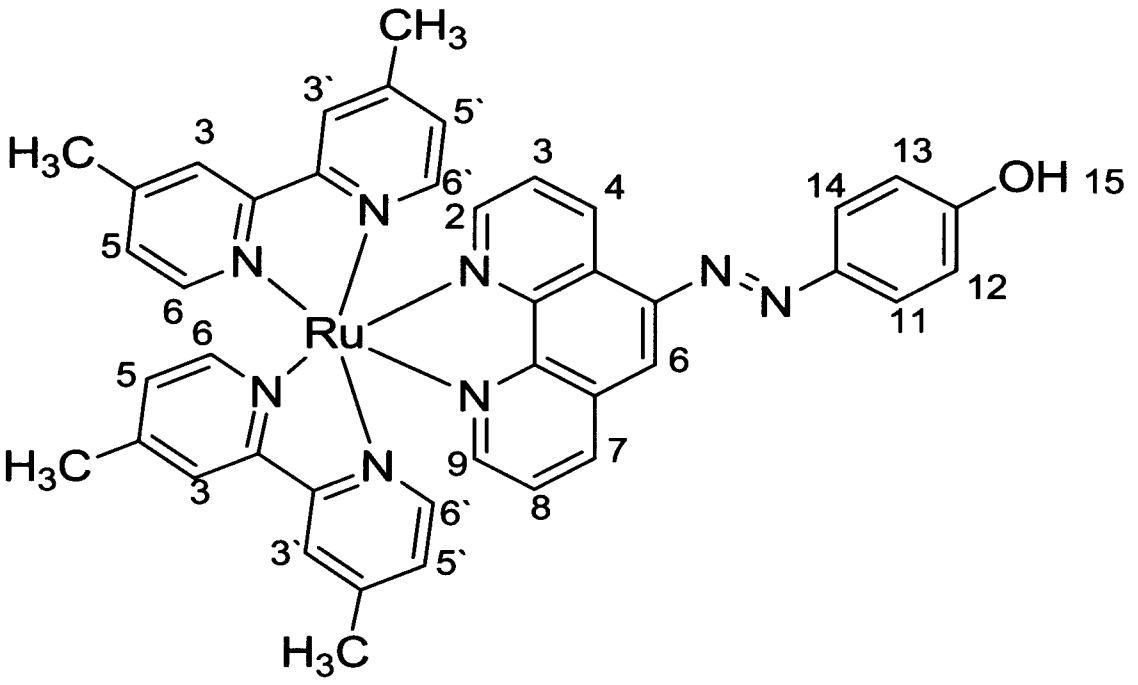

II.9 $[(dcbpy)_2Ru^{II}(phen\text{-}azo\text{-}phenol)](PF_6)_2$

The ^{1}H-NMR for this complex was recorded in d_6-DMSO (not completely dissolved). The spectrum is shown in Figures 9f-g. The peaks from the 4,4'-dicarboxy-2,2'-bipyridine ligands were not clear (possibly due to extensive H-bonding and deprotonation equilibrium) so they were difficult to assign. The doublet centered at 7.06 ppm is assigned as arising from the H-12/H-13 positions on the phenol ring. Likewise, the doublet centered at 8.08 ppm would appear to be a good match for the H-11/H-14 positions, although it is curious that this doublet integrates to 3H (relative to assigned 2H at 7.06 ppm). The singlet at 8.50 ppm seems reasonable (as in the previous mcbpy complex) to assign as arising from the H-6 position on the phen-azo-phenol.

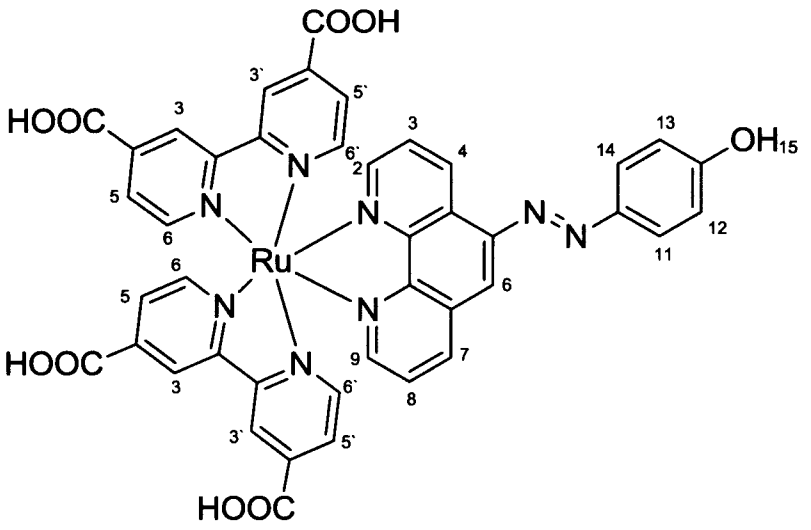

II.10 ^{1}H-NMR for [(mcbpy)$_2$Ru^{II}(phen-azo-phenol)](PF$_6$)$_2$

The spectrum for the 4th fraction from size exclusion chromatography was recorded using d_6-DMSO. It was found that this fraction was completely soluble in d_6-DMSO compared to the 3rd and 5th fractions which were either poorly or partially soluble. ^{1}H-NMR signal was obtained for the 4th fraction as shown in Figures 5m-o. The peaks from the phen-azo-phenol ligand were clear to observe whereas the ones from the bipyridine moiety were overlapped and difficult to distinguish. For example, the doublets centered at 7.05 ppm and 8.08 ppm can be assigned to the H-12/H-13 and H-11/H-14 signals on the phenol. The broad singlet at 10.8 ppm can be assigned to the –OH group on the phenol. In addition, the singlet at 8.48 ppm can be identified as H-6 on the phen-azo-phenol. Based on an assigned integration of 1.00 for the H-6 signal, the region from 11 to 6.5 ppm integrates to approximately 26 H. This compares fairly well with the expected integration of 24 H (excluding –CH_3 signal).

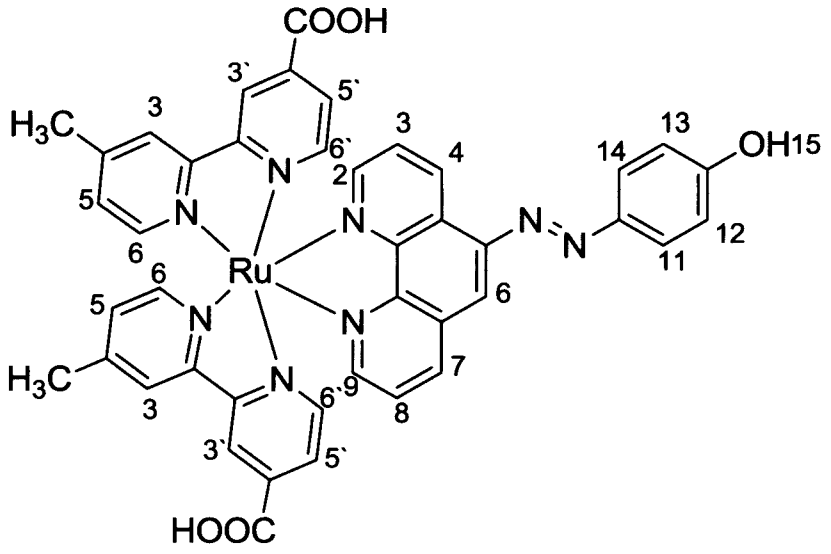

II.11 ^{1}H-NMR for the reduction of isatin:

The ^{1}H-NMR spectrum was recorded in d_6-DMSO and the peaks were referenced against the DMSO peak at 2.50 ppm (Figures 14a-d). The spectrum showed a mixture of three compounds: the pyridine solvent used for the reduction process, isatin and indigo dye. The formation of indigo occurred when the isatin was reduced to indolin-3-ol (indoxyl). This reduction is favored in a basic medium and the presence of pyridine was apparently sufficient. The ^{1}H-NMR spectrum of an authentic sample of indigo dye was recorded in d_6-DMSO and the peaks were compared to the product of isatin reduction (Figure 14c). It is clear that the formation of indigo dye resulted from the reduction process. Table 8 shows the ^{1}H-NMR chemical shifts for indigo dye; the values are based on Figure 14f. Two functional groups in the indoline ring would affect the position of the ^{1}H-NMR peaks: (C=O) and (-NH). The protons at positions (H-1, H-1') were shifted downfield due to their relative position to the (C=O) group and appeared as a doublet due to coupling with the protons at positions H-2, H-2'. The protons at positions H-2, H-2' and H-3, H-3' produced triplets since they each coupled to the two adjacent protons. The

chemical shift positions for the protons at H-2, H-2' appeared at 6.95 ppm since they were at the p-position of the amine group and m-position from the (C=O) group. The protons H-3, H-3'appeared downfield from H-2/H-2' since they were in p-positions from the carbonyl group (C=O). The amine protons (H-5, H-5') appeared downfield and broad due the possibility of forming hydrogen bonds with the oxygen in the carbonyl group as shown in the structure below.

The UV-Vis spectra of both the authentic sample of indigo dye and the product from the reduction of isatin were recorded in DMSO (Figure 14g). The spectra showed that both had a band maximum at ~619 nm which confirmed the synthesis of indigo dye. However, the UV-Vis spectra differ in the UV region since the possible formed indigo dye was not pure and contained pyridine in addition to un-reduced isatin which both absorb in the UV region.

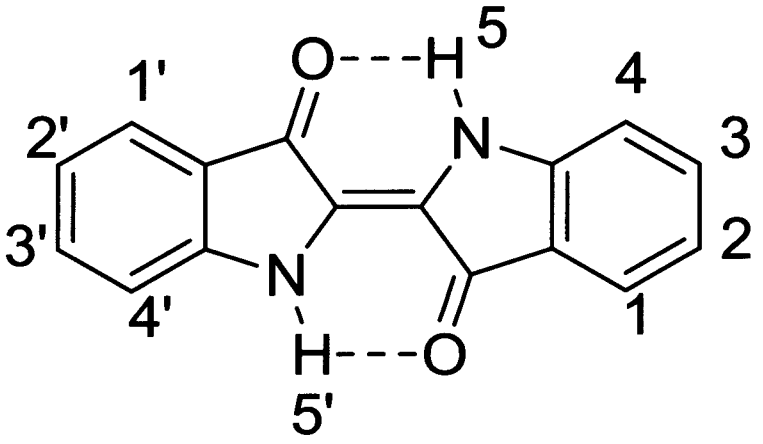

(E)-[2,2'-biindolinylidene]-3,3'-dione (Indigo dye)

Table 8: ^{1}H-NMR chemical shift for indigo dye.

Chemical shift δ (ppm)	10.50 (s broad)	7.61 (d)	7.51 (t)	7.33 (d)	6.95 (t)
# H	2	2	2	2	2
Position	H-5, H-5'	H-1, H-1'	H-3, H-3'	H-4,4'	H-2, H-2'

III. IR data

The IR for 4,4'-dicarboxy-2,2'-bipyridine (dcbpy) was obtained by making a KBr pellet of the ligand. The vibrational stretching of the carbonyl (Figure 6o) $\bar{\upsilon}$(C=O) was 1720 cm^{-1} (lit.[3] 1721 cm^{-1}). When dcbpy was esterified to the methyl ester (dmcbpy), $\bar{\upsilon}$C=O shifted to a slightly higher energy (1732 cm^{-1}, Figure 7a). The IR for $[Ru^{II}(dmcbpy)_2Cl_2]^{2+}$ was recorded (Figure 8c) and $\bar{\upsilon}$(C=O) was 1726 cm^{-1} (lit.[3] 1725 cm^{-1}). This value is a reflection of the small but measurable effect of coordination of a Ru(II) metal and the σ and π-donating ability of the Cl^- ligand. IR spectrum for 4'-carboxy-4-methyl-2,2'-bipyridine (mcbpy) were recorded and are shown in Figures 10c-d, $\bar{\upsilon}$(C=O) = 1707 cm^{-1}. The IR for $[Ru^{II}(dmcbpy)_2Cl_2]^{2+}$ was recorded and gave $\bar{\upsilon}$(C=O) 1606 cm^{-1} (Figure 9c).

IV. X-ray crystallography of phen-azo-phenol

The crystal structure of phen-azo-phenol is shown in Figures 3j-k. Crystals were grown by slow evaporation from THF and concentrated HCl. The acid was added to protonate at least one of the N-atoms in the phenanthroline ring. It turned out that only one of the N-atoms of the phenanthroline ring was protonated, but this protonation probably helped in growing crystals from this ligand. It was found from the crystal structure of phen-azo-phenol that weak intermolecular interaction exists between the chlorine atom and the hydrogen attached to N2 (Cl1...H-N2). The N2-H...Cl1 distance (D...A) was 3.1077 (19) Å and the N2-H...Cl1 angle (D-H...A) was 145(2)°. The crystal packing was stabilized by this weak interaction (Figure 3k) and strong H-bonding interaction between O1-H4...O2 ((D...A) = 2.586 (2) Å, (D-H...A) =166(3)°). The

dihedral angle between the phenanthroline and the phenol ring was 14.40 (19)° as shown in the diagram below.

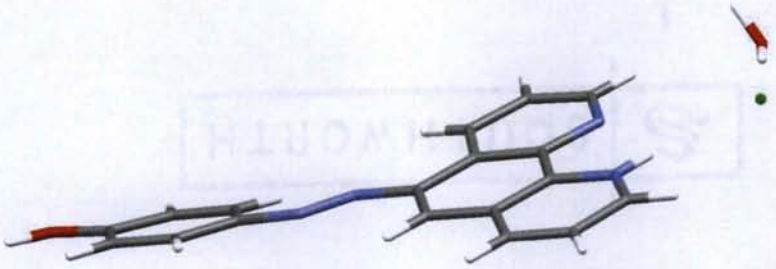

V. UV-Vis spectra

V.1 UV-Vis of phen-azo-phenol

The UV-Vis spectra of phen-azo-phenol in different solvents are shown in Figures 3e-f. The phen-azo-phenol was dissolved in MeOH first then 200 μL aliquots were diluted into 3 mL of the selected solvents to overcome the solubility issue with this ligand in the selected solvents and to maintain a consistent concentration. Investigation of the UV-Vis spectra showed that there were two absorption maxima in the visible region: one in the 380-400 nm range and the other in the 490-520 nm range. One of the bands was dominant over the other depending on the solvent and the presence of added acid or base. The 380-400 nm absorbance range predominated in 1,4-dioxane, $CHCl_3$, and MeOH. The higher wavelength maximum dominated when CH_3CN, pyridine, DMSO and DMF were used.

Scheme 1 shows that deprotonation of the phenol could cause delocalization of the electrons on both the phenol and phenanthroline rings. This could cause the absorption maximum to red shift. Evidence of this comes from the UV-Vis of the previously

mentioned spectra of phen-azo-phenol in various organic solvents (Figures 3e-f). The solvents containing nitrogen bases (DMF, pyridine, CH_3CN) which are expected to be more basic lead to spectra where the higher wavelength maxima (equated with the deprotonated form of phen-azo-phenol) are favored. MeOH (somewhat acidic), $CHCl_3$ and the cyclic ether 1,4-dioxane appear not to be capable of effectively deprotonating the phenol. While DMSO may not be as basic as pyridine and DMF, it has been measured to be more basic than acetone, diethyl ether, and MeOH.[8]

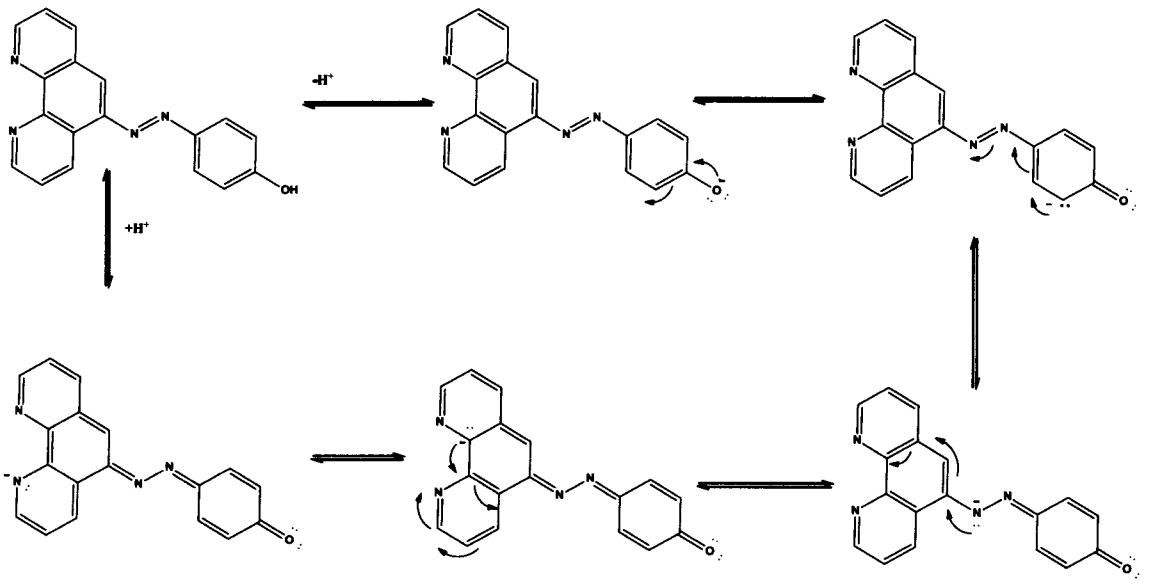

Scheme 1: Resonance structures upon deprotonation of phenol in phen-azo-phenol.

To investigate further the spectral solvent dependence and acid-base properties, the absorptivity was recorded in three different organic solvents in the presence added H^+ or OH^- (Figures 3g-i). The absorption in basic medium was obtained by the addition of one drop of 10% NaOH to the diluted solutions of phen-azo-phenol in DMSO, acetone and MeOH. In all of these solvents the absorbance was red shifted and the intensity increased as expected due to the deprotonation and delocalization of electrons (Scheme 2).

However, in acidic medium, where one drop of 2 M HCl was added to the diluted solutions of phen-azo-phenol, the maximum at ~500 nm disappeared and the absorption at ~ 400 nm dominated.

V.2 UV-Vis spectra of ruthenium polypyridyl complexes

The absorption spectra of these complexes in the visible region arose from both metal-ligand charge transfer (MLCT) transitions and the transitions involving azo dyes. The MLCT transitions involved promotion of an electron from a metal $d\pi$ orbital to a ligand π^* orbital. The assignment of the MLCT transitions for the studied complexes was based on the prototype $Ru^{II}(bpy)_3^{2+}$.

The UV-Vis spectrum of $Ru^{II}(bpy)_3^{2+}$ in MeOH is shown in Figure 9k. This is identical to Figure I-5 from the Introduction. Ru(II)-polypyridyl complexes generally show a broad MLCT absorption around 450 nm which has a high energy shoulder (around 420 nm in $Ru^{II}(bpy)_3^{2+}$). A barely noticeable metal-centered (MC) transition (d-d transition) is found in the 320 to 340 nm range. Intense π-π^* ligand centered (LC) transitions are typical for Ru(II) polypyridyl complexes in the 270-300 nm range. Finally, a higher energy MLCT can be observed in $Ru^{II}(bpy)_3^{2+}$ at approximately 240 nm. As stated previously, it would be expected that Ru(II) polypyridyl complexes involving azo-dye ligands to show UV-Vis spectra similar to the $Ru^{II}(bpy)_3^{2+}$ with additional absorptions due to the azo-dye chromophore.

The spectra of the third and fourth fractions for the complex $[(mcbpy)_2Ru^{II}$(phen-azo-phenol)$](PF_6)_2$ were recorded in MeOH (Figures 5i-j). Each spectrum showed three bands in the visible region. The first peak at ~ 460-462 nm along with the peak at 420 nm represent the broad MLCT absorption typical of Ru(II) polypyridyl complexes. The peak

at approximately 388-390 nm is assigned as arising from the absorption of the phen-azo-phenol ligand. The absorption maximum in the UV region at 288 nm for the 3rd fraction and the broad absorption envelope centered at 273 nm (4th fraction) are assigned as arising from intraligand π-π^* transitions centered on the 4-methyl-4'-carboxy-2,2'-bipyridine ligands and the 1,10-phenanthroline portion of phen-azo-phenol. The absorption maxima at around 250 nm most likely correspond to the higher energy MLCT transitions.

The UV-Vis spectrum of $[(dmbpy)_2Ru^{II}(phen\text{-}azo\text{-}phenol)](PF_6)_2$ in MeOH is shown in Figure 6i. The MLCT absorption is at 460 nm with the shoulder at approximately 434 nm. The absorption of the coordinated phen-azo-phenol is at 384 nm and appears slightly lower in intensity than the MLCT bands. A maximum at 280 nm (π-π^* bpy and phen absorption) and a high energy MLCT (just over 250 nm) are observed.

The third complex $[(dcbpy)_2Ru^{II}(phen\text{-}azo\text{-}phenol)](PF_6)_2$ was also dissolved in MeOH and the UV-Vis spectrum was recorded (Figure 9e). The MLCT absorptions are once again apparent at 460 nm and 430 nm. The peak due to phen-azo-phenol (390 nm) is red shifted slightly (compared to the other two complexes) but also noticeably more intense. The π-π^* band is also red-shifted (to 300 nm). The higher energy MLCT is centered at around 250 nm.

A very common solvent used for spectroscopic and electrochemical work on Ru(II) polypyridyl complexes is CH_3CN. This solvent shows particularly wide spectroscopic and electrochemical windows and typically dissolves PF_6^- salts of Ru(II) polypyridyl complexes quite well. Therefore, UV-Vis spectra in neat CH_3CN were taken for the Ru(II) complexes presented here (Figures 9i-j). This led to two unexpected results. The

first was that $[(mcbpy)_2Ru^{II}(phen\text{-}azo\text{-}phenol)]^{2+}$ was completely insoluble in CH_3CN.Therefore, only the spectra of $[(dmbpy)_2Ru^{II}(phen\text{-}azo\text{-}phenol)]^{2+}$ (Figure 9i) and $[(dcbpy)_2Ru^{II}(phen\text{-}azo\text{-}phenol)]^{2+}$ (Figure 9j) were recorded in CH_3CN. The second unexpected result was dramatic change in the visible absorption for $[(dmbpy)_2Ru^{II}(phen\text{-}azo\text{-}phenol)]^{2+}$ in CH_3CN. This complex turns a bright purple color in this solvent. In addition, it appears that it involves a different mechanism besides simple deprotonation of the phen-azo-phenol. The origin of this spectral change is still under investigation.

All three Ru(II) complexes have at least one ionizable H-atom. Therefore, it was decided to record the UV-Vis spectra for the three complexes in the presence of added acid or base. No significant change in the spectrum was observed for these complexes in MeOH after the addition of 1 drop of concentrated H_2SO_4. The UV-Vis spectrum of $[(mcbpy)_2Ru^{II}(phen\text{-}azo\text{-}phenol)]$ was obtained and is shown in Figure 9h. The complex didn't dissolve in CH_3CN. However, when base is added to the solution in MeOH the absorbance at 390 nm due to the coordinated phen-azo-phenol shifted to approximately 500 nm and increased in intensity. This shift is most likely due to deprotonation of the phenol –OH in phen-azo-phenol. The MLCT band didn't shift but appeared to increase in intensity, most likely due to the additive effect of the intense phen-azo-phenol observation. The UV region showed no noticeable peak shifts.

The UV-Vis spectra of $[(dmbpy)_2Ru^{II}(phen\text{-}azo\text{-}phenol)]^{2+}$ in MeOH and CH_3CN is shown in Figure 9i. The complex was soluble in both MeOH and CH_3CN. The spectrum in CH_3CN was different than the one in MeOH. The absorbance maximum at 390 nm in MeOH appears to shift to 590 nm in CH_3CN. The maximum at 460 nm in MeOH was assigned before to the MLCT[9]; however, the band at 590 nm in CH_3CN can be due to the

absorption of phen-azo-phenol and the effect of CH_3CN polarity on MLCT. The band at 455 nm in CH_3CN might be assigned to the MLCT transition band of the complex. The UV-Vis spectrum in acidic medium had a slight changes compared to the spectrum in MeOH. The absorbance band of phen-azo-phenol in acidified MeOH was enhanced compared to MLCT band in MeOH.

The spectrum of $[(dcbpy)_2Ru^{II}(phen\text{-}azo\text{-}phenol)](PF_6)_2$ was recorded under similar conditions and is shown in Figure 9j. As with $[(mcbpy)_2Ru^{II}(phen\text{-}azo\text{-}phenol)]^{2+}$, there was no evidence of phen-azo-phenol deprotonation in neat MeOH. The addition of base caused the expected shift in the phen-azo-phenol absorption maximum (380 nm to around 506 nm). As with the $[(mcbpy)_2Ru^{II}(phen\text{-}azo\text{-}phenol)]^{2+}$ complex, there was a small change in UV absorption. The peak at approximately 300 nm does show a slight blue-shift in the presence of added base, probably reflective of deprotonation of the acid groups on the bpy ligands.

VI. Cyclic voltammetry for Ruthenium(II) polypyridyl complexes

The complexes $[(dcbpy)_2Ru^{II}(phen\text{-}azo\text{-}phenol)]^{2+}$ and $[(mcbpy)_2Ru^{II}(phen\text{-}azo\text{-}phenol)]^{2+}$ were dissolved in DMF and $[(dmbpy)_2Ru^{II}(phen\text{-}azo\text{-}phenol)]^{2+}$ in CH_3CN. It was found that the complexes and the ligands were soluble in DMSO but this solvent has a limited range at positive potentials (up to around 1V). In this solvent the redox properties of R^{III}/Ru^{II} complexes can't be studied since their oxidative potentials are typically > + 1 V. The electrochemical properties of the ligand (phen-azo-phenol) were also studied in both CH_3CN and DMF to compare them with the complexes.

VI.1 Cyclic voltammetry (CV) for phen-azo-phenol:

The values of the redox potentials for this ligand are shown in Table 9. The CVs were recorded in both DMF and CH_3CN using either glassy carbon (GC) or platinum (Pt)

electrodes (Figures 18-20). The CV's were recorded in these two solvents since the ruthenium complexes studied here were soluble in either CH_3CN or DMF. It was found that somewhat better signal could be obtained when the GC working electrode was used compared to a Pt working electrode as shown in Figure 19. This was thought to be due to the larger surface area of the GC (3.0 mm) compared to the Pt electrode (1.6 mm).

In DMF, the phen-azo-phenol was found to have three reduction waves (one of them irreversible) and two irreversible oxidation waves when DMF was used as shown in Figure 18. The two oxidation waves were at +0.12 V and +0.54 V versus the ferrocenium/ferrocene (Fc^+/Fc) internal standard. The three reductions were at Ec = -1.46, and $E_{1/2}$ = -2.07 and -2.52 V vs Fc^+/Fc. The first reduction was irreversible and it was assigned as arising from the diazo group. The second and third reductions ($E_{1/2}$ = -2.07 V, -2.52 V) were assigned to the phenanthroline moiety. In CH_3CN, one oxidation (E_a = +0.71 V) and two reductions (Ec = -1.32 V, $E_{1/2}$ = -1.32 V vs Fc^+/Fc) were observed (Figure 20). Both the oxidation and the reduction were shifted to more positive potentials in CH_3CN compared to DMF.

Table 9: Redox potentials for phen-azo-phenol vs Fc^+/Fc.

Figure #	Oxidation $E_{1/2}$ (V), ΔE_p (mV)	Reduction $E_{1/2}$ (V), ΔE_p (mV)
18[a,GC]	+0.12[irr]	-1.46[irr]
	+0.54[irr]	-2.07 (82.2)
		-2.52 (41.3)
20[b, GC]	+0.71[irr]	-1.32[irr], -1.97 (74.9)

[GC] Glassy carbon working electrode. [irr] Irreversible. [Pt] Platinum working electrode. [a] DMF /0.1 M TBAH. [b] CH_3CN/0.1M TBAH.

VI.2- Cyclic voltammetry of ruthenium(II) polypyridyl complexes

The redox properties of the ruthenium(II) complexes were investigated either in DMF or CH_3CN. The values of the redox potentials are shown in Tables 10 and 11. The

three Ru(II)-phen-azo-phenol complexes showed three to five reduction waves and two of them showed one oxidation wave. The reference compound, $[(bpy)_2Ru(phen)]^{2+}$ gave three reduction waves and one oxidation wave. The structures of all four complexes are shown in Scheme 3.

The results for the reference $[(bpy)_2Ru(phen)]^{2+}$ will be discussed first. In DMF this complex had three reduction waves and one oxidation wave (Figure 21). The three reduction waves were centered at $E_{1/2}$ = -1.73, -1.92 and -2.19 V respectively. The first two waves can be assigned as 1 ē reduction of each bpy ligand and the last wave (-2.19 V) as a reduction of the phen-ligand. Support of these assignments comes from Bard et. al.[10] where the CV's of both $Ru^{II}(bpy)_3^{2+}$ and $Ru^{II}(phen)_3^{2+}$ were recorded in CH_3CN. In this work, both $Ru^{II}(bpy)_3^{2+}$ and $Ru^{II}(phen)_3^{2+}$ show three closely-spaced reduction waves, with the $Ru^{II}(phen)_3^{2+}$ reductions consistently more negative than those of $Ru^{II}(bpy)_3^{2+}$. With regard to the oxidations of Ru(II) metal center, the $[(bpy)_2Ru(phen)]^{2+}$ complex gave a wave centered at +1.30 V in CH_3CN vs SSCE (Figure 22). This compares to +1.354 V and +1.40 V (vs SCE) obtained by Bard et al.[10] for $Ru^{II}(bpy)_3^{2+}$ and $Ru^{II}(phen)_3^{2+}$, respectively.

Table 10: Electrochemical date for $[(dcbpy)_2Ru^{II}(phen\text{-}azo\text{-}phenol)]^{2+}$, $[(mcbpy)_2Ru^{II}(phen\text{-}azo\text{-}phenol)]^{2+}$ and the reference compound $[(bpy)_2Ru^{II}(phen\text{-}azo\text{-}phenol)]^{2+}$ vs Fc^+/Fc in DMF (0.1 M TBAH, sample concentrated 1×10^{-3} M, WE: GC, Aux: Pt, Ref: Ag wire, scan rate: 100 mV s^{-1}).

Complex	Figure #	Oxidation $E_{1/2}$ (V), ΔE_p (mV)	Reduction $E_{1/2}$ (V), ΔE_p (mV)
$[(dcbpy)_2Ru^{II}(phen\text{-}azo\text{-}phenol)]$ **3**	24	ND	-2.35 (14.6) -2.07 (26.2) -1.86 (50.2) -1.25^{irr}
$[(mcbpy)_2Ru^{II}(phen\text{-}azo\text{-}phenol)]^{2+}$ **2**	26	+0.54 (43.6)	-2.34 (74.7) -2.13 (134.7) -1.93 (99.9) -1.78^{irr}, -1.19^{irr}
$[(bpy)_2Ru^{II}(phen)]^{2+}$ **4**	21	+0.82 (77.7)	-2.19 (74.1) -1.92 (72.2) -1.74 (76.1)

ND Not detected. irr Irreversible.

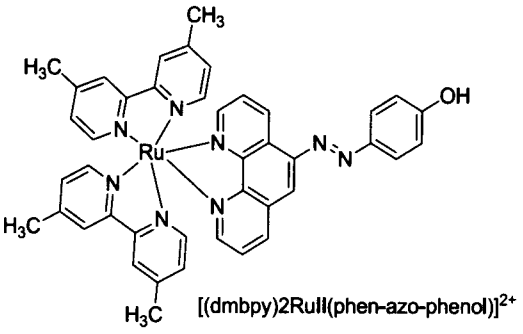

1

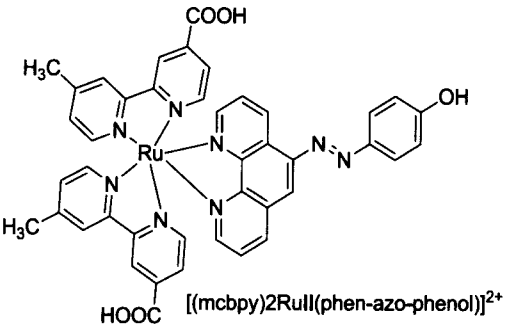

2

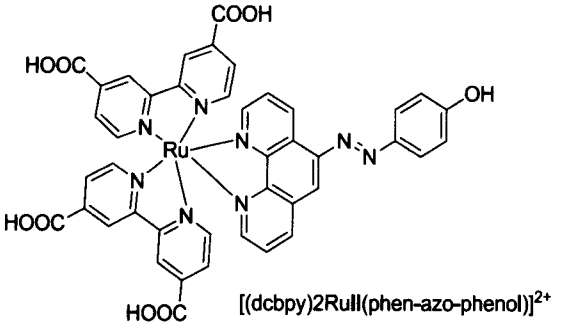

3

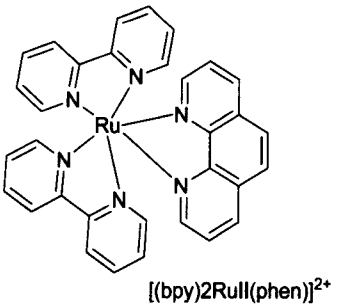

4

Scheme 3: Ruthenium(II) polypyridyl complexes

$[(dcbpy)_2Ru^{II}(phen\text{-}azo\text{-}phenol)]^{2+}$

The CV of this complex was obtained in DMF (Table 10 and Figure 24). This complex had an irreversible reduction at -1.25 V which was assigned to the azo group. The reductions at $E_{1/2}$ = -1.86 V and -2.07 V were assigned to the two dcbpy ligands. The third reduction $E_{1/2}$ = -2.35 V was assigned to the phenanthroline moiety. The peak separations (ΔE_p) were abnormally small for the two most negative reductions (26.2 mV and 14.6 mV, respectively). This may simply be due to the difficulty in pinpointing the maximum values in these weak and broad signals.

A metal-centered oxidation wave was not observed for $[(dcbpy)_2Ru^{II}(phen\text{-}azo\text{-}phenol)]^{2+}$. It is possible that the oxidation is shifted too far in the positive direction (outside of solvent cut-off, Figure 24). The presence of the electron withdrawing groups (-COOH) on the bpy ligands would remove the electron density from the bipyridine ring which in turn decrease the electron density on the metal center making the oxidation of Ru^{II} difficult.[11]

$[(mcbpy)_2Ru^{II}(phen\text{-}azo\text{-}phenol)]^{2+}$

This complex gave five reduction waves and one oxidation wave (Table 10 and Figures 25-26). The oxidation wave was at $E_{1/2}$ = +0.54 V and was assigned to the oxidation of the Ru^{II} metal center. The first (irreversible) reduction wave at -1.19 V was assigned as reduction of the azo dye group. The second (irreversible) reduction at -1.78 V was an unexpected wave. It would tempting to assign this as the reduction of the carboxyl group as shown in eq 1.[12]

$$-COOH + \bar{e} \longrightarrow -CO_2^{\cdot} + \tfrac{1}{2} H_2 \quad \text{eq 1}$$

However, this would mean that this reduction would have been observed for the $[(dcbpy)_2Ru^{II}(phen\text{-}azo\text{-}phenol)]^{2+}$ unless the two complexes show significantly different

pKa values for the –COOH groups. The third and fourth reduction waves were assigned to the mcbpy ligands and the fifth for the reduction of the phenanthroline ring.

$[(dmbpy)_2Ru^{II}(phen\text{-}azo\text{-}phenol)]^{2+}$

Electrochemical data for this complex were obtained in CH_3CN (Table 11, Figure 28). The results using a platinum working electrode (Figure 27) and GC working electrode (Figure 28) were very similar but peaks appeared slightly enhanced with GC. The complex showed four reduction waves and one oxidation wave (Table 11). The oxidation wave was centered at +0.82 V was assigned as oxidation of the Ru(II) center. There is some evidence for an oxidation wave before this one. The first (irreversible) reduction Ec = -1.34 V was for the reduction of the azo dye. The reduction wave centered at $E_{1/2}$ = -2.08 V and -2.27 V can be assigned as reduction of a bpy ligand and the phenanthroline portion of phen-azo-phenol, as with the other complexes. The reduction wave centered at -1.59 V is somewhat problematic to assign. Although it is one of four (expected) reductions for this complex, the positive shift compared to complexes (2) and (3) is difficult to explain. This result is more evidence (along with ^{1}H-NMR and UV-Vis data) that the true identity (and structure) of this complex is not clear.

Table 11: Electrochemical data for $[(dmbpy)_2Ru^{II}(phen\text{-}azo\text{-}phen)]^{2+}$ and the reference compound $[(bpy)_2Ru^{II}(phen)]^{2+}$ in CH_3CN (0.1 M TBAH, sample concentrated 1×10^{-3} M, scan rate: 100 mV s^{-1}). All potentials reported vs Fc^+/ Fc internal standard.

Complex	Figure #	Oxidation $E_{1/2}$ (V), ΔE_p (mV)	Reduction $E_{1/2}$ (V), ΔE_p (mV)
$[(dmbpy)_2Ru^{II}(phen\text{-}azo\text{-}phenol)]^{2+}$ **1** WE: GC, Aux: Pt wire, Ref: Ag wire	28	+0.82 (95.9)	-2.27 (111.2) -2.08 (156.0) -1.59 (148.6) -1.34[irr]
$[(bpy)_2Ru^{II}(phen)]^{2+}$ **4** WE: GC, Aux: Pt wire, Ref: SCE	22, 23	+0.89 (57.2)	-2.19 (79.5) -1.92 (100.5) -1.73 (41.1)

[irr] Irreversible.

VII. Future work

This thesis can be divided into parts: the first part was the synthesis and purification of phen-azo-phenol (and Ru(II) complexes) and the second was the synthetic attempts at phen-indigo. The UV-Vis, ^{1}H-NMR and the CV results of $[(dmbpy)_2Ru^{II}(phen\text{-}azo\text{-}phenol)]^{2+}$ showed unexpected results compared to $[(mcbpy)_2Ru^{II}(phen\text{-}azo\text{-}phenol)]^{2+}$ and $[(dcbpy)_2Ru^{II}(phen\text{-}azo\text{-}phenol)]^{2+}$. The identity and structure of this complex is not truly known so a further study of this complex can be conducted for a future project. The second part of this thesis can be regarded as a survey of the possible methods for the synthesis of the phen-indigo ligand. The synthesis of phen-indigo was not completed so a possible future project would be the synthesis of this ligand. One possible approach would involve using 5-NH_2-phen and diethyl ketomalonate hydrate[13] followed by the reduction of the phen-isatin using $LiAlH_4$.[14]

References:

1. Reactions of Arenes. Electrophilic Aromatic Substitution. http://www.chem.-ucalgary.ca/courses/351/Carey5th/Ch12/ch12-3.html (accessed 6/1/2012).
2. Mao, Minchong. MS. Thesis, Eastern Illinois University, July. 1997.
3. Görl, H.; Henry, W.; Popp, J.; Rau, S.; Schäfer, B.; Schmitt, M.; Schwalbe, M.; Tschiervel, S.; Vaughan, G.; Vos, J.G. Synthesis and Characterization of Poly(bipyridine)ruthenium Complexes as Building Blocks for Heterosupramolecular Arrays. *Eur. J. Inorg. Chem.* **2008**, 3310-3319.
4. Jiang, H.Z., Wang, S.; Wu, H. Synthesis of cis-Dithiocyanato bis(4,4'-Dicarboxylic acid-2,2'-bipyridine)ruthenium and its Application in Dye-Sensitized Solar Cells. *Asian J. Chem.* **2008**, *20*, 3438-3446.
5. Lu, Z.; Twieg, R.J. Copper-Catalyzed Aryl Amination in Aqueous Media with 2-Dimethylaminoethanol Ligand. *Tetrahedron Lett.* **2005**, *46*, 2997-3001.
6. Hendrickson, J.B.; Hussoin, Md.S. Reactions of Carboxylic Acids with "Phosphonium Anhydrides". *J. Org. Chem.* **1989**, *54*, 1144-1149.
7. Hennig, A.; Huber, S.M.; Pühlhofer, F.G.; Weiss, R. A Novel and General One-Pot Synthesis of Isatine and Its N-Unsubstituted Derivatives via Nucleophilic Substitution Reactions on 1,2-Bis(dimethylamino)-1,2-dichloroethene. *J. Heterocyclic Chem.* **2009**, *46*, 421-427.
8. Perdoncin, G.; Scorran0, G. Protonation Equilibrium in Water at Several Temperatures of Alcohols, Ethers, Acetone, Dimethyl Sulfide, and Dimethyl Sulfoxide. *J. Am. Chem. Soc.* **1977**, *99*, 6983-6986.

9. Felix, F.; Ferguson, J.; Güdel, U.H.; Ludi, A. The Electronic Spectrum of $Ru(bpy)_3^{2+}$. *J. Am. Chem. Soc.* **1980**, *102*, 4096-4102.

10. Tokel-Takvoryan, N.; Hemingway, R.E.; Bard, A.J. Electrogenerated Chemilumiluminescence. XIII. Electrochemical and Electrogenrated Chemiluminescence Studies of Ruthenium Chelates. *J. Am. Chem. Soc.* **1973**, *95*, 6582-6589.

11. Hou, Y.J.; Cao, Y.; Shen, J.C.; Tia, W.J.; Wu, F.; Xie, P.H.; Zhang, B.W. Spectroscopic and electrochemical properties of ruthenium(II) polypyridyl complexes. *J. Chem. Soc., Dalton Trans.* **1999**, 4217-4221.

12. Ahlgrén, M.; Eskelinen, E.; Haukka, M.; Luukkanen, S.; Pakkanen, T.A. Redox and Photochemical Behavior of Ruthenium(II) Complexes with H_2dcbpy Ligand (H_2dcbpy = 2,2'-bipyridine-4,4'-dicarboxylic acid). *J. Chem. Soc., Dalton Trans.*, **2000**, 2745-2752.

13. Boone, B.J.; Rauls, T.J.; Rice, K.C.; Rubin, A.B. Synthesis, Antimalarial Activity, and Phototoxicity of some Benzo[h]quinoline-4-methanols. *J. Med. Chem.* **1976**, *19*, 887-892.

14. Khoshtanya, T.E.; Kurkovskaya, L.N.; Mirziashrili, N.T.; Sikharnlidze, M.I.; Tsintsadze, T.G. Novel Route For Obtaining Isomeric Benzo[b]Thiophenoindolines. *Chem. Heterocycl. Comp.* **2002**, *38*, 472-476.

Figures:

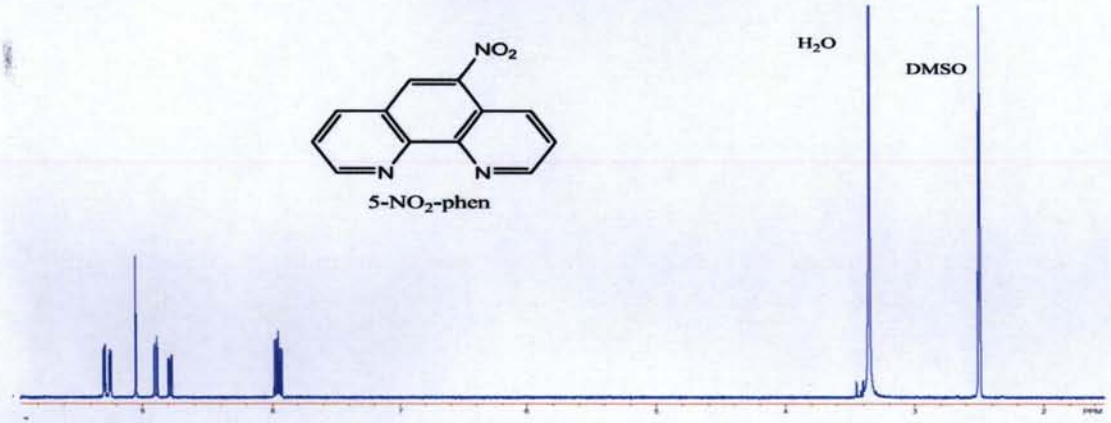

Figure 1a: ^{1}H-NMR spectrum (MEM2A373) of 5-NO_2-phen (111511-A-AH) in d_6-DMSO.

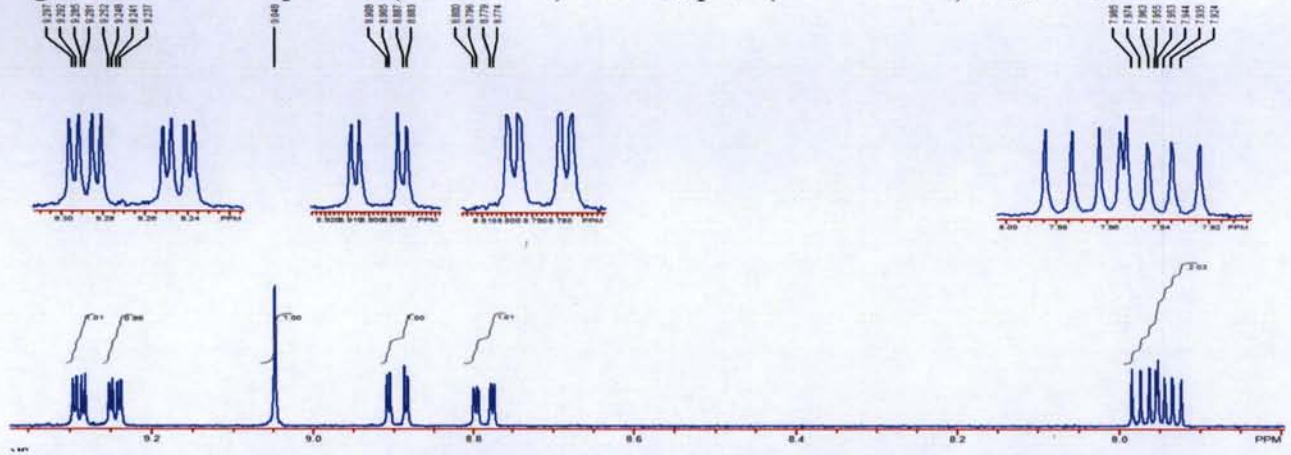

Figure 1b: ^{1}H-NMR spectrum (MEM2A373) for 5-NO_2-phen (111511-A-AH) in d_6-DMSO.

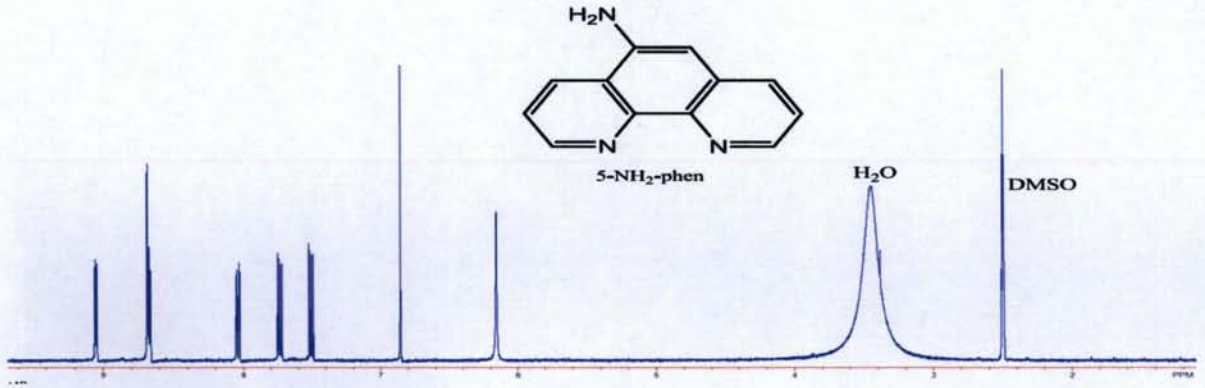

Figure 2a:[1]H-NMR spectrum (MEM2A374) of 5-NH_2 -phen (111611-A-AH) in d_6-DMSO.

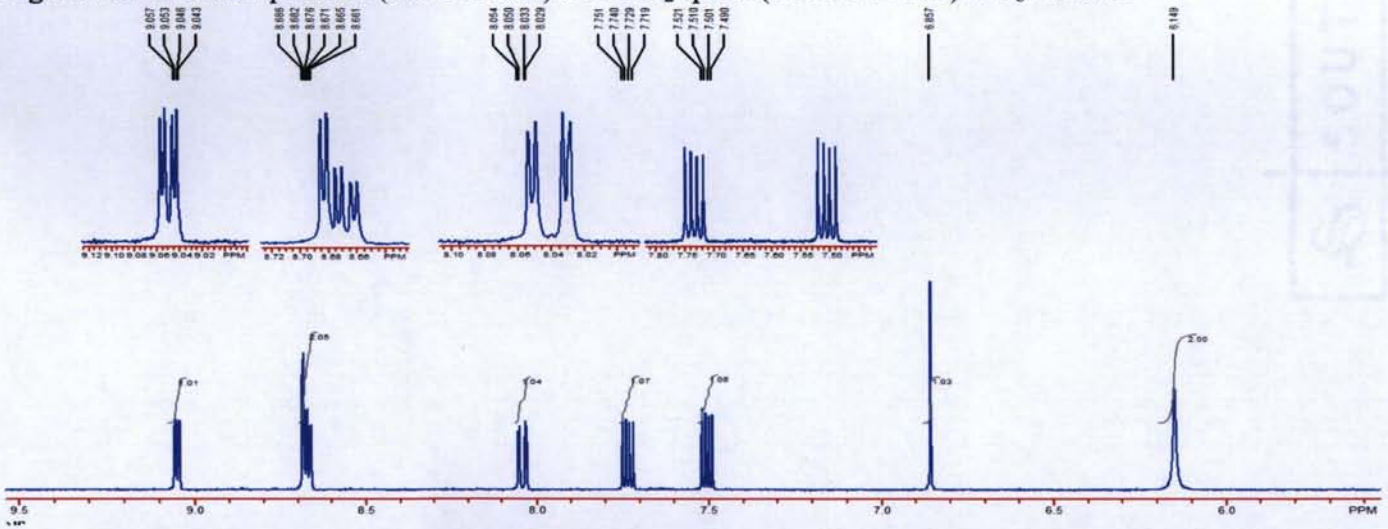

Figure 2b: 1H-NMR spectrum (MEM2A374) of 5-NH2 -phen (111611-A-AH) in d6-DMSO expanded.

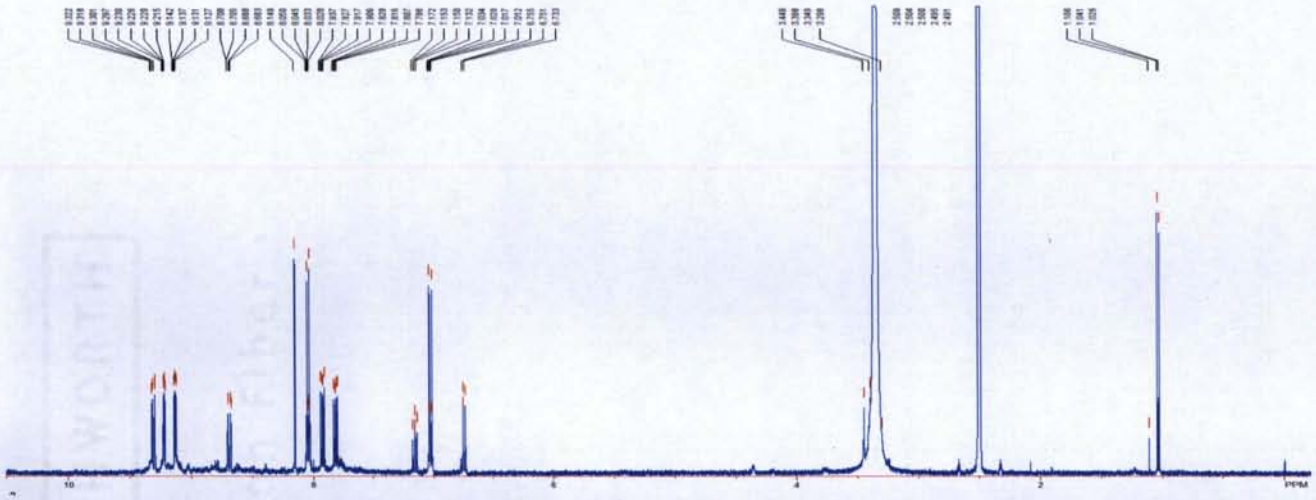

Figure 3a: ^{1}H-NMR (MEM2A243) of phen-azo-phenol crude product (053011-A-AH) in d_6-DMSO.

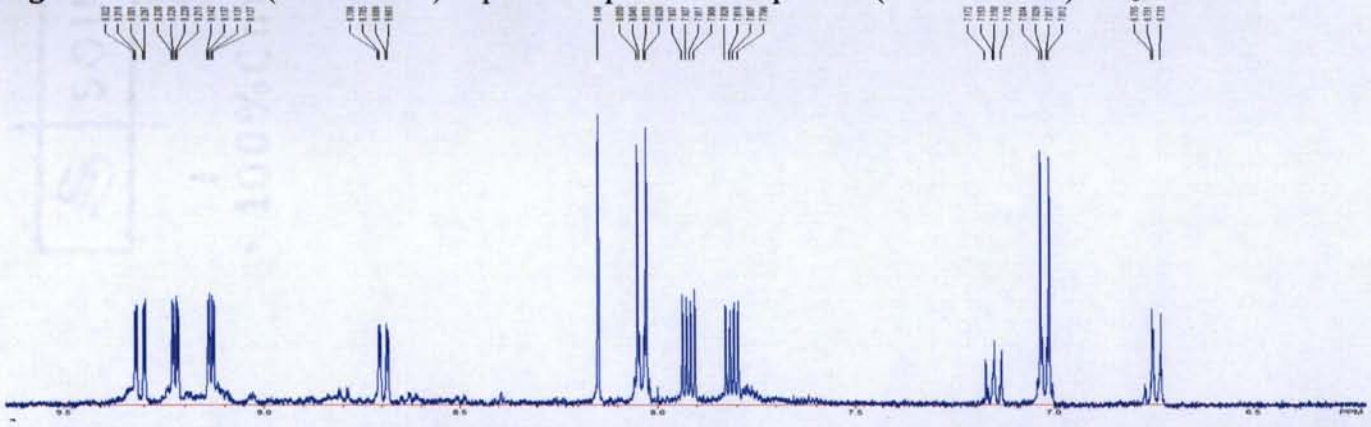

Figure 3b: ^{1}H-NMR spectrum (MEM2A243) of phen-azo-phenol crude product (053011-A-AH) in d_6-DMSO expanded.

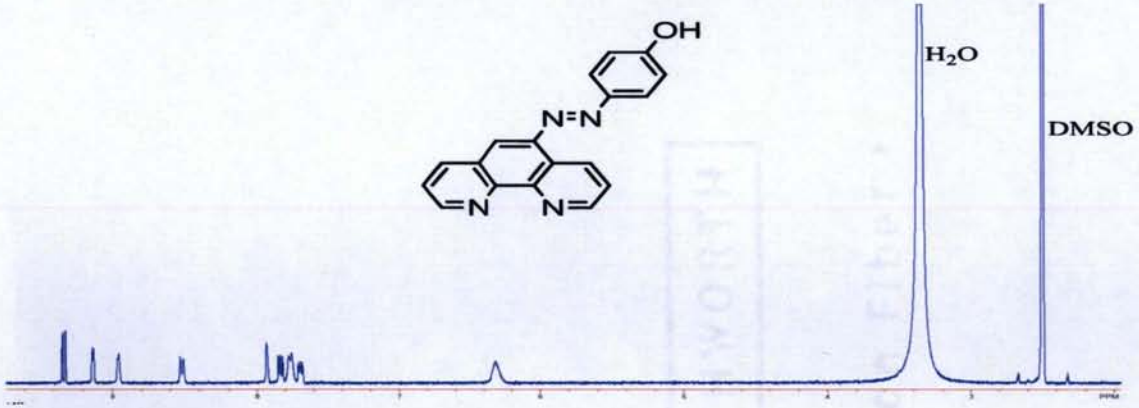

Figure 3c:[1]H-NMR spectrum (MEM2A246) for phen-azo-phenol (053111-A-AH) in d_6-DMSO.

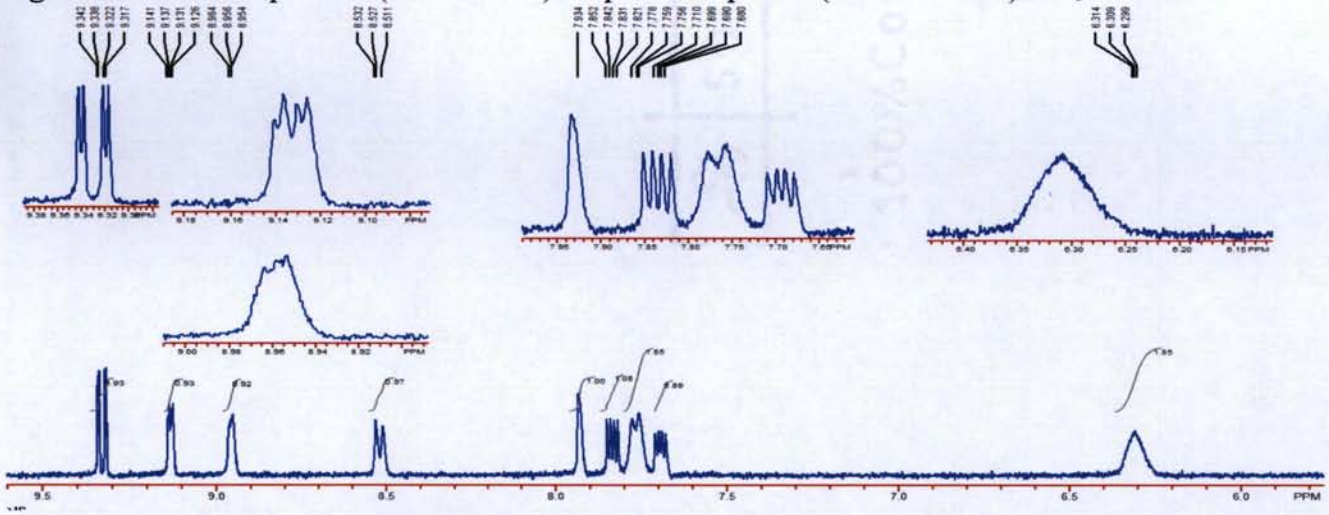

Figure 3d:[1]H-NMR spectrum (MEM2A246) for phen-azo-phenol (053111-A-AH) in d_6-DMSO.

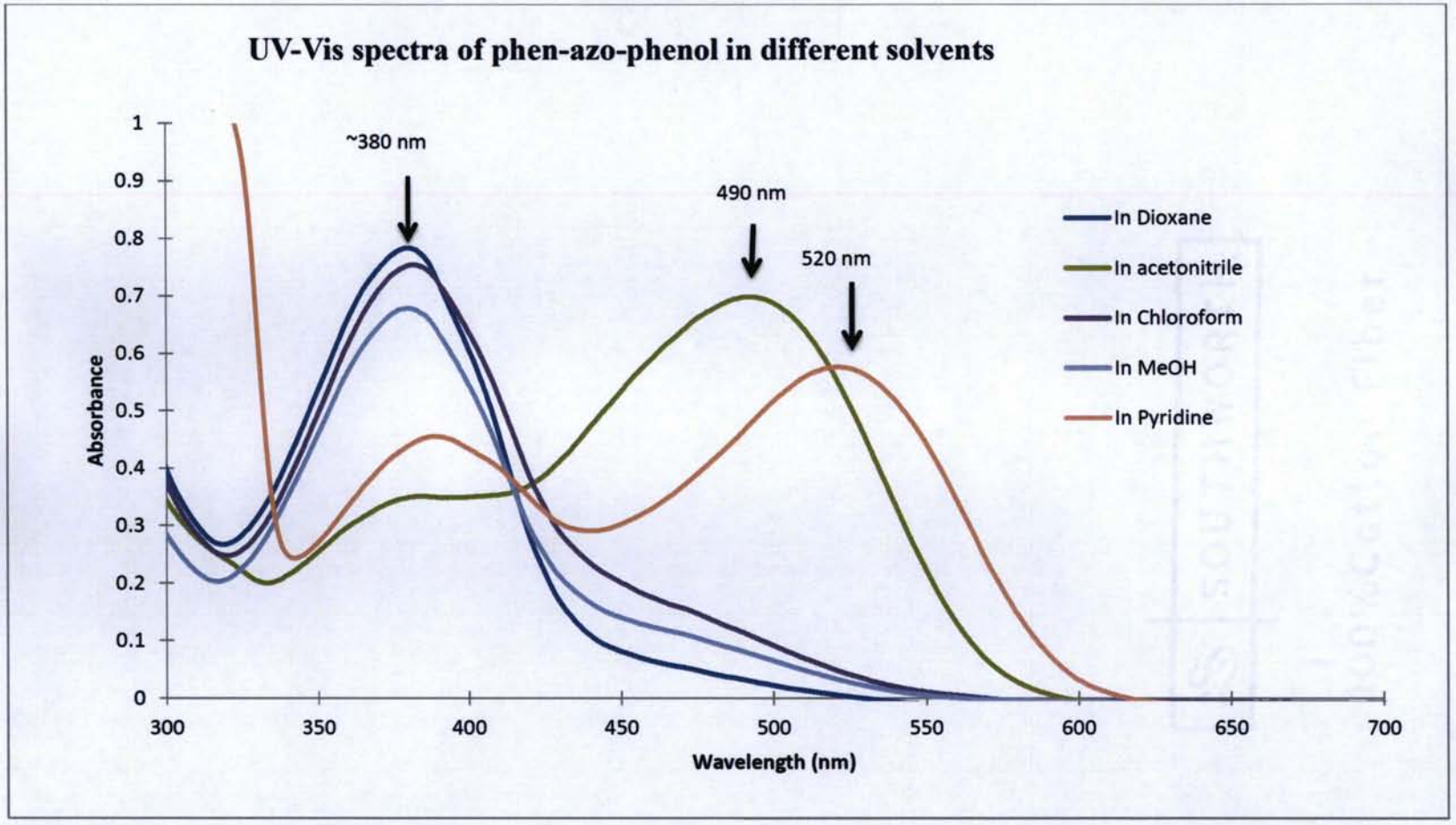

Figure 3e: UV-Vis spectra of phen-azo-phenol (053111-A-AH).

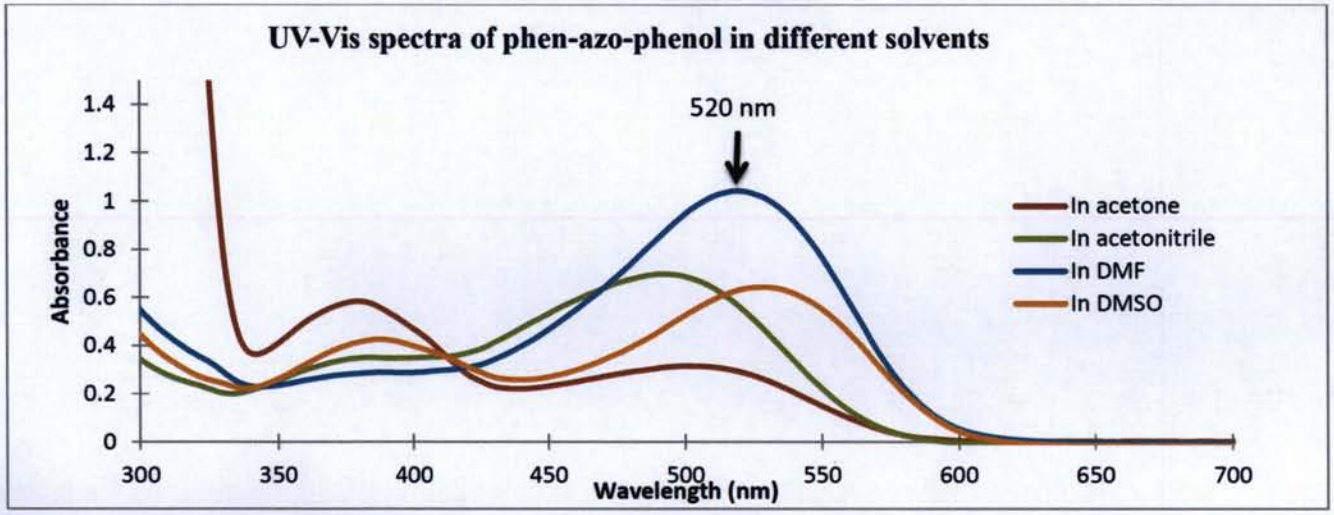

Figure 3f: UV-Vis spectra of phen-azo-phenol (053111-A-AH).

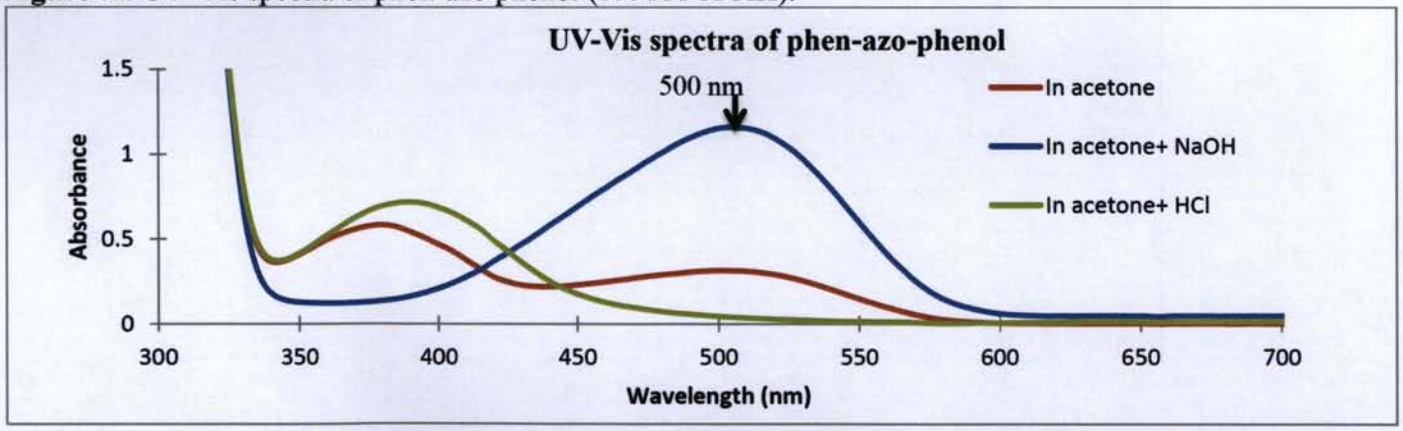

Figure 3g: UV-Vis spectra of phen-azo-phenol (053111-A-AH) in acetone and in acetone with added acid or base.

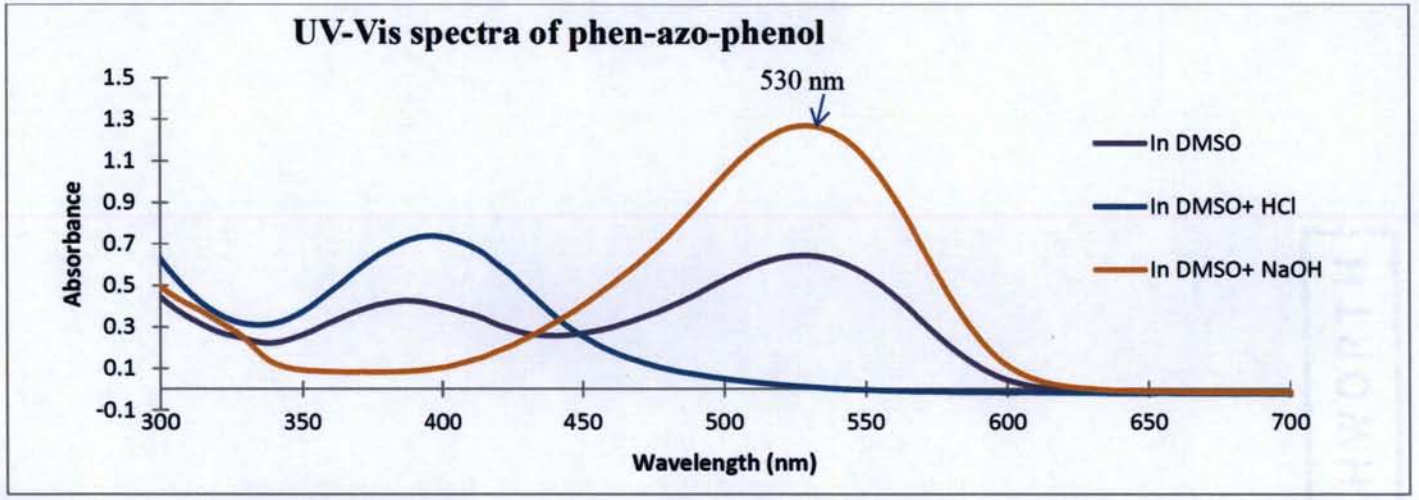

Figure 3h: UV-Vis spectra of phen-azo-phenol (053111-A-AH) in DMSO and in DMSO with added acid or base.

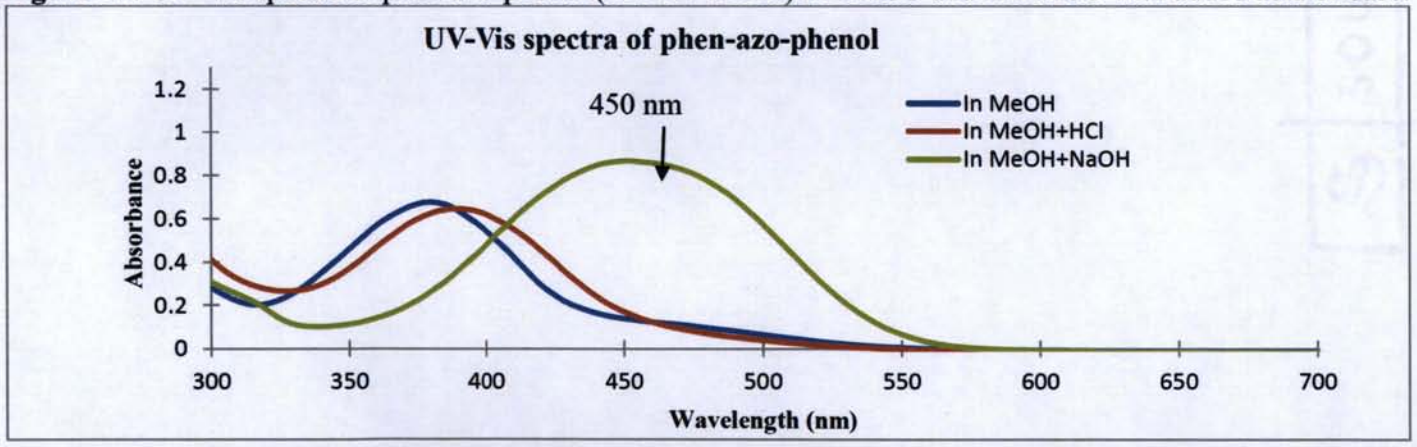

Figure 3i: UV-Vis spectra of phen-azo-phenol (053111-A-AH) in MeOH and in MeOH with added acid and base.

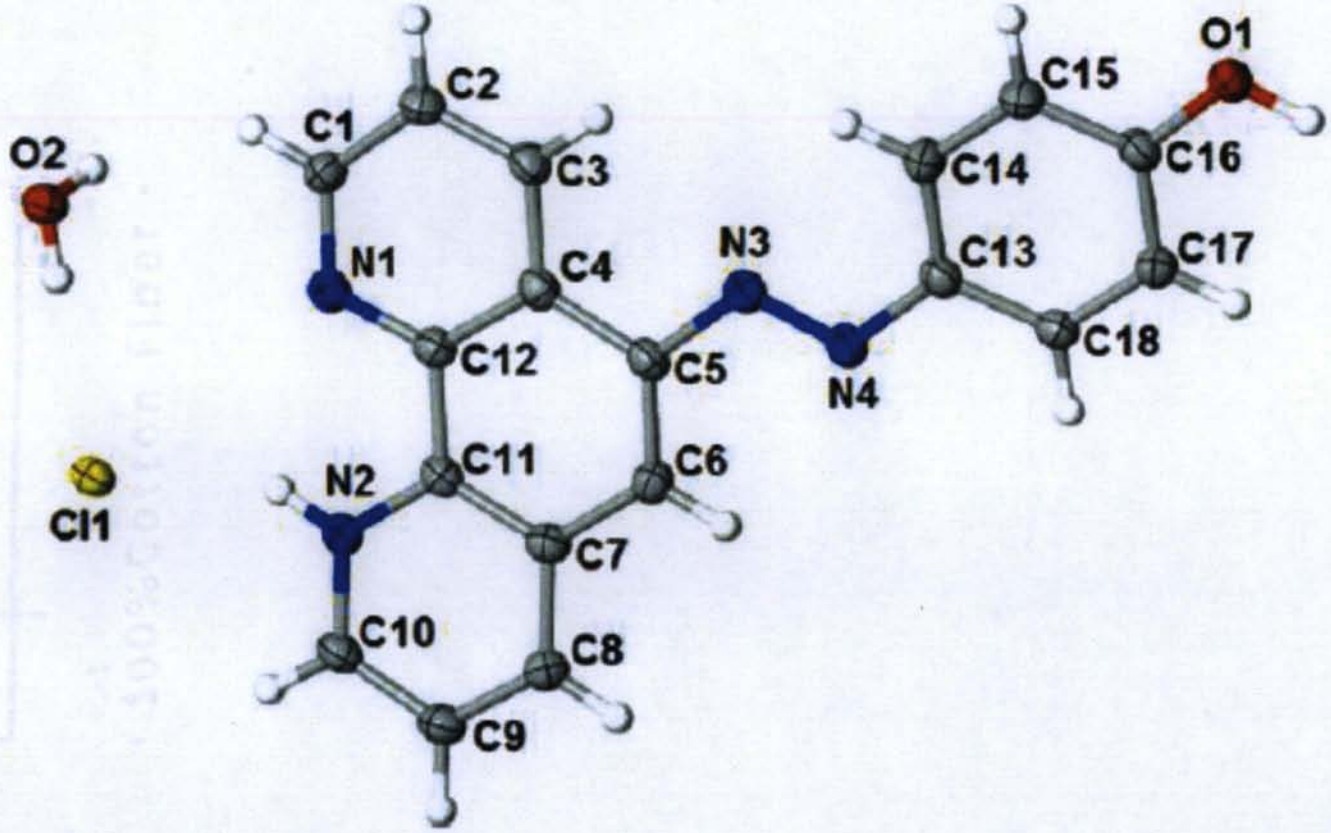

Figure 3j: Crystal structure of phen-azo-phenol (053111-A-AH).

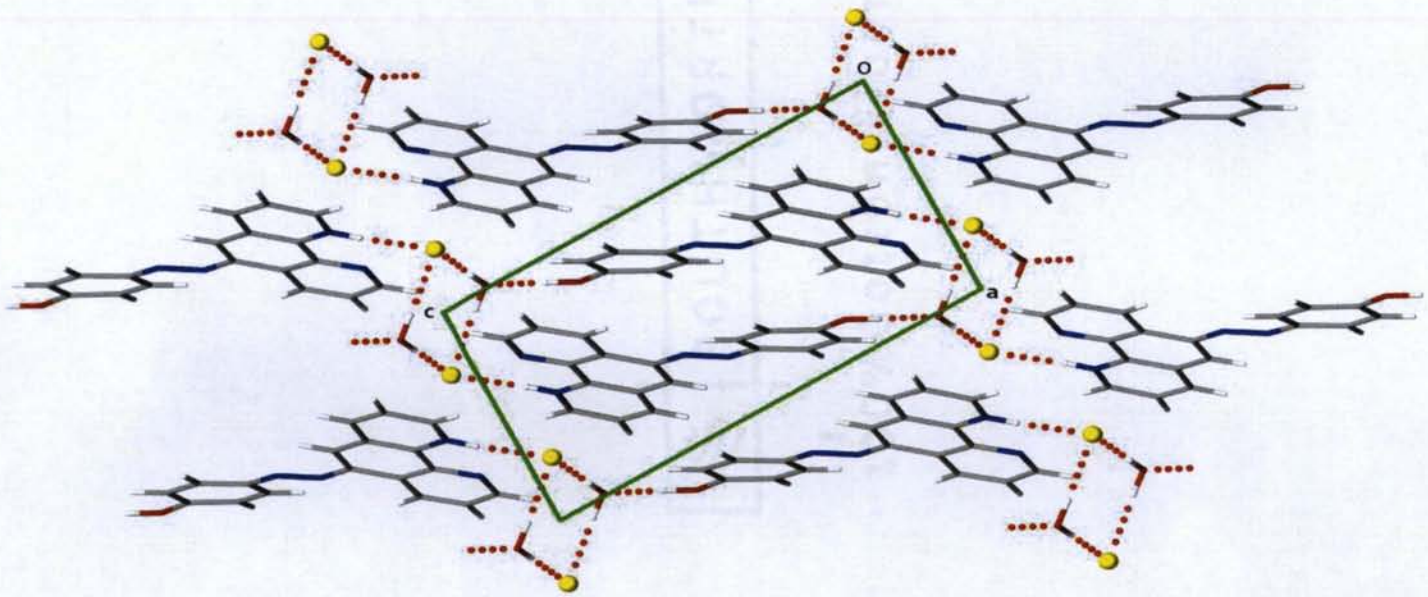

Figure 3k: Crystal packing of phen-azo-phenol (053111-A-AH).

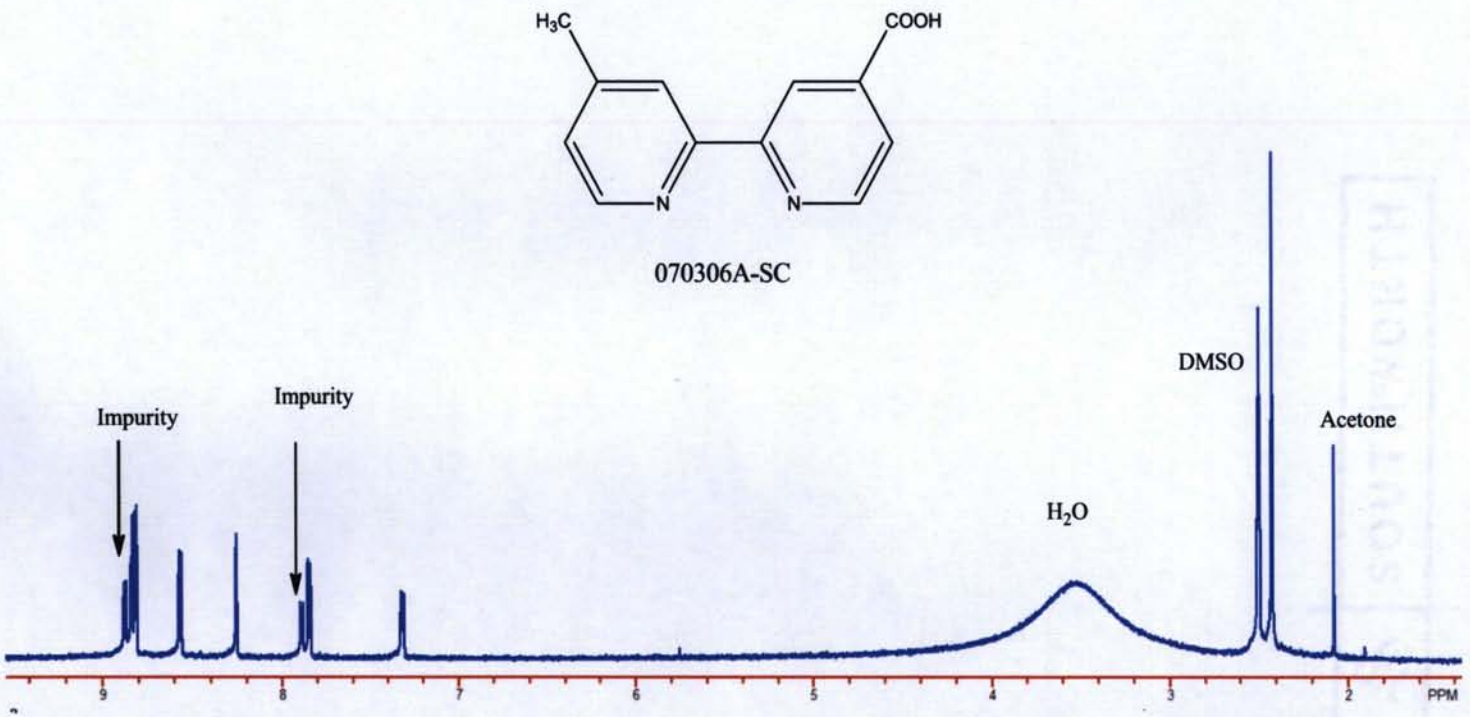

Figure 4a: ^{1}H-NMR (MEM2A404) of 4-carboxy-4'-methyl-2,2'-bipyridine (070306A-SC) in d_6-DMSO.

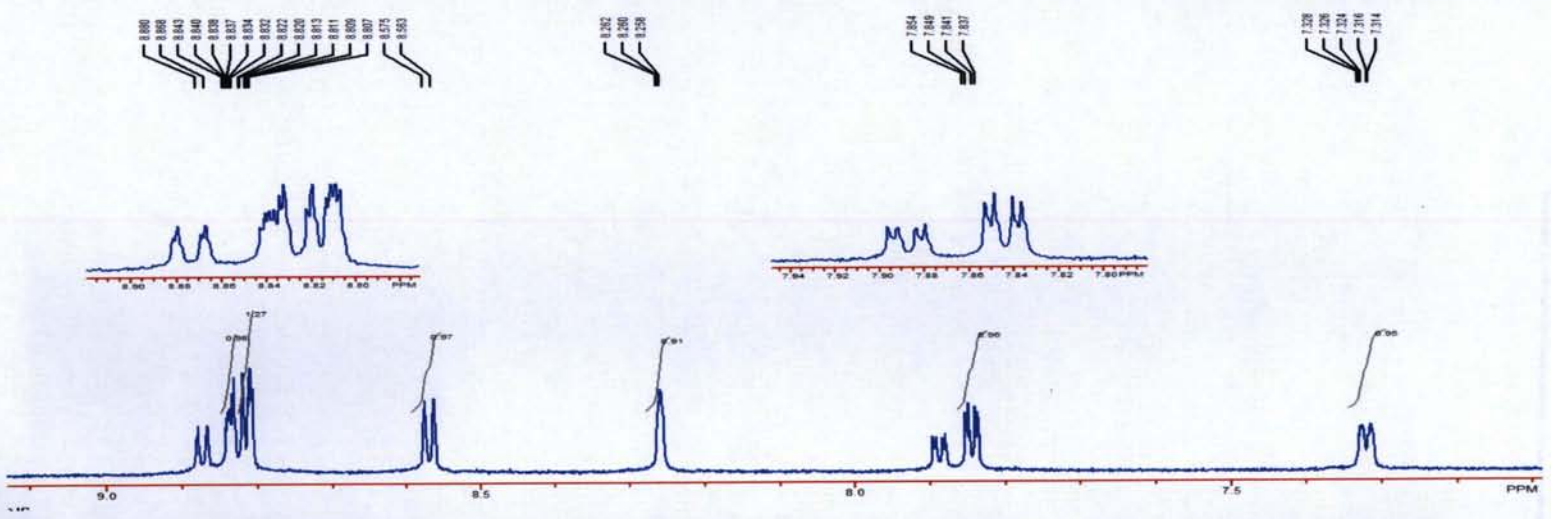

Figure 4b: ^{1}H-NMR (MEM2A404) of 4-carboxy-4'-methyl-2,2'-bipyridine (070306A-SC) in d_6-DMSO expanded.

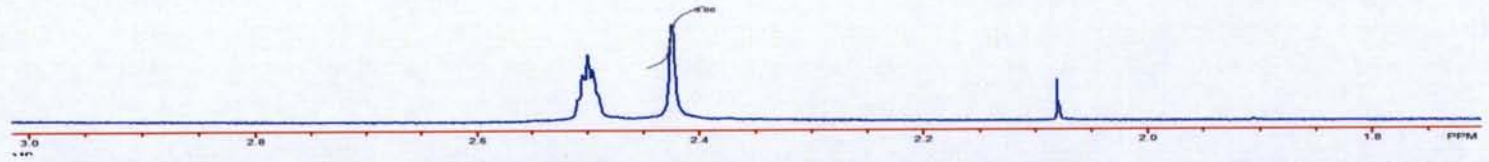

Figure 4c: ^{1}H-NMR (MEM2A404) of 4-carboxy-4'-methyl-2,2'-bipyridine (070306A-SC) in d_6-DMSO expanded showing the methyl protons.

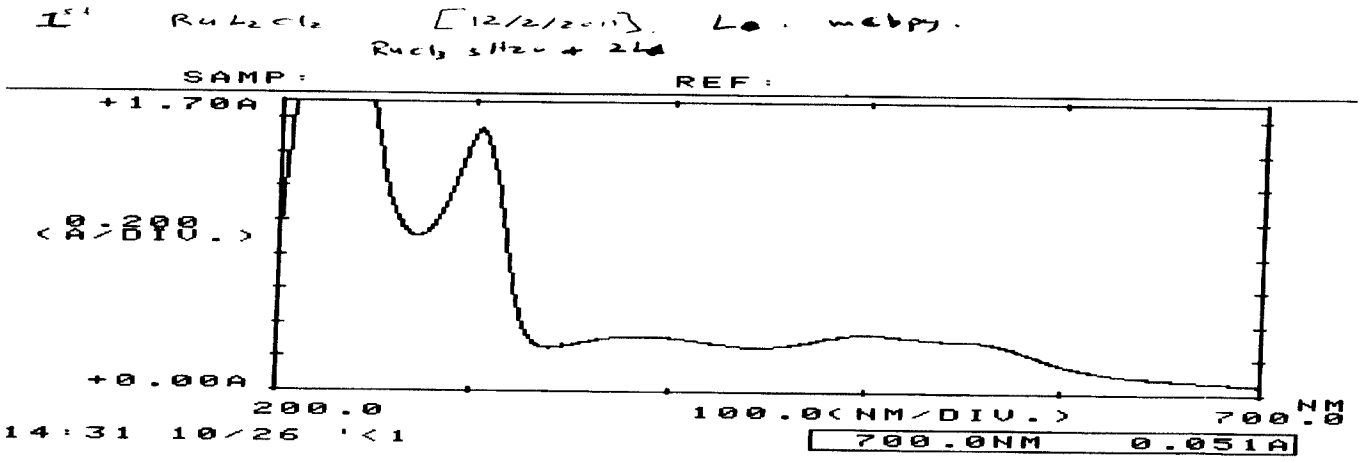

Figure 4d: UV-Vis spectrum in MeOH for the reaction of $RuCl_3.3H_2O$ with 4-carboxy-4'-methyl-2,2'-bipyridine initially after mixing.

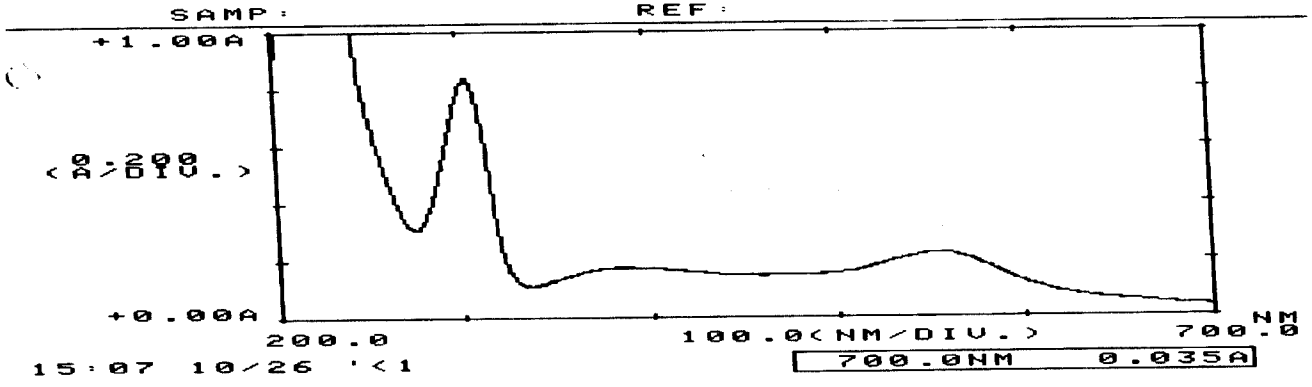

Figure 4e: UV-Vis spectrum in MeOH for the reaction of $RuCl_3.3H_2O$ with 4-carboxy-4'-methyl-2,2'-bipyridine after 1 h of the reaction.

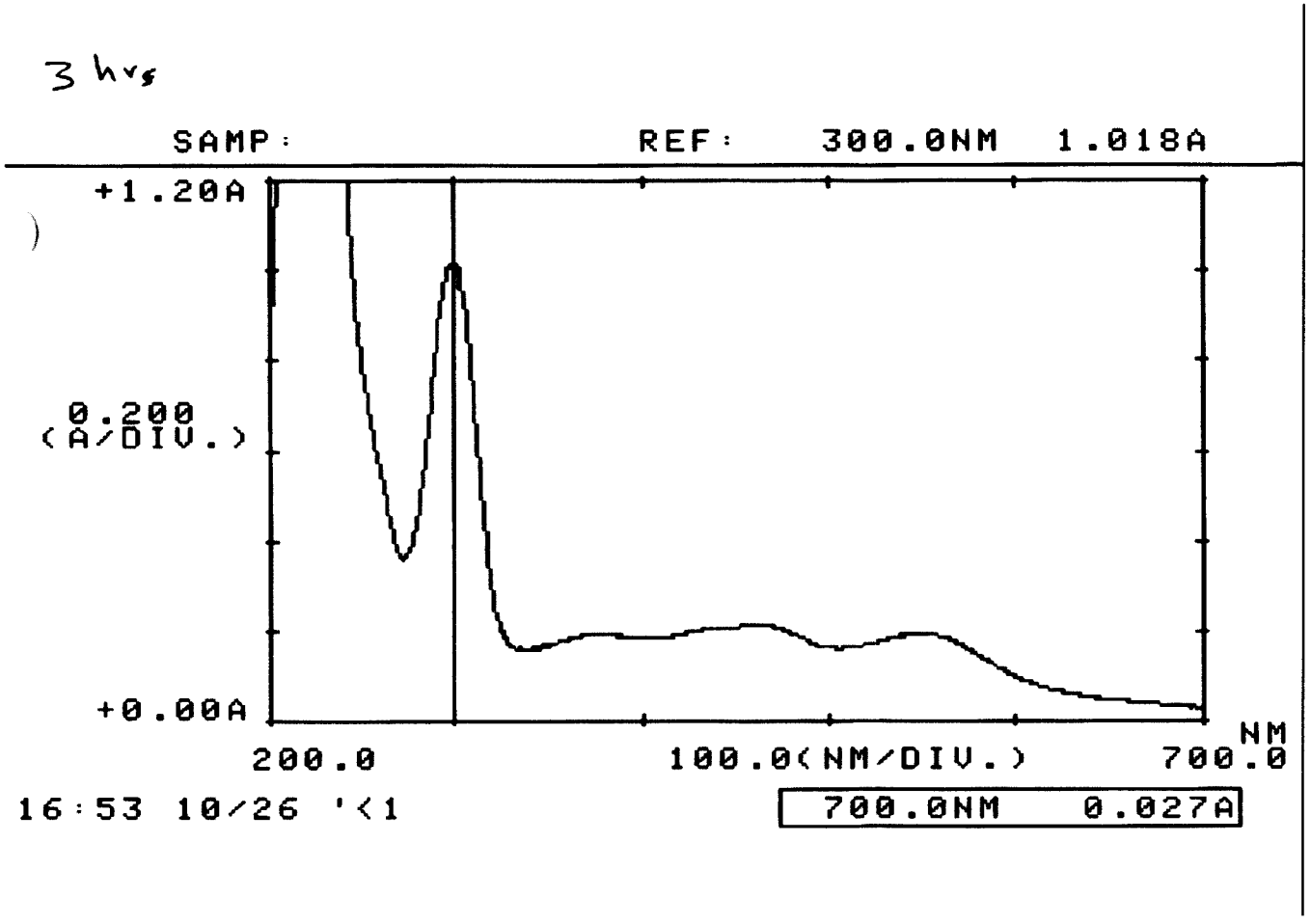

Figure 4f: UV-Vis spectrum in MeOH for the reaction of $RuCl_3.3H_2O$ with 4-carboxy-4'-methyl-2,2'-bipyridine after 3 h of the reaction.

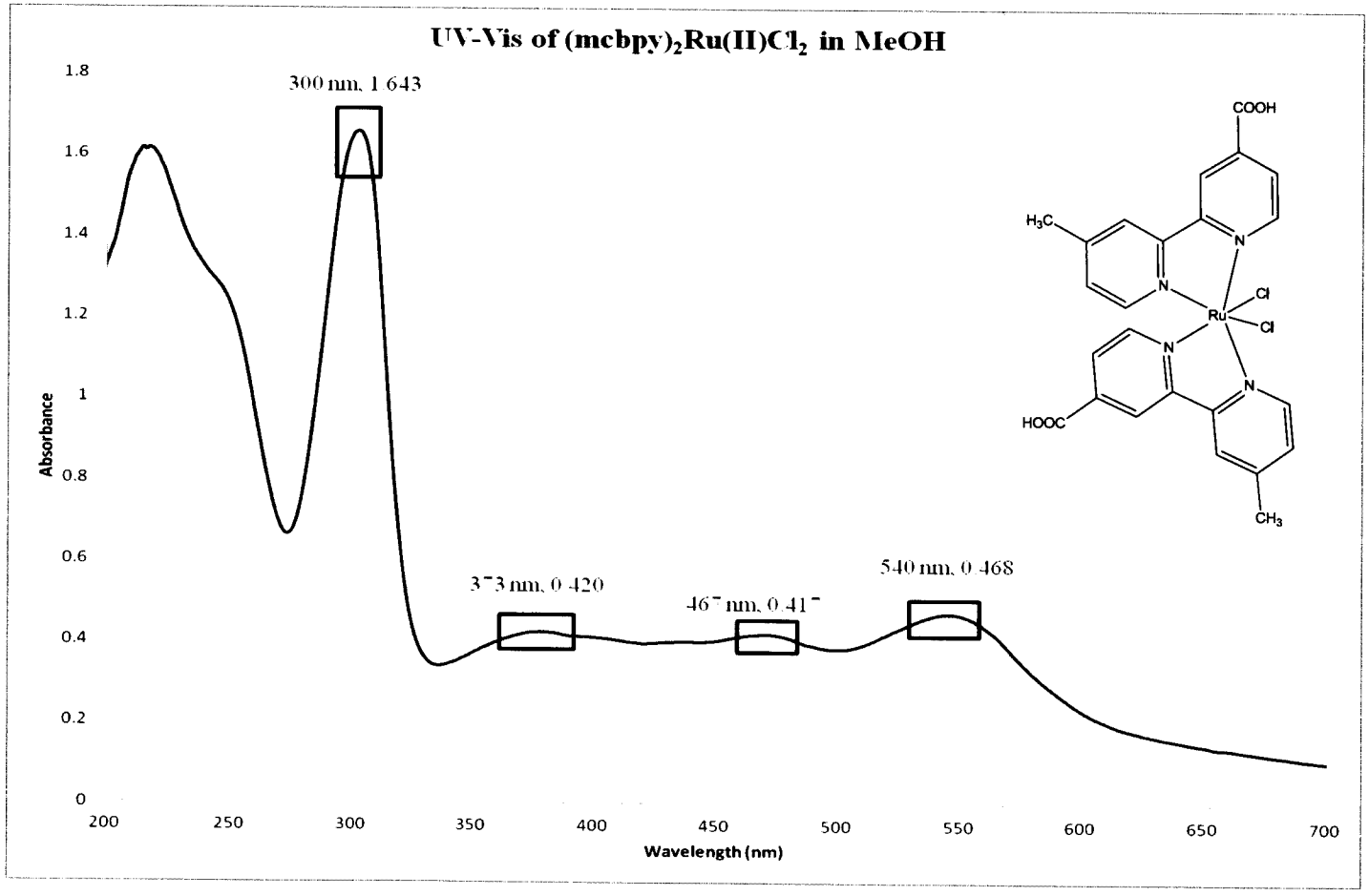

Figure 4g: UV-Vis of $Ru^{II}(mcbpy)_2Cl_2$ (120511-B-AH) in MeOH.

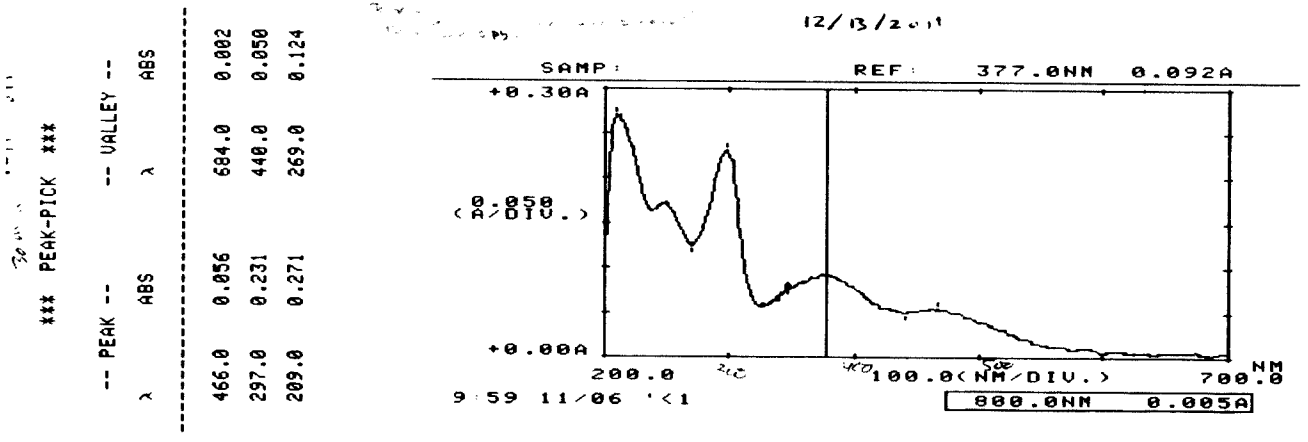

Figure 5a: UV-Vis for the reaction of $Ru^{II}(mcbpy)_2Cl_2$ with phen-azo-phenol after 30 min of reaction using MeOH as a solvent.

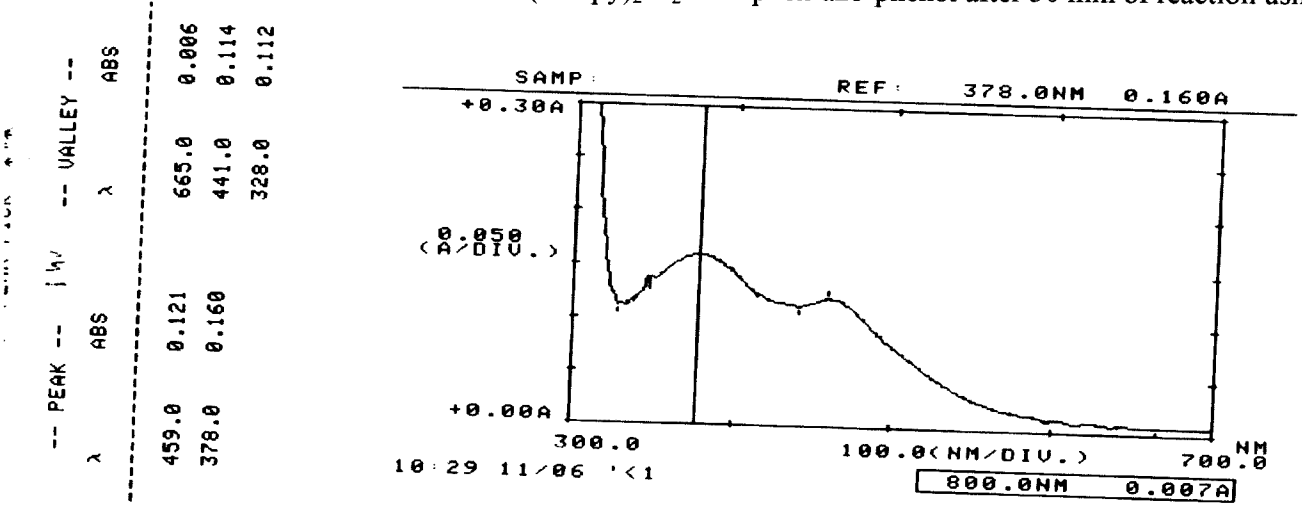

Figure 5b: UV-Vis for the reaction of $Ru^{II}(mcbpy)_2Cl_2$ with phen-azo-phenol after 1 h of reaction using MeOH as a solvent.

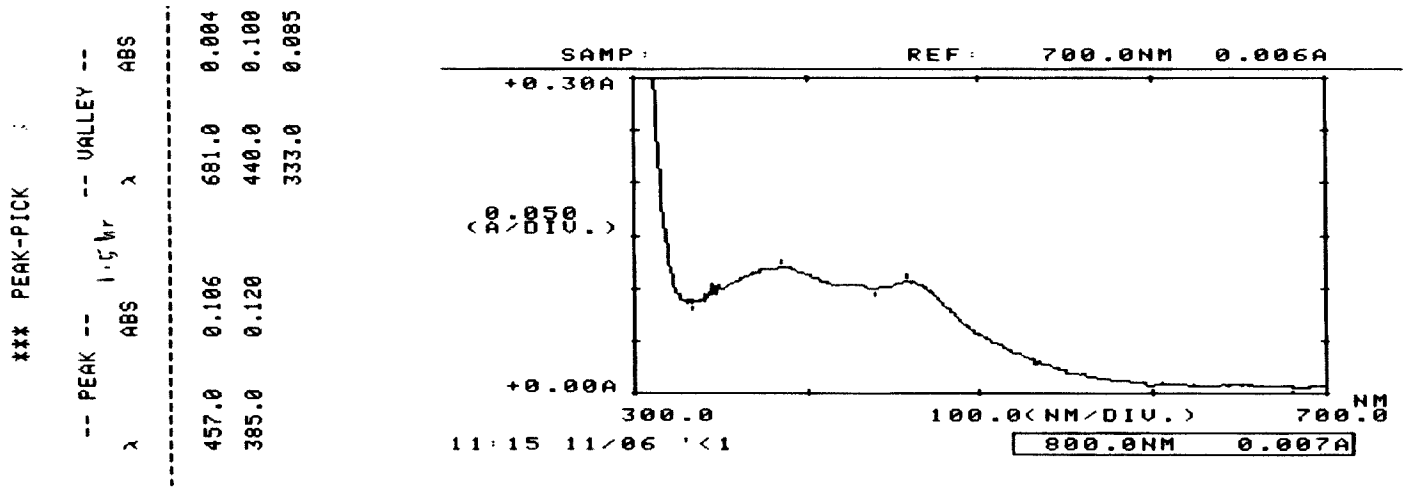

Figure 5c: UV-Vis for the reaction of $Ru^{II}(mcbpy)_2Cl_2$ with phen-azo-phenol after 1.5 h of reaction using MeOH as a solvent.

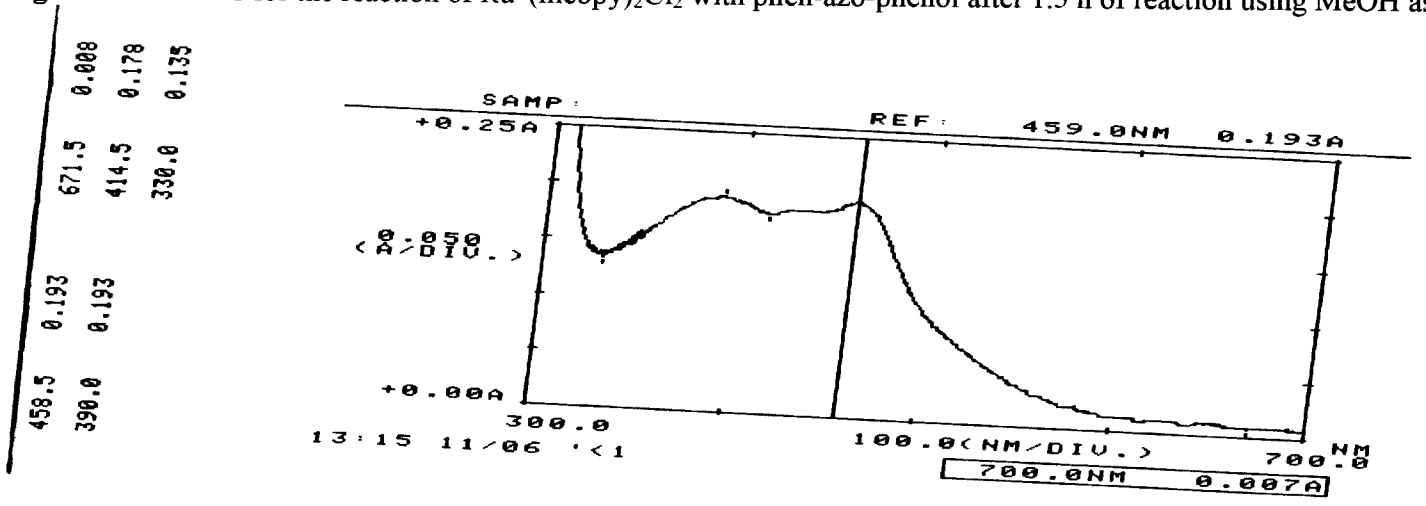

Figure 5d: UV-Vis for the reaction of $Ru^{II}(mcbpy)_2Cl_2$ with phen-azo-phenol after 3.5 h of reaction using MeOH as a solvent.

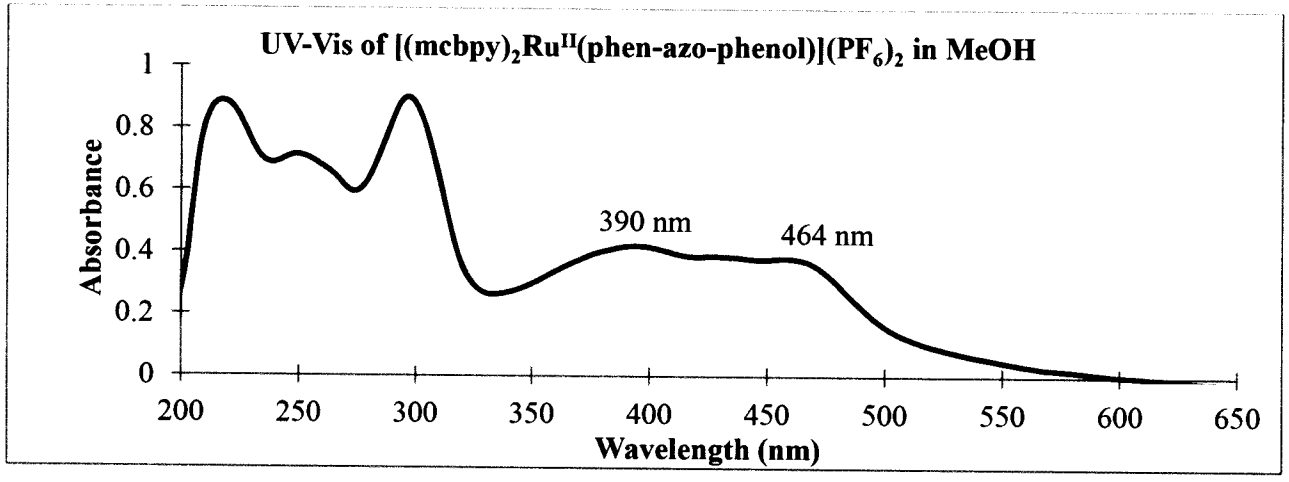

Figure 5e: UV-Vis spectrum of $[(mcbpy)_2Ru^{II}(phen\text{-}azo\text{-}phenol)](PF_6)_2$ (032812-B-AH) crude product in MeOH.

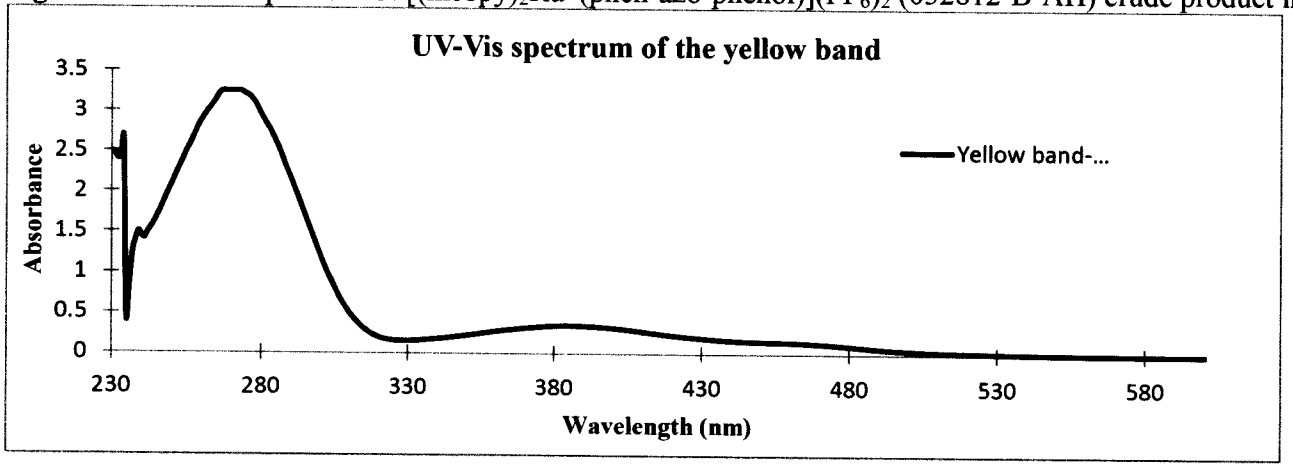

Figure 5f: The UV-Vis spectrum of the yellow band from purification of $[(mcbpy)_2Ru^{II}(phen\text{-}azo\text{-}phenol)](PF_6)_2$ (121311-A-AH) in CH_3OH:CH_3COOH (90:10).

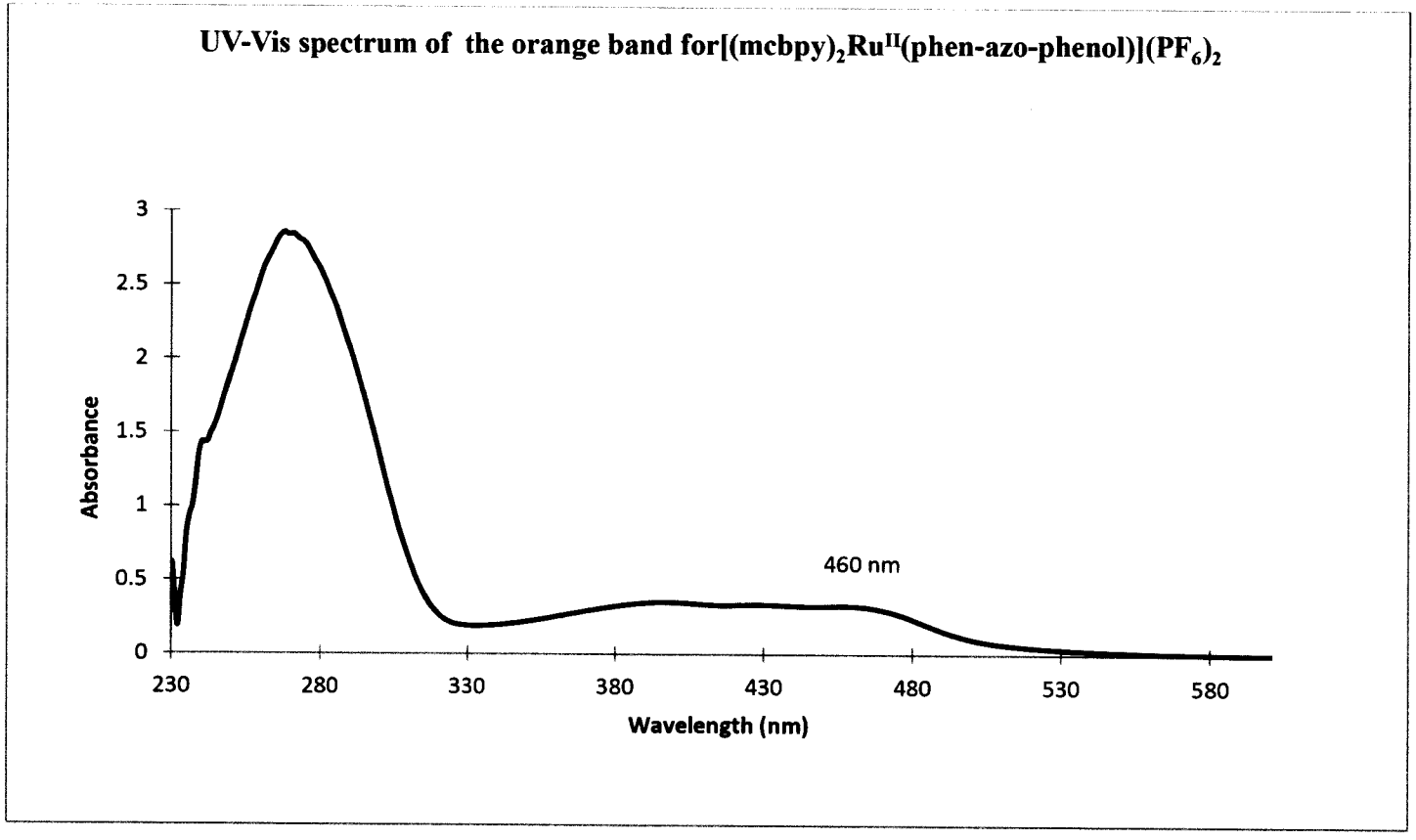

Figure 5g: UV-Vis spectrum of the orange band (032812-B-AH) from the purification of $[(mcbpy)_2Ru^{II}(phen\text{-}azo\text{-}phenol)](PF_6)_2$(121311-A-AH) in MeOH:$CH_3COOH$ (90:10).

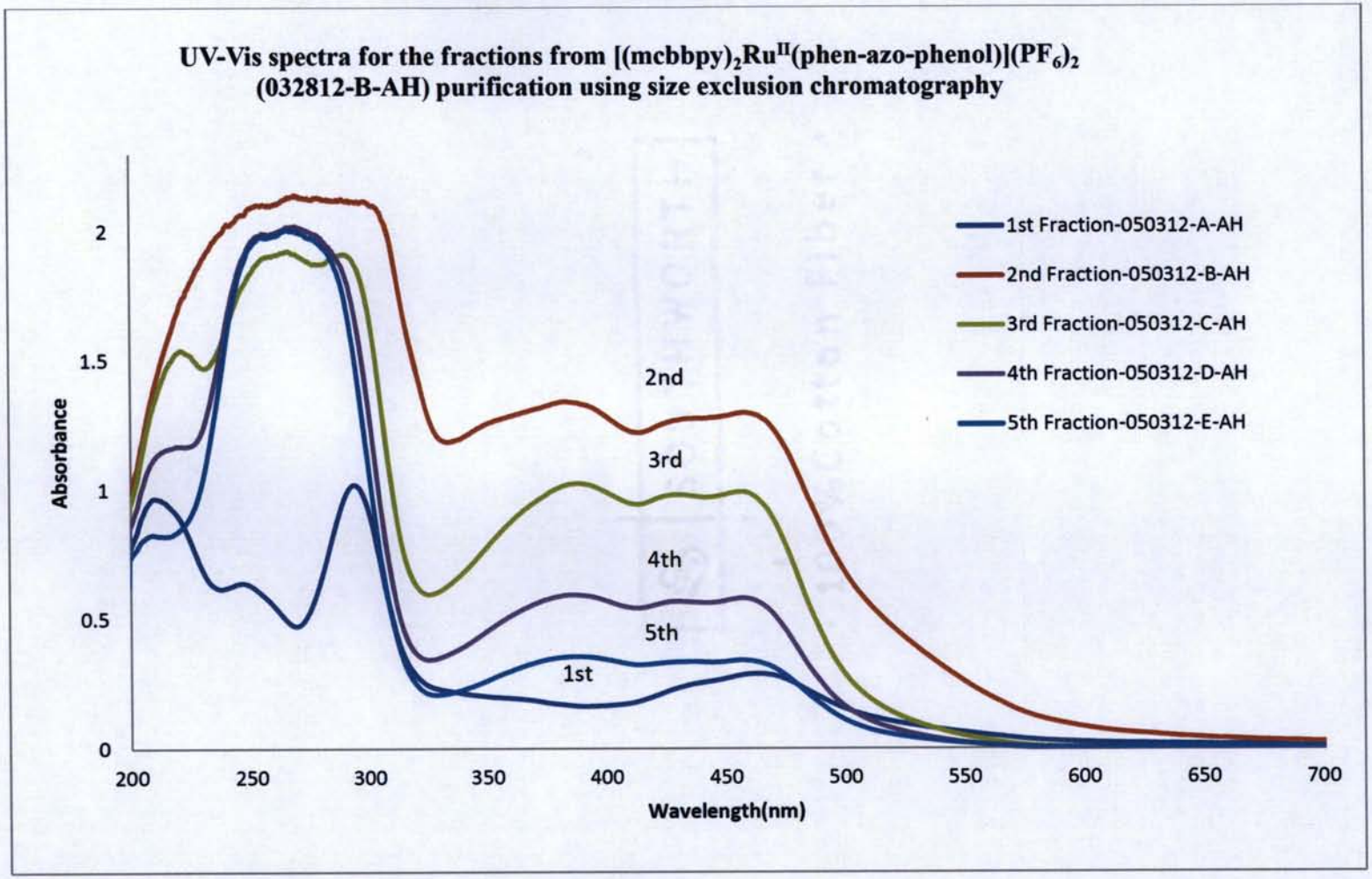

Figure 5h: UV-Vis spectra from size exclusion chromatography.

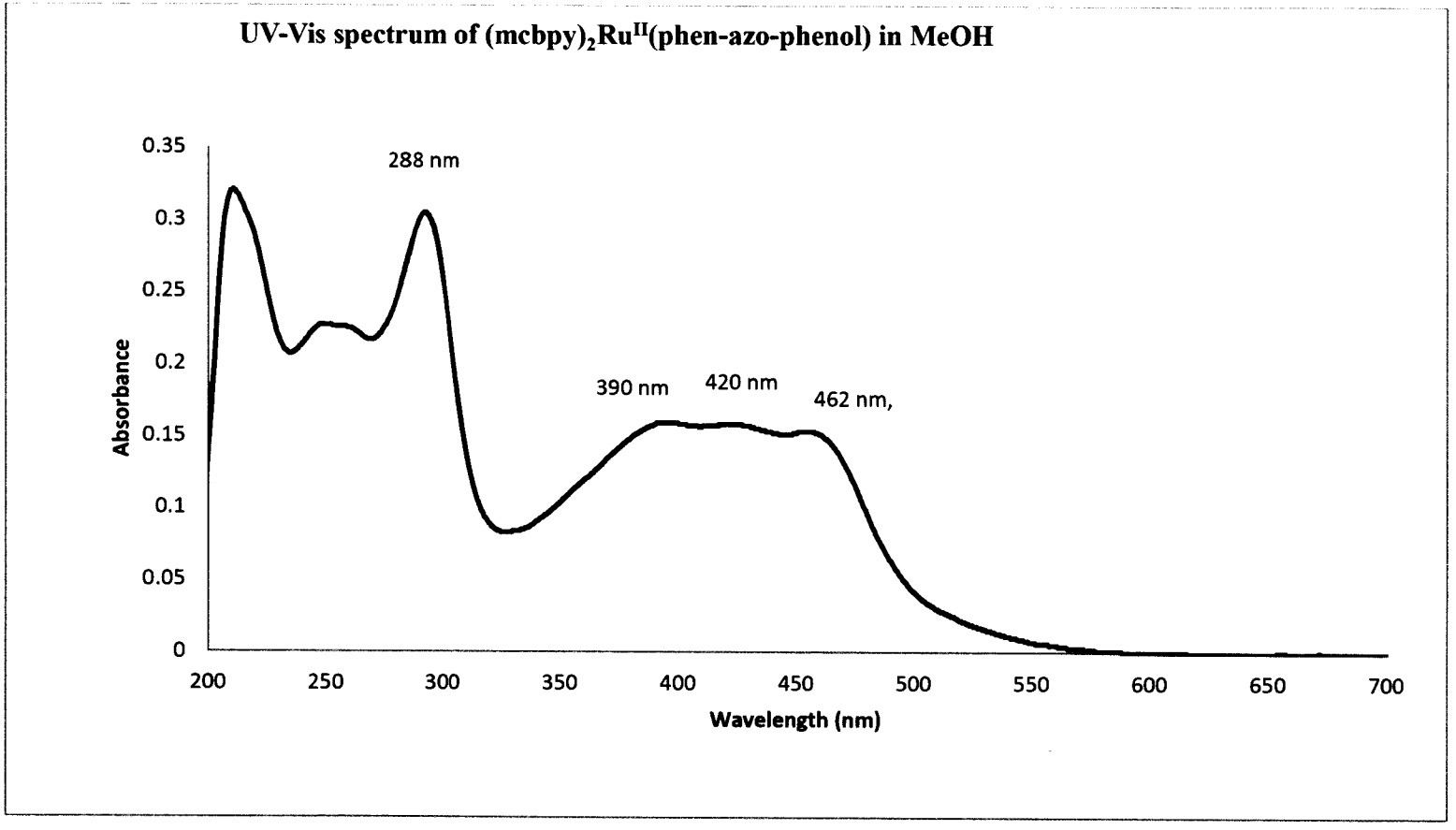

Figure 5i: UV-Vis of $[(mcbpy)_2Ru^{II}(phen\text{-}azo\text{-}phenol)](PF_6)_2$ (3rd fraction-050312-C-AH) in MeOH.

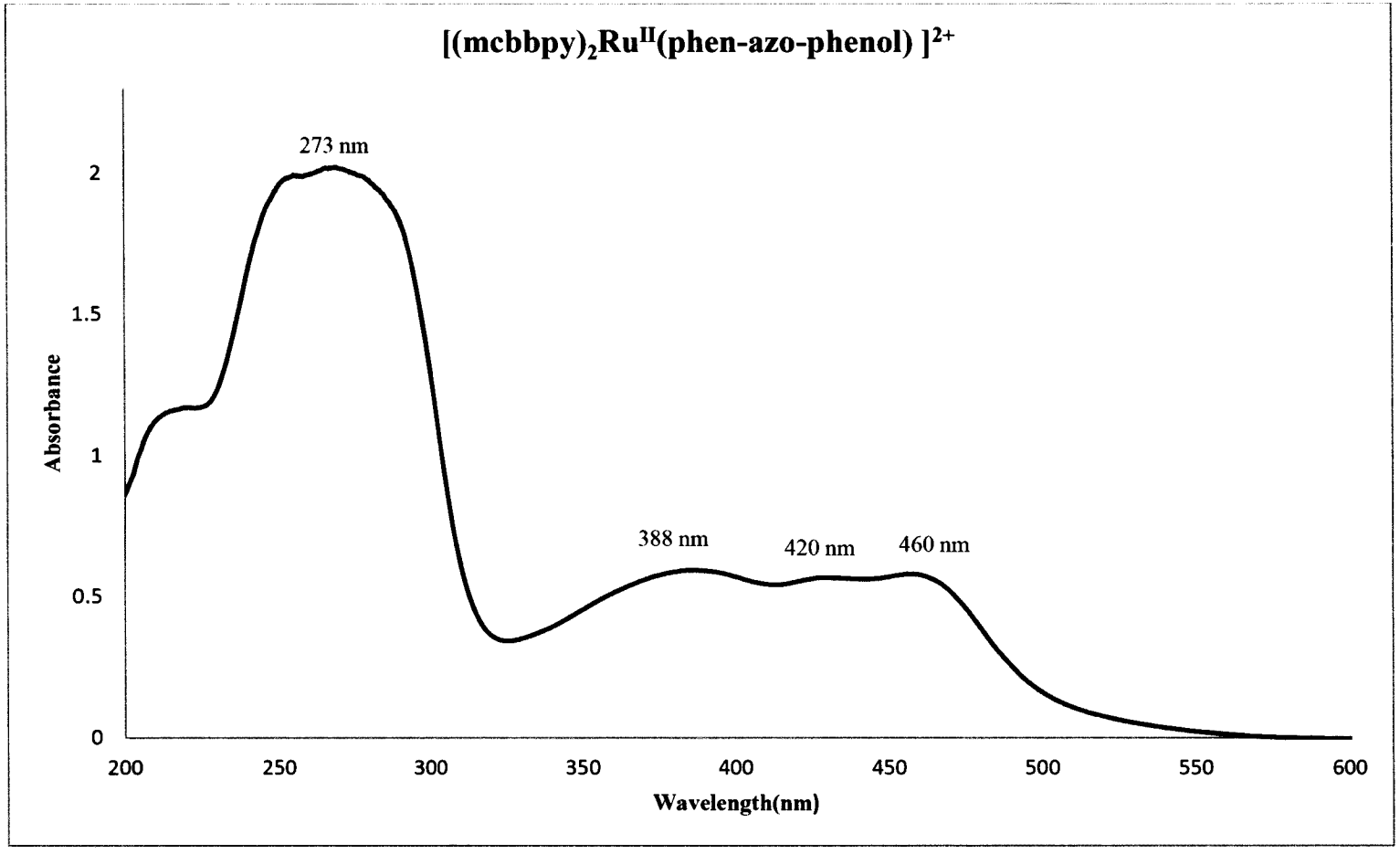

Figure 5j: UV-Vis of $[(mcbpy)_2Ru^{II}(phen\text{-}azo\text{-}phenol)](PF_6)_2$ (4^{th} fraction-050312-D-AH) in MeOH.

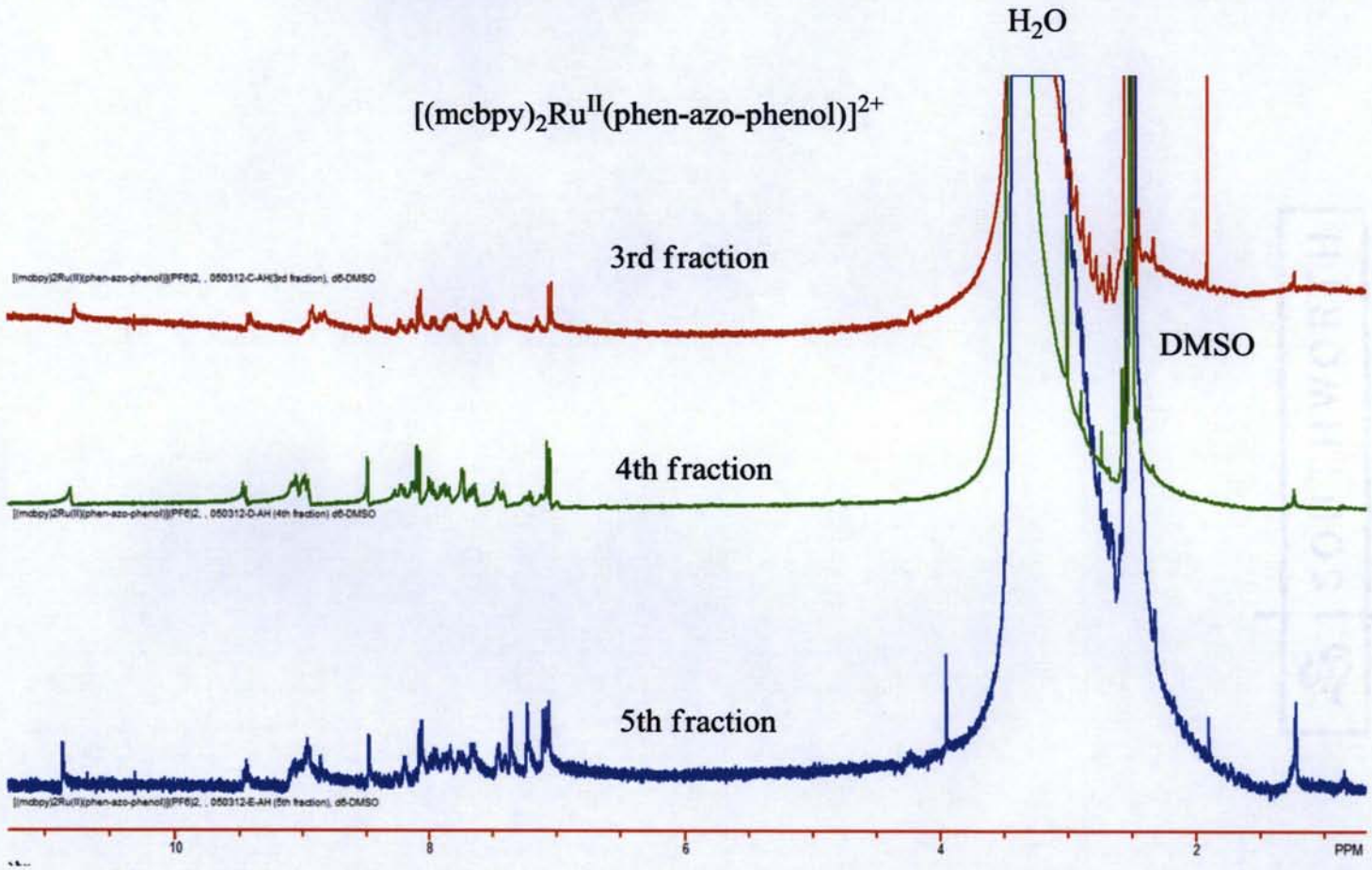

Figure 5k: ^{1}H-NMR (MEM2A409, MEM2A411 and MEM2A410) for the last three fractions (3rd, 4th, and 5th) of [(mcbpy)$_2$Ru^{II}(phen-azo-phenol)](PF$_6$)$_2$ in d$_6$-DMSO.

$[(mcbpy)_2Ru^{II}(phen\text{-}azo\text{-}phenol)]^{2+}$

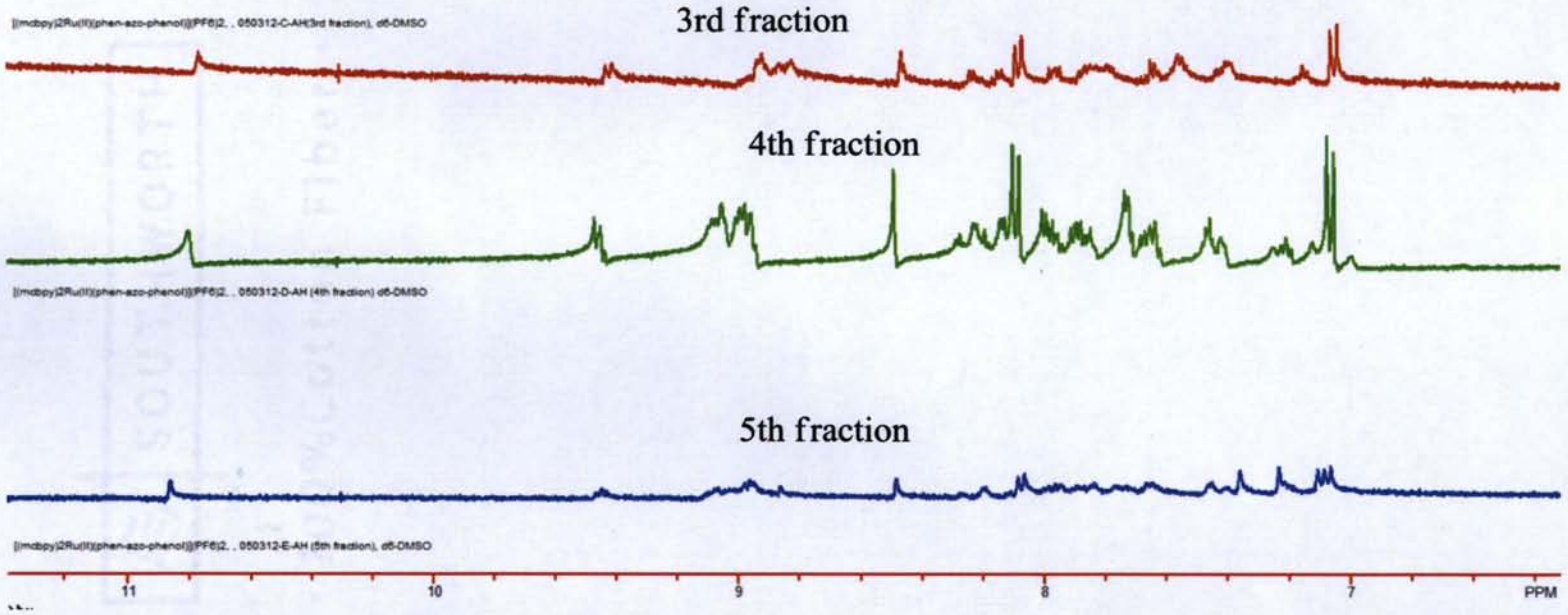

Figure 5l: ^{1}H-NMR (MEM2A409, MEM2A411 and MEM2A410) for the last three fractions (3rd, 4th, and 5th) of $[(mcbpy)_2Ru^{II}(phen\text{-}azo\text{-}phenol)](PF_6)_2$ in d_6DMSO expanded.

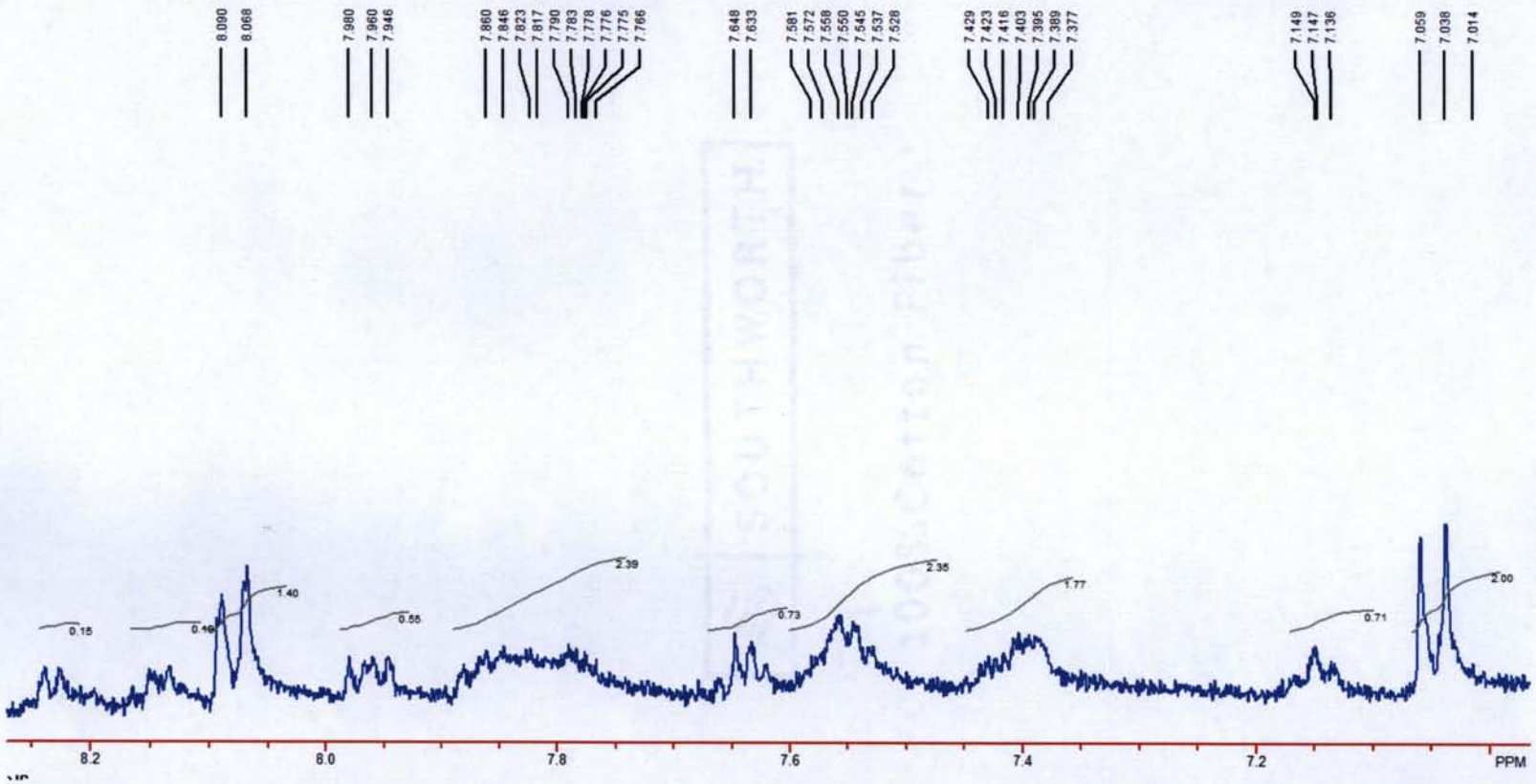

Figure 5m: ^{1}H-NMR (MEM2A409) for $[(mcbpy)_2Ru^{II}(phen\text{-}azo\text{-}phenol)](PF_6)_2$ (050312-C-AH) 3rd fraction in d_6-DMSO.

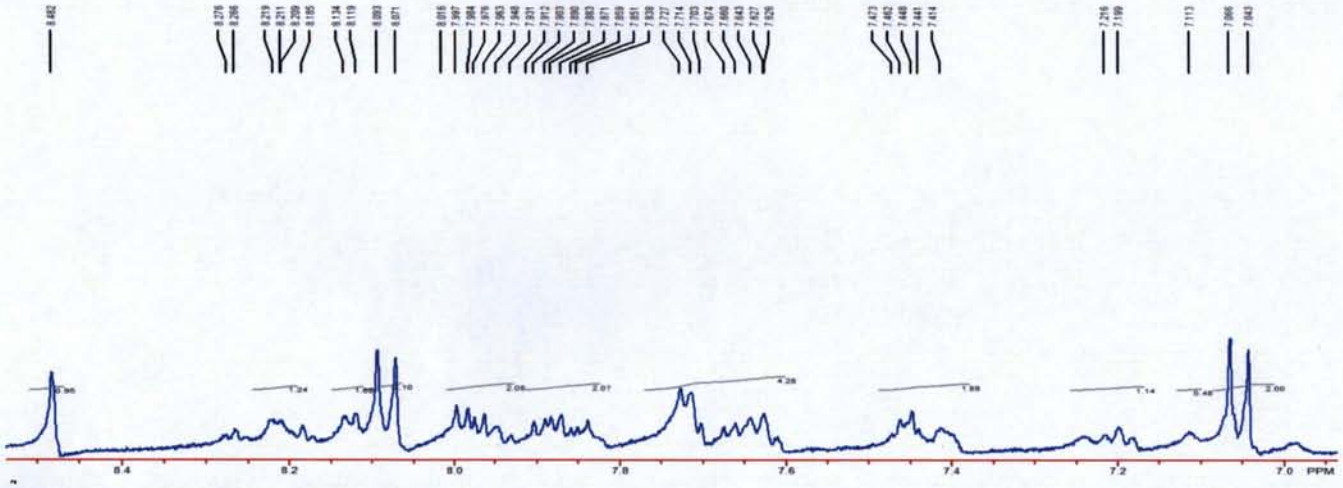

Figure 5n: ^{1}H-NMR (MEM2A411) for [(mcbpy)$_2$Ru^{II}(phen-azo-phenol)](PF$_6$)$_2$ (050312-D-AH) 4th fraction in DMSO.

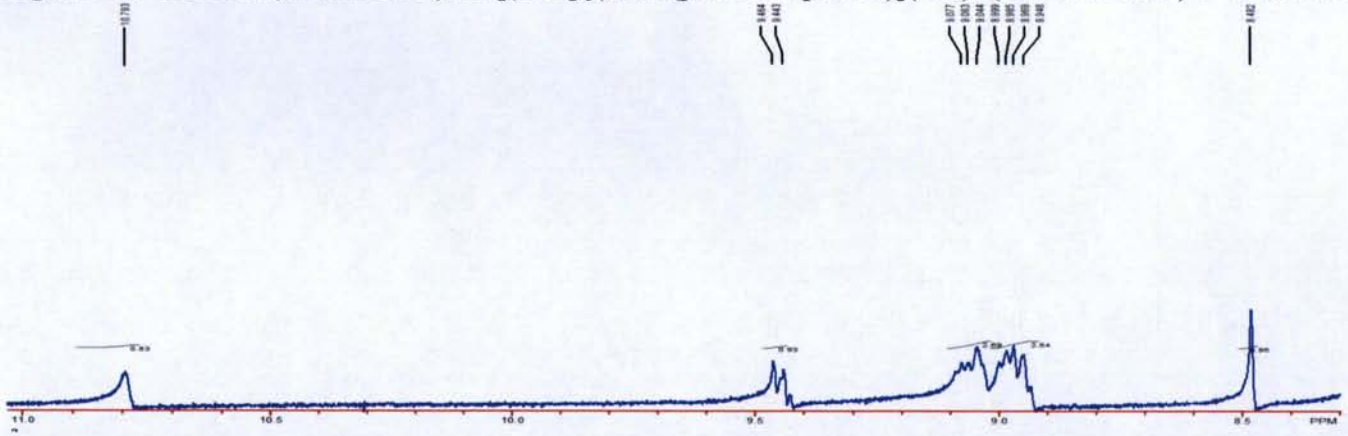

Figure 5o: ^{1}H-NMR (MEM2A411) for [(mcbpy)$_2$Ru^{II}(phen-azo-phenol)](PF$_6$)$_2$ (050312-D-AH) in d$_6$-DMSO for the 4th fraction showing the rest of the spectrum.

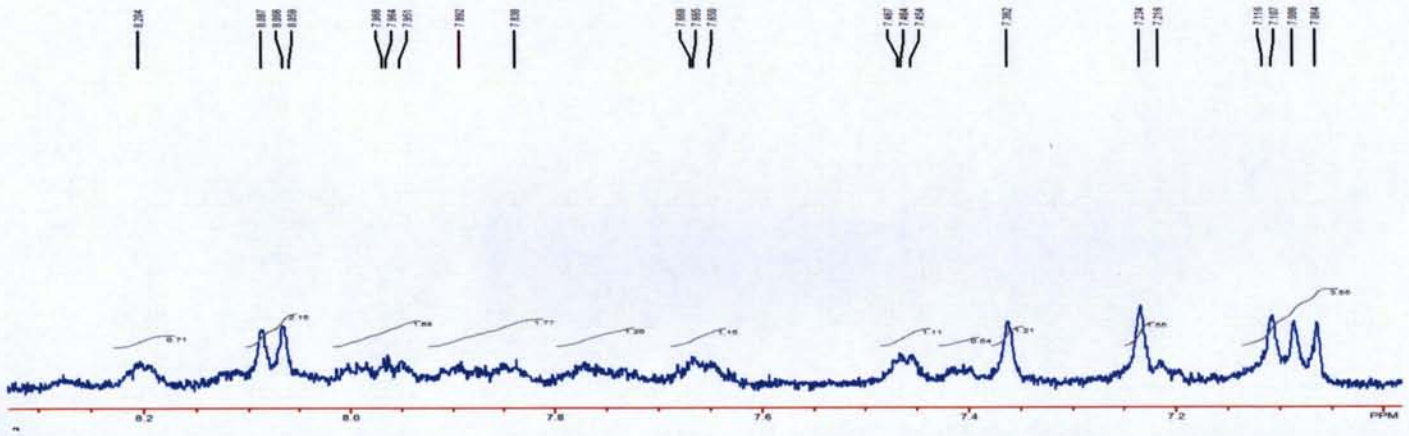

Figure 5p: ^{1}H-NMR (MEM2A410) for [(mcbpy)$_2$Ru^{II}(phen-azo-phenol)](PF$_6$)$_2$ (050312-E-AH) 5th fraction in d$_6$-DMSO.

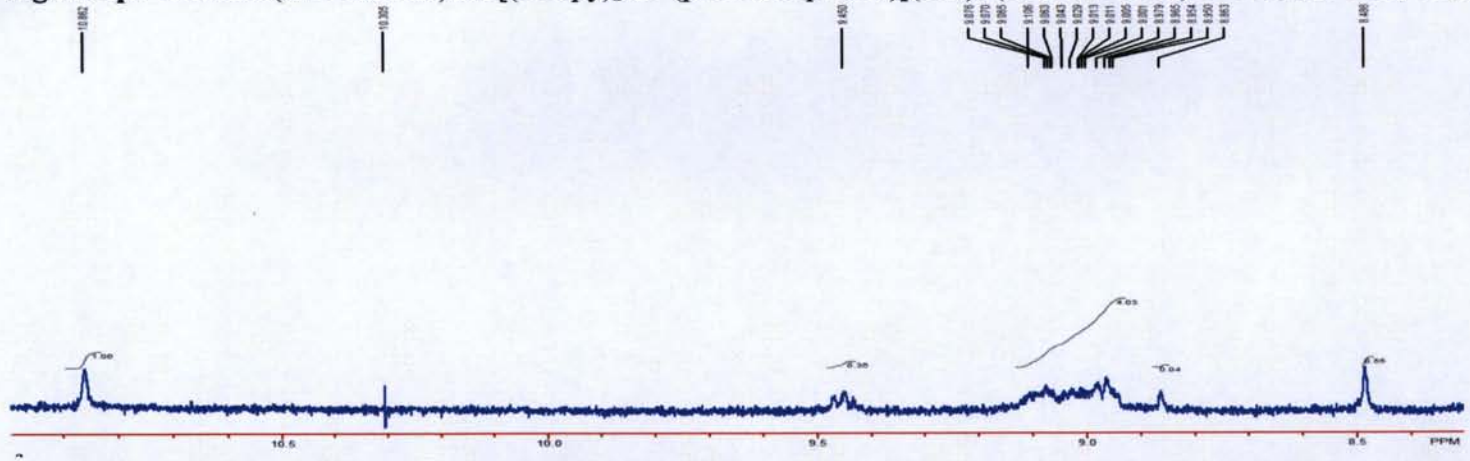

Figure 5q: ^{1}H-NMR (MEM2A410) for [(mcbpy)$_2$Ru^{II}(phen-azo-phenol)](PF$_6$)$_2$ (050312-E-AH) 5th fraction expanded in d$_6$-DMSO

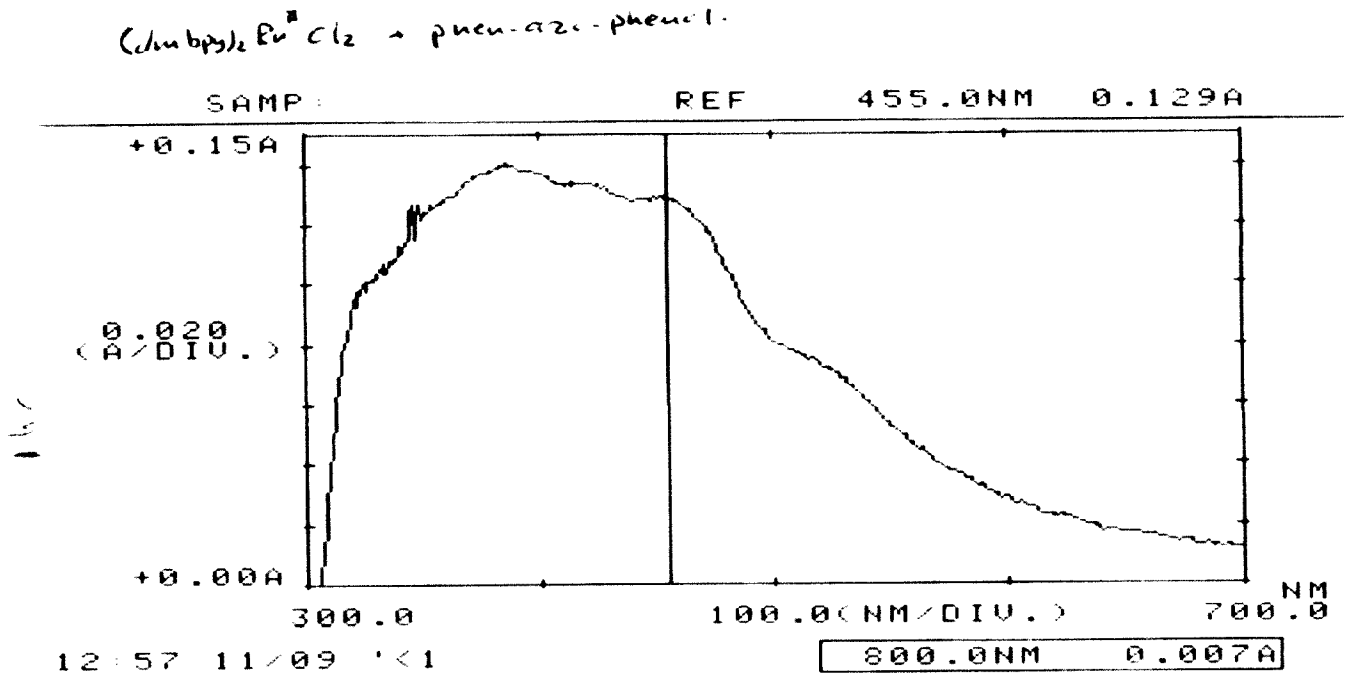

Figure 6a: UV-Vis spectrum for the reaction of $Ru^{II}(dmbpy)_2Cl_2$ with phen-azo-phenol using 95% EtOH as a solvent after 1 h of reflux.

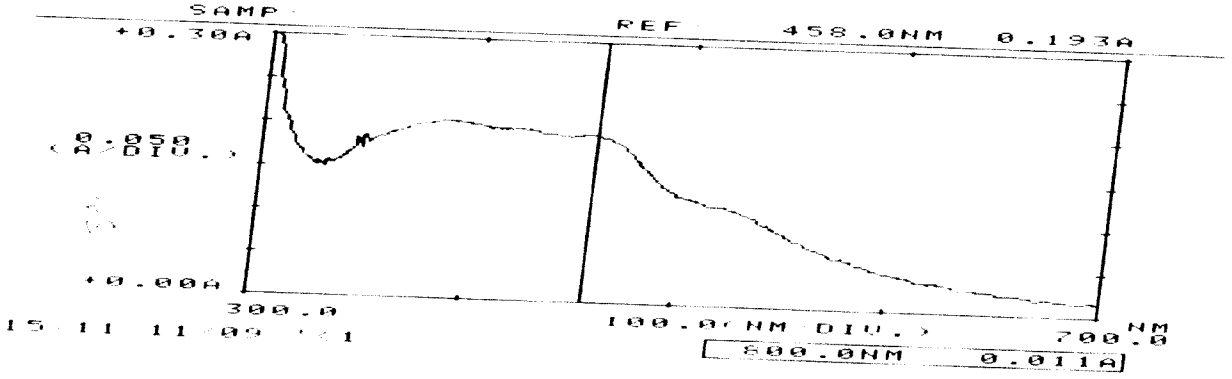

Figure 6b: UV-Vis spectrum for the reaction of $Ru^{II}(dmbpy)_2Cl_2$ with phen-azo-phenol using 95% EtOH as a solvent after 3 h of reflux.

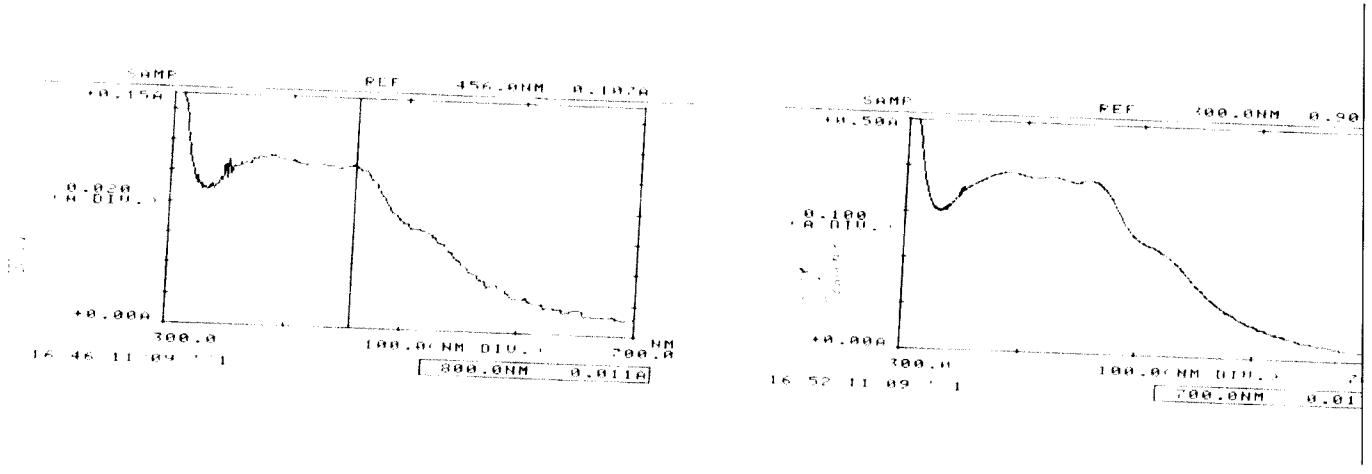

Figure 6c: UV-Vis spectrum for the reaction of $Ru^{II}(dmbpy)_2Cl_2$ with phen-azo-phenol using 95% EtOH as a solvent after 5 h of reflux.

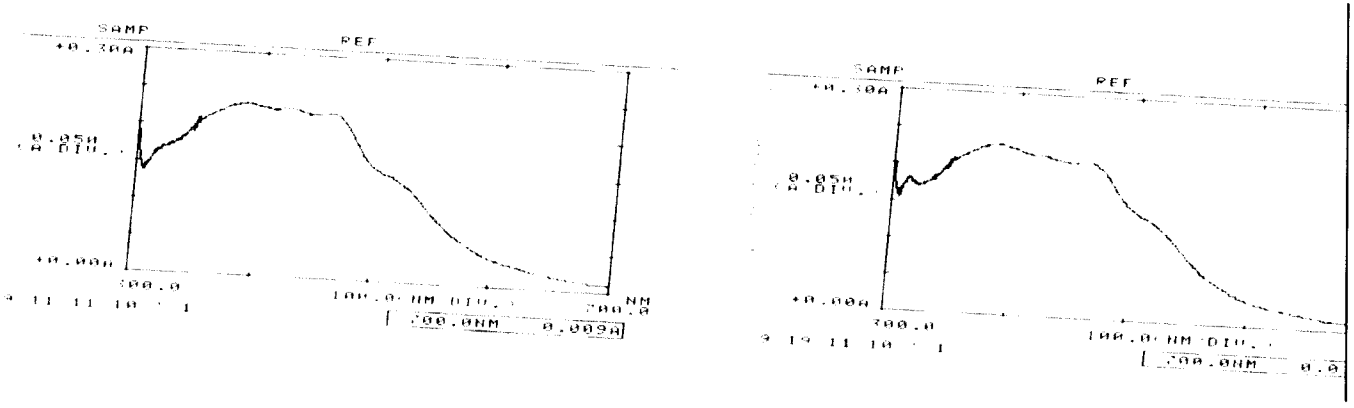

Figure 6d: UV-Vis spectrum for the reaction of $Ru^{II}(dmbpy)_2Cl_2$ with phen-azo-phenol using 95% EtOH as a solvent after 21 h of reflux

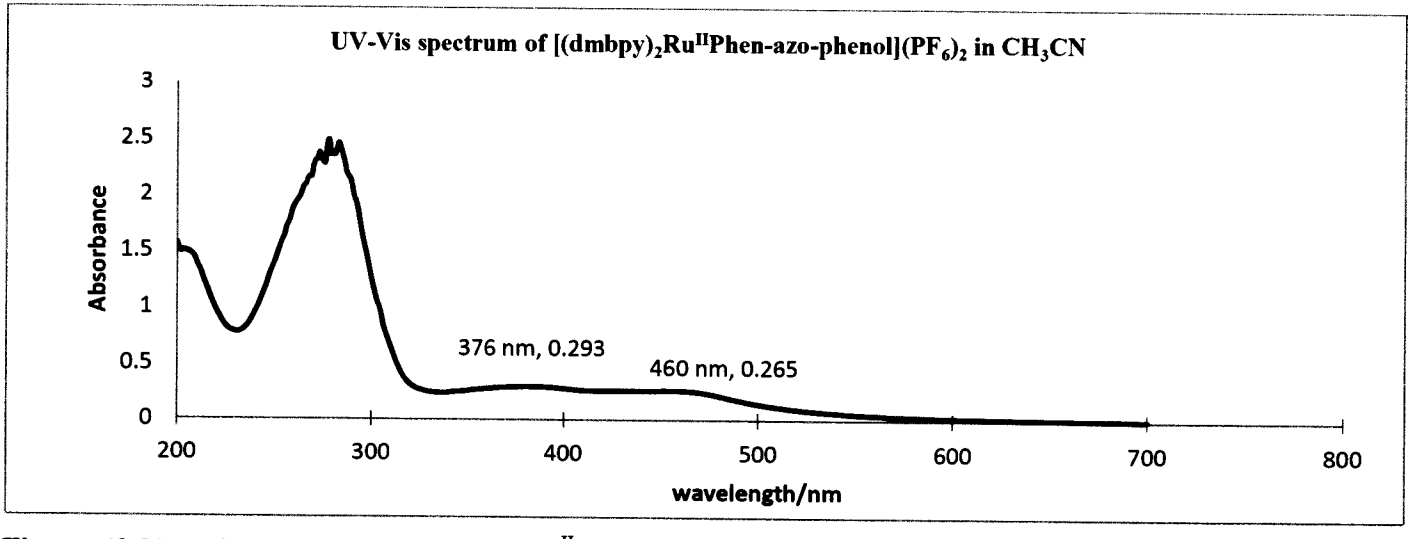

Figure 6f: UV-Vis spectrum of $[(dmbpy)_2Ru^{II}(phen\text{-}azo\text{-}phenol)](PF_6)_2$ (010512-A-AH) in CH_3CN.

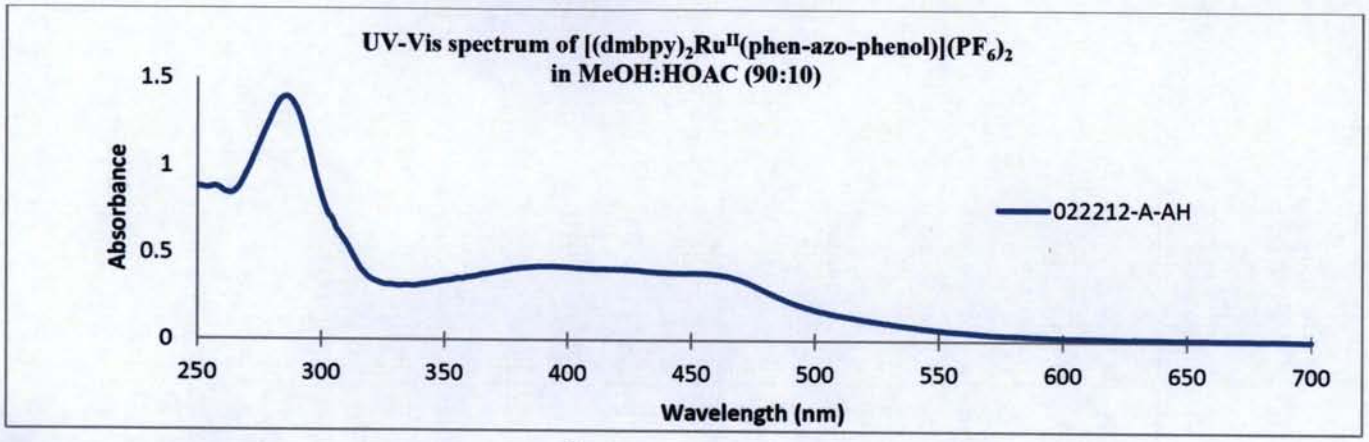

Figure 6g: UV-Vis spectrum of $[(dmbpy)_2Ru^{II}(phen\text{-}azo\text{-}phenol)](PF_6)_2$ (022212-A-AH) for the red fraction from alumina column.

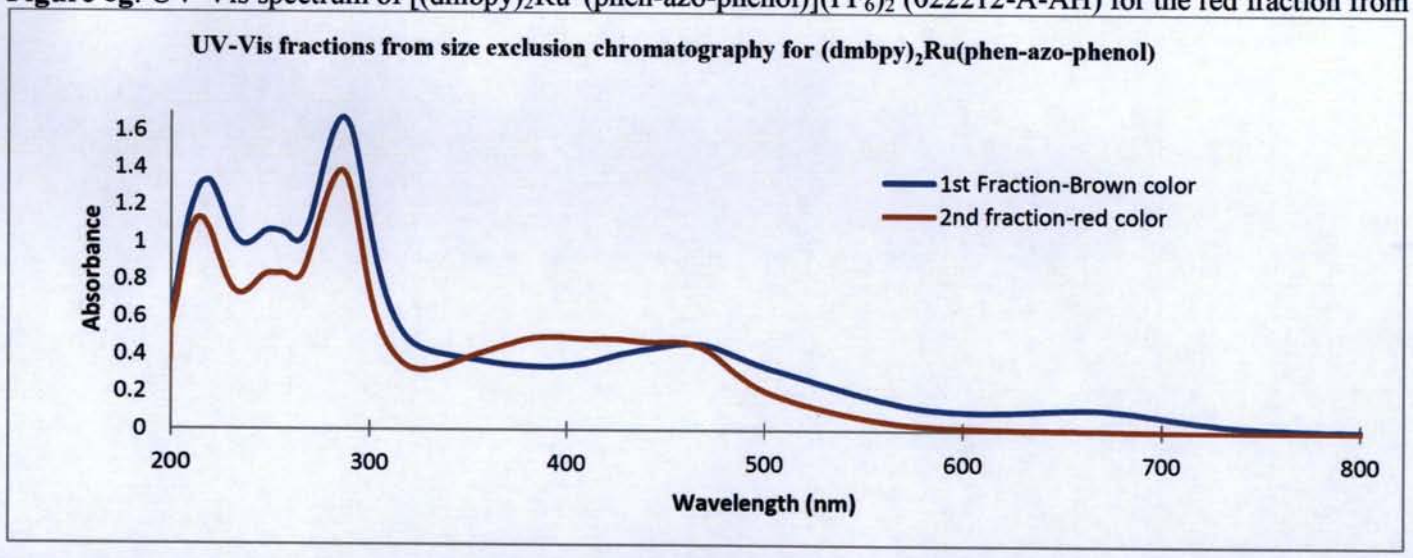

Figure 6h: UV-Vis spectra for the two fractions from size exclusion chromatography using 80:20 $MeOH/H_2O$ as a solvent.

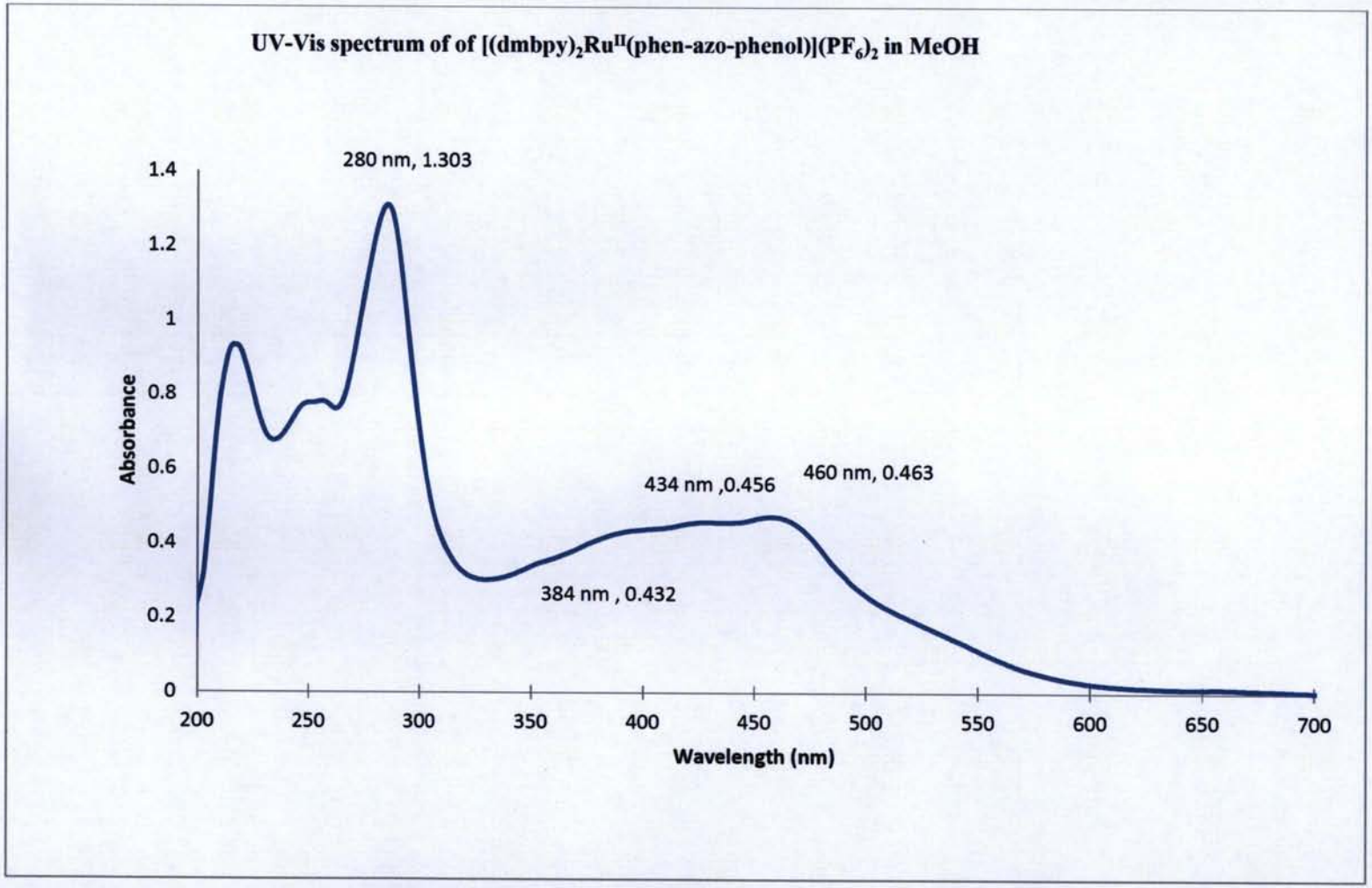

Figure 6i: UV-Vis spectrum of $[(dmbpy)_2Ru^{II}(phen\text{-}azo\text{-}phenol)](PF_6)_2$ (050712-B-AH) in MeOH.

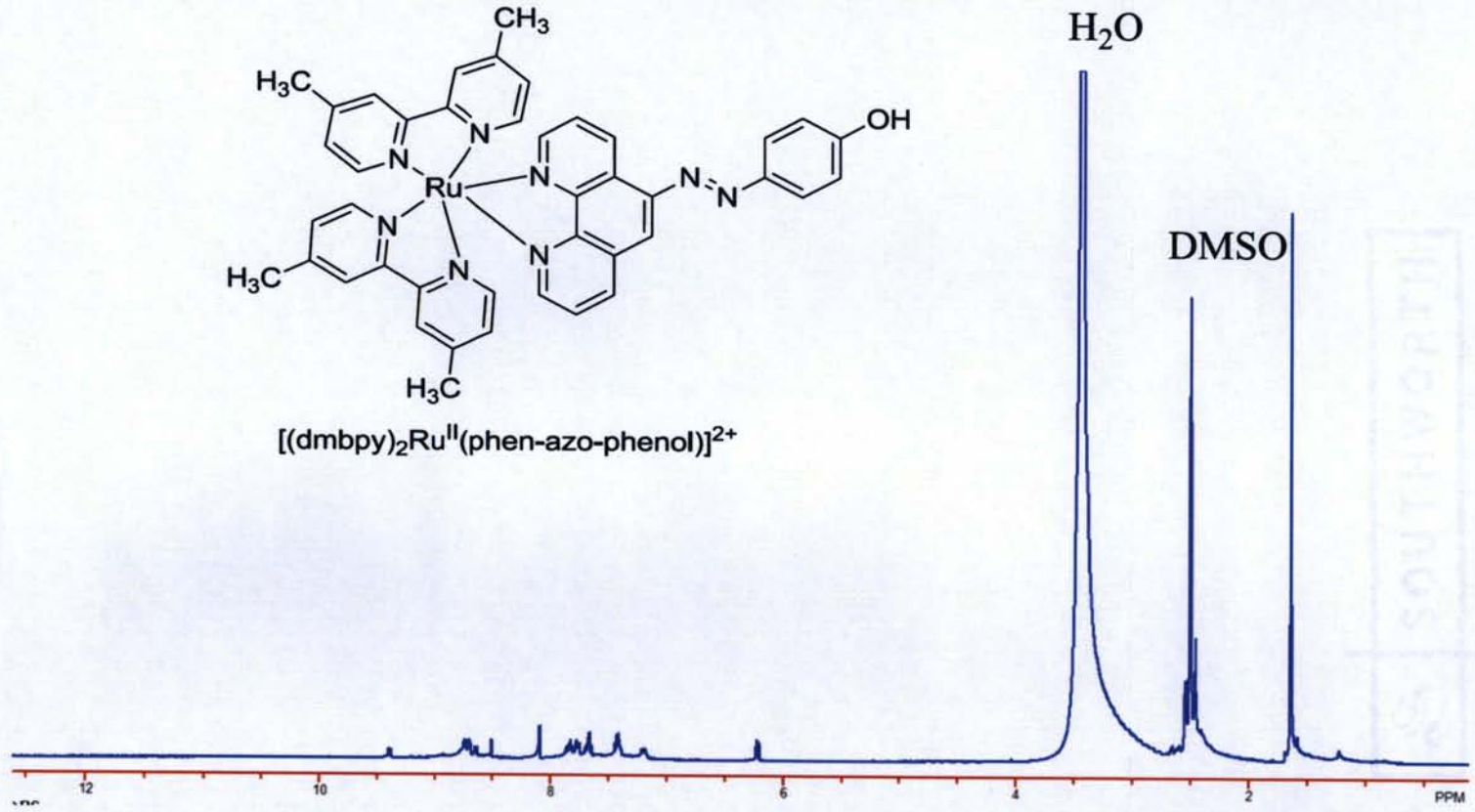

Figure 6j: ^{1}H-NMR (MEM2A412) for [(dmbpy)$_2$Ru^{II}(phen-azo-phenol)](PF$_6$)$_2$ (050712-B-AH) in d$_6$-DMSO.

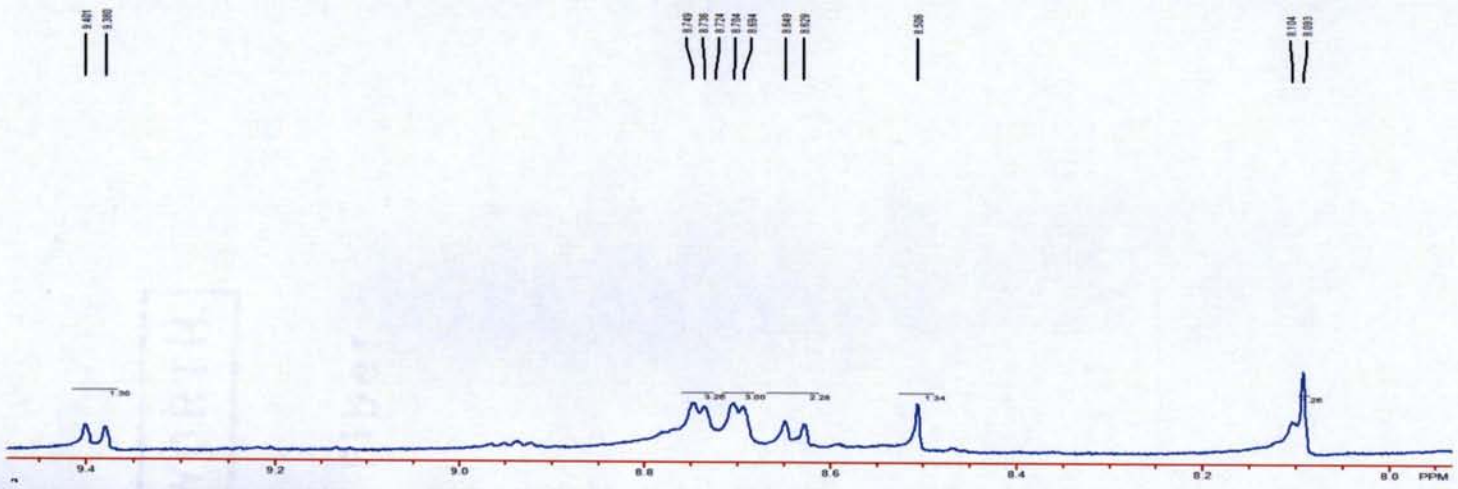

Figure 6k: ^{1}H-NMR (MEM2A412) for [(dmbpy)$_2$Ru^{II}(phen-azo-phenol)](PF$_6$)$_2$ (050712-B-AH) in d$_6$-DMSO expanded.

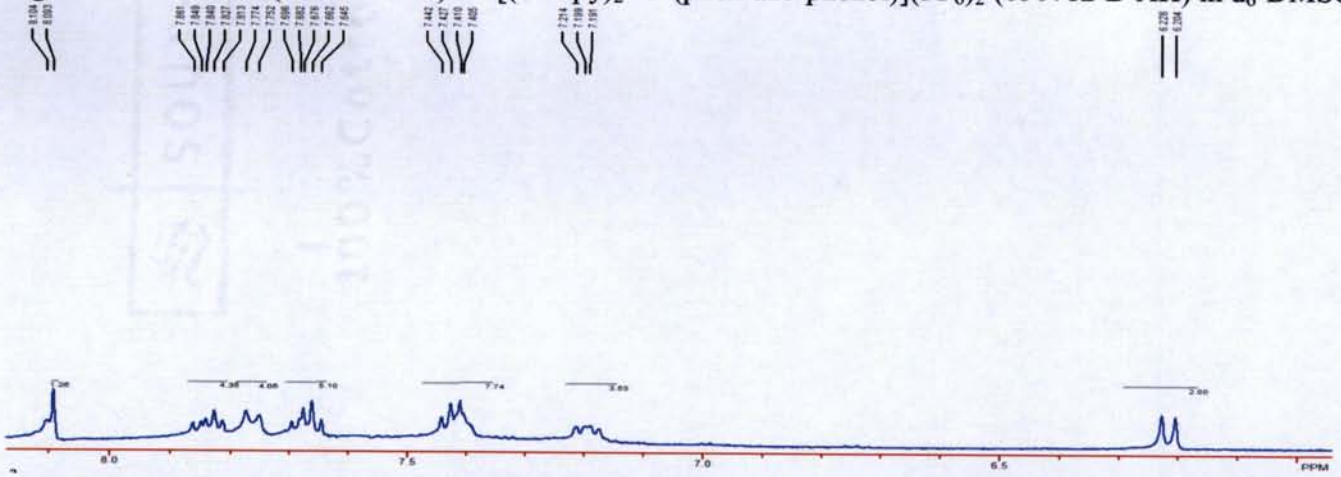

Figure 6l: ^{1}H-NMR (MEM2A412) for [(dmbpy)$_2$Ru^{II}(phen-azo-phenol)](PF$_6$)$_2$ (050712-B-AH) in d$_6$-DMSO expanded.

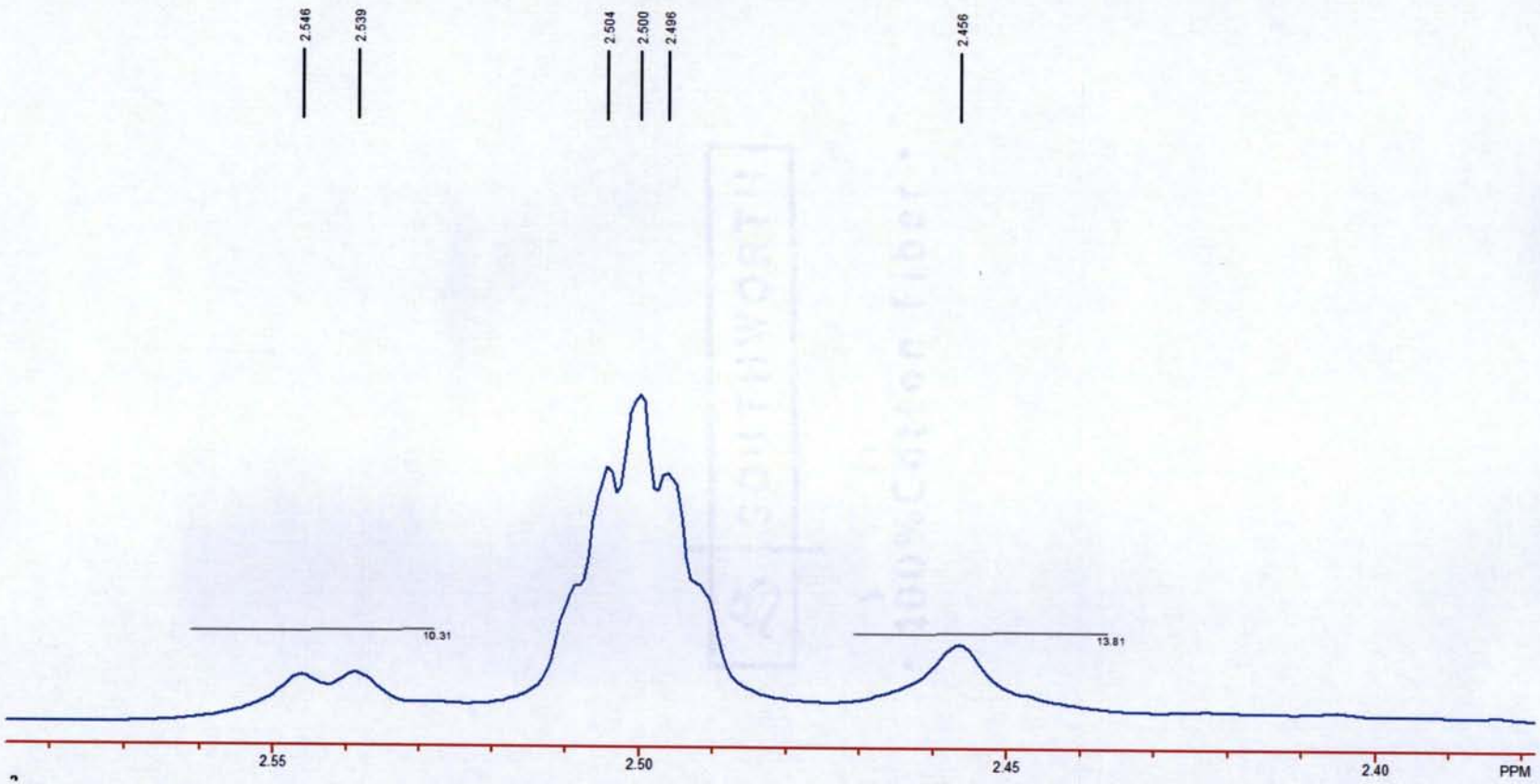

Figure 6m: ^{1}H-NMR (MEM2A412) for [(dmbpy)$_2$Ru^{II}(phen-azo-phenol)](PF$_6$)$_2$ (050712-B-AH) in d$_6$-DMSO expanded showing the methyl protons.

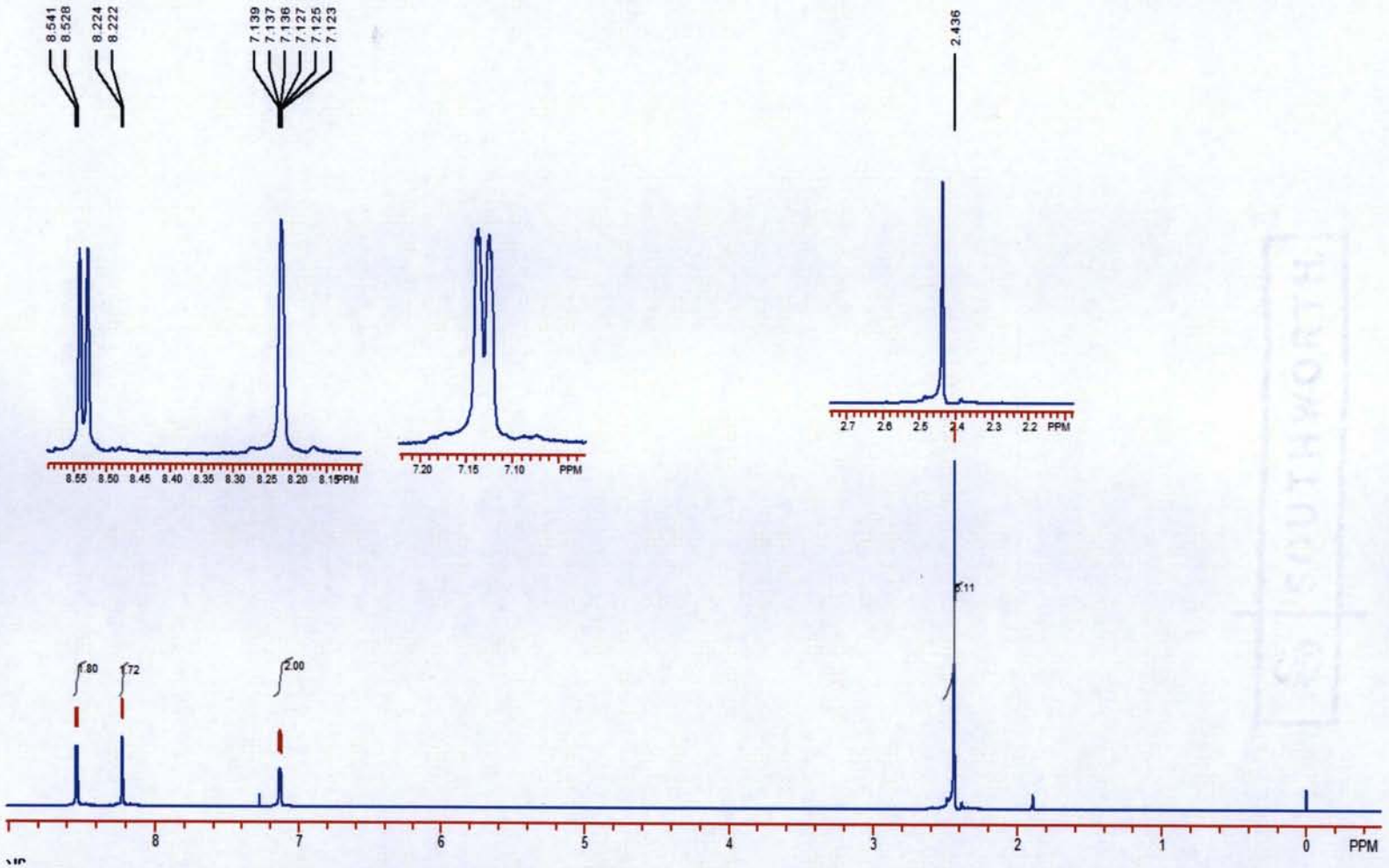

Figure 6n: ^{1}H-NMR (MEM2A414) of an authentic sample of 4,4'-dimethyl-2,2'-bipyridine in $CDCl_3$.

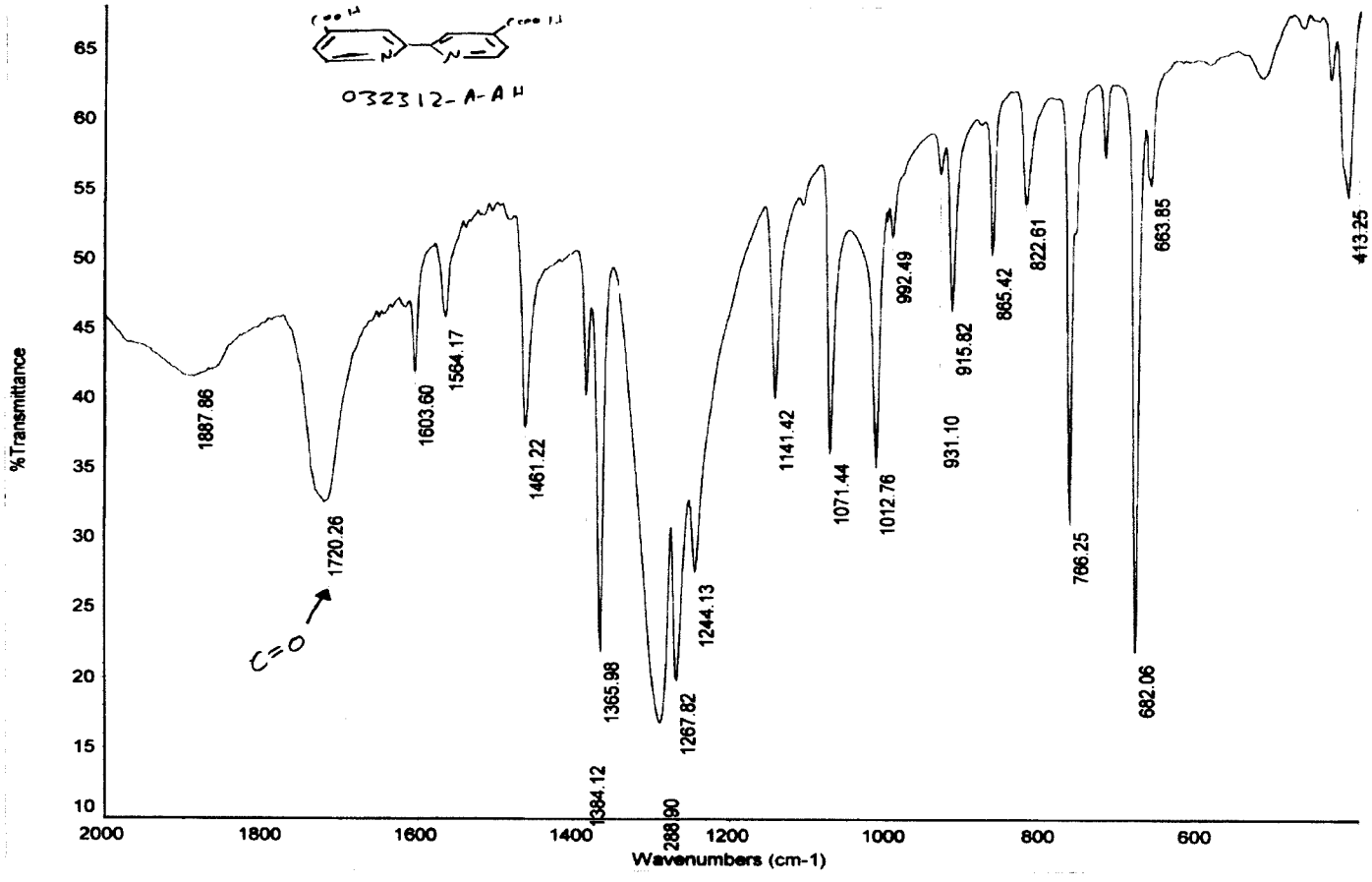

Figure 6o: IR spectrum for 4,4'-dicarboxy-2,2'-bipyridine (032312-A-AH).

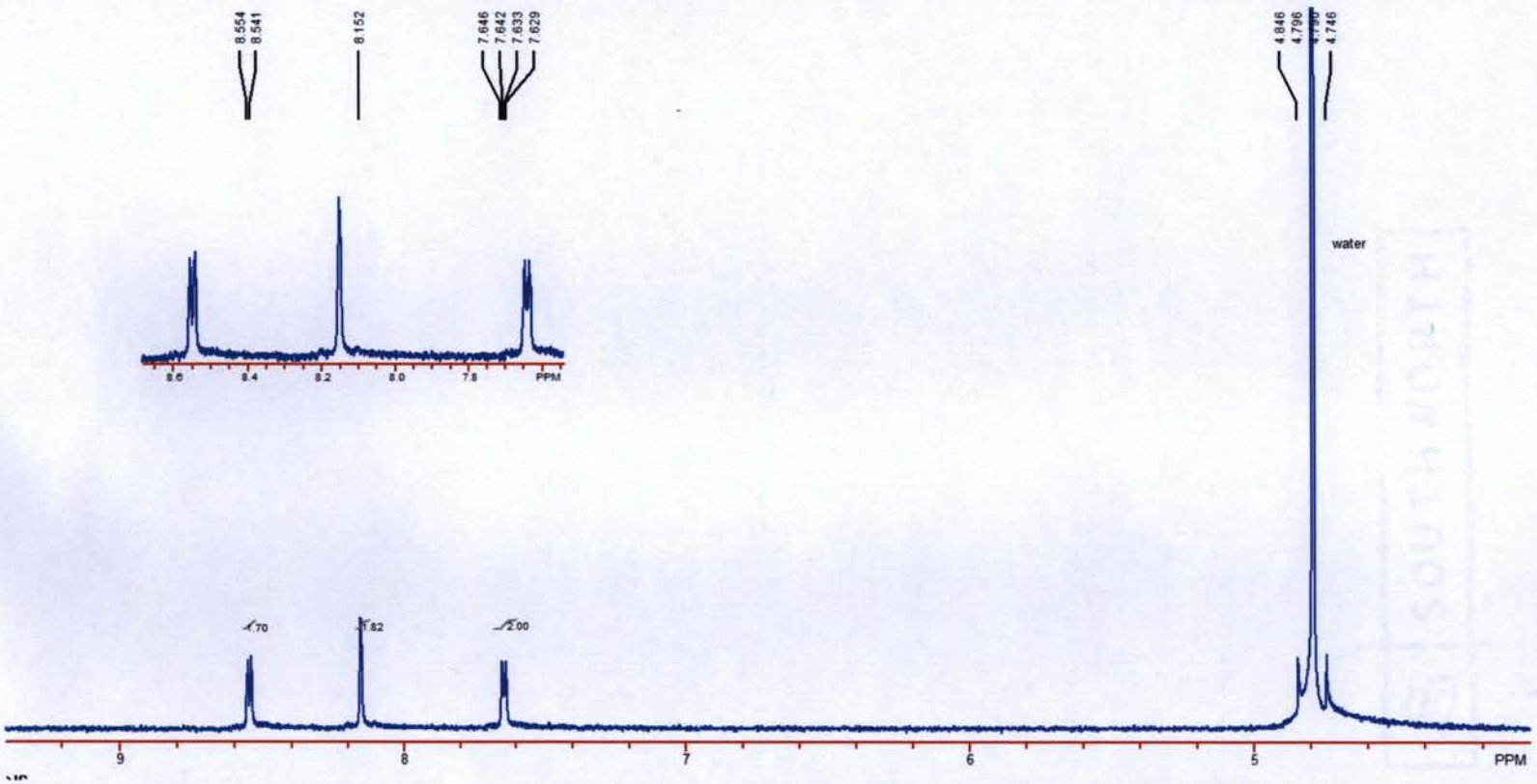

Figure 6p: ^{1}H-NMR (MEM2A413) for 4,4'-dicarboxy-2,2'-bipyridine (032312-A-AH) in D_2O/NaOD.

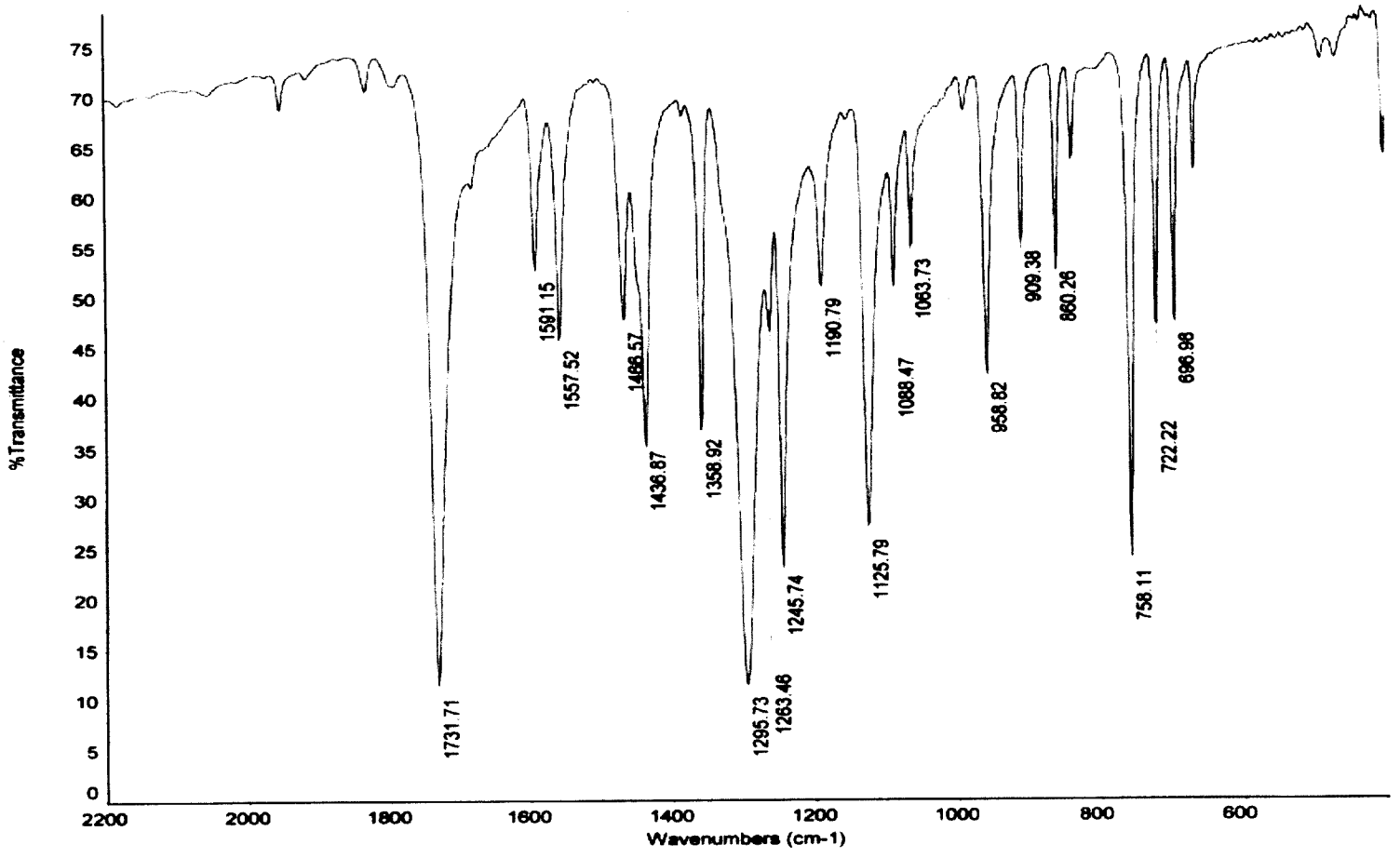

Figure 7a: IR spectrum of 4,4'-dimethoxycarbonyl-2,2'-bipyridine (032412-A-AH) (expanded).

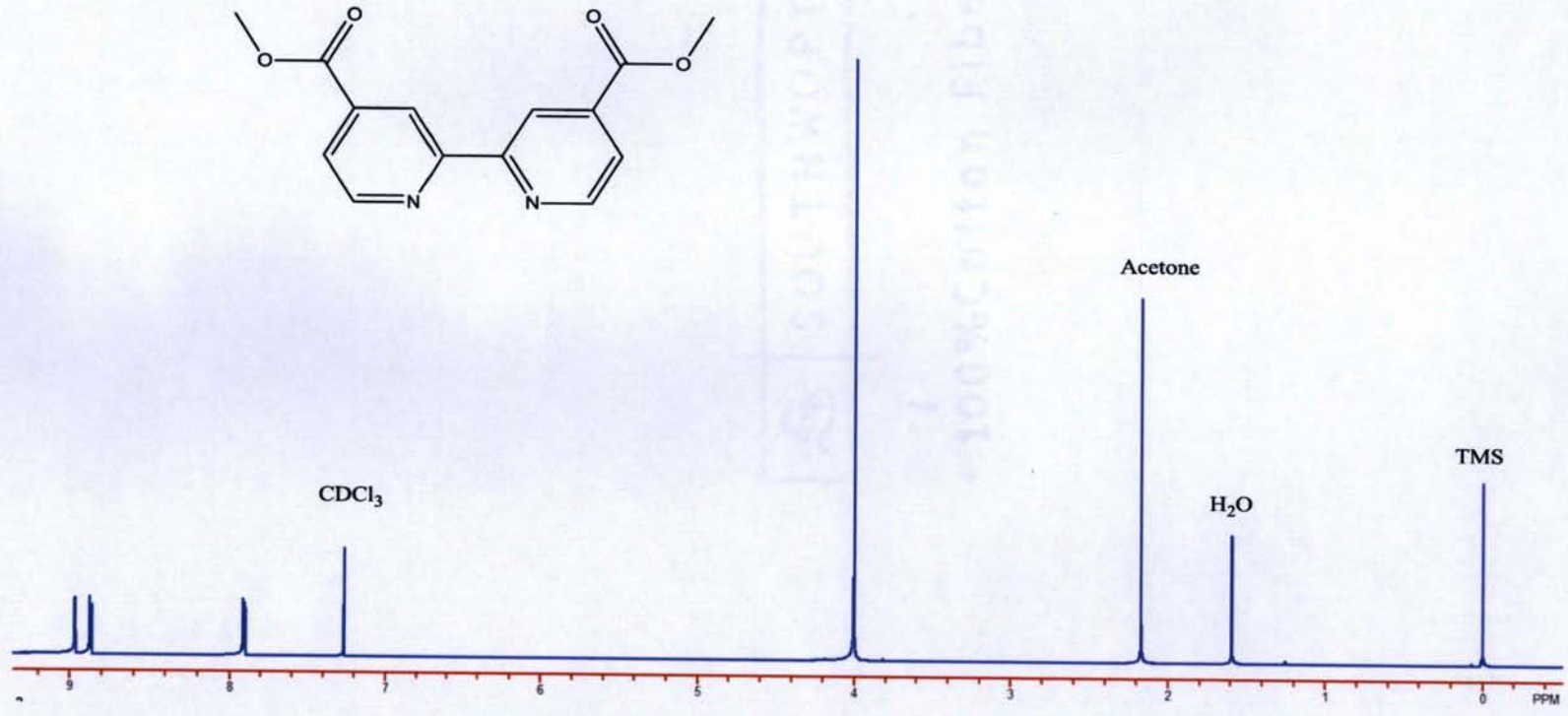

Figure 7b:^{1}H-NMR (MEM2A381) of 4,4'-dimethoxycarbonyl-2,2'-bipyridine (032412-A-AH) in $CDCl_3$.

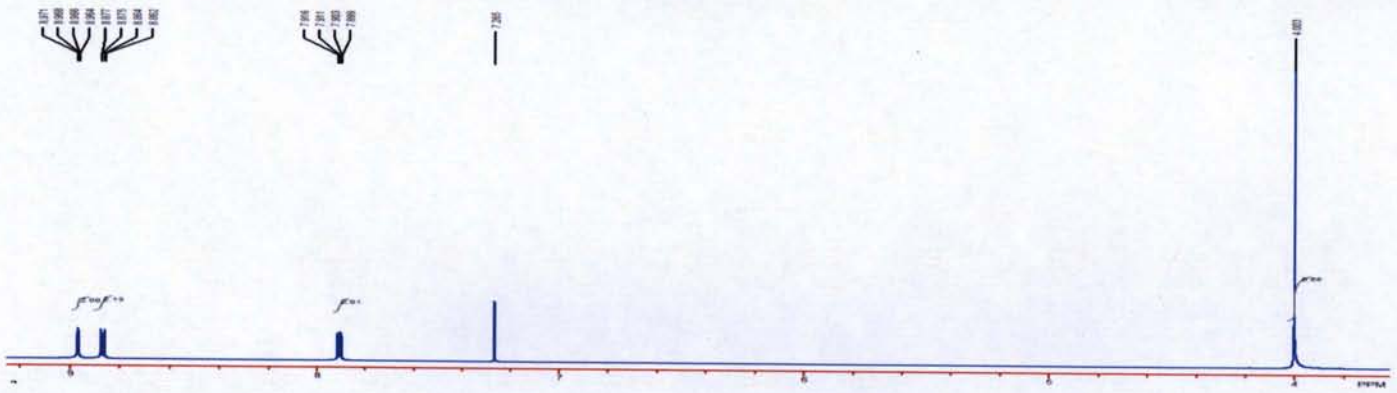

Figure 7c: ^{1}H-NMR (MEM2A381) of 4,4'-dimethoxycarbonyl-2,2'-bipyridine (032412-A-AH) in $CDCl_3$ expanded.

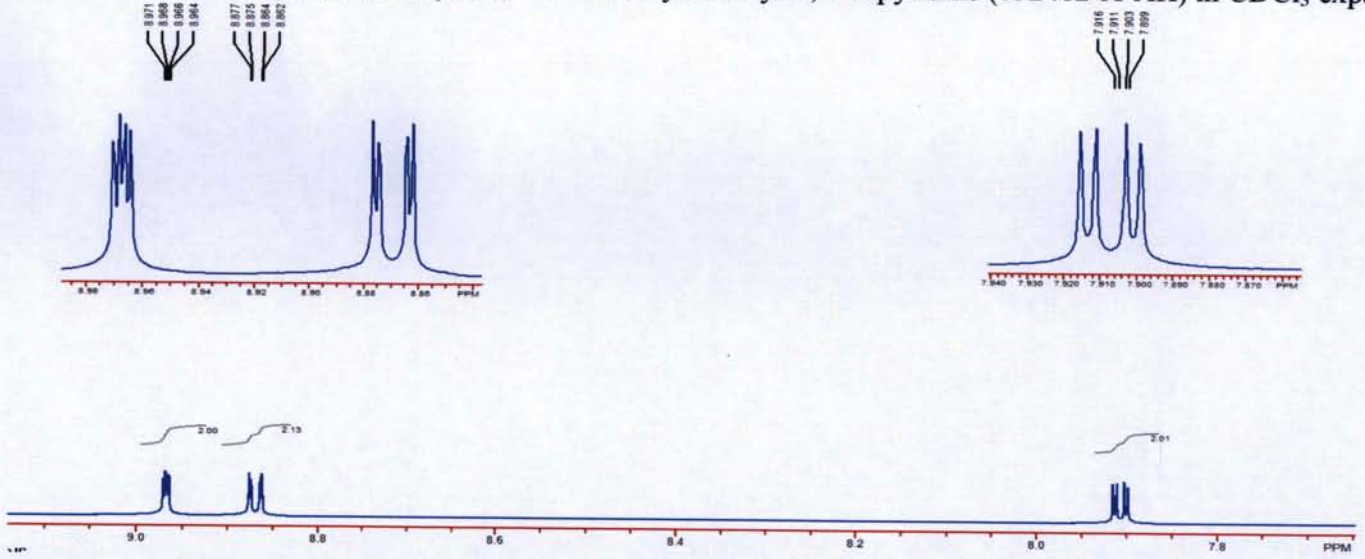

Figure 7d: ^{1}H-NMR (MEM2A381) of 4,4'-dimethoxycarbonyl-2,2'-bipyridine (032412-A-AH) in $CDCl_3$ expanded in the aromatic region.

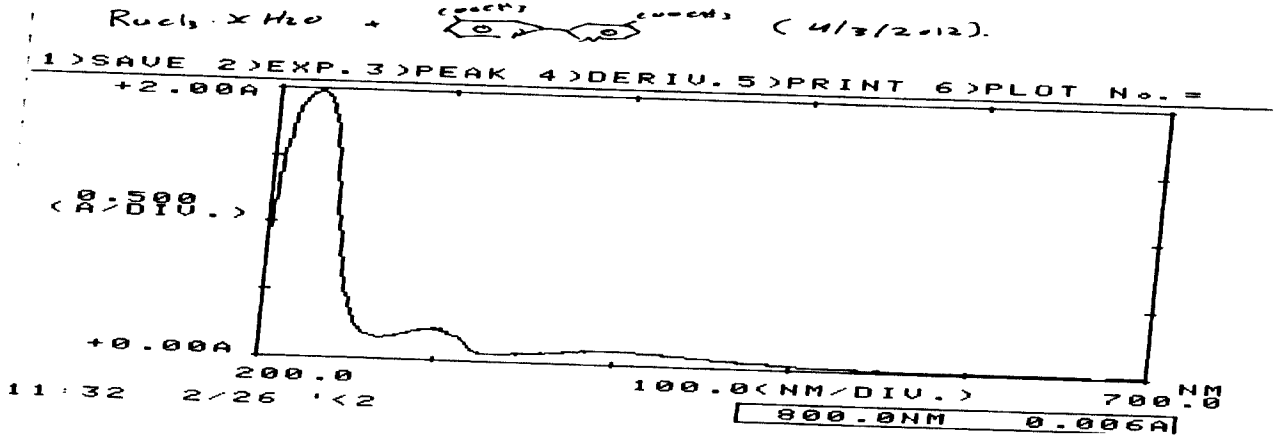

Figure 8a: UV-Vis spectrum for the reaction of $RuCl_3.3H_2O$ with (4,4'-dimethoxy-2,2'-bipyridine) in abs. EtOH initially after mixing.

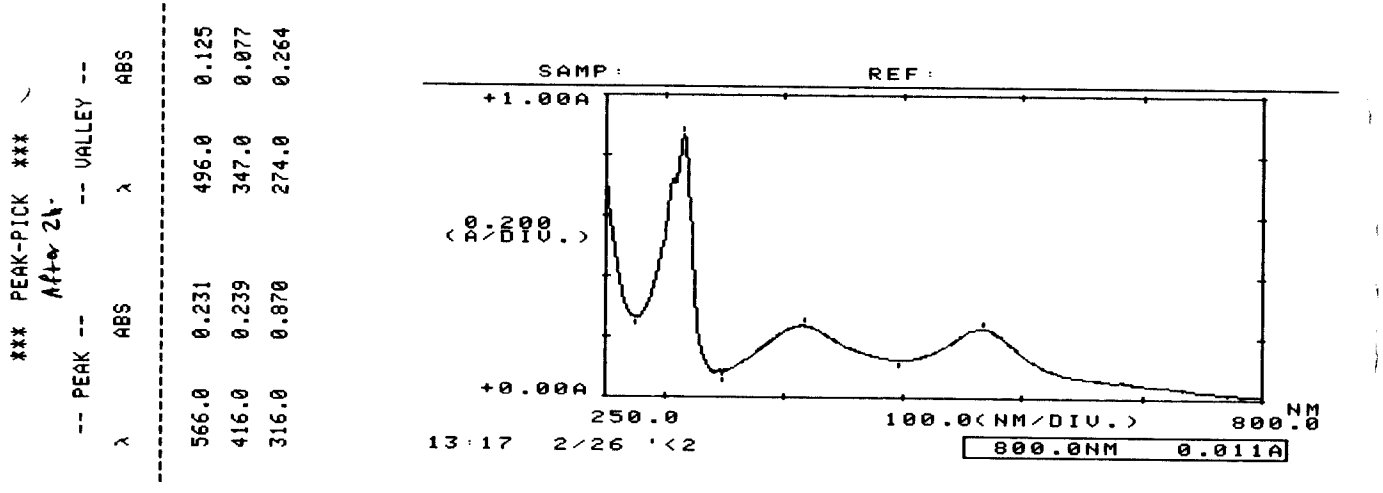

Figure 8b: UV-Vis spectrum for the reaction of $RuCl_3.3H_2O$ with (4,4'-dimethoxy-2,2'-bipyridine) in abs. EtOH after 2 h.

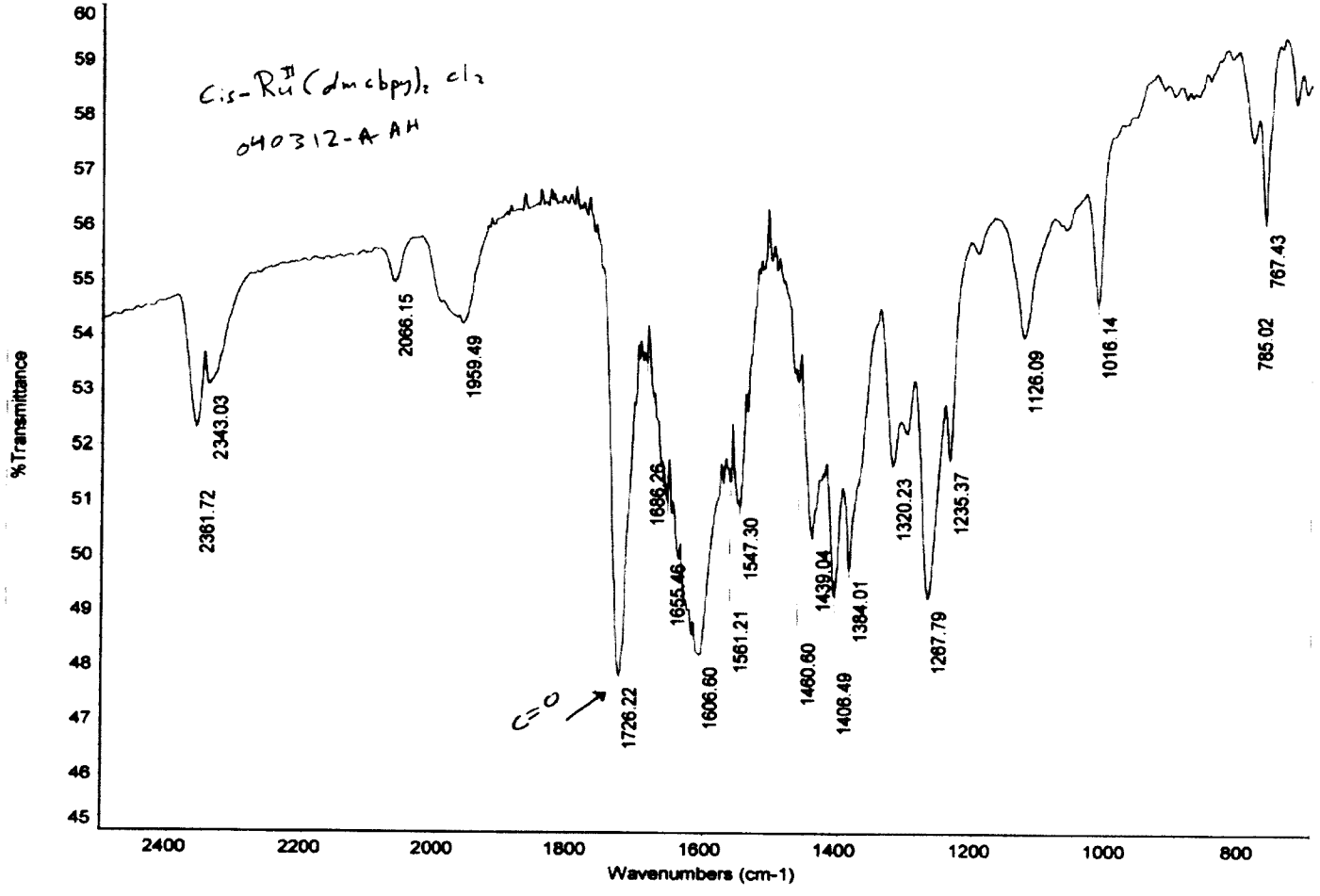

Figure 8c: IR spectrum of $Ru^{II}(dmcbpy)_2Cl_2$ (040312-A-AH).

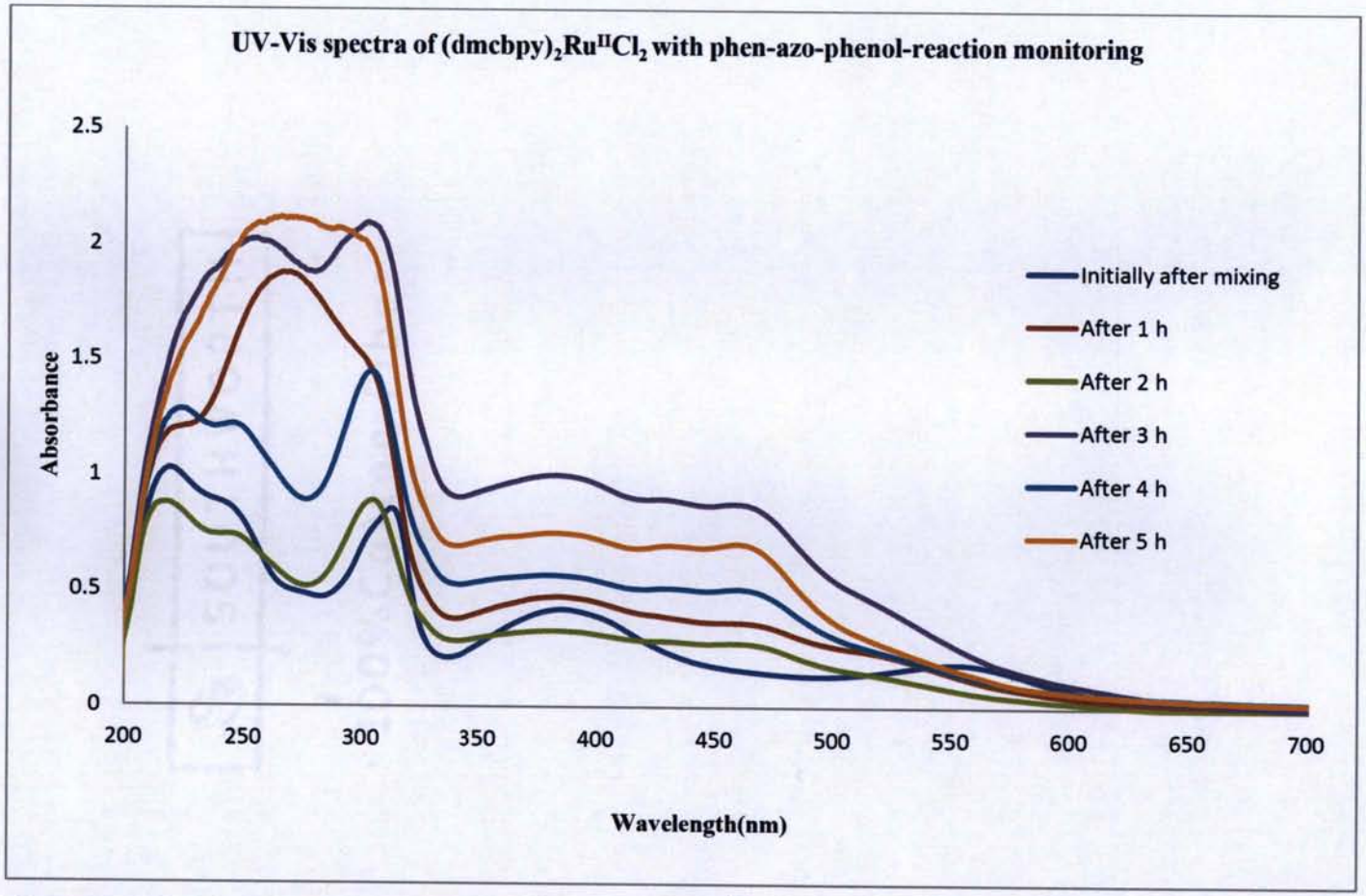

Figure 9a: UV-Vis spectra for the reaction monitoring of $Ru^{II}(dmcbpy)_2Cl_2$ with phen-azo-phenol using MeOH as a solvent.

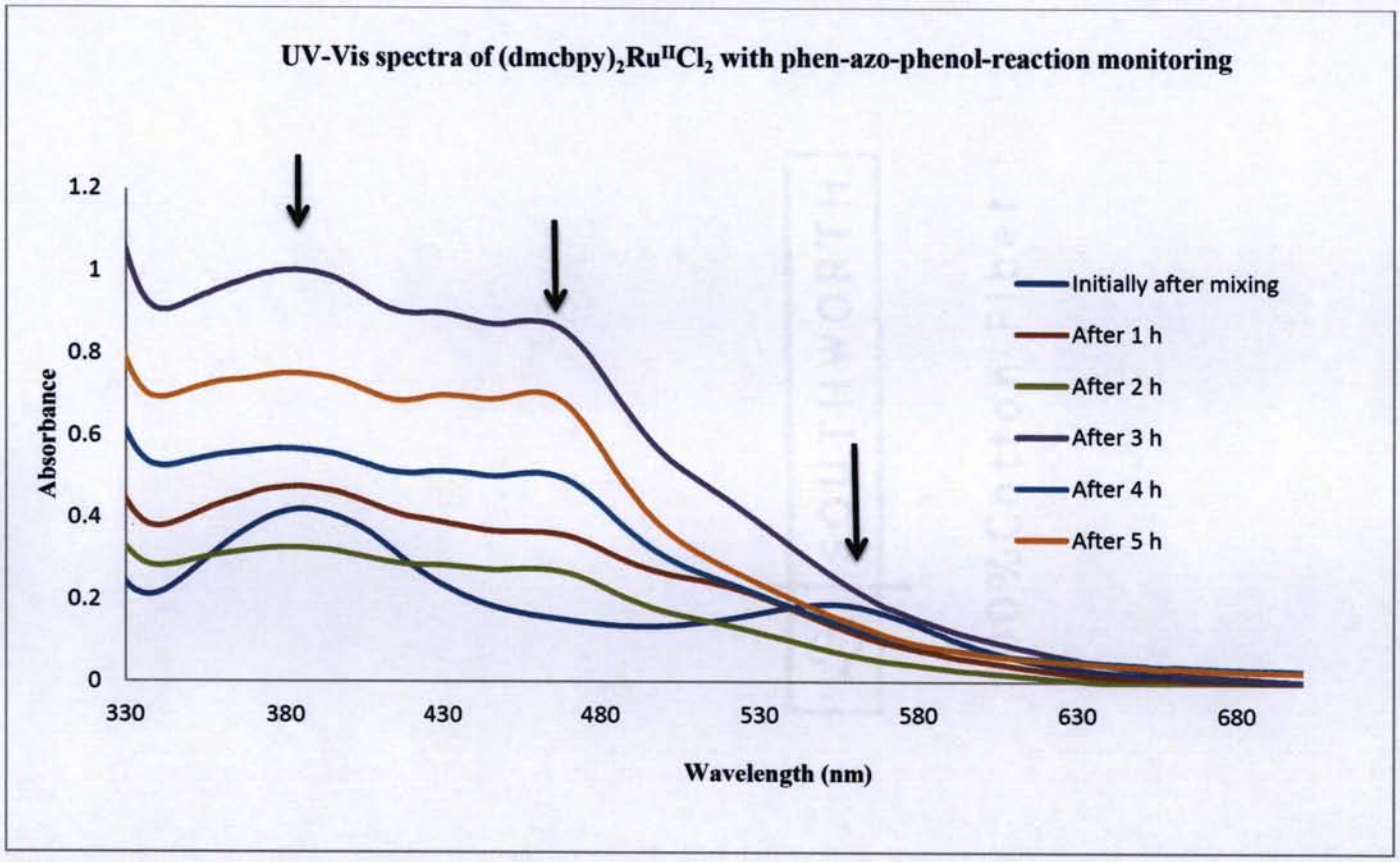

Figure 9b: UV-Vis spectra for the reaction monitoring of $Ru^{II}(dmcbpy)_2Cl_2$ with phen-azo-phenol in MeOH expanded. The arrows indicate the shift in wavelength as the reaction proceeds.

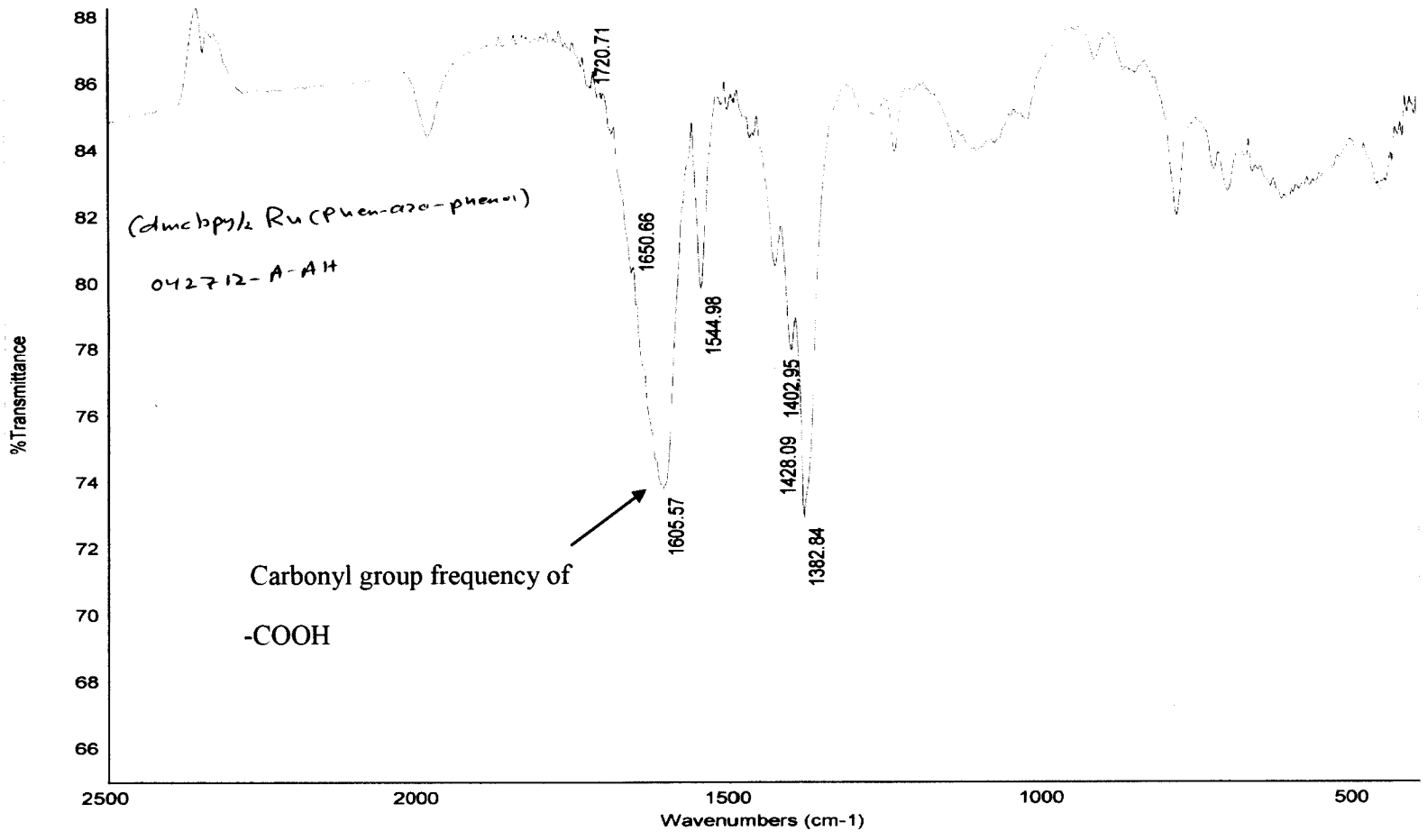

Figure 9c: IR spectrum of $[(dmcbpy)_2Ru^{II}(phen\text{-}azo\text{-}phenol)](PF_6)_2$ (042712-A-AH).

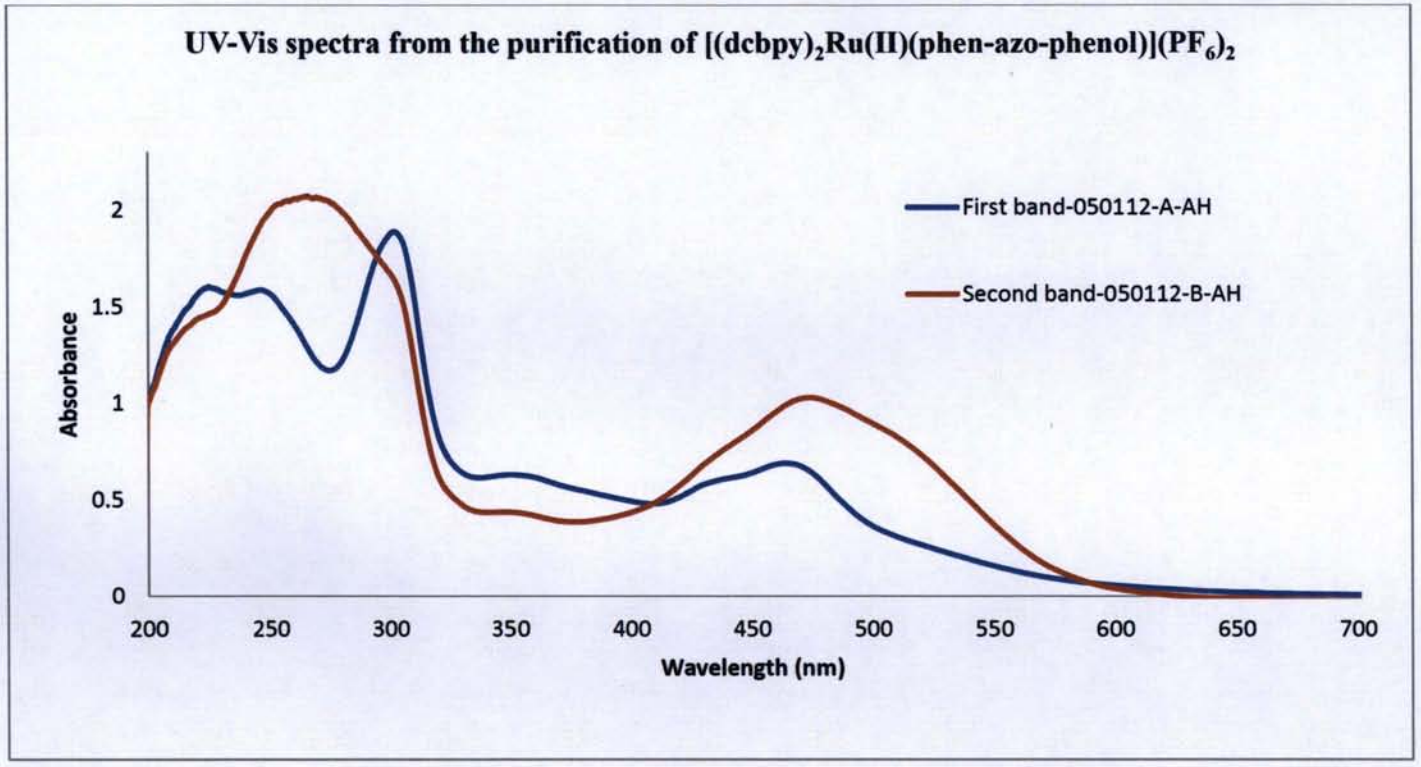

Figure 9d: UV-Vis spectra for the two bands collected from size exclusion chromatography in 1:1 MeOH:H_2O.

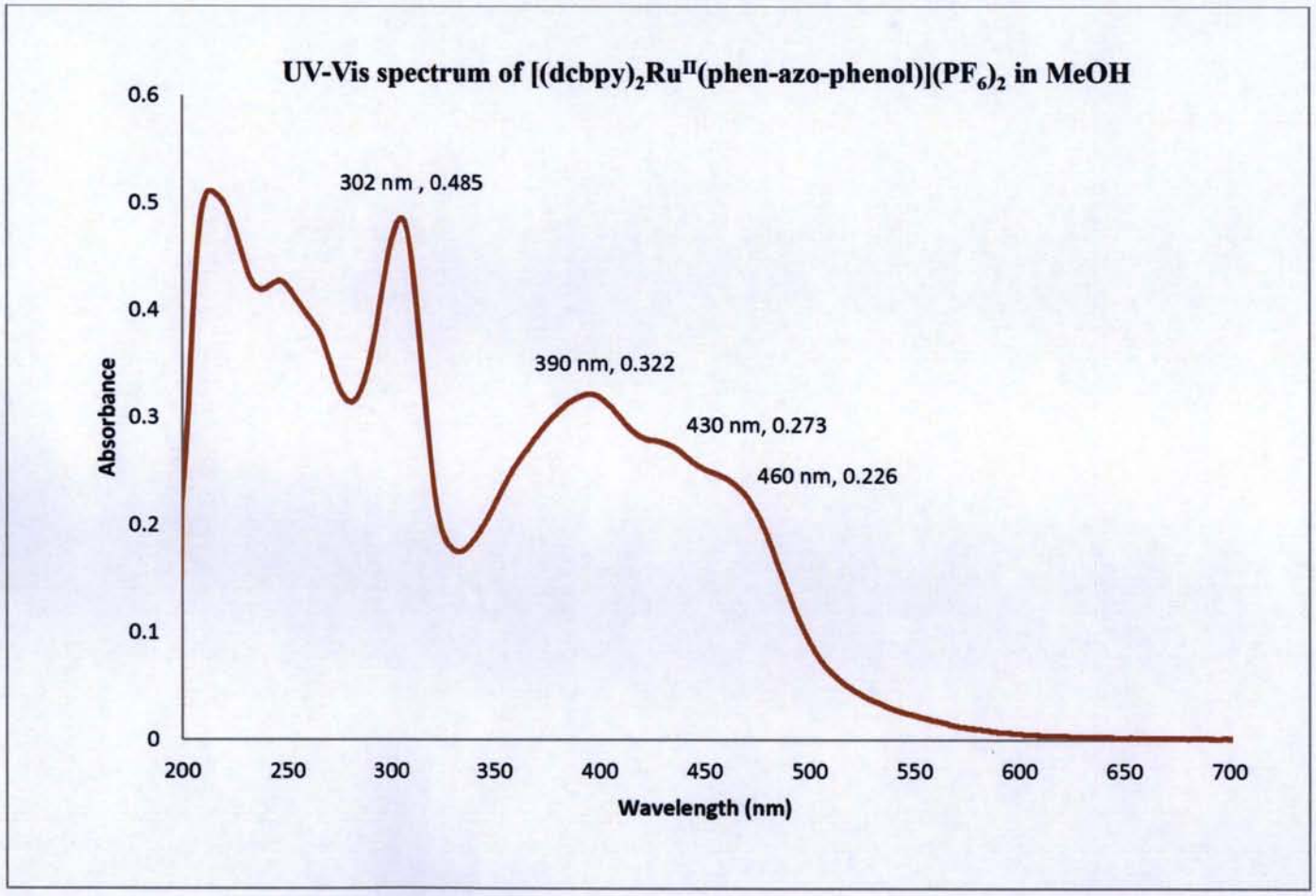

Figure 9e: UV-Vis spectrum of $[(dcbpy)_2Ru^{II}(phen\text{-}azo\text{-}phenol)](PF_6)_2$ (050112-B-AH) in MeOH.

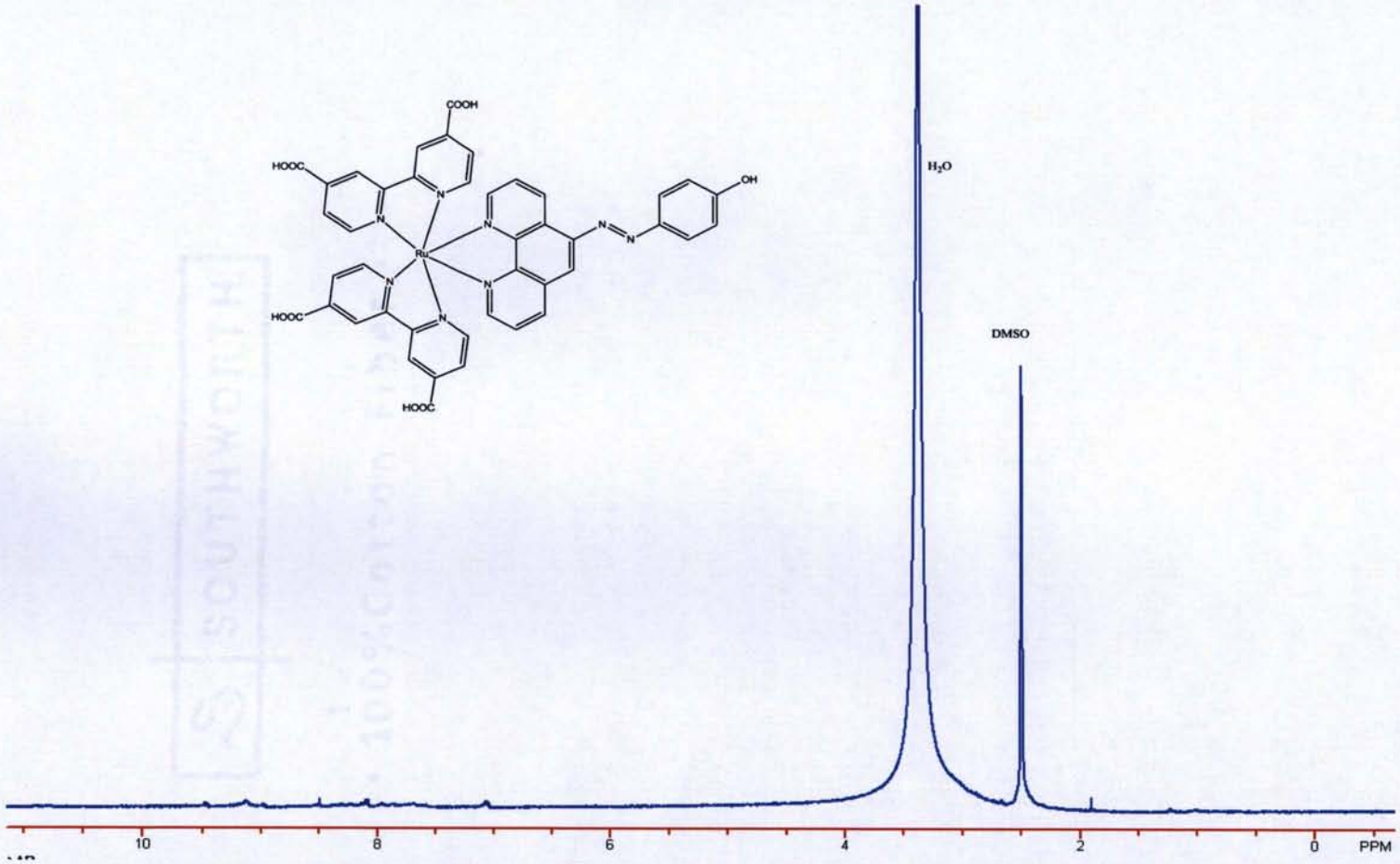

Figure 9f: ^{1}H-NMR (MEM2A400) of [(dcbpy)$_2$Ru^{II}(phen-azo-phenol)](PF$_6$)$_2$ (050112-B-AH) in d$_6$-DMSO.

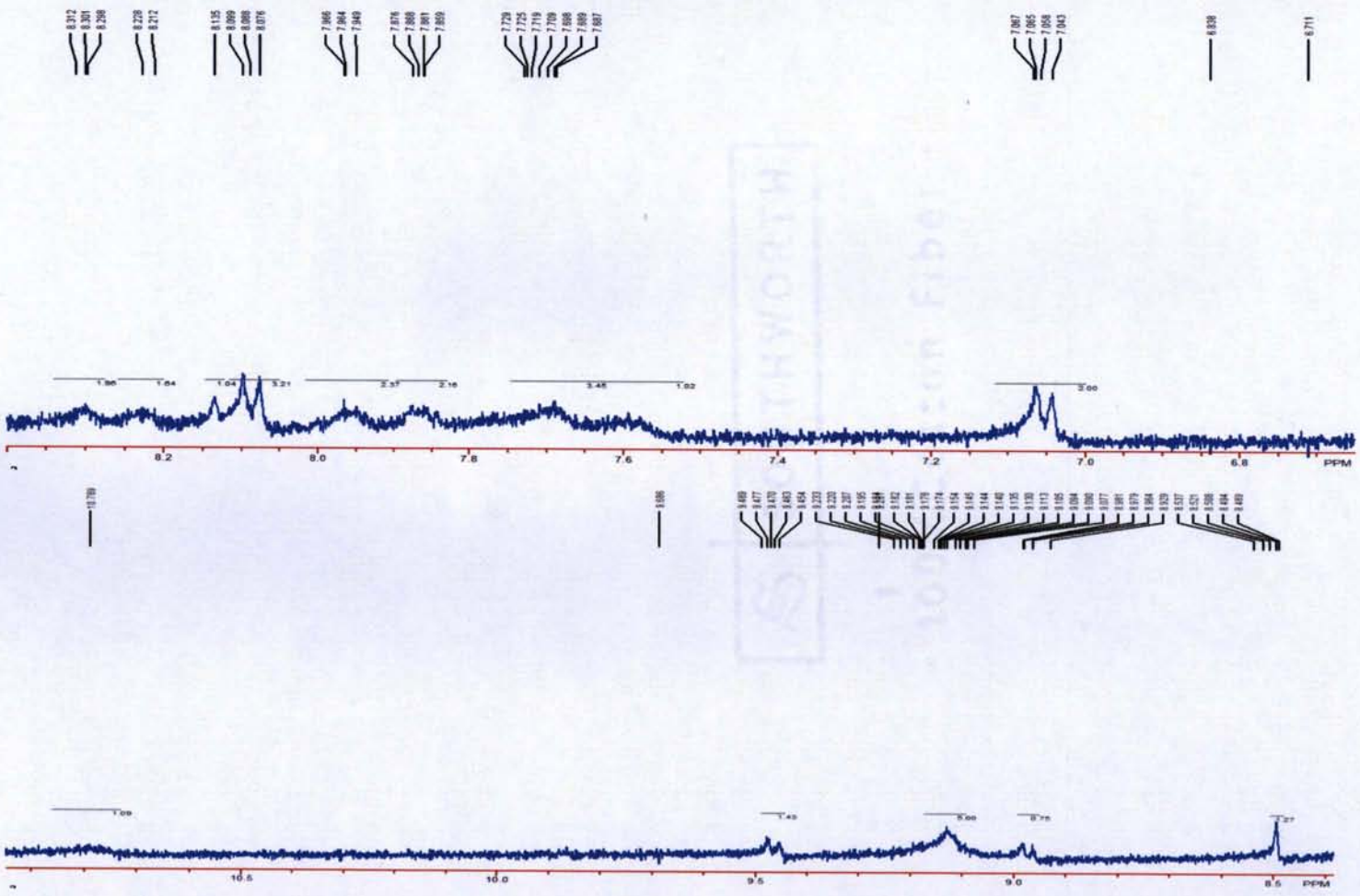

Figure 9g: ^{1}H-NMR (MEM2A400) of [(dcbpy)$_2$Ru^{II}(phen-azo-phenol)](PF$_6$)$_2$ (050112-B-AH) in d$_6$-DMSO expanded.

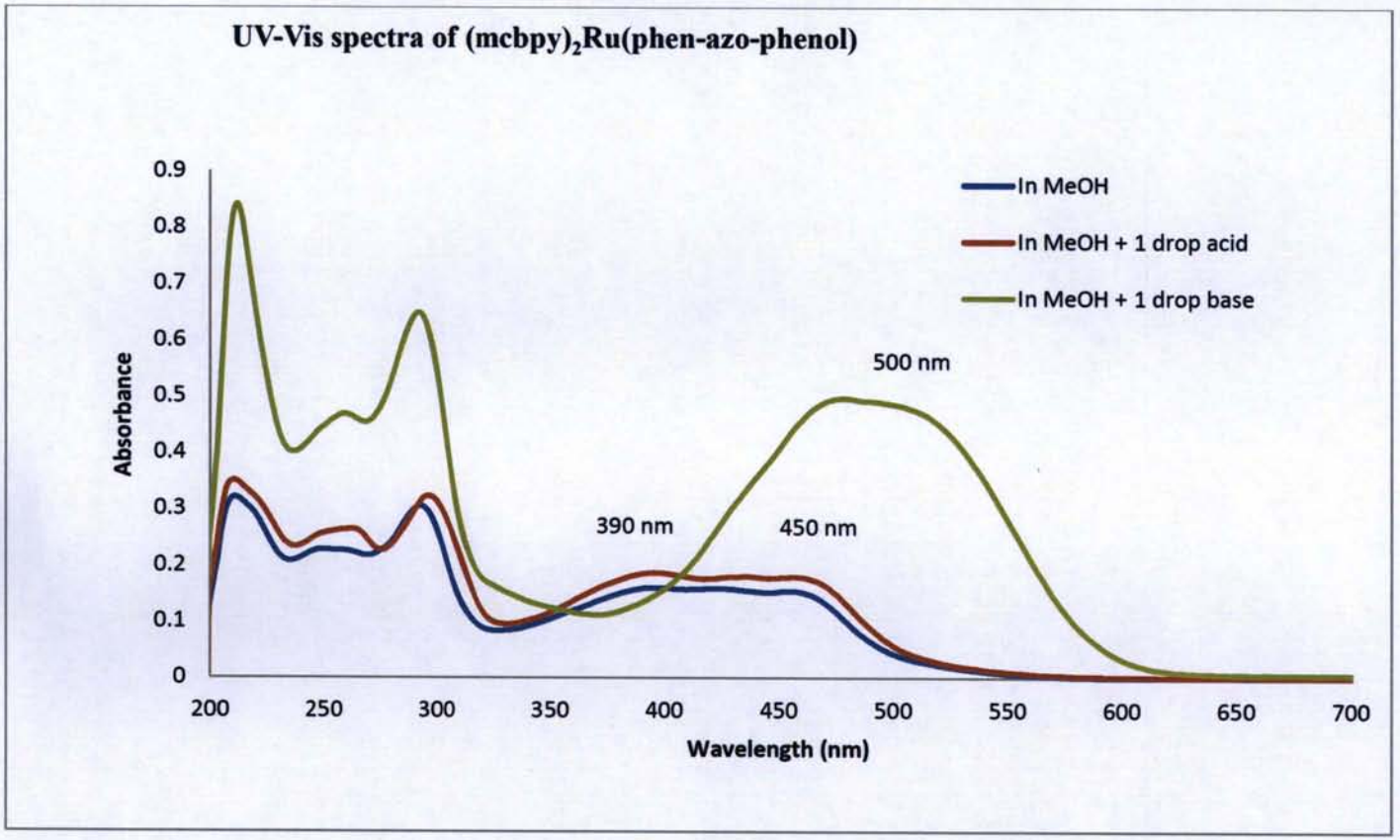

Figure 9h: UV-Vis spectra of $[(mcbpy)_2Ru^{II}(phen\text{-}azo\text{-}phenol)](PF_6)_2$ (050312C-AH).

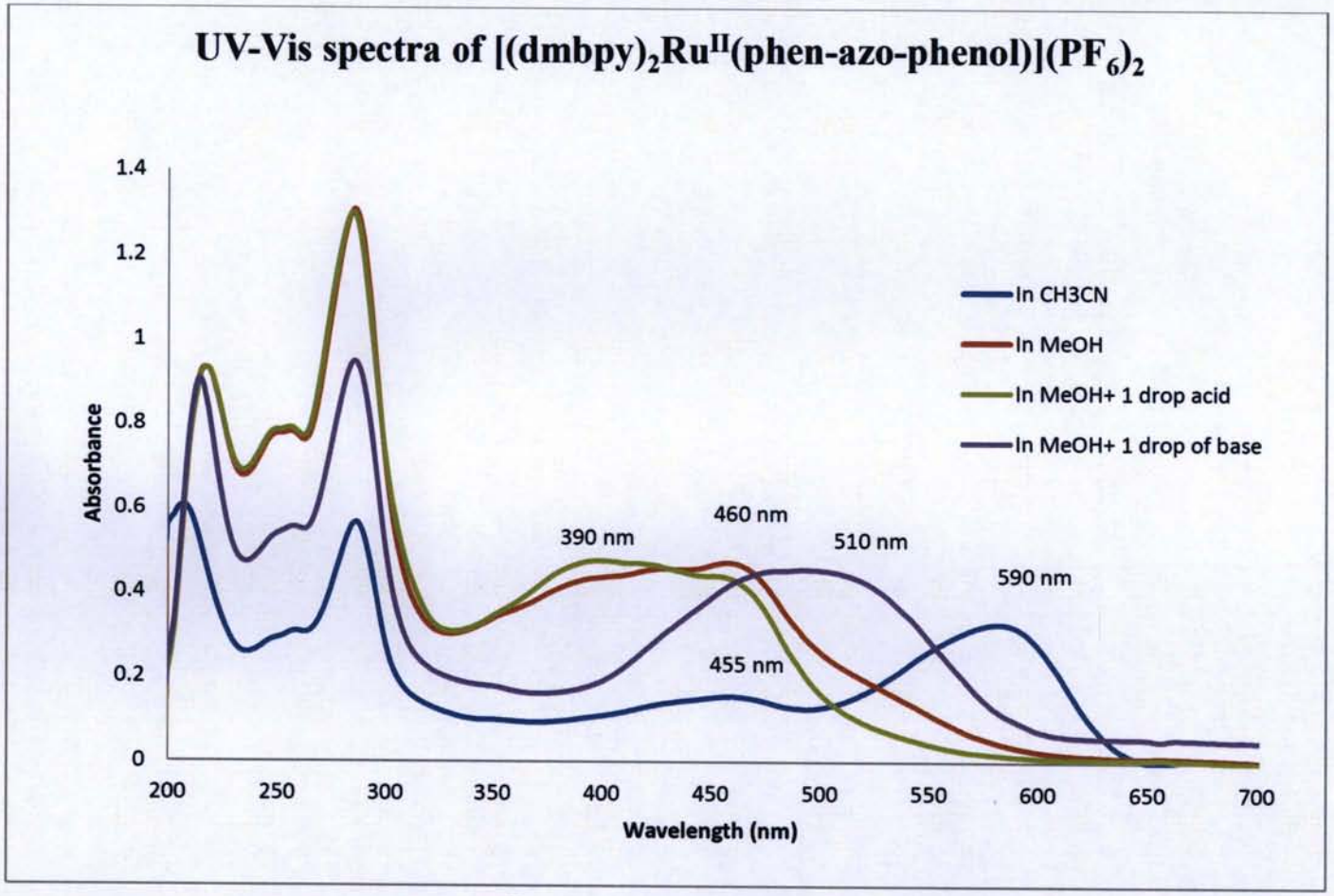

Figure 9i: UV-Vis spectra of $[(dmbpy)_2Ru^{II}(phen\text{-}azo\text{-}phenol)](PF_6)_2$ (050712-B-AH).

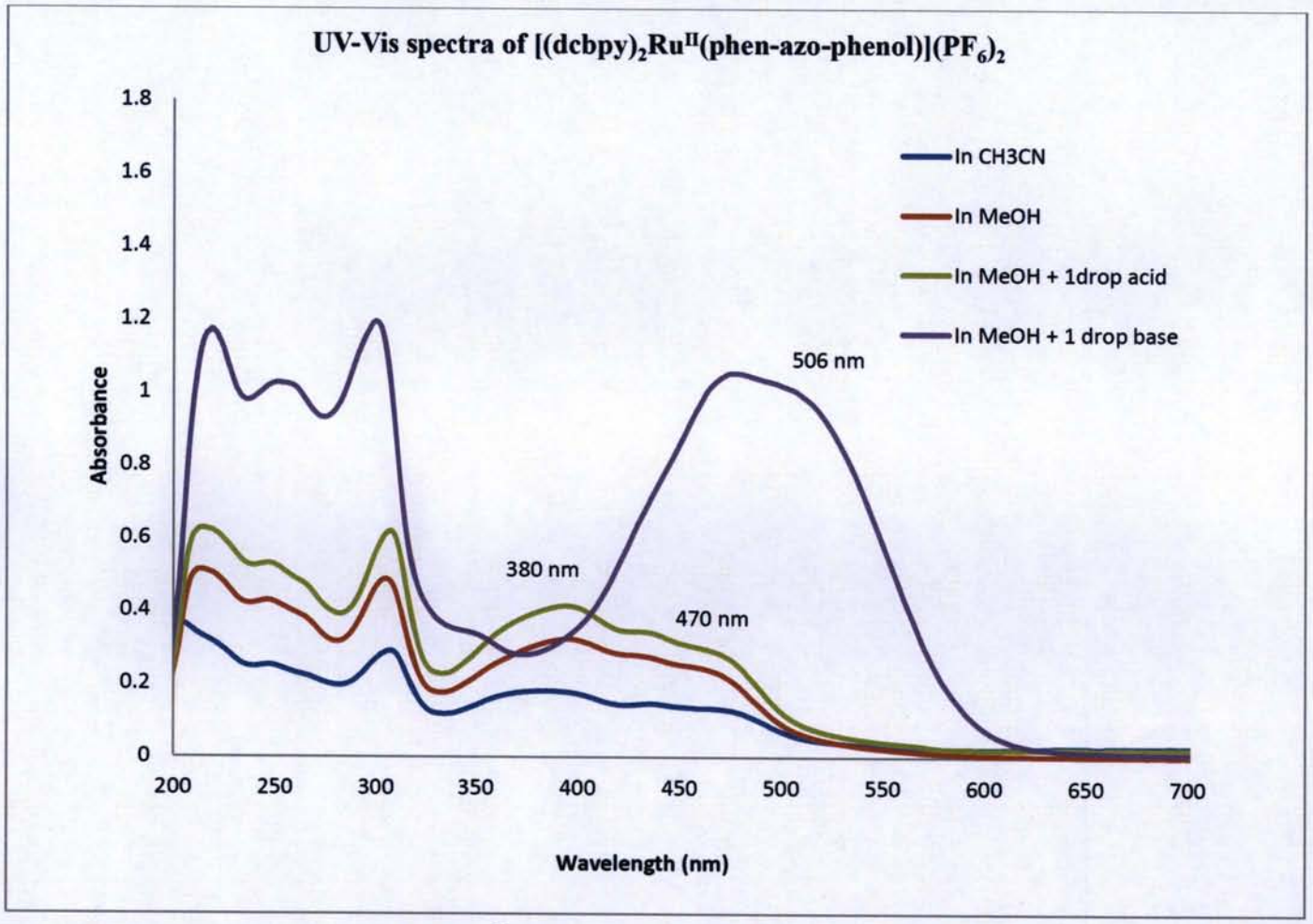

Figure 9j: UV-Vis spectra of $[(dcbpy)_2Ru^{II}(phen\text{-}azo\text{-}phenol)](PF_6)_2$ (050112-B-AH).

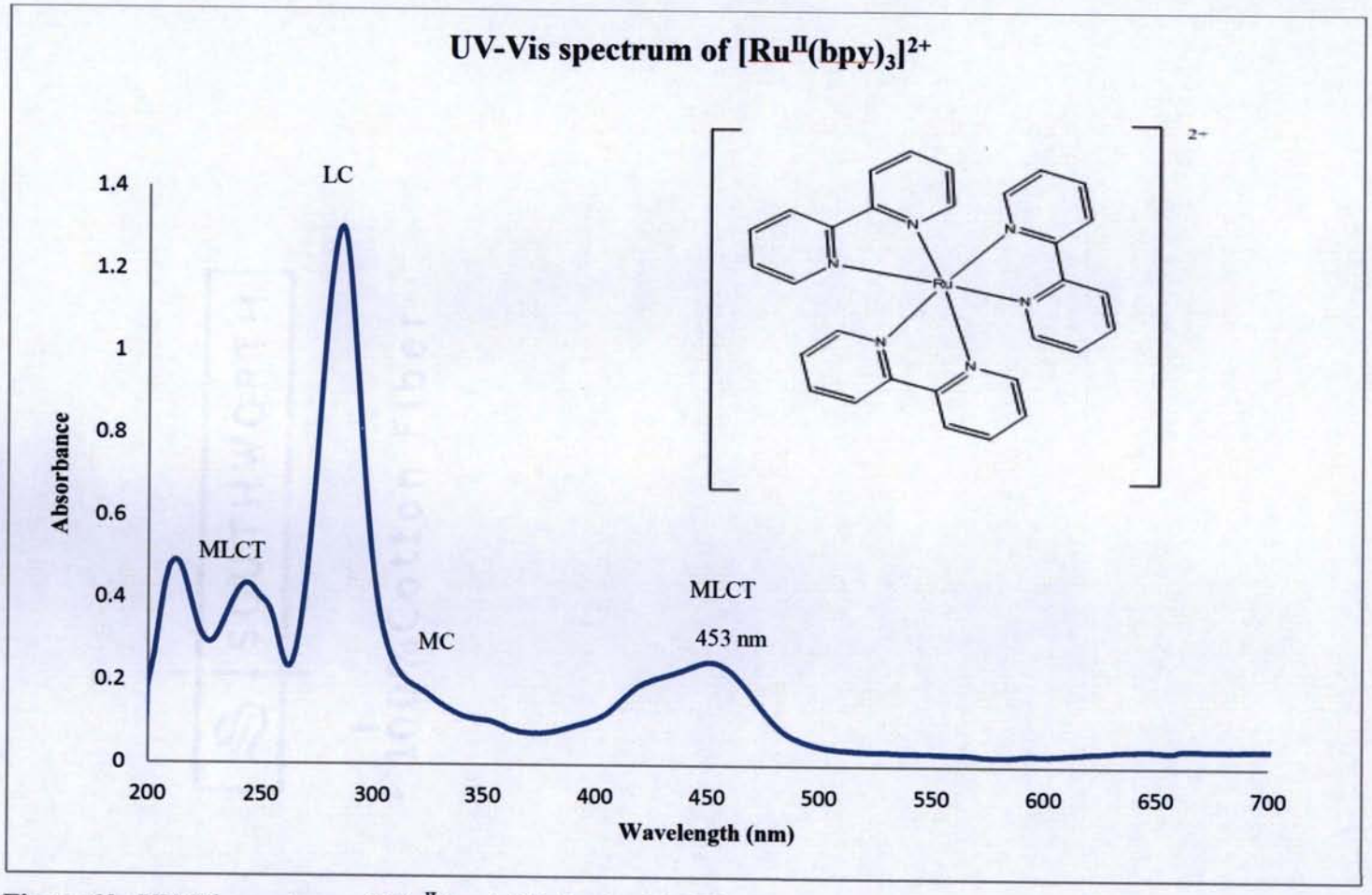

Figure 9k: UV-Vis spectrum of [Ru^{II}(bpy)$_3$]Cl$_2$ in abs. MeOH.

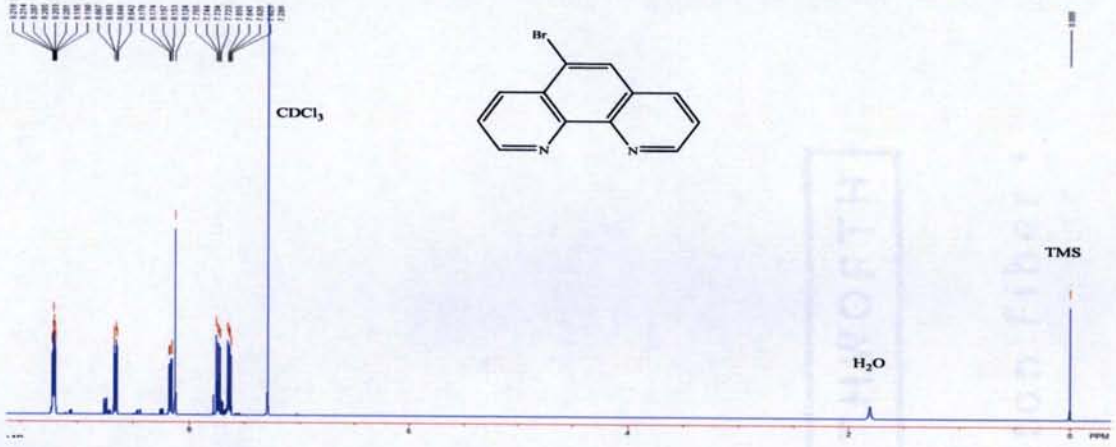

Figure 10a: ^{1}H-NMR (MEM2A282) for 5-Br-phen (070811-A-AH) in $CDCl_3$.

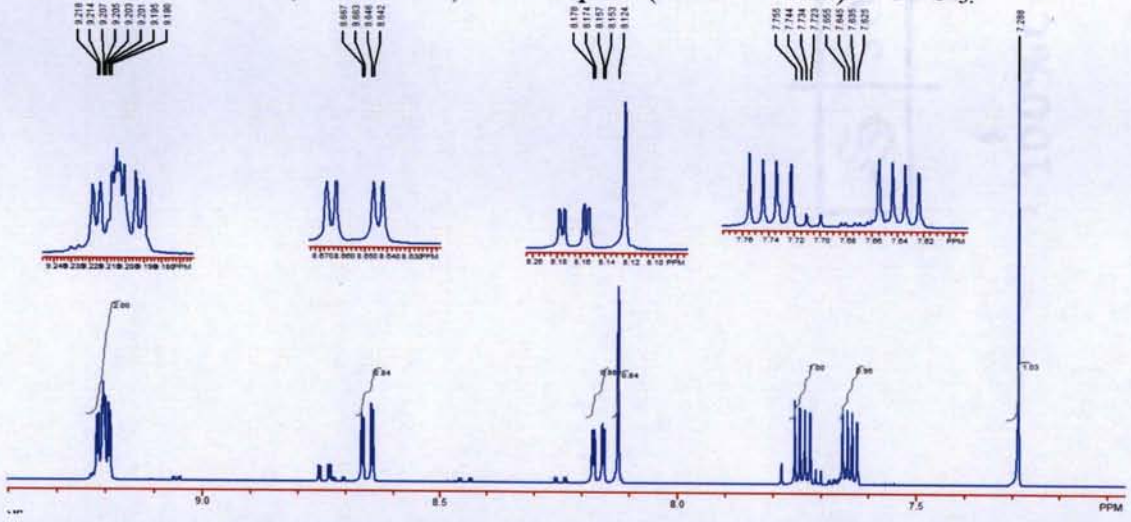

Figure 10b: ^{1}H-NMR (MEM2A282) for 5-Br-phen (070811-A-AH) in $CDCl_3$ expanded.

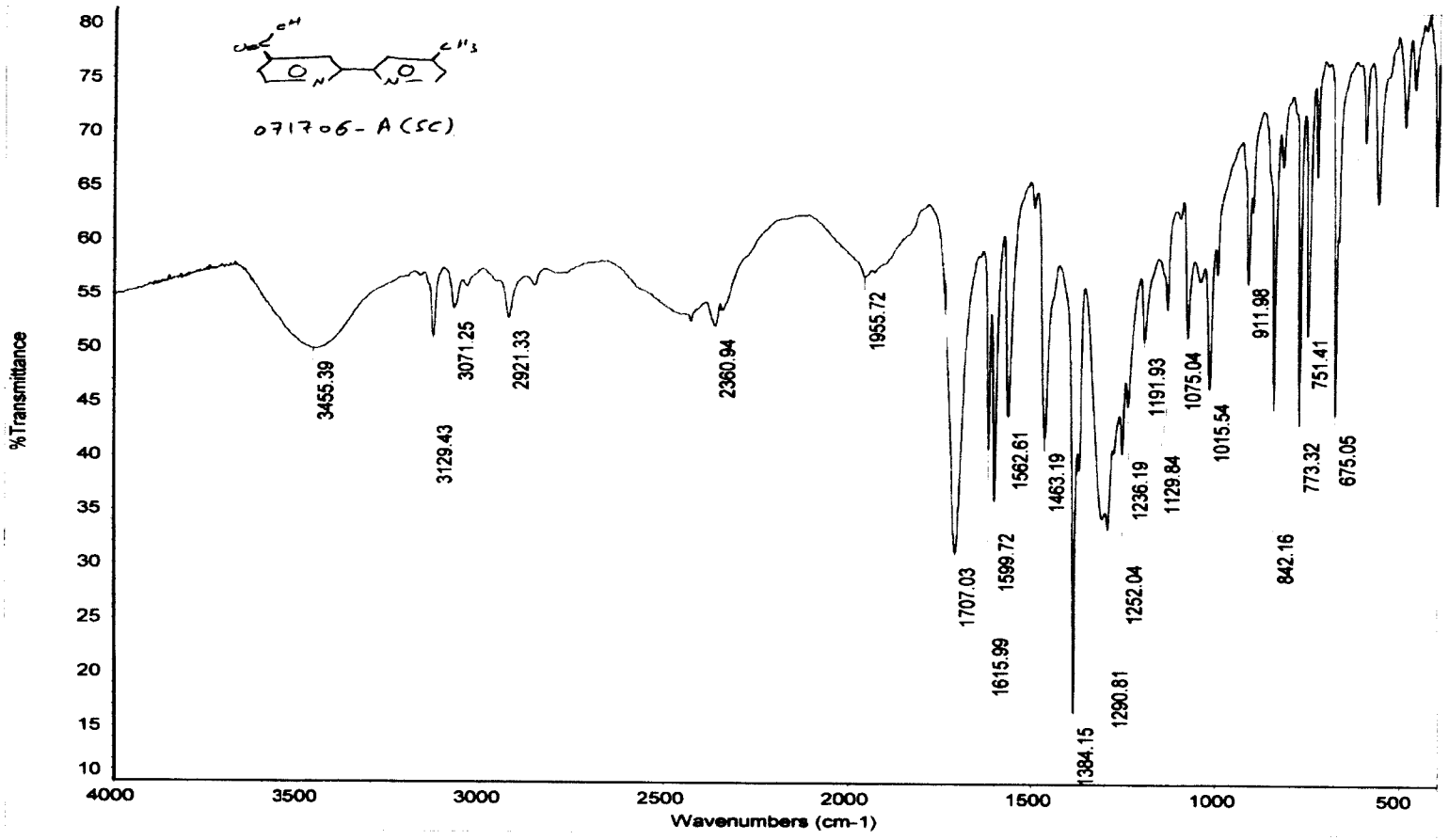

Figure 10c: IR of 4'-carboxy-4-methyl-2,2'-bipyridine (071706-A(SC).

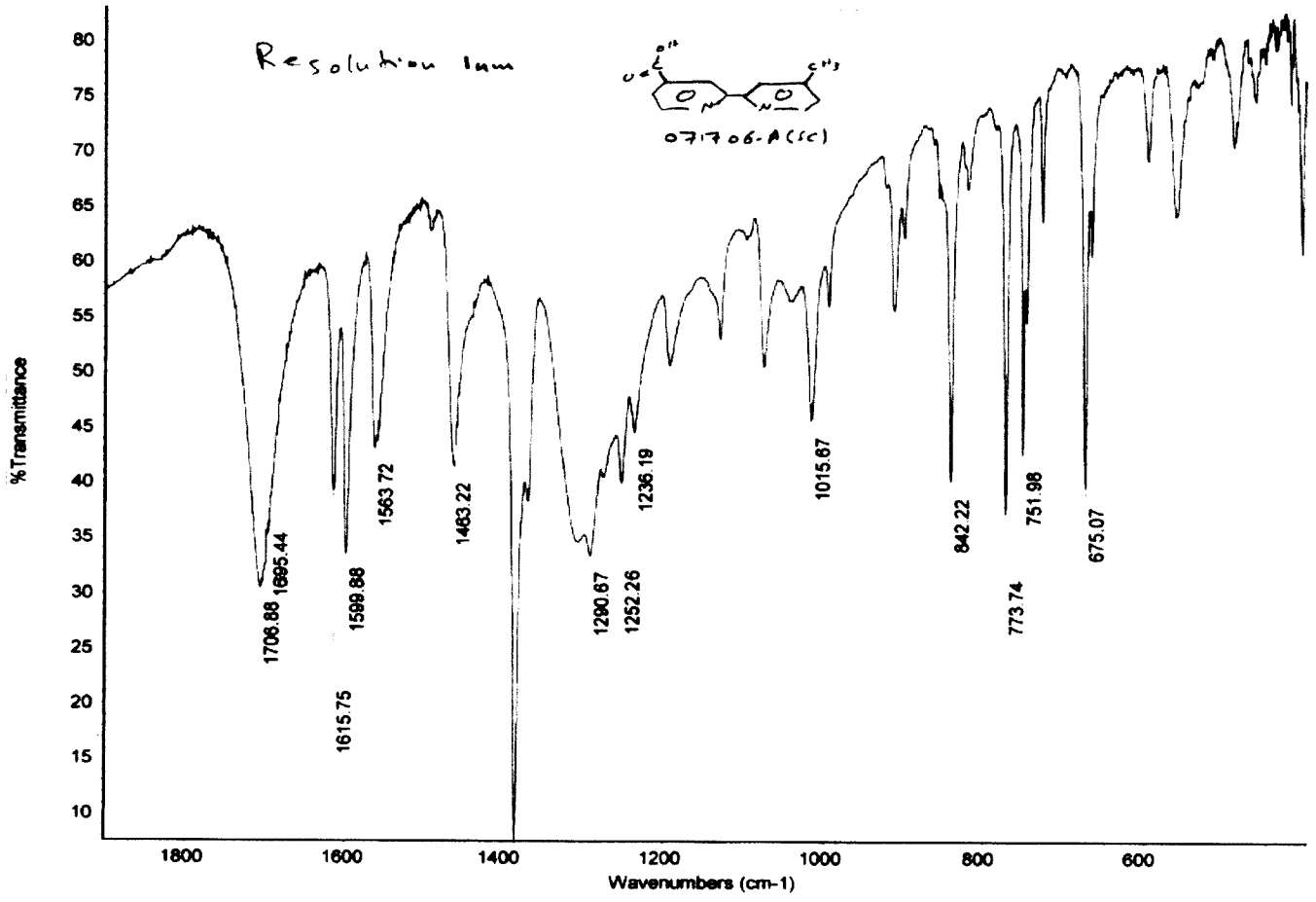

Figure 10d: IR of 4'-carboxy-4-methyl-2,2'-bipyridine (071706-A(SC) at high resolution.

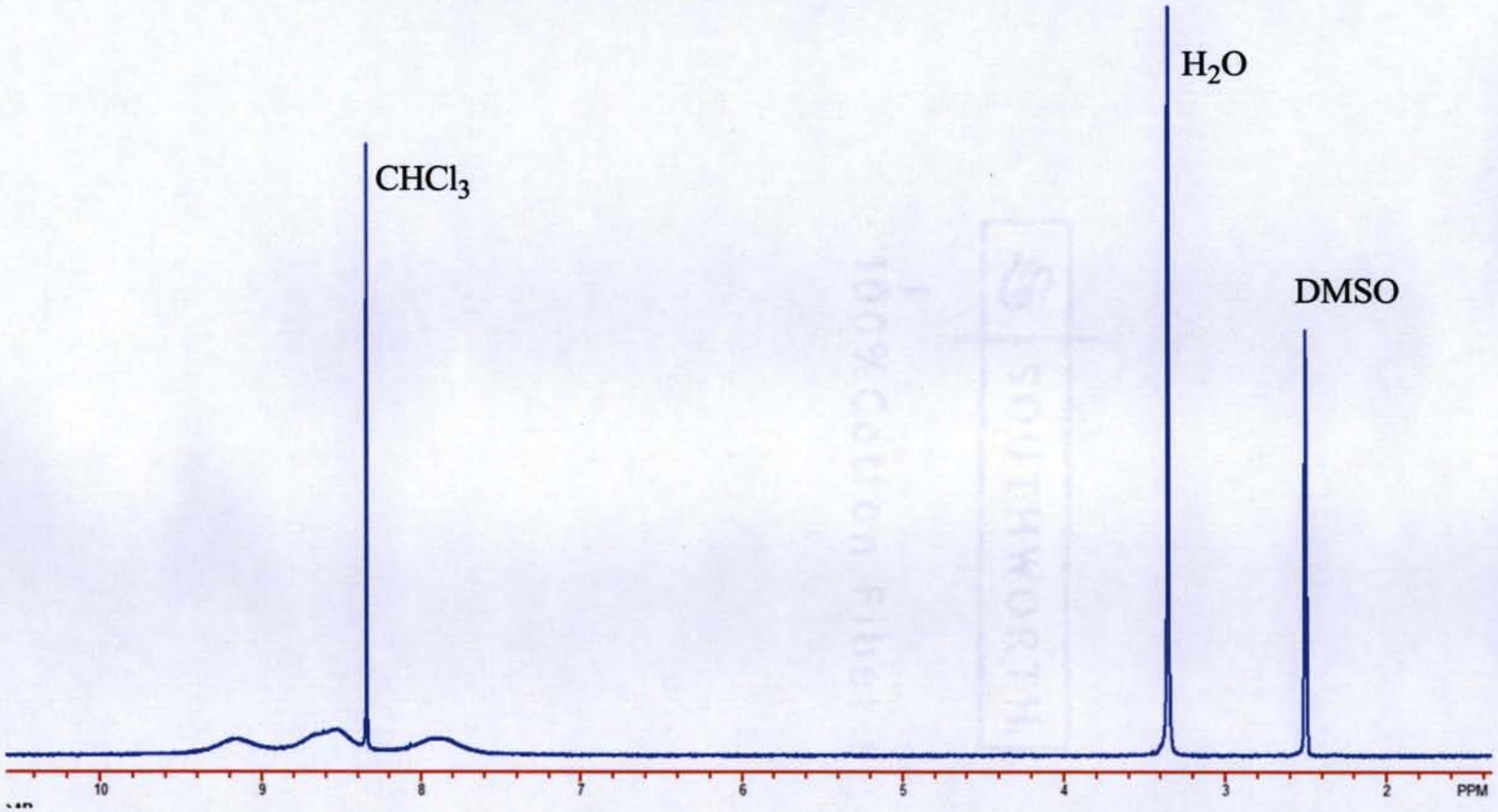

Figure 11a: ^{1}H-NMR (MEM2A287) for the synthetic attempt of 2-((1,10-phenanthrolin-5-yl)amino)acetic acid (071911A-AH) in d_6-DMSO.

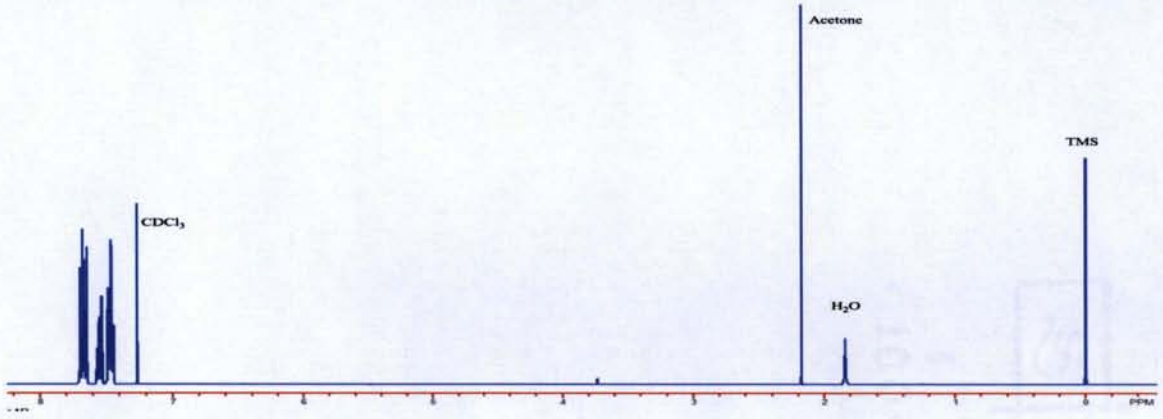

Figure 12a: ^{1}H-NMR (MEM2A302) for the synthetic attempt of indoxyl (080211-B-AH) in $CDCl_3$.

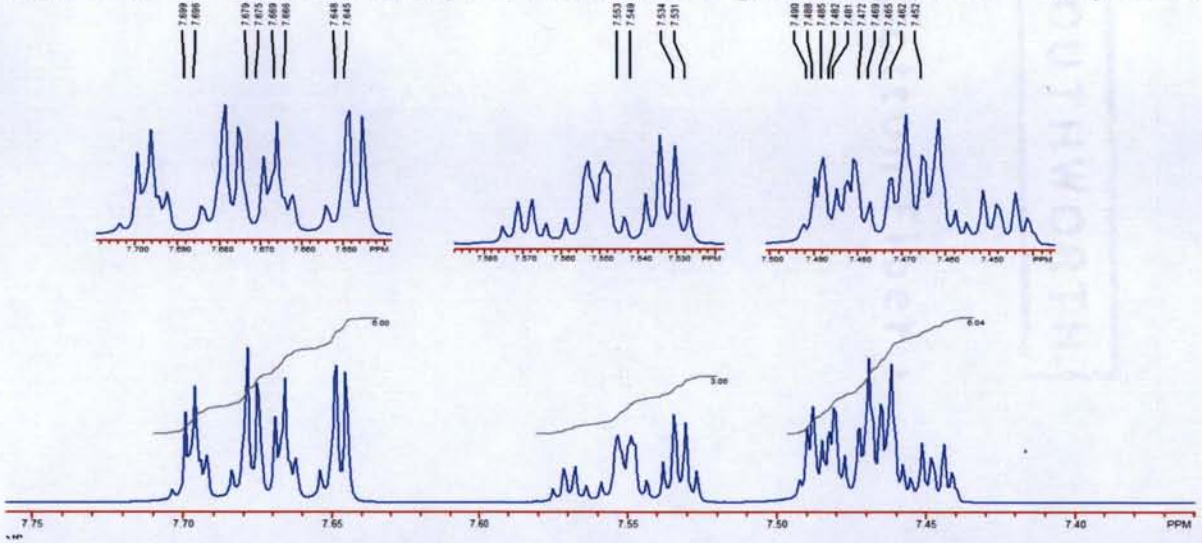

Figure 12b:^{1}H-NMR (MEM2A302) for the synthetic attempt of indoxyl (080211-B-AH) in $CDCl_3$ (expanded).

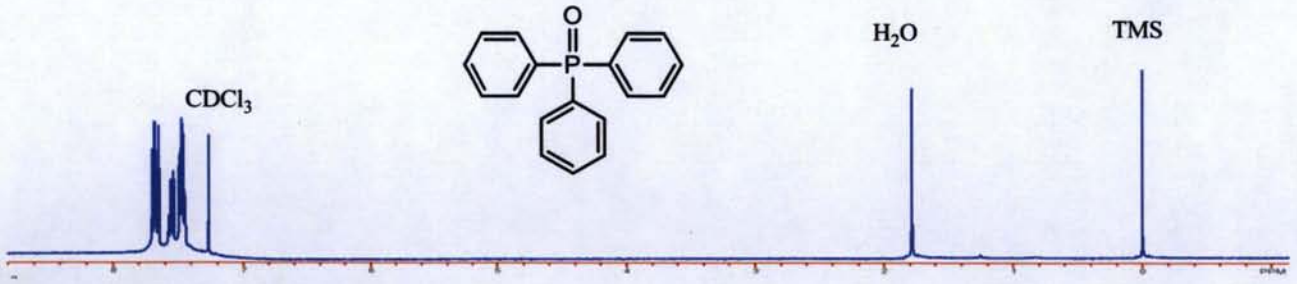

Figure 12c: ^{1}H-NMR (MEM2A415) for an authentic sample of triphenylphosphine oxide in $CDCl_3$.

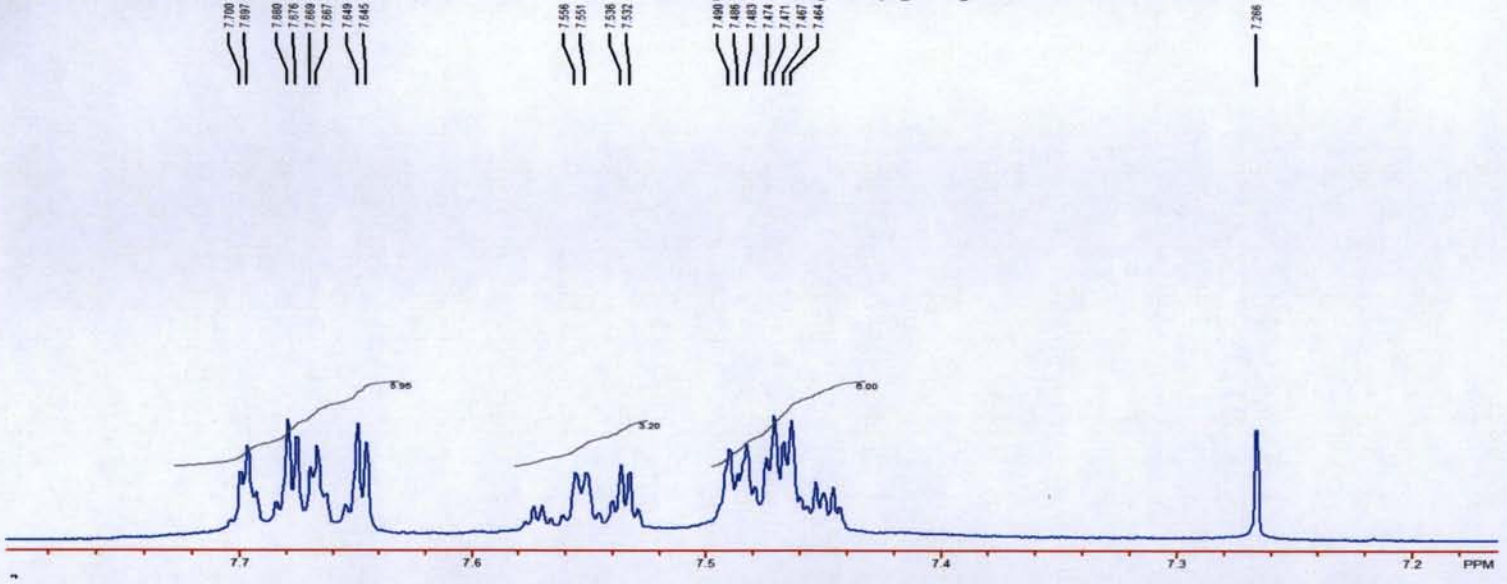

Figure 12d: ^{1}H-NMR (MEM2A415) for an authentic sample of triphenylphosphine oxide in $CDCl_3$ expanded.

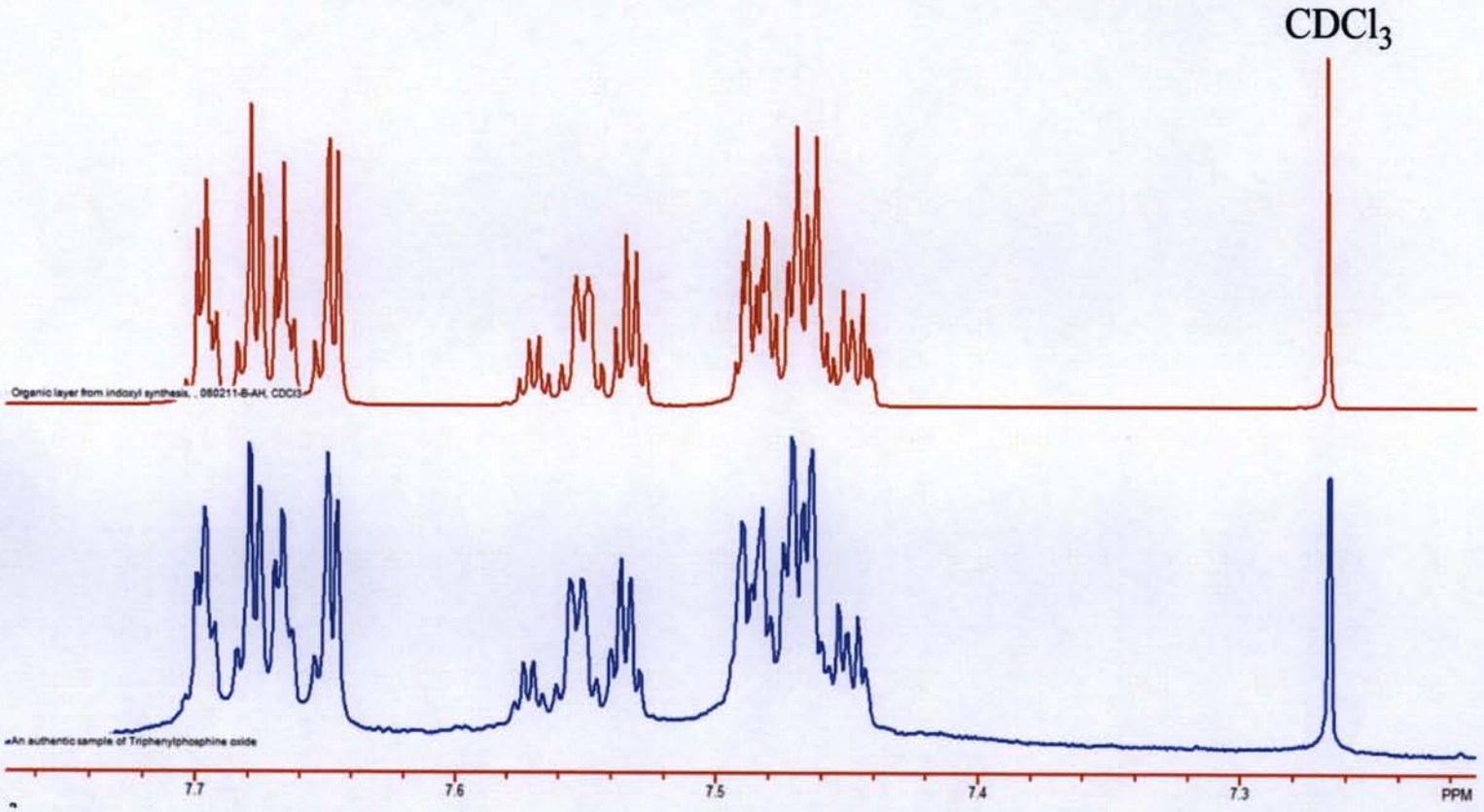

Figure 12e: ^{1}H-NMR for the indoxyl attempt upper graph (MEM2A302) and an authentic sample of triphenylphosphine oxide lower graph (MEM2A415) in $CDCl_3$.

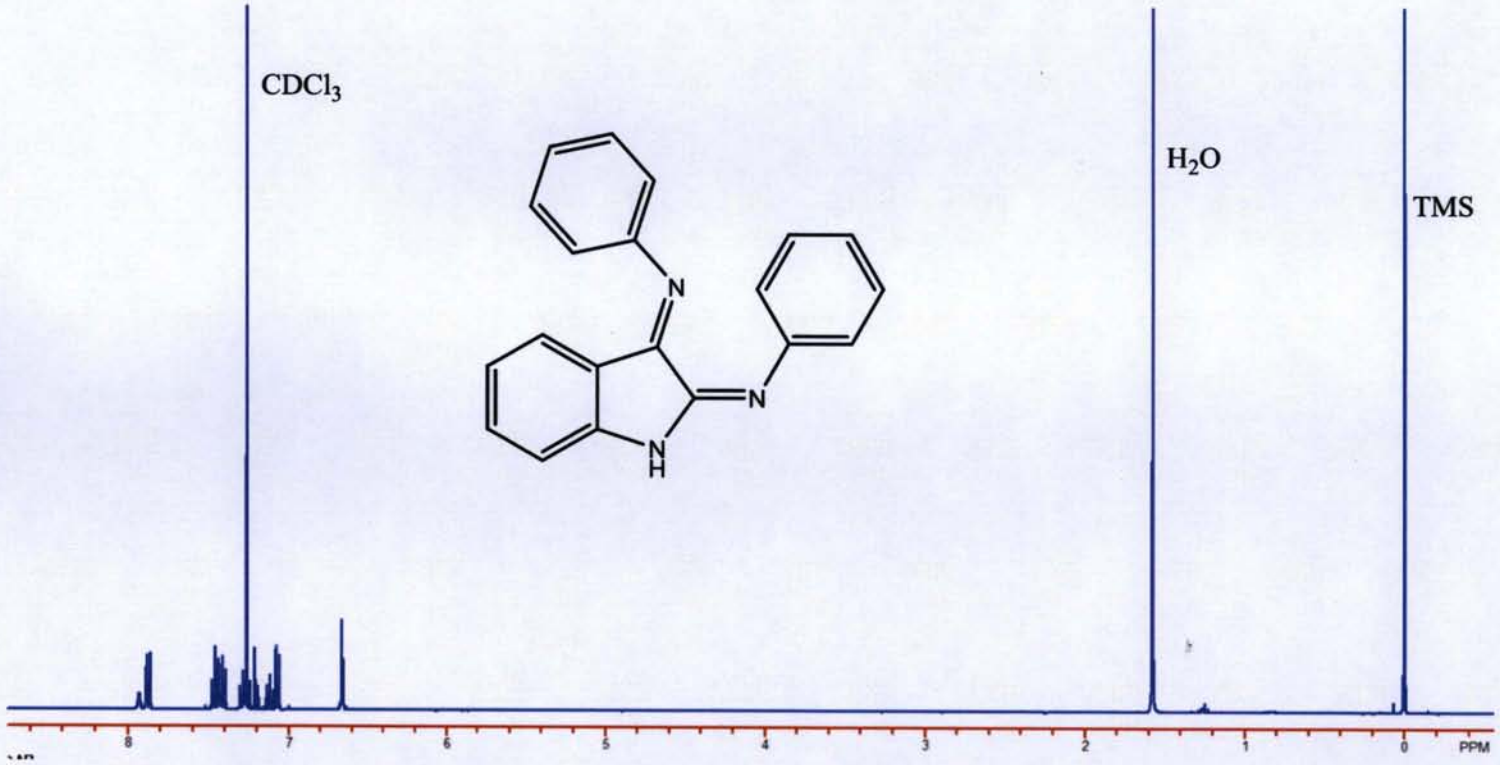

Figure 13a: ^{1}H NMR (MEM2A311) spectrum of 2-phenylamino-3-phenylimino-3H-indole (081211-A-AH) in $CDCl_3$.

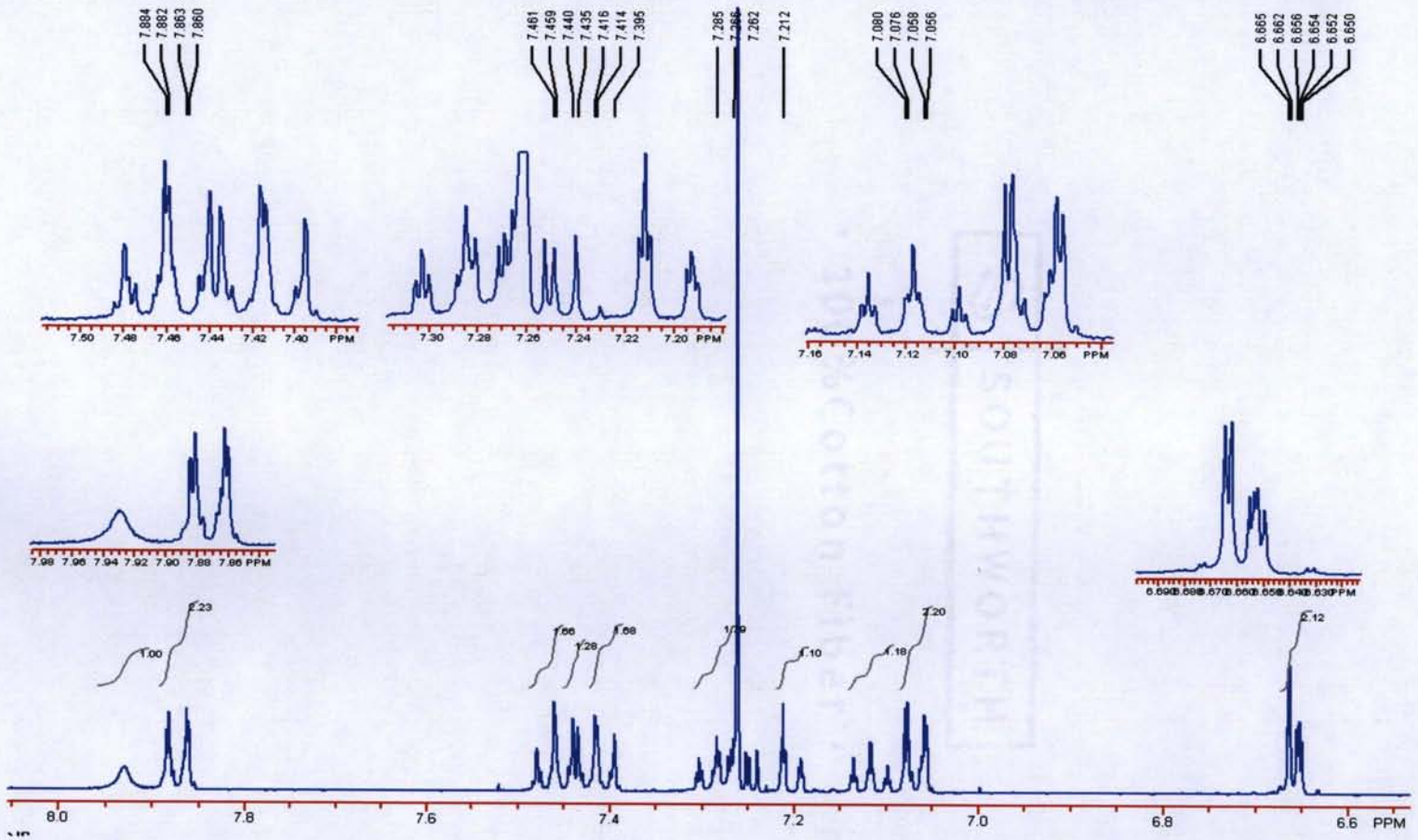

Figure 13b: ^{1}H-NMR (MEM2A311) spectrum for 2-phenylamino-3-phenylimino-3H-indole (081211-A-AH) in $CDCl_3$ (expanded).

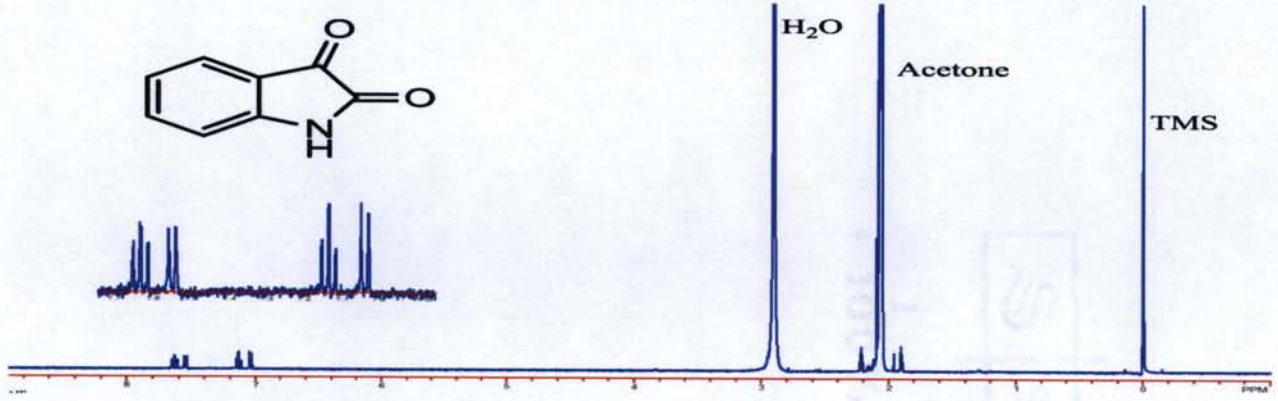

Figure 14a:[1]H- NMR (MEM2A312) spectrum of isatin (081311-A-AH) in acetone-d_6.

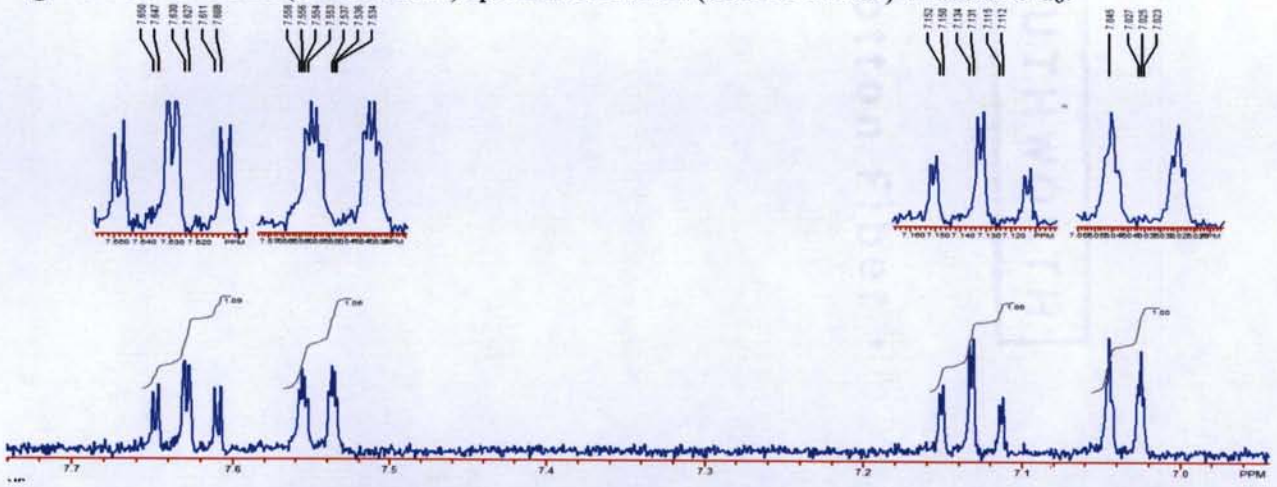

Figure 14b:[1]H-NMR (MEM2A312) spectrum for isatin (081311-A-AH) in acetone-d_6 (expanded).

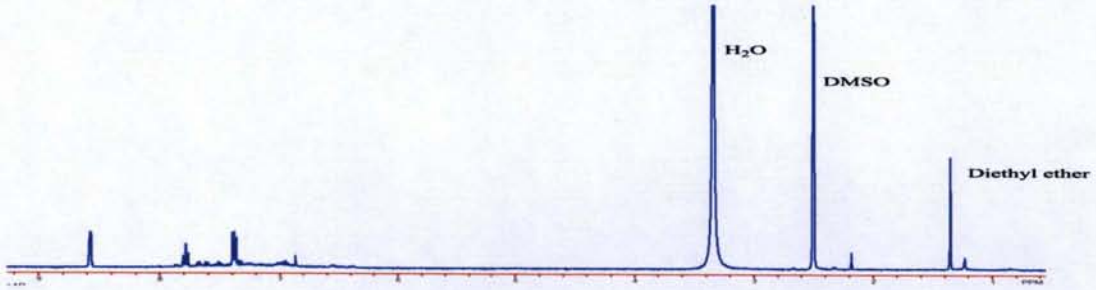

Figure 14a: ^{1}H-NMR (MEM2A313) spectrum for the product of isatine reduction (081711-A-AH) in d_6-DMSO.

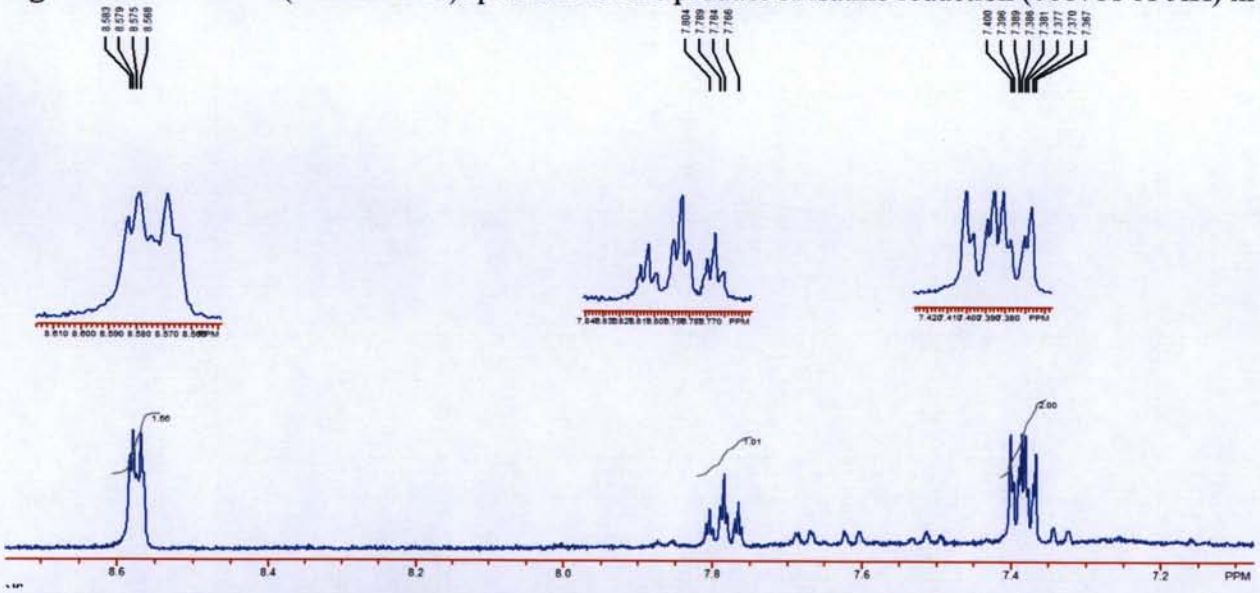

Figure 14b:^{1}H-NMR (MEM2A313) spectrum for the product of isatin reduction (081711-A-AH) in d_6-DMSO showing pyridine peaks in the spectrum as the major impurity.

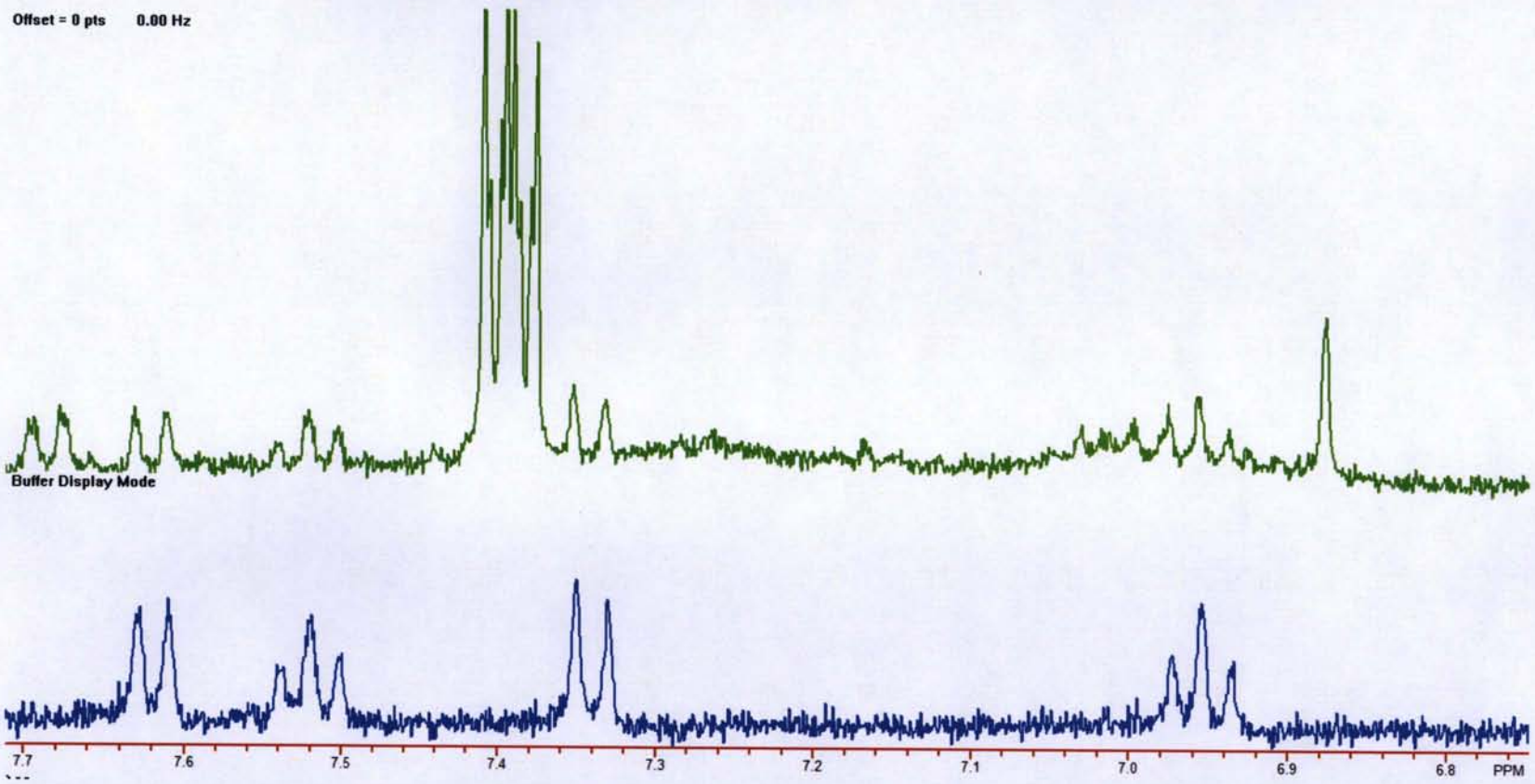

Figure 14c: ^{1}H-NMR (MEM2A313) spectra for the product of isatin reduction (081711-A-AH) upper spectrum (green color) and an authentic sample of indigo dye lower spectrum (blue color) in d_6-DMSO.

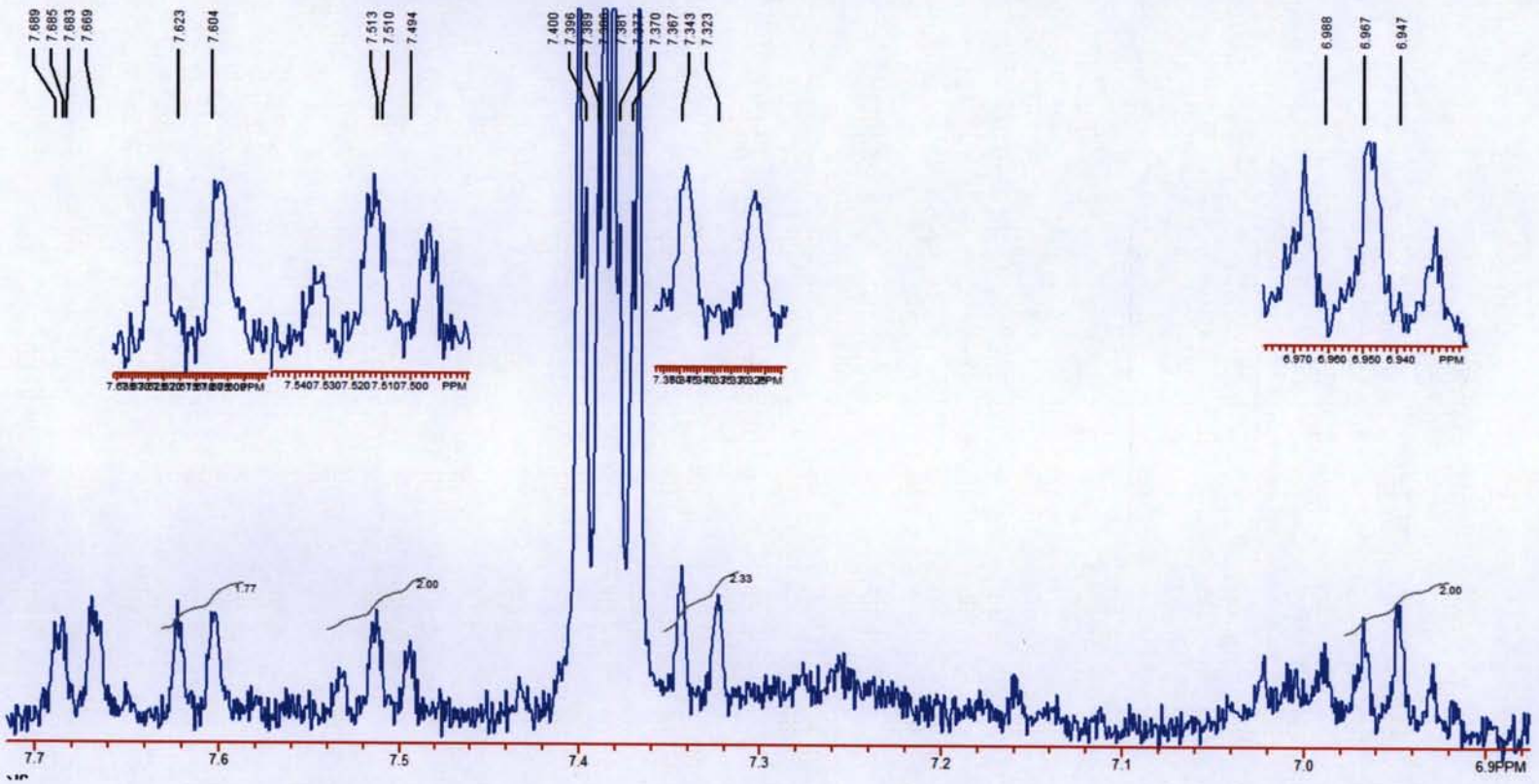

Figure 14d: ^{1}H-NMR (MEM2A313) spectrum for the product of isatin reduction (081711-A-AH) in d_6-DMSO showing the integration values of indigo dye peaks.

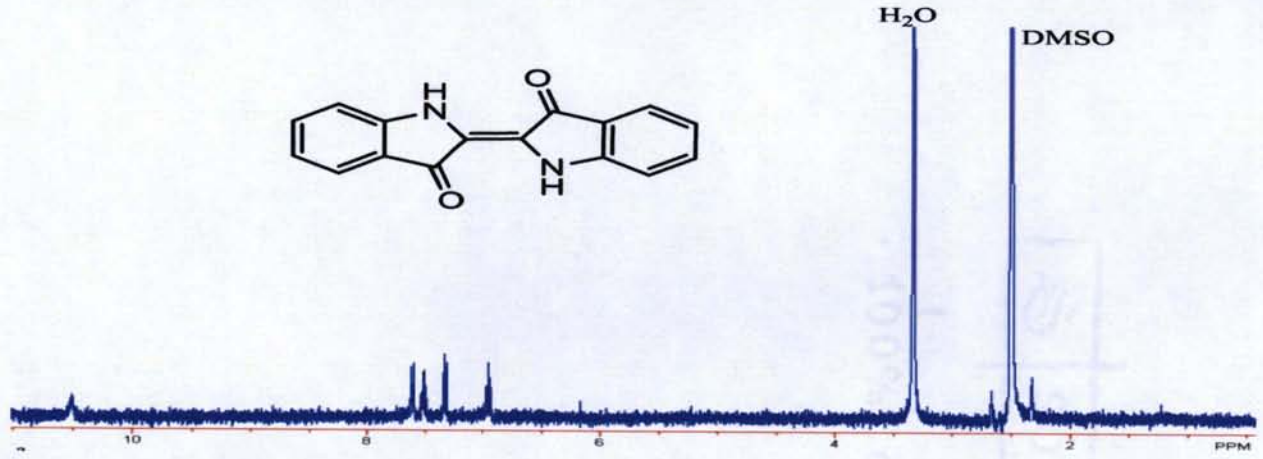

Figure 14e: ^{1}H-NMR spectrum (MEM2A305) for an authentic sample of indigo dye in d_6-DMSO.

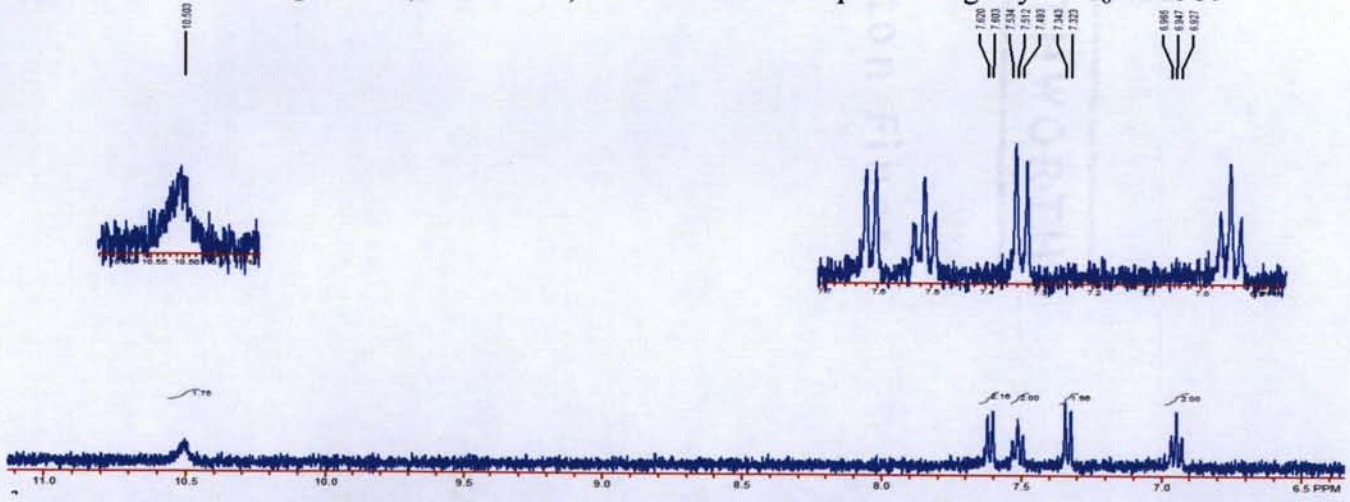

Figure 14f: ^{1}H-NMR spectrum (MEM2A305) for an authentic sample of indigo dye in d_6-DMSO expanded.

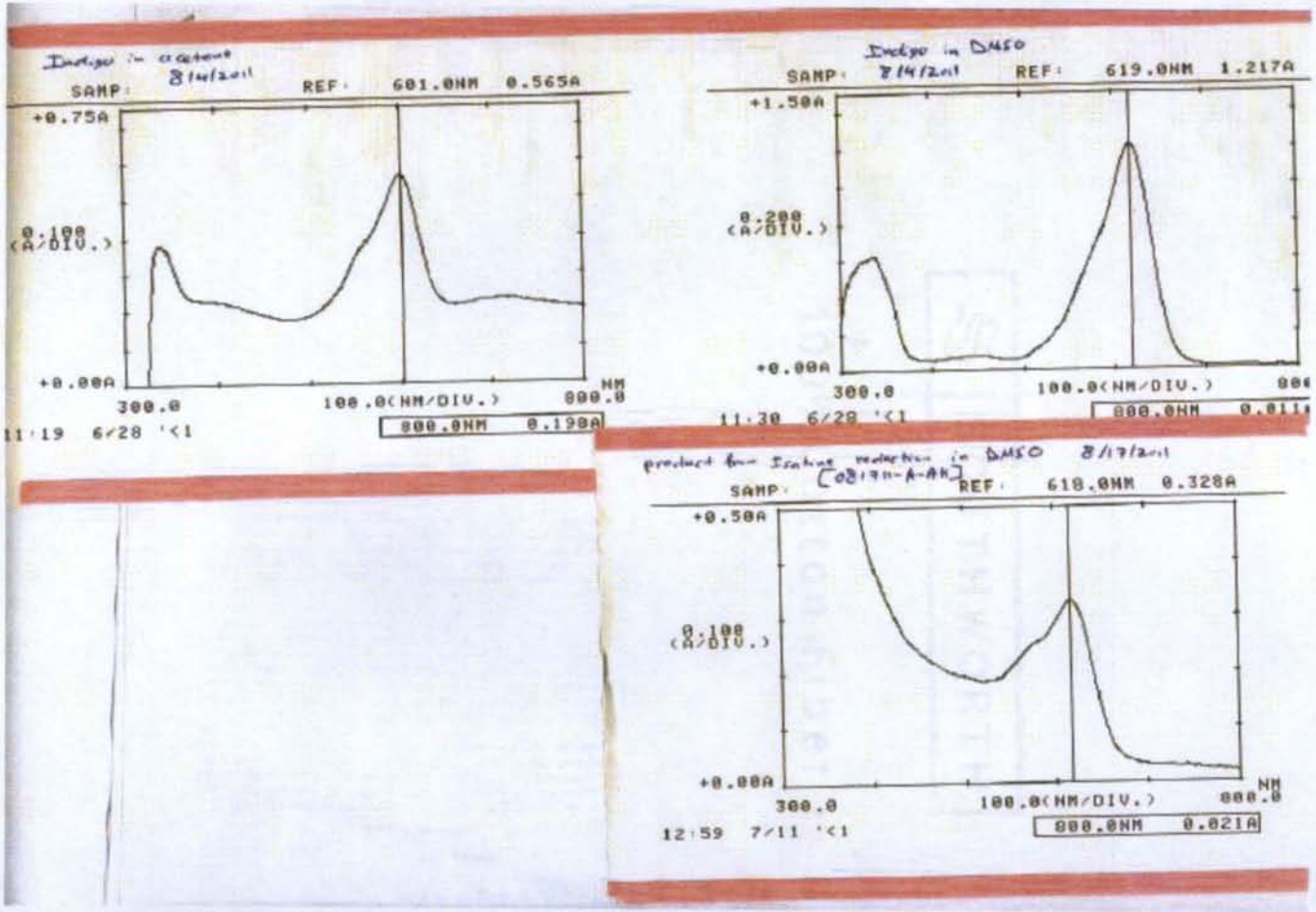

Figure 14g: UV-Vis spectra of an authentic sample of indigo dye and the product of isatin reduction (081711-A-AH) in DMSO.

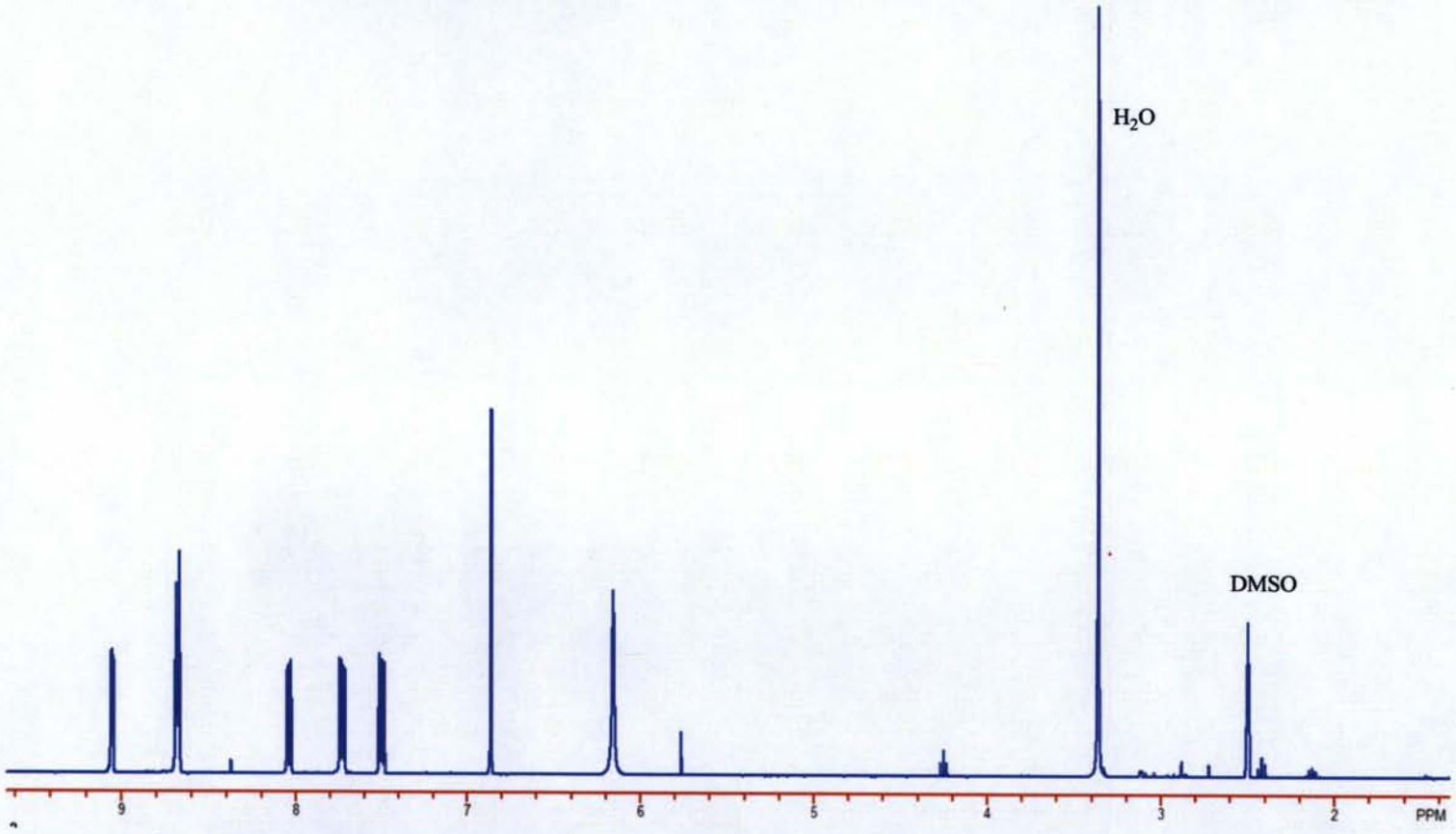

Figure 16a: ^{1}H- NMR (MEM2A316) spectrum for the synthetic attempt at phen-isatin (082511-A-AH) in d_6-DMSO.

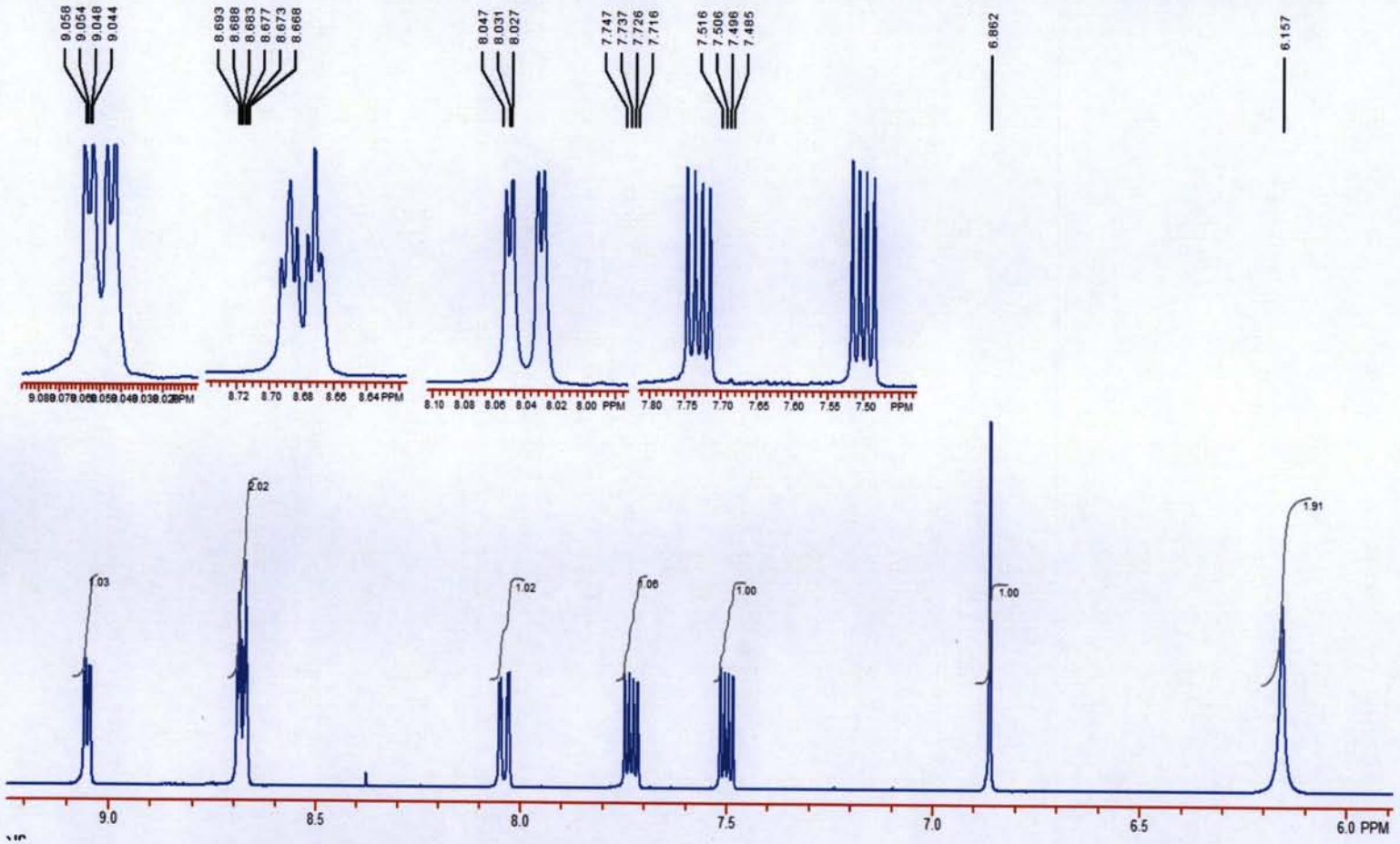

Figure 16b: ^{1}H- NMR (MEM2A316) spectrum for the synthetic attempt at phen-isatin (082511-A-AH) in d_6-DMSO. The spectrum matched the starting material 5-NH_2-phen (Figure 2b).

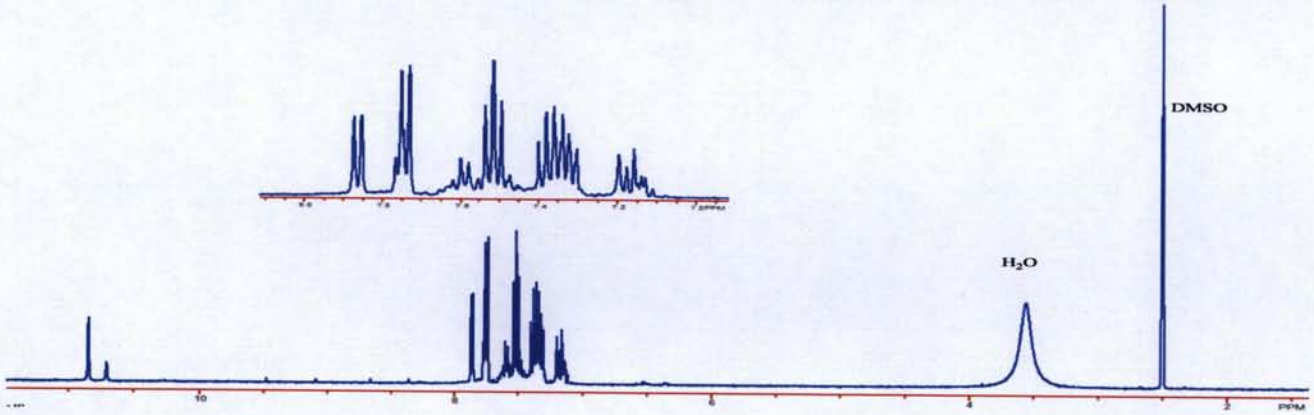

Figure 17a: ^{1}H-NMR (MEM2A319) for the synthetic attempt of isatin (090711-A-AH) in d_6-DMSO.

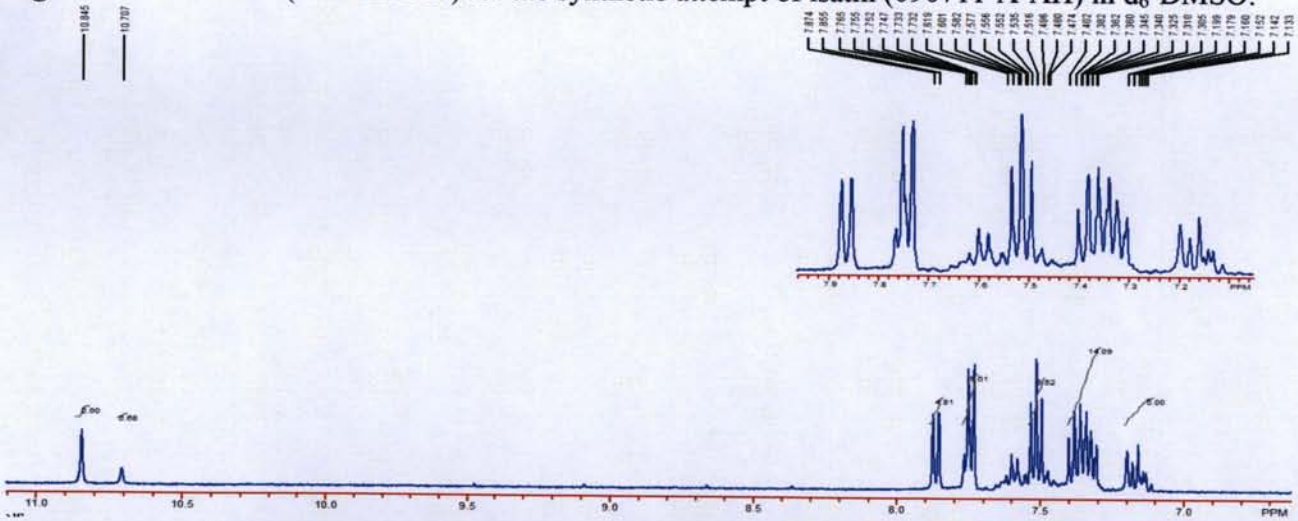

Figure 17b: ^{1}H-NMR (MEM2A319) for the synthetic attempt of isatin (090711-A-AH) in d_6-DMSO (expanded).

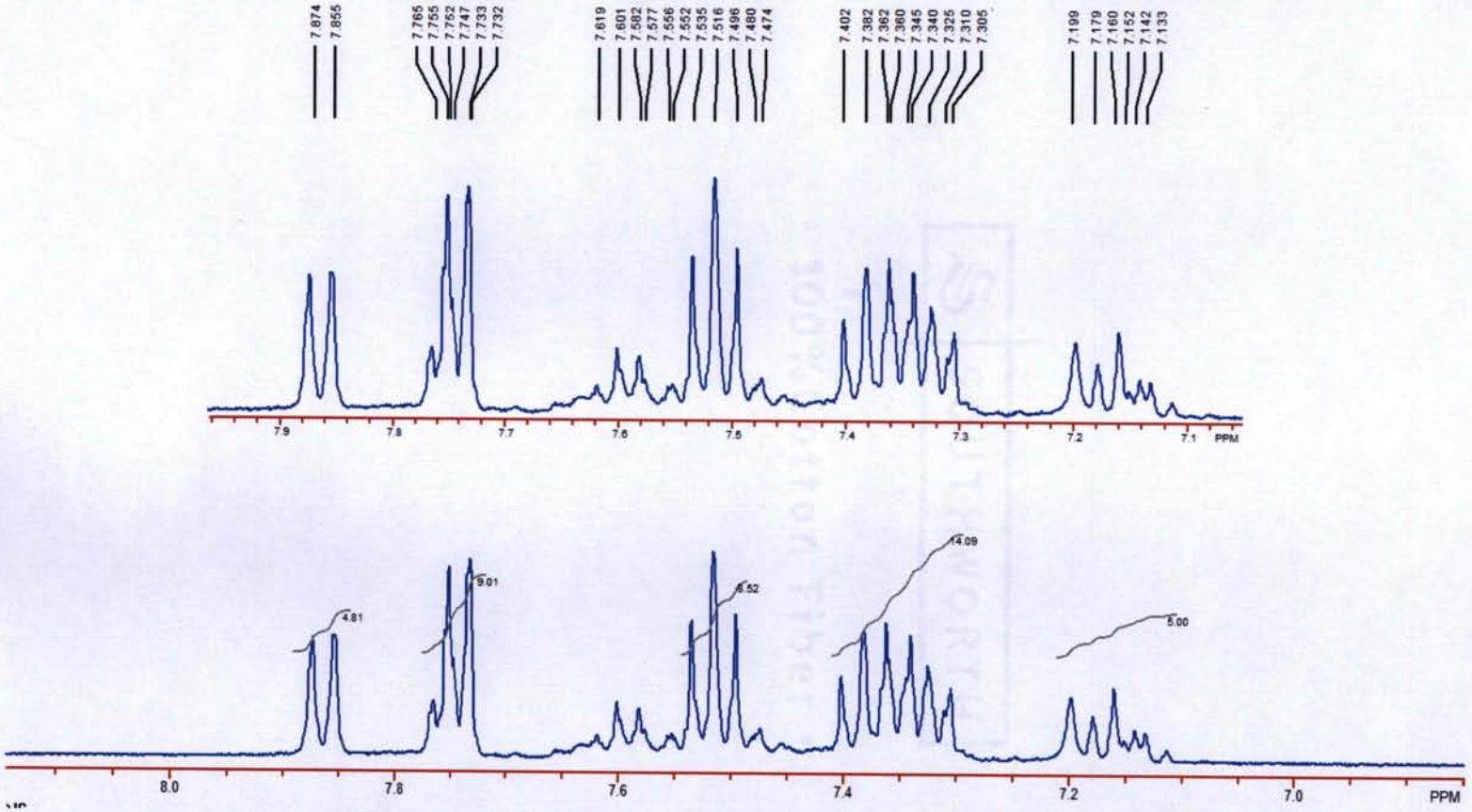

Figure 17c: ^{1}H-NMR (MEM2A319) for the synthetic attempt of isatin (090711-A-AH) in d_6-DMSO (expanded).

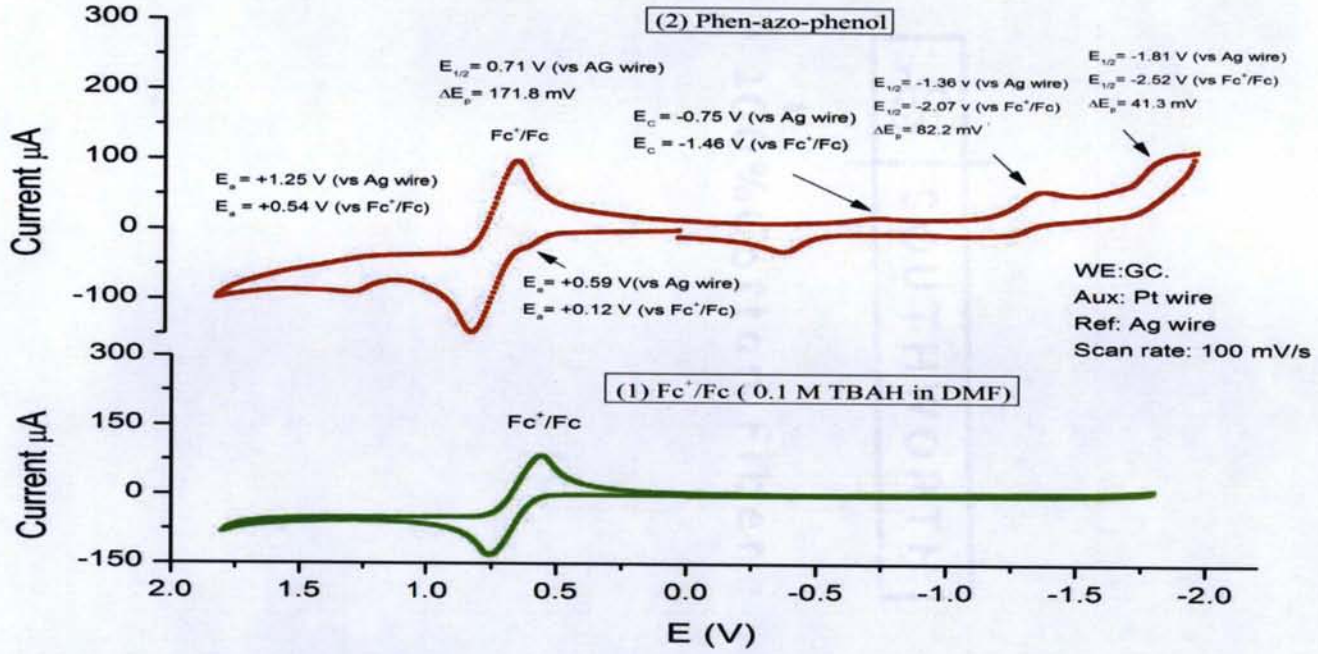

Figure 18: CV plots of: (1) Background (CV-060912P-AK), (2) phen-azo-phenol (CV-060912U-AK). They were recorded in DMF (0.1 M TBAH, sample concentrated 5×10^{-3} M).

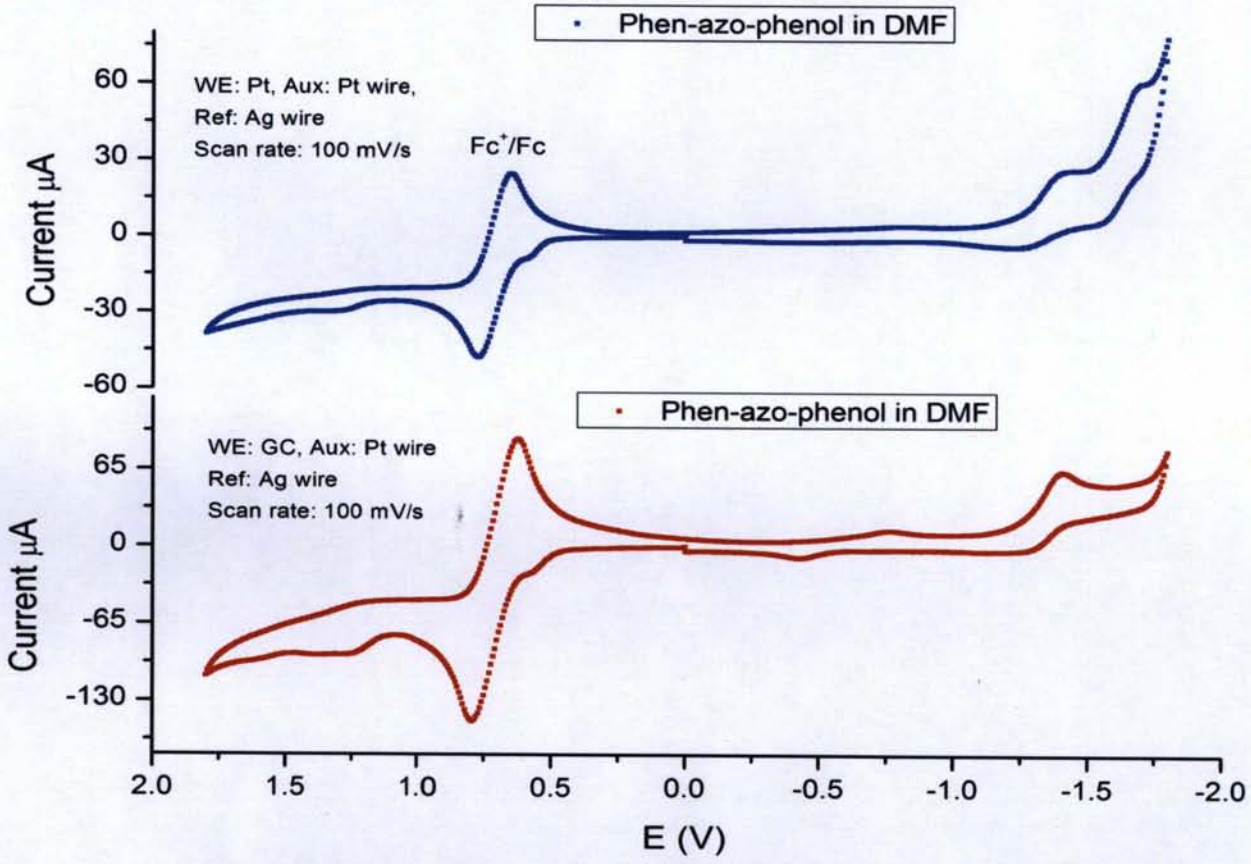

Figure 19: CV of phen-azo-phenol (CV-060912Q-AK) lower graph using glassy carbon electrode and upper graph (CV-060912R-AK) using a platinum electrode. Both CVs were recorded in DMF (0.1 M TBAH, sample concentrated 5×10^{-3} M).

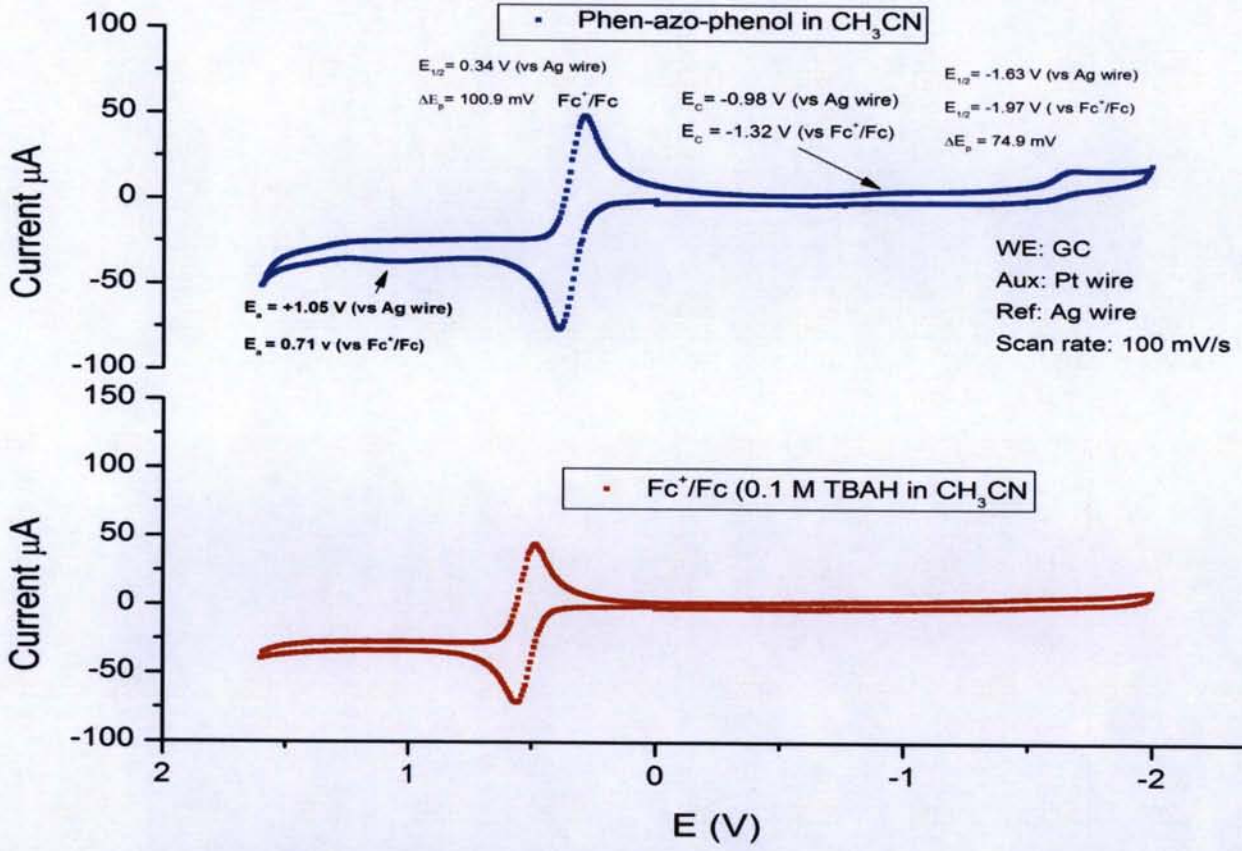

Figure 20: CV plots of phen-azo-phenol (CV-051512Z-AK) upper graph vs the background (CV-051512X-AK) lower graph. Both CVs were recorded in CH_3CN (0.1 M TBAH, sample concentrated 1×10^{-3} M).

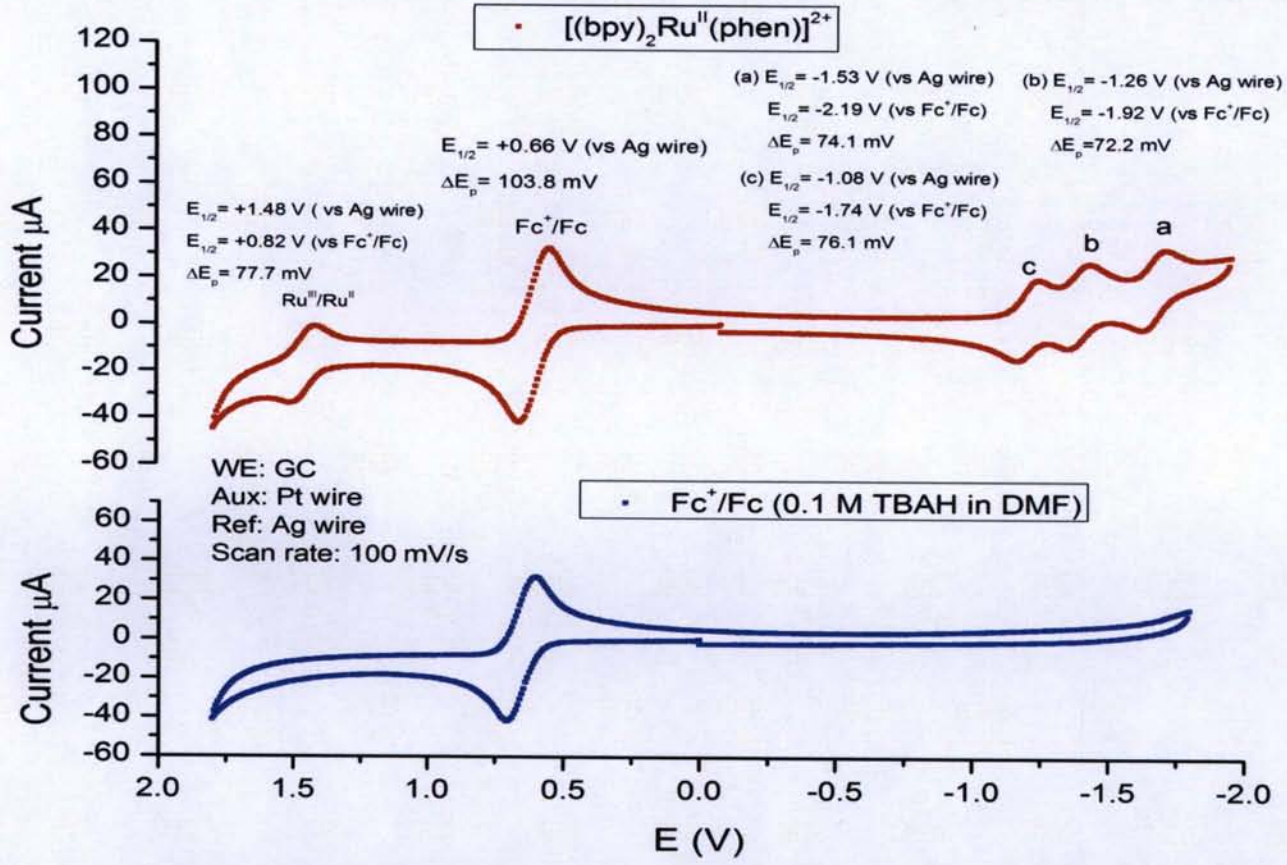

Figure 21: CV of $[(bpy)_2Ru^{II}(phen)]^{2+}$ upper graph (CV-060912E-AK) and the scan background (CV-060912C-AK) recorded in DMF (0.1 M TBAH, sample concentrated 1×10^{-3} M).

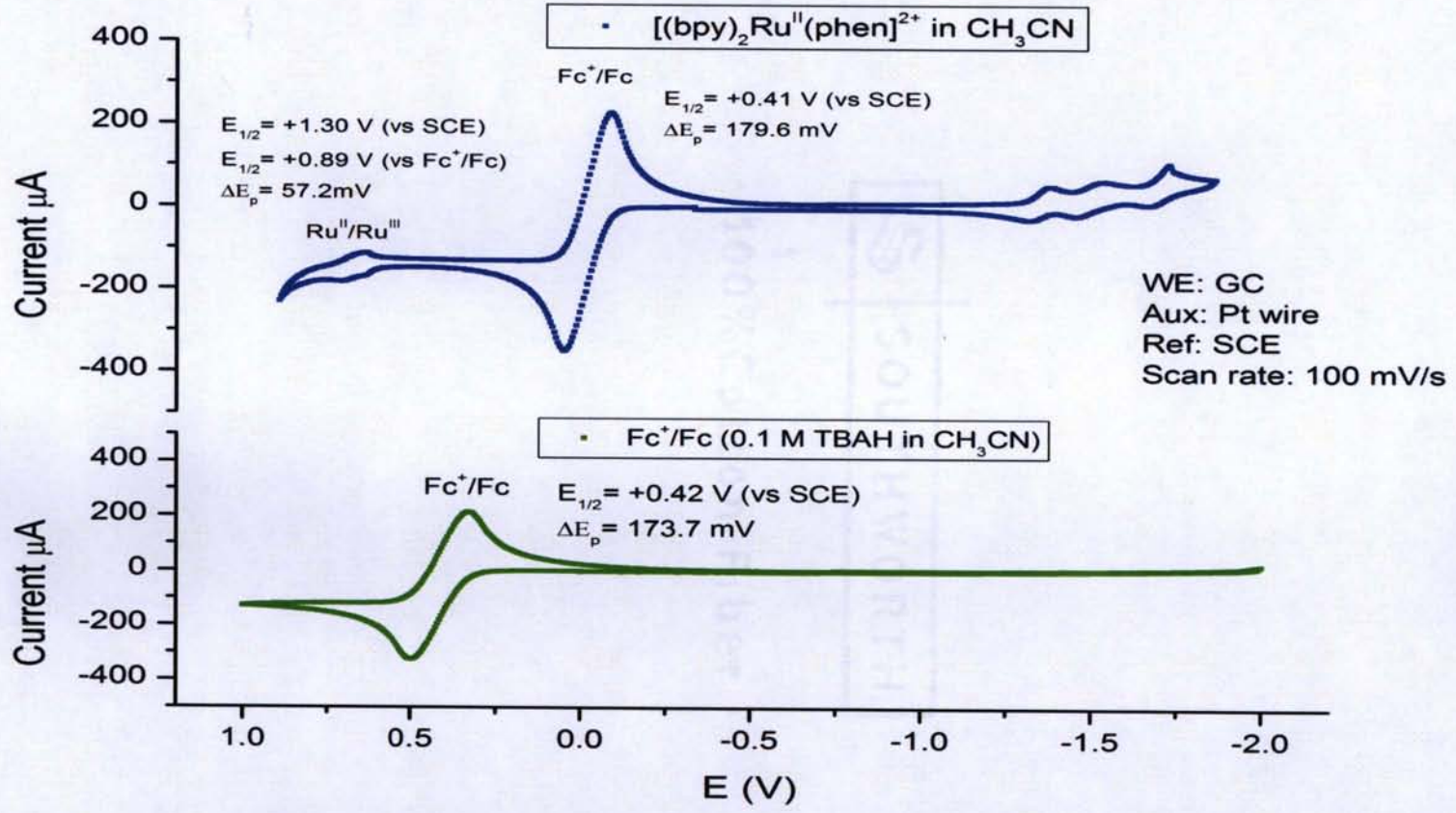

Figure 22: CV of [(bpy)2Ru^{II}(phen-azo-phenol)]$^{2+}$ upper graph (CV-051412G-AK) and the background scan (CV-051412C-AK) recorded in CH_3CN (0.1 M TBAH, sample concentrated 1×10^{-3} M).

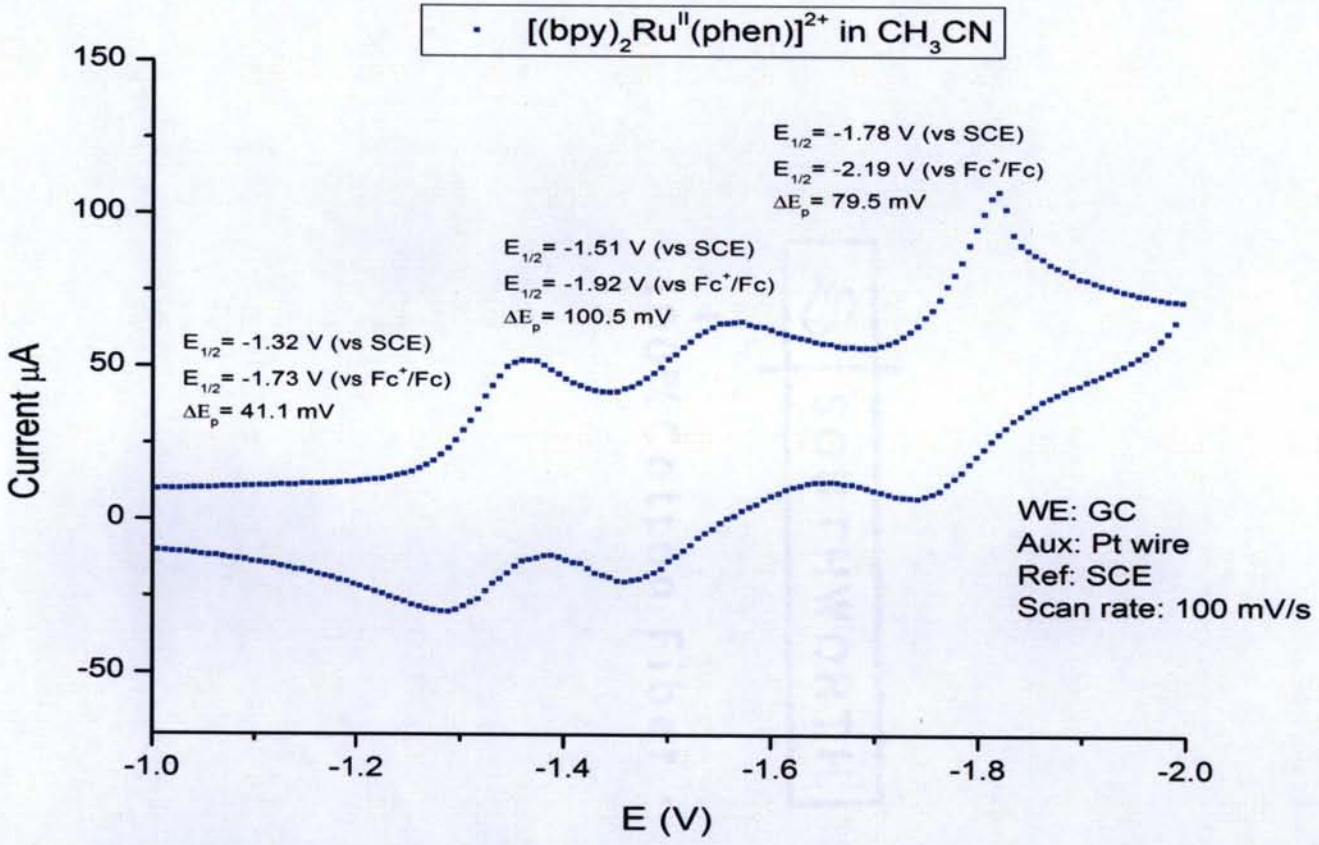

Figure 23: CV of [(bpy)2Ru^{II}(phen-azo-phenol)]$^{2+}$ (CV-051412G-AK) showing the reductive part. It was recorded in CH_3CN (0.1 M TBAH, sample concentrated 1×10^{-3} M).

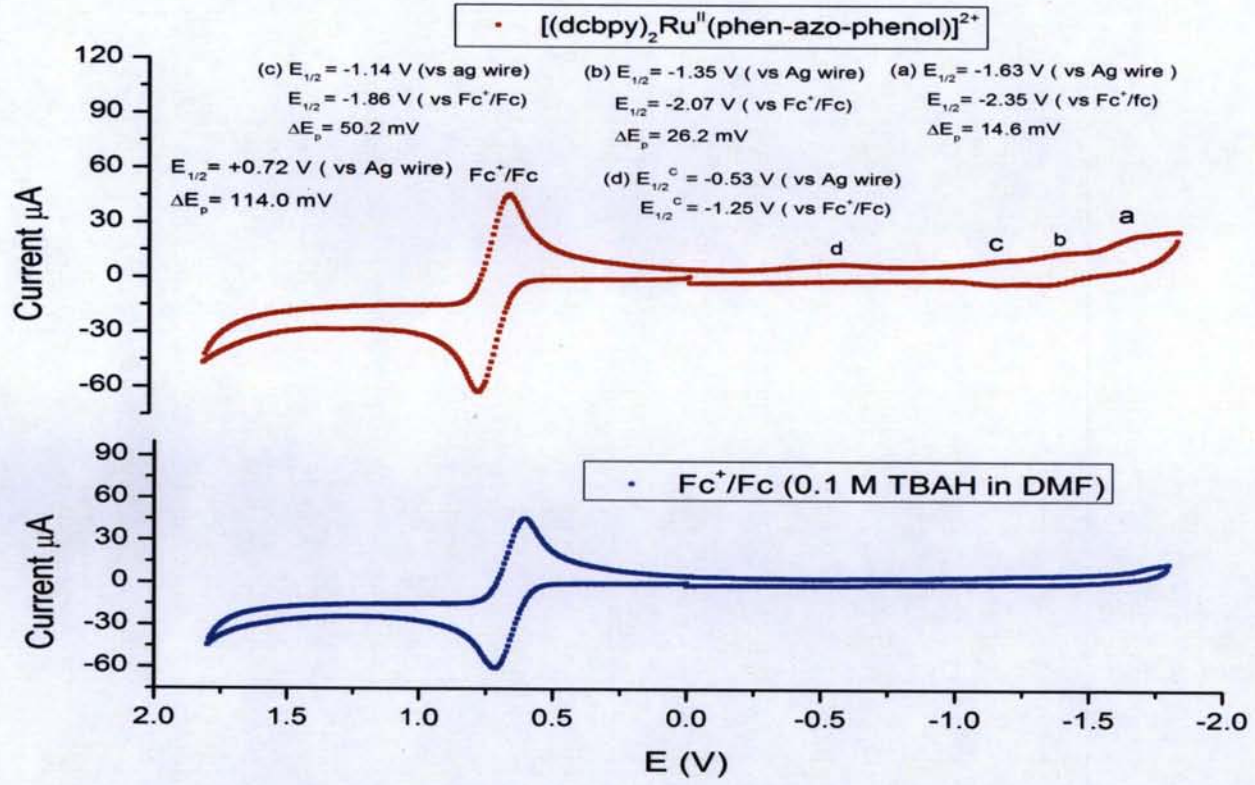

Figure 24: CV of $[(dcbpy)_2Ru^{II}(phen\text{-}azo\text{-}phenol)]^{2+}$ (CV-060912K-AK) upper graph and the background scan (CV-060912J-AK) recorded in DMF (0.1 M TBAH, sample concentrated 1×10^{-3} M, WE:GC, Aux; Pt, Ref: Ag wire, scan rate: 100 mV s^{-1}).

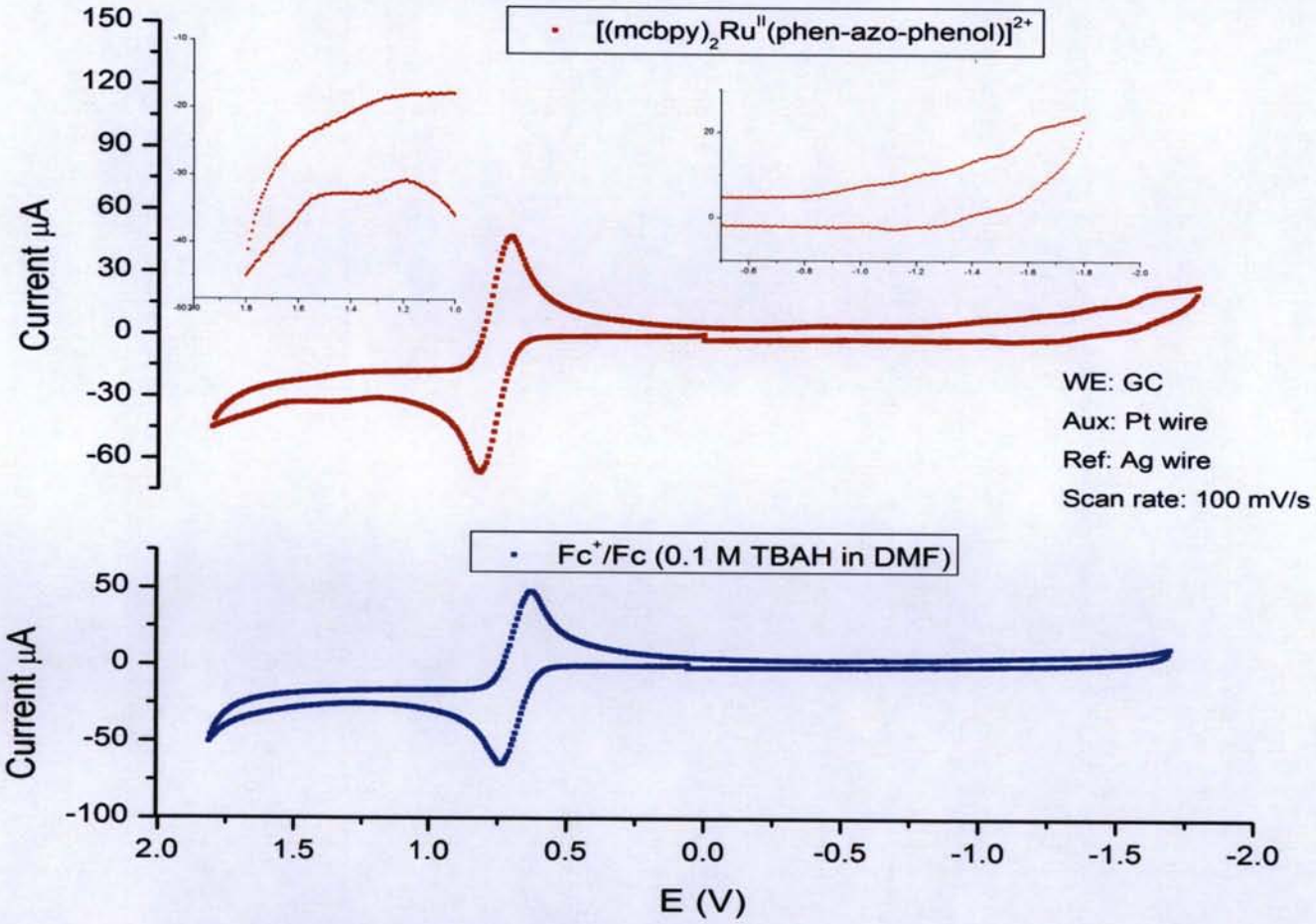

Figure 25: CV for $[(mcbpy)_2Ru^{II}(phen\text{-}azo\text{-}phenol)]^{2+}$ (CV-060912H-AK) upper graph and the background lower graph (CV-060912F-AK) recorded in DMF (0.1 M TBAH, sample concentrated 1×10^{-3} M).

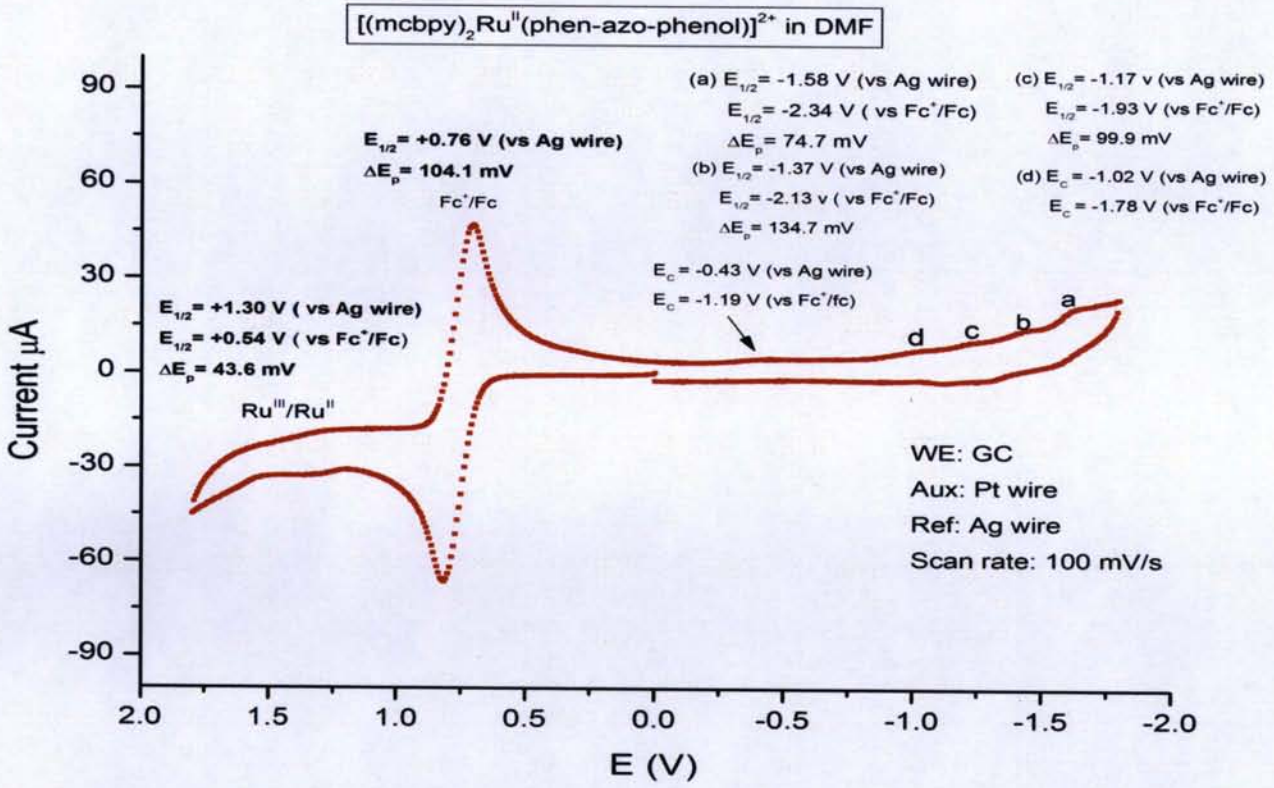

Figure 26: CV for $[(mcbpy)_2Ru^{II}(phen\text{-}azo\text{-}phenol)]^{2+}$ (CV-060912H-AK) recorded in DMF (0.1 M TBAH, sample concentrated 1×10^{-3} M).

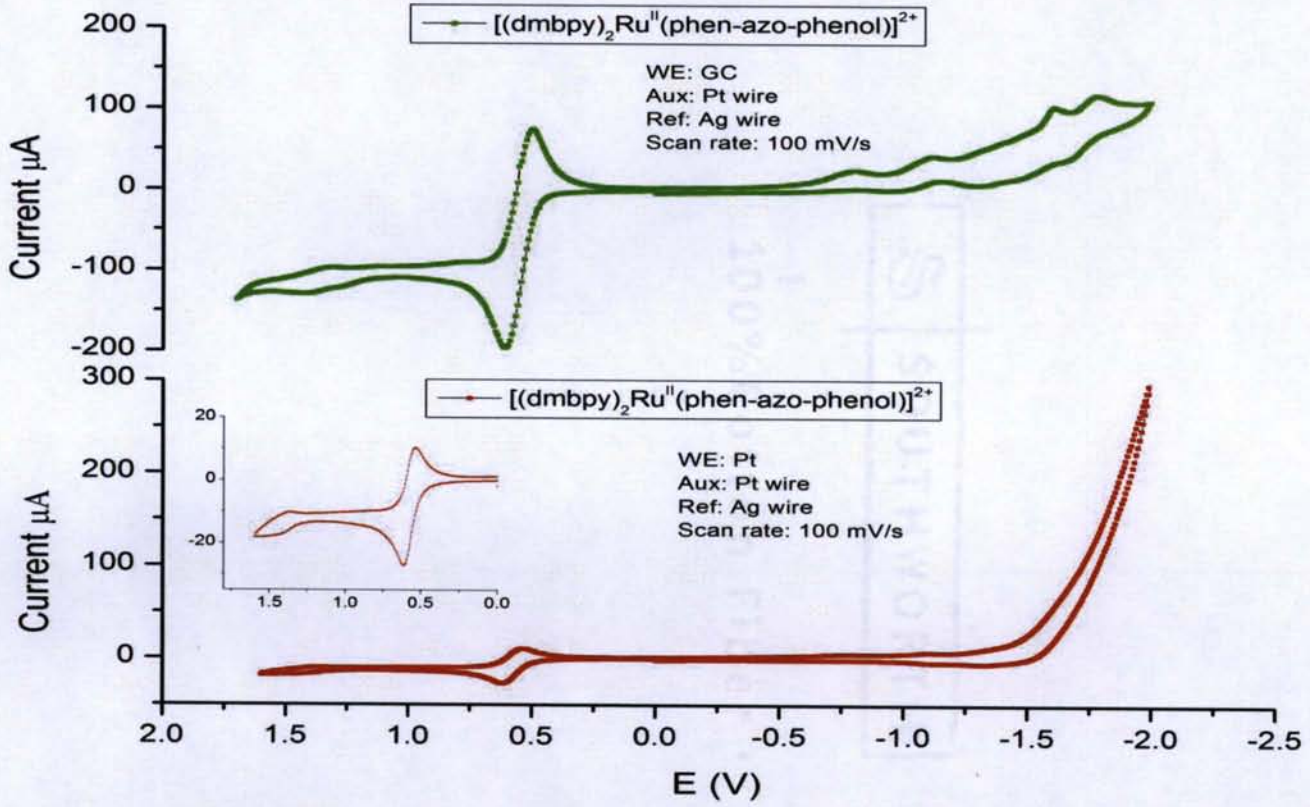

Figure 27: CV of $[(dmbpy)_2Ru^{II}(phen\text{-}azo\text{-}phenol)]^{2+}$ using Pt working electrode lower graph (CV-051512C-AK) and using GC electrode upper graph (CV-051512Q-AK) recorded in CH_3CN (0.1 M TBAH, sample concentrated 1×10^{-3} M).

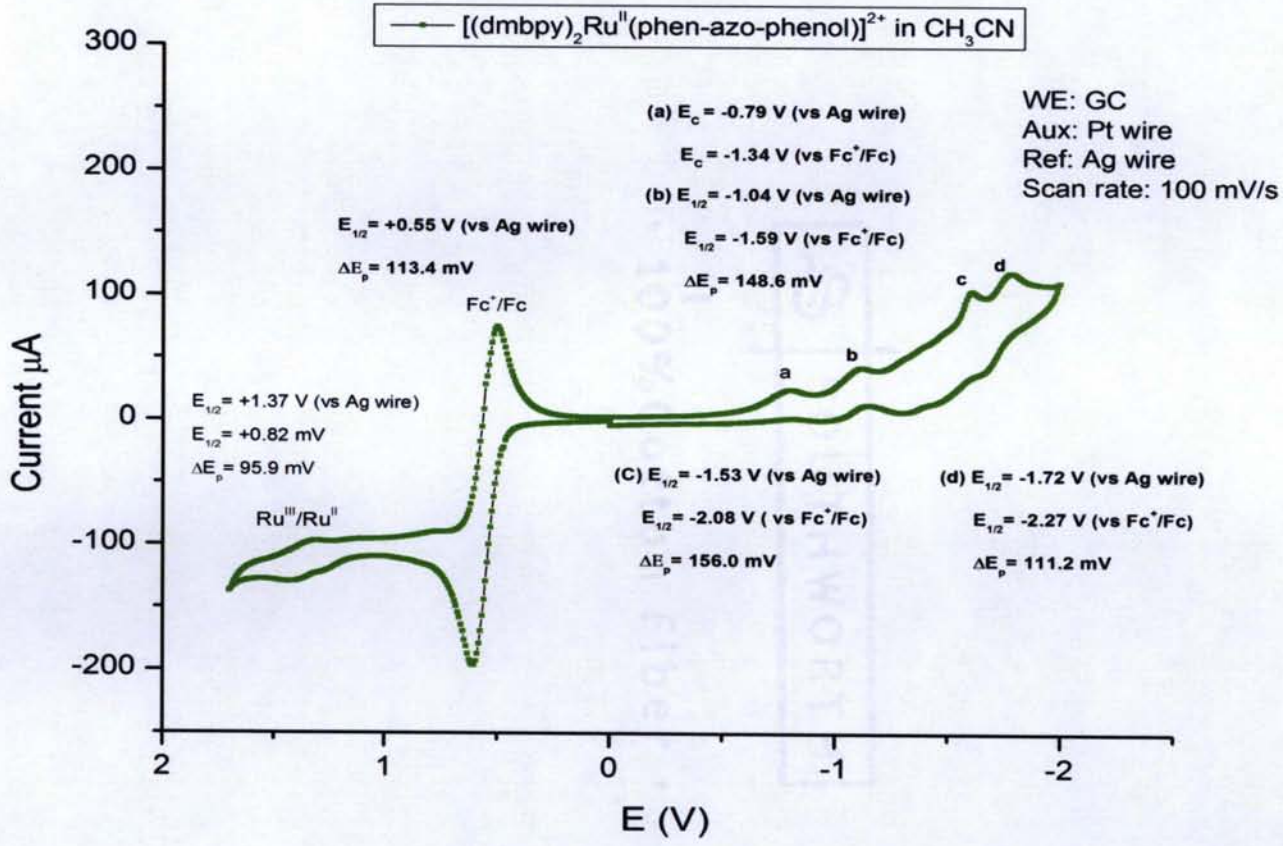

Figure 28: CV of $[(dmbpy)_2Ru^{II}(phen\text{-}azo\text{-}phenol)]^{2+}$ (CV-051512Q-AK) recorded in CH_3CN (0.1 M TBAH, sample concentrated 1×10^{-3} M).

Appendix 1:

Refinement

H atoms attached to N and O atoms were found in a difference Fourier map and refined independently using isotropic atomic displacement parameters. All of the H atoms bonded to aromatic C atoms were placed in geometrically calculated positions (C—H = 0.95 Å) and were included in the refinement in a riding model approximation, with $U_{iso}(H) = 1.2U_{eq}(C)$.

6-[(4-Hydroxyphenyl)diazenyl]-1,10-phenanthrolin-1-ium chloride monohydrate

Crystal data

$C_{18}H_{13}N_4O^+ \cdot Cl^- \cdot H_2O$	$Z = 2$
$M_r = 354.79$	$F(000) = 368$
Triclinic, $P\bar{1}$	$D_x = 1.468$ Mg m^{-3}
Hall symbol: -P 1	Cu $K\alpha$ radiation, $\lambda = 1.54178$ Å
$a = 7.6732$ (4) Å	Cell parameters from 4384 reflections
$b = 7.7894$ (4) Å	$\theta = 3.2$–$66.7°$
$c = 14.1225$ (7) Å	$\mu = 2.28$ mm^{-1}
$\alpha = 78.535$ (3)°	$T = 100$ K
$\beta = 80.379$ (3)°	Transparent plate, orange
$\gamma = 78.212$ (3)°	0.41 × 0.26 × 0.04 mm
$V = 802.73$ (7) Å^3	

Data collection

Bruker APEXII CCD diffractometer	2806 independent reflections
Radiation source: fine-focus sealed tube	2407 reflections with $I > 2\sigma(I)$
graphite	$R_{int} = 0.051$

Detector resolution: 8.33 pixels mm^{-1}

phi and ω scans

Absorption correction: multi-scan (*SADABS*; Bruker, 2008)

$T_{min} = 0.454$, $T_{max} = 0.914$

15401 measured reflections

$\theta_{max} = 67.4°$, $\theta_{min} = 3.2°$

$h = -9 \rightarrow 9$

$k = -7 \rightarrow 9$

$l = -16 \rightarrow 16$

Refinement

Refinement on F^2

Least-squares matrix: full

$R[F^2 > 2\sigma(F^2)] = 0.043$

$wR(F^2) = 0.118$

$S = 1.03$

2806 reflections

242 parameters

0 restraints

Primary atom site location: structure-invariant direct methods

Secondary atom site location: difference Fourier map

Hydrogen site location: inferred from neighbouring sites

H atoms treated by a mixture of independent and constrained refinement

$w = 1/[\sigma^2(F_o^2) + (0.0805P)^2 + 0.1676P]$ where $P = (F_o^2 + 2F_c^2)/3$

$(\Delta/\sigma)_{max} < 0.001$

$\Delta\rho_{max} = 0.40$ e $Å^{-3}$

$\Delta\rho_{min} = -0.21$ e $Å^{-3}$

Special details

Geometry. All e.s.d.'s (except the e.s.d. in the dihedral angle between two l.s. planes) are estimated using the full covariance matrix. The cell e.s.d.'s are taken into account individually in the estimation of e.s.d.'s in distances, angles and torsion angles; correlations between e.s.d.'s in cell parameters are only used when they are defined by crystal symmetry. An approximate (isotropic) treatment of cell e.s.d.'s is used for estimating e.s.d.'s involving l.s. planes.

Refinement. Refinement of F^2 against ALL reflections. The weighted *R*-factor *wR* and goodness of fit *S* are based on F^2, conventional *R*-factors *R* are based on *F*, with *F* set to zero for negative F^2. The threshold expression of $F^2 > \sigma(F^2)$ is used only for calculating *R*-factors(gt) *etc*. and is not relevant to the choice of reflections for refinement. *R*-factors based on F^2 are statistically about twice as large as those based on *F*, and *R*- factors based on ALL data will be even larger.

Fractional atomic coordinates and isotropic or equivalent isotropic displacement parameters ($Å^2$)

	x	*y*	*z*	U_{iso}*/U_{eq}
Cl1	0.24720 (6)	0.24063 (6)	0.05019 (3)	0.02974 (18)
O1	0.8362 (2)	1.58116 (19)	−0.72107 (11)	0.0356 (4)
O2	0.0147 (2)	0.5892 (2)	0.10617 (11)	0.0319 (4)
N1	0.3212 (2)	0.6808 (2)	−0.09907 (12)	0.0286 (4)
N2	0.5247 (2)	0.3608 (2)	−0.12489 (13)	0.0278 (4)
N3	0.6421 (2)	0.9679 (2)	−0.39335 (12)	0.0289 (4)
N4	0.7403 (2)	0.9508 (2)	−0.47300 (12)	0.0288 (4)
C1	0.2241 (3)	0.8387 (3)	−0.08742 (15)	0.0301 (5)
H1	0.1353	0.8451	−0.0320	0.036*
C2	0.2451 (3)	0.9963 (3)	−0.15216 (16)	0.0307 (5)
H2	0.1716	1.1059	−0.1405	0.037*
C3	0.3723 (3)	0.9915 (3)	−0.23242 (15)	0.0289 (5)
H3	0.3878	1.0975	−0.2771	0.035*
C4	0.4799 (3)	0.8273 (3)	−0.24789 (14)	0.0265 (4)
C5	0.6165 (3)	0.8060 (3)	−0.33052 (14)	0.0272 (4)
C6	0.7152 (3)	0.6433 (3)	−0.34203 (15)	0.0281 (4)
H6	0.8043	0.6327	−0.3970	0.034*
C7	0.6860 (3)	0.4882 (3)	−0.27224 (15)	0.0277 (4)
C8	0.7851 (3)	0.3169 (3)	−0.27964 (15)	0.0302 (5)
H8	0.8755	0.3004	−0.3335	0.036*
C9	0.7517 (3)	0.1734 (3)	−0.20927 (16)	0.0314 (5)
H9	0.8194	0.0580	−0.2139	0.038*
C10	0.6177 (3)	0.1993 (3)	−0.13131 (15)	0.0298 (5)
H10	0.5928	0.1010	−0.0826	0.036*
C11	0.5531 (3)	0.5072 (3)	−0.19183 (14)	0.0263 (4)
C12	0.4470 (3)	0.6768 (3)	−0.17871 (14)	0.0258 (4)
C13	0.7674 (3)	1.1138 (3)	−0.53279 (15)	0.0273 (4)
C14	0.6952 (3)	1.2806 (3)	−0.50623 (16)	0.0337 (5)
H14	0.6267	1.2879	−0.4441	0.040*
C15	0.7232 (3)	1.4333 (3)	−0.56975 (16)	0.0344 (5)
H15	0.6758	1.5458	−0.5508	0.041*
C16	0.8206 (3)	1.4250 (3)	−0.66197 (15)	0.0302 (5)
C17	0.8979 (3)	1.2599 (3)	−0.68827 (15)	0.0283 (4)
H17	0.9682	1.2527	−0.7499	0.034*
C18	0.8705 (3)	1.1070 (3)	−0.62302 (15)	0.0284 (4)
H18	0.9236	0.9943	−0.6405	0.034*
H4	0.902 (4)	1.565 (4)	−0.783 (2)	0.052 (8)*
H19	0.442 (4)	0.377 (3)	−0.076 (2)	0.045 (7)*
H20	0.077 (4)	0.494 (4)	0.091 (2)	0.054 (8)*
H21	−0.055 (4)	0.622 (4)	0.062 (2)	0.050 (8)*

Atomic displacement parameters ($Å^2$)

	U^{11}	U^{22}	U^{33}	U^{12}	U^{13}	U^{23}
Cl1	0.0299 (3)	0.0235 (3)	0.0305 (3)	0.00016 (18)	−0.00177 (19)	0.00097 (18)
O1	0.0425 (9)	0.0243 (8)	0.0323 (8)	−0.0014 (6)	0.0041 (7)	0.0007 (6)
O2	0.0383 (9)	0.0256 (8)	0.0288 (8)	0.0005 (6)	−0.0038 (7)	−0.0041 (6)
N1	0.0299 (9)	0.0255 (9)	0.0280 (9)	−0.0050 (7)	−0.0016 (7)	−0.0011 (7)
N2	0.0282 (9)	0.0249 (9)	0.0272 (9)	−0.0021 (7)	−0.0023 (7)	−0.0013 (7)
N3	0.0283 (9)	0.0280 (9)	0.0276 (9)	−0.0033 (7)	−0.0025 (7)	−0.0010 (7)
N4	0.0277 (9)	0.0292 (10)	0.0262 (9)	−0.0026 (7)	−0.0035 (7)	0.0005 (7)
C1	0.0291 (11)	0.0284 (11)	0.0298 (11)	−0.0026 (8)	0.0014 (8)	−0.0049 (8)
C2	0.0345 (11)	0.0226 (11)	0.0330 (11)	−0.0016 (8)	−0.0031 (9)	−0.0048 (8)
C3	0.0324 (11)	0.0233 (11)	0.0298 (11)	−0.0056 (8)	−0.0043 (8)	−0.0011 (8)
C4	0.0256 (10)	0.0268 (11)	0.0268 (10)	−0.0040 (8)	−0.0065 (8)	−0.0017 (8)
C5	0.0279 (10)	0.0253 (11)	0.0267 (10)	−0.0035 (8)	−0.0067 (8)	0.0005 (8)
C6	0.0268 (10)	0.0307 (11)	0.0251 (10)	−0.0040 (8)	−0.0005 (8)	−0.0040 (8)
C7	0.0261 (10)	0.0264 (11)	0.0290 (11)	−0.0014 (8)	−0.0049 (8)	−0.0034 (8)
C8	0.0286 (11)	0.0291 (11)	0.0309 (11)	−0.0008 (8)	−0.0024 (8)	−0.0059 (8)
C9	0.0321 (11)	0.0235 (11)	0.0358 (11)	−0.0001 (8)	−0.0045 (9)	−0.0033 (8)
C10	0.0321 (11)	0.0215 (11)	0.0337 (11)	−0.0022 (8)	−0.0067 (9)	−0.0002 (8)
C11	0.0277 (10)	0.0236 (10)	0.0274 (10)	−0.0047 (8)	−0.0067 (8)	−0.0014 (8)
C12	0.0254 (10)	0.0246 (11)	0.0269 (10)	−0.0032 (8)	−0.0049 (8)	−0.0032 (8)
C13	0.0258 (10)	0.0268 (11)	0.0271 (10)	−0.0022 (8)	−0.0054 (8)	−0.0001 (8)
C14	0.0363 (12)	0.0315 (12)	0.0280 (11)	−0.0025 (9)	0.0030 (9)	−0.0026 (9)
C15	0.0403 (12)	0.0244 (11)	0.0334 (12)	−0.0009 (9)	0.0024 (9)	−0.0040 (8)
C16	0.0306 (11)	0.0268 (11)	0.0300 (11)	−0.0031 (8)	−0.0046 (8)	0.0013 (8)
C17	0.0274 (10)	0.0286 (11)	0.0267 (10)	−0.0024 (8)	−0.0023 (8)	−0.0029 (8)
C18	0.0281 (10)	0.0266 (11)	0.0276 (10)	0.0007 (8)	−0.0053 (8)	−0.0025 (8)

Geometric parameters (Å, °)

O1—C16	1.347 (2)	C6—C7	1.430 (3)
O1—H4	0.95 (3)	C6—H6	0.9500
O2—H20	0.84 (3)	C7—C11	1.404 (3)
O2—H21	0.85 (3)	C7—C8	1.408 (3)
N1—C1	1.327 (3)	C8—C9	1.376 (3)
N1—C12	1.355 (3)	C8—H8	0.9500
N2—C10	1.326 (3)	C9—C10	1.391 (3)
N2—C11	1.358 (3)	C9—H9	0.9500
N2—H19	0.87 (3)	C10—H10	0.9500
N3—N4	1.259 (2)	C11—C12	1.432 (3)
N3—C5	1.419 (3)	C13—C18	1.388 (3)
N4—C13	1.411 (3)	C13—C14	1.402 (3)
C1—C2	1.398 (3)	C14—C15	1.372 (3)
C1—H1	0.9500	C14—H14	0.9500
C2—C3	1.368 (3)	C15—C16	1.396 (3)
C2—H2	0.9500	C15—H15	0.9500
C3—C4	1.409 (3)	C16—C17	1.395 (3)
C3—H3	0.9500	C17—C18	1.384 (3)
C4—C12	1.405 (3)	C17—H17	0.9500
C4—C5	1.444 (3)	C18—H18	0.9500
C5—C6	1.362 (3)		
C16—O1—H4	112.0 (17)	C7—C8—H8	119.8
H20—O2—H21	103 (3)	C8—C9—C10	119.17 (19)
C1—N1—C12	116.57 (17)	C8—C9—H9	120.4
C10—N2—C11	123.09 (19)	C10—C9—H9	120.4
C10—N2—H19	120.1 (18)	N2—C10—C9	120.14 (19)
C11—N2—H19	116.8 (18)	N2—C10—H10	119.9
N4—N3—C5	115.16 (16)	C9—C10—H10	119.9
N3—N4—C13	113.91 (16)	N2—C11—C7	119.06 (18)
N1—C1—C2	123.65 (19)	N2—C11—C12	119.30 (18)
N1—C1—H1	118.2	C7—C11—C12	121.64 (18)
C2—C1—H1	118.2	N1—C12—C4	124.37 (18)
C3—C2—C1	119.52 (18)	N1—C12—C11	117.06 (17)
C3—C2—H2	120.2	C4—C12—C11	118.57 (18)
C1—C2—H2	120.2	C18—C13—C14	118.72 (19)
C2—C3—C4	119.12 (18)	C18—C13—N4	117.59 (18)

C2—C3—H3	120.4	C14—C13—N4	123.69 (18)
C4—C3—H3	120.4	C15—C14—C13	120.14 (19)
C12—C4—C3	116.77 (18)	C15—C14—H14	119.9
C12—C4—C5	119.30 (17)	C13—C14—H14	119.9
C3—C4—C5	123.92 (18)	C14—C15—C16	120.64 (19)
C6—C5—N3	124.55 (18)	C14—C15—H15	119.7
C6—C5—C4	121.23 (18)	C16—C15—H15	119.7
N3—C5—C4	114.16 (17)	O1—C16—C17	123.39 (19)
C5—C6—C7	120.71 (19)	O1—C16—C15	116.79 (18)
C5—C6—H6	119.6	C17—C16—C15	119.82 (19)
C7—C6—H6	119.6	C18—C17—C16	118.89 (19)
C11—C7—C8	118.16 (19)	C18—C17—H17	120.6
C11—C7—C6	118.55 (18)	C16—C17—H17	120.6
C8—C7—C6	123.28 (19)	C17—C18—C13	121.70 (18)
C9—C8—C7	120.38 (19)	C17—C18—H18	119.2
C9—C8—H8	119.8	C13—C18—H18	119.2
C5—N3—N4—C13	−178.33 (16)	C8—C7—C11—C12	179.75 (18)
C12—N1—C1—C2	0.2 (3)	C6—C7—C11—C12	0.2 (3)
N1—C1—C2—C3	−0.2 (3)	C1—N1—C12—C4	0.2 (3)
C1—C2—C3—C4	−0.2 (3)	C1—N1—C12—C11	179.76 (18)
C2—C3—C4—C12	0.6 (3)	C3—C4—C12—N1	−0.6 (3)
C2—C3—C4—C5	179.22 (19)	C5—C4—C12—N1	−179.33 (18)
N4—N3—C5—C6	13.2 (3)	C3—C4—C12—C11	179.85 (18)
N4—N3—C5—C4	−169.79 (17)	C5—C4—C12—C11	1.1 (3)
C12—C4—C5—C6	−0.7 (3)	N2—C11—C12—N1	−0.5 (3)
C3—C4—C5—C6	−179.33 (19)	C7—C11—C12—N1	179.51 (18)
C12—C4—C5—N3	−177.80 (17)	N2—C11—C12—C4	179.09 (17)
C3—C4—C5—N3	3.6 (3)	C7—C11—C12—C4	−0.9 (3)
N3—C5—C6—C7	176.79 (18)	N3—N4—C13—C18	−178.43 (17)
C4—C5—C6—C7	0.0 (3)	N3—N4—C13—C14	1.1 (3)
C5—C6—C7—C11	0.2 (3)	C18—C13—C14—C15	1.5 (3)
C5—C6—C7—C8	−179.3 (2)	N4—C13—C14—C15	−178.00 (19)
C11—C7—C8—C9	−0.3 (3)	C13—C14—C15—C16	1.2 (3)

C6—C7—C8—C9	179.22 (19)	C14—C15—C16—O1	177.6 (2)
C7—C8—C9—C10	0.7 (3)	C14—C15—C16—C17	−3.1 (3)
C11—N2—C10—C9	0.0 (3)	O1—C16—C17—C18	−178.53 (18)
C8—C9—C10—N2	−0.5 (3)	C15—C16—C17—C18	2.3 (3)
C10—N2—C11—C7	0.4 (3)	C16—C17—C18—C13	0.5 (3)
C10—N2—C11—C12	−179.60 (18)	C14—C13—C18—C17	−2.4 (3)
C8—C7—C11—N2	−0.3 (3)	N4—C13—C18—C17	177.18 (17)
C6—C7—C11—N2	−179.78 (17)		

Hydrogen-bond geometry (Å, °)

D—H···*A*	*D*—H	H···*A*	*D*···*A*	*D*—H···*A*
O1—H4···O2^{i}	0.95 (3)	1.65 (3)	2.586 (2)	166 (3)
N2—H19···Cl1	0.87 (3)	2.35 (3)	3.1077 (19)	145 (2)
O2—H20···Cl1	0.84 (3)	2.25 (3)	3.0959 (16)	180 (3)
O2—H21···Cl1^{ii}	0.85 (3)	2.30 (3)	3.1467 (17)	170 (2)

Symmetry codes: (i) $x+1, y+1, z-1$; (ii) $-x, -y+1, -z$.